Universidade de Aveiro
Ano 2019
Departamento de Economia, Gestão, Engenharia Industrial e Turismo
Departamento de Engenharia Mecânica

Wagd Ajeeb

Transferência de calor por convecção em escoamentos de nanofluidos não newtonianos em micro permutadores de calor

Convective heat transfer of non-Newtonian nanofluids in micro heat exchanger

Universidade de Aveiro
Ano 2019

Departamento de Economia, Gestão, Engenharia Industrial e Turismo

Departamento de Engenharia Mecânica

Wagd Ajeeb

Transferência de calor por convecção em escoamentos de nanofluidos não newtonianos em micro permutadores de calor

Convective heat transfer of non-Newtonian nanofluids in micro heat exchanger

Tese apresentada à Universidade de Aveiro para cumprimento dos requisitos necessários à obtenção do grau de Doutor em Sistemas Energéticos e Alterações Climáticas, realizada sob a orientação científica do Doutor Nelson Amadeu Dias Martins e da Doutora Mónica Sandra Abrantes de Oliveira Correia, Professores Auxiliares do Departamento de Engenharia Mecânica da Universidade de Aveiro.

This thesis is presented to the University of Aveiro to fulfil the requirements necessary to obtain a PhD in Energy Systems and Climate Change, under the scientific guidance of Doctor Nelson Amadeu Dias Martins and Doctor Mónica Sandra Abrantes de Oliveira Correia, Assistant Professors at the Department of Mechanical Engineering of Aveiro University.

Apoio financeiro da Plataforma Global para Estudantes Sírios, especialmente do ex-Presidente de Portugal Dr. Jorge Sampaio e a Dra. Helena Barroco (Fundação da Casa do Regalo, Lisboa).

Financial support from Global Platform for Syrian Students, especially the former President of Portugal Dr Jorge Sampaio and Dr Helena Barroco (Foundation of Casa do Regalo, Lisbon).

“True knowledge exists in knowing that you know nothing.” – Socrates

“The secret of change is to focus your energy, not on fighting the old but on building the new.” – Socrates

o júri

presidente

Doutor Joaquim Manuel Vieira
Professor Catedrático da Universidade de Aveiro

Doutor Fernando José Neto da Silva
Professor Auxiliar da Universidade de Aveiro

Doutor Nelson Amadeu Dias Martins
Professor Auxiliar da Universidade de Aveiro (Orientador)

Doutor Adélio Manuel de Sousa Cavadas
Professor Adjunto da Escola Superior de Tecnologia de Gestão, Instituto Politécnico de Viana do Castelo

Doutor Hugo Miguel Filipe Calisto
Investigador da European Commission, Joint Research Centre (JRC), Petten, Netherlands

Doutor Bruno Alexandre Abreu Silva
Diretor Executivo da SCUBIC

acknowledgements

I express my gratitude and my very great appreciation to my supervisors Doctor Mónica Oliveira and Doctor Nelson Martins, assistant professors at the Department of Mechanical Engineering from the University of Aveiro, for their assistance and guidance.

Also, I would like to offer my special thanks to Dr Bruno Abreu for his generous assistance. My special thanks are extended to the valuable database provided by Dr Bruno Abreu and Dr Bruno Lamas in their previous experimental investigations and their assistance to comprehend and tailoring their results. In addition, I would like to thank the various people for their contribution to this project; researchers and past students who worked on CNTs nanofluid and heat transfer in the University of Aveiro, also, the employees and the experts for their valuable technical support.

In addition, I acknowledge Global Platform for Syrian Students, especially to former President of Portugal Dr Jorge Sampaio and to Dr Helena Barroco, for the financial support and providing the requirements of being in Portugal.

Finally, I am very grateful for my wonderful parents, Adnan Ajeeb and Waheba Robah for the continuous and unconditional love and support. Also, I would like to dedicate this success to my parents, my country Syria and to all young people who couldn't have the chance to complete their education under the war conditions, and to those who are in the holy position of protecting the people, particularly my martyred friends.

palavras-chave

Nanotubos de carbono, nanofluidos, Microcanal, escoamento laminar, FLUENT-ANSYS.

resumo

Neste trabalho é estudado numericamente o impacto do uso de fluidos não-newtonianos como meio de transferência de calor em micro permutadores de calor (MCHE). O estudo da utilização de fluidos não newtonianos para fins de transferência de calor é uma área de pesquisa com interesse crescente como resultado do desenvolvimento de nanofluidos com características de transferência de calor melhoradas, já que estes geralmente apresentam um comportamento reológico complexo, i.e., não newtoniano. No presente trabalho, foram considerados nanofluidos de base aquosa produzidos a partir de nanotubos de carbono (MWCNT), caracterizados por um comportamento reológico pseudoplástico. O desempenho da transferência de calor destes nanofluidos em microcanais é avaliado para uma extensiva gama de condições de operação e compreendendo variações nos parâmetros constitutivos e morfológicos do fluido de trabalho, identificados como determinantes das propriedades termofísicas e de transporte deste tipo de fluido, nomeadamente, fluido de base, geometria da nanopartícula e concentração. O problema em análise é estudado computacionalmente usando ferramentas de CFD, considerando escoamento monofásico bidimensional, em condições estacionárias e regime laminar, para uma geometria específica de micro permutador de calor. As propriedades termofísicas dos nano fluídos considerados, obtidas experimentalmente, foram disponibilizadas e convenientemente modeladas, de modo a serem integradas neste estudo. Como as propriedades físicas dos fluidos considerados estão diretamente relacionadas à composição e morfologia dos fluidos, os resultados deste estudo podem ser usados para estabelecer a influência relativa da propriedades deste tipo de nanofluido sobre a transferência de calor e eficácia do processo de transferência neste tipo de sistema (micro canais), proporcionando uma forma de indireta de estabelecer as características do fluido de trabalho em função da aplicação específica pretendida, por exemplo: micro sistemas eletromecânicos, energia solar, aplicações aeroespaciais, sensores, atuadores etc.

Esta tese aborda vários objetivos da Agenda 2030 para o Desenvolvimento Sustentável, adotada por todos os estados-membro das nações Unidas em 2015, nomeadamente as relacionadas direta e indiretamente com a utilização e disponibilidade de energia (7, 9, 11 e 13, ver: https://sustainabledevelopment.un.org/SDGs), uma vez que a eficácia da transferência de calor dita a eficiência energética da maioria dos sistemas térmicos, potenciando uma utilização mais racional das fontes de energia disponíveis, e consequentemente, um menor impacto ambiental quando se considera o ciclo de vida do sistema.

keywords MWCNTs, nanofluids, Microchannel, Laminar flow, FLUENT-ANSYS.

abstract

The effect of using non-Newtonian fluids as a heat transfer medium in microchannel heat exchangers (MCHE) is numerically investigated. The study of Non-Newtonian fluids for heat transfer purposes is a research area with growing interest as a result of the development of nanofluids with enhanced heat transfer characteristics, as these usually show a complex rheologic behaviour. In the present work, water-based carbon multi-walled carbon nanotubes (MWCNT) fluids, showing a shear-thinning rheological behaviour were considered. The heat transfer performance of MWCNTs nanofluids in microchannels is assessed for a wide range of operating conditions and comprising the parameters known to directly influence the thermophysical and transport properties of this sort of heat transfer fluid, namely base fluid, nanoparticle geometry and concentration. The overall problem is computationally solved using CFD tools, considering a single-phase, 2D, laminar, steady state flow numerical model for a specific micro heat exchanger geometry. The thermophysical properties of the considered MWCNTs nanofluids, experimentally obtained, were made available and conveniently modelled. As the physical properties of the considered fluids are directly related to the fluids morphology, the study provides a means to establish the relative influence of MWCNTs nanofluids properties on the overall heat transfer and fluid flow effectiveness of such systems, providing a mean to indirectly support the tailoring of the heat transfer fluid to specific heat exchanger applications, e.g.: micro-electromechanical systems, solar energy, aerospace applications.

This thesis addresses several goals of the 2030 Agenda for Sustainable Development, adopted by all United Nations Member States in 2015, namely those directly and indirectly related with energy use and availability (7, 9, 11 and 13, see: https://sustainabledevelopment.un.org/sdgs), since heat transfer effectiveness dictates the overall energy efficiency of most thermal systems, broadening the scope towards more rational use of energy sources and hence mitigate the environmental impact of the system's life cycle.

TABLE OF CONTENTS

TABLE OF CONTENTS **1**

LIST OF FIGURES **5**

LIST OF TABLES **11**

NOMENCLATURE **13**

CHAPTER 1- INTRODUCTION **21**

1.1 THESIS BACKGROUND AND MOTIVATION 21

1.2 STATEMENT OF THE PROBLEM AND GENERAL OBJECTIVES 23

1.3 LITERATURE REVIEW 24

1.3.1 Microchannel 24

1.3.2 Nanofluids and its applications 25

1.3.2.1. Carbon nanotubes (CNTs) nanofluids (Structure) 25

1.3.2.2. Applications 27

1.3.2.3. Research trends 28

1.3.3 Nanofluids in Microchannels 30

1.3.4 Heat transfer of CNTs nanofluid 35

1.3.5 Characteristics of CNTs nanofluids in heat transfer studies 35

1.3.6 Computational fluid dynamic (CFD) 39

1.3.6.1. Numerical approach process 40

1.3.6.2. Governing equations 43

1.3.7 Numerical studies of CNTs nanofluid 46

1.3.8 Synthesis (State of the art identifying gaps in knowledge) 50

1.4 THESIS SPECIFIC OBJECTIVES AND RESEARCH QUESTIONS 52

1.5 THESIS CONTRIBUTION 53

1.6 THESIS ORGANIZATION 56

CHAPTER 2- Experimental and numerical study of convective heat transfer and laminar flow of MWCNTs nanofluid in a horizontal macroscale-tube **59**

2.1 CHAPTER SYNTHESIS AND PURPOSE 59

2.2 INTRODUCTION 59

2.3 EXPERIMENTAL SET-UP 62

2.3.1 Experimental methodology 64
2.3.2 Repeatability and uncertainty analysis 65
2.3.3 The preparation of the nanofluid 65
2.3.4 The nanofluid properties 66
2.4 MATHEMATICAL MODELLING 71
2.4.1 Geometric configuration 71
2.4.2 Governing equations 72
2.4.3 Boundary conditions 72
2.5 RESULTS AND DISCUSSION 73
2.5.1 Mesh optimisation and validation 73
2.5.2 Heat transfer 75
2.5.3 Nusselt Number 86
2.5.4 Pressure Drop, Wall Shear Stress and Friction coefficient 88
2.5.5 Wall Shear Stress 91
2.6 CHAPTER CONCLUSION 93

CHAPTER 3- FUNDAMENTALS OF FLUID FLOW AND HEAT TRANSFER IN MICROCHANNELS 95

3.1 CHAPTER SYNTHESIS 95
3.2 INTRODUCTION 95
3.3 NEWTONIAN FLUID FLOW IN MICROCHANNELS 96
3.3.1 Surface roughness effect and Transition Reynolds number. 97
3.3.2 Viscous dissipation effect 98
3.3.3 Microchannels numerical modelling analysis 99
3.4 Microchannel numerical model development and validation. 104
3.4.1 Mathematical modelling 104
3.4.2 Assumptions and methodology 104
3.4.3 Mesh optimisation 105
3.4.4 The validation of the numerical methodology 106
3.5 CHAPTER CONCLUSION 113

CHAPTER 4- HEAT TRANSFER BEHAVIOUR OF MWCNTS NANOFLUIDS IN MICROCHANNELS 115

4.1 CHAPTER SYNTHESIS 115
4.2 INTRODUCTION 116
4.3 NUMERICAL MODEL 119
4.4 NUMERICAL PARAMETERS AND PROCEDURE 129

4.5 THE RESULTS 143
4.6 CHAPTER CONCLUSION 162

CHAPTER 5- CONCLUSIONS 165

5.1 CONCLUSIONS 166
5.2 FUTURE WORK 170

REFERENCES 173

A. Thermophysical properties 191

B. Conductivity 193

C. Viscosity 194

LIST OF FIGURES

Fig. 1-1: Some applications of the micro heat exchangers [40]. 28
Fig. 1-2: The number of articles on nanofluid and CNTs nanofluid published from 1993 to 2018..... 29
Fig. 1-3: A scheme of the numerical approach process of CFD [95]..... 41
Fig. 1-4: A scheme of solving the governing equations by CFD tools [95]..... 42
Fig. 1-5: A scheme clarifies the thesis contribution for the CNTs nanofluid in MCHE. 55
Fig. 2-1 Photography of the experimental device. 63
Fig. 2-2: Deviation of the proposed correlations of thermal conductivity in comparison with experimental data. 68
Fig. 2-3: The deviation of the proposed correlations of viscosity in comparison with experimental data for 0.25% and 0.5% MWCNTs nanofluids. 70
Fig. 2-4: Schematic diagram of the numerical region (test part). 72
Fig. 2-5: Mesh independency for water flow according to Nusselt number as a function of Re number. 73
Fig. 2-6: Numerical and experimental Nusselt number as a function of axial position along the tube for distilled water, for Re=1620. 74
Fig. 2-7: The test section model showing the resulted temperature field at the outlet of the tube for deferent cases: (a: 0.5%CNTs-Re=1000, b: 0.25% CNTs, R e=1000, c: 0.5%CNTs-Re=2000 and d: 0.25%CNTs-Re=2000). 76
Fig. 2-8: Numerical and experimental wall temperature as a function of axial position along the tube for the base fluid and (0.25% and 0.5%) CNTs nanofluids for Reynolds numbers of (Re=2000,1500, and Re=1000). 77
Fig. 2-9: Numerical and experimental fluid temperature at the outlet of the tube as a function of Reynolds number for (a:0.5%CNTs. b:0.25%CNTs. c: EG30%.). 78
Fig. 2-10: Numerical and experimental convective heat transfer coefficient as a function of axial position along the tube for Re=1000 (a:0.25%CNTs, b:0.5%CNTs, c: EG30%). 81

Fig. 2-11: Numerical and experimental convective heat transfer coefficient as a function of axial position along the tube for Re=1500 (a: 0.25%CNTs, b: 0.5%CNTs, c: EG30%). 82
Fig. 2-12: Numerical and experimental convective heat transfer coefficient as a function of axial position along the tube for Re=2000 (a: 0.25%CNTs, b: 0.5%CNTs, c: EG30%). 83
Fig. 2-13: Average convective heat transfer coefficient as a function of nanoparticle concentration. (a: Re =1000, b: Re = 1500, c; Re=2000). 85
Fig. 2-14: Numerical and experimental Average Nusselt numbers as a function of Reynolds number. 87
Fig. 2-15: Pressure drop for MWCNTs nanofluids and the base fluid as a function of Reynolds number. 90
Fig. 2-16: Friction coefficient for MWCNTs nanofluids and the base fluid as a function of Reynolds number. 90
Fig. 2-17: Wall Shear Stress for MWCNTs nanofluids and base fluid as a function of Re number. 91
Fig. 2-18: Wall Shear Stress for MWCNTs nanofluids as a function of axial position along the tube for both cases: variable- thermophysical properties and constant-properties (a: 0.5%CNTs, b: 0.25%CNTs). 92
Fig. 3-1: Local distribution of Nu number of the tube (Di=373μm) at Re=200. . 107
Fig. 3-2: Pressure drop (kPa) of water flow in microtube (D_i=130μm) as a function of Re number. 108
Fig. 3-3: Pressure drop (kPa) of water flow in microtube (D_i=200μm) as a function of Re number. 108
Fig. 3-4: Friction constant ($f \cdot Re$) of water flow in microtube as a function of Re number. 109
Fig. 3-5: Local Nusselt number of water flow in microtube as a function of the axial length of the tube for electrical power of Q=2 W and Re= 774. 110
Fig. 3-6: The numerical results of several turbulence models in terms of Nusselt number as a function of Reynolds number. 113
Fig. 4-1: The polynomial fitting curve of conductivity for the experimental data of Sample A and Sample B nanofluids. 122

Fig. 4-2: The deviation of the proposed correlations of viscosity in comparison with experimental data of Sample B nanofluids. 123
Fig. 4-3: Local heat transfer coefficient of Sample-A and Sample-B nanofluids flow in microtube (Di=1.55 mm) as a function of axial distance along the tube at a: Re=1200 and b: Re=1200. 124
Fig. 4-4: The deviation of the proposed correlations of Non-Newtonian viscosity in comparison with experimental data for the concentrations of MWCNTs particles: a: 0.125 wt.% and b: 0.25 wt.%. 127
Fig. 4-5: Numerical and experimental convective heat transfer coefficient as a function of axial position along the tube for a: Re=200 and b: Re=470 128
Fig. 4-6: Numerical results of pressure drop compared with the available experimental data of Hussien et al. [82]. 129
Fig. 4-7: Schematic diagram of the numerical region (test part). 130
Fig. 4-8: The thermal diffusivity as a function of viscosity for the 60 nanofluid samples. 132
Fig. 4-9: The equivalent nanofluid in terms of thermal conductivity as a function of temperature. 135
Fig. 4-10: The centreline velocity along the tube (L=2.2 m). 138
Fig. 4-11: The parabolic velocity profile at several axial locations along the tube. 138
Fig. 4-12: The dimensionless temperature profile at several axial locations along the tube. 139
Fig. 4-13: The laminar velocity profiles for shear-thinning Non-Newtonian fluids (Pseudoplastic fluids) [166]. 140
Fig. 4-14: The Nusselt number along the tube 140
Fig. 4-15: Mesh independence for the base fluid (30% EG +70% DW) flow in the tube. 142
Fig. 4-16: The test section model showing the resulted temperature field at the outlet of the tube for deferent cases: (a: NF_{group1}-Re=100, b: NF_{group1}-Re=1400, c: NF_{group4}-Re=100 and d: NF_{group4}-Re=1400) 145
Fig. 4-17: Average heat transfer coefficient as a function of Reynolds number. 147

Fig. 4-18: Total pressure drop as a function of Reynolds number. 148
Fig. 4-19: Fanning Friction factor as a function of Re number. 152
Fig. 4-20: JF number as a function of Re number. 152
Fig. 4-21: Thermal resistance number as a function of Re number. 154
Fig. 4-22: Heat transfer coefficient as a function of axial distance along the tube for the same fluid flow value. 155
Fig. 4-23: The numerical results of Average Nu number in comparison with the results of the correlation for the Non-Newtonian fluids (**a** and **b**) and Newtonian fluids (**c**) 157
Fig. 4-24: The results of the new Average Nu number correlation in comparison with the numerical data as a function of Reynolds number. 161
Fig. B-1: The deviation of the proposed correlations of thermal conductivity in comparison with experimental data (NF-group3 and NF-group4). 193
Fig. C-1: The deviation of the proposed correlations of viscosity in comparison with experimental data for EG60% and EG30% base fluids. 195
Fig. C-2: Deviation of the proposed correlations of viscosity in comparison with experimental data for 0.25%, 0. 5%, 0.75%, 1.0% and 1.5% MWCNTs nanofluids (NF1-5) for the particle dimensions of l_p/d_p=231 (d_p=50-80 nm and l_p= 10-20 μm) and 30%EG+DW as a base fluid. 197
Fig. C-3: Deviation of the proposed correlations of viscosity in comparison with experimental data for 0.25%, 0. 5%, 0.75%, 1.0% and 1.5% MWCNTs nanofluids (NF6-10) for the particle dimensions of l_p/d_p=667 (d_p=20-40 nm and l_p= 10-30 μm) and 30%EG+DW as a base fluid. 198
Fig. C-4: Deviation of the proposed correlations of viscosity in comparison with experimental data for 0.25%, 0. 5%, 0.75%, 1.0% and 1.5% MWCNTs nanofluids (NF11-15) for the particle dimensions of l_p/d_p=50 (d_p=20-40 nm and l_p= 1-2 μm) and 30%EG+DW as a base fluid. 199
Fig. C-5: Deviation of the proposed correlations of viscosity in comparison with experimental data for 0.25%, 0. 5%, 0.75%, 1.0% and 1.5% MWCNTs nanofluids (NF26-30) for the particle dimensions of l_p/d_p=333 (d_p=20-40 nm and l_p= 5-15 μm) and 30%EG+DW as a base fluid. 200

Fig. C-6: Deviation of the proposed correlations of viscosity in comparison with experimental data for 0.25%, 0. 5%, 0.75%, 1.0% and 1.5% MWCNTs nanofluids (NF31-35) for the particle dimensions of lp/dp=231 (d_p=50-80 nm and l_p= 10-20 μm) and 60%EG+DW as a base fluid. 201
Fig. C-7: Deviation of the proposed correlations of viscosity in comparison with experimental data for 0.25%, 0. 5%, 0.75%, 1.0% and 1.5% MWCNTs nanofluids (NF41-45) for the particle dimensions of l_p/d_p=50 (d_p=10-20 nm and l_p= 1-2 μm) and 60%EG+DW as a base fluid. 202
Fig. C-8: Deviation of the proposed correlations of viscosity in comparison with experimental data for 0.25%, 0. 5%, 0.75%, 1.0% and 1.5% MWCNTs nanofluids (NF46-50) for the particle dimensions of l_p/d_p=125 (d_p=60-100 nm and l_p= 5-15 μm) and 60%EG+DW as a base fluid. 203

LIST OF TABLES

Table 1-1: Most important effects behaviour parameters of nanofluids in microchannels – Literature highlights..... 34

Table 1-2: Experimental investigations on heat transfer performance of CNTs nanofluids..... 39

Table 1-3: Heat transfer of CNTs Nanofluids– numerical modelling and fluid property definition..... 49

Table 1-4: Mechanism concepts that affect heat transfer and fluid flow of CNTs nanofluid. 54

Table 2-1: The general characteristics of the experimental facility..... 63

Table 2-2: Thermophysical properties of the nanofluids at the tube inlet (293.15 K). 67

Table 2-3 Thermal conductivity correlations. 68

Table 2-4: Average deviation between numerically predicted data and experimental results..... 86

Table 3-1: Transition Reynolds number in microchannels in some previous studies. 98

Table 3-2: Summary of some investigations studying the validity of using a numerical approach for microscale fluid flow..... 103

Table 3-3: Summary of the reproduced studies for heat transfer and pressure drop of single-phase Laminar fluid flow in microchannels..... 111

Table 4-1: Summary of some investigations on heat transfer performance of nanofluids with a reference to the hydrodynamic diameter of the microchannel (D_h) and the nanoparticle size (d_p). 118

Table 4-2: The parameters of the viscosity correlations for Sample A and Sample B nanofluids. 122

Table 4-3: Thermal conductivity correlations. 123

Table 4-4: The velocity of the nanofluids at the inlet of the tube..... 123

Table 4-5: The viscosity correlations. 126

Table 4-6: The velocity of the nanofluids at the inlet of the tube..... 126

Table 4-7: Thermal conductivity correlations. 127
Table 4-8: The available samples of MWCNT nanofluids in the database. 131
Table 4-9: The equivalent nanofluid in terms of rheological view for each group. 134
Table 4-10: The equivalent nanofluid in terms of density and specific heat. 134
Table 4-11: The velocity of the nanofluids at the inlet of the tube. 138
Table 4-12: Summary of some studies for heat transfer and Laminar fluid flow in microchannels with reference to the hydraulic developed conditions. 141
Table 4-13: The velocity of the nanofluids at the inlet of the tube for each Re number. 141
Table 4-14: Average increase of heat transfer coefficient and pressure drop. 149
Table 4-15: The enhancement of the heat transfer coefficient for several Reynolds numbers. 149
Table 4-16: Some correlations of Nusselt number for Laminar flow. 156
Table 4-17: The constants values of the correlation Eq. 4-37. 158
Table 4-18: The constants values of the correlation Eq. 4-38. 159
Table A-1: Thermophysical properties of the nanofluid samples (30%EG base fluid). 191
Table A-2: Thermophysical properties of the nanofluid samples (60%EG base fluid). 192
Table B-1: Thermal conductivity correlations of the four nanofluids and basfluids. 193
Table C-1: Rheological parameters of the nanofluid samples. 196

NOMENCLATURE

Q: Heat transfer flow (W)

P: Pressure (Pa).

$\dot{m}$: Mass flow (Kg/s).

Re: Reynold number.

NF: Nanofluid.

BF: Base fluid.

HTC: Heat Transfer Coefficient.

CHE: Compact Heat Exchanger.

MCHS: Microchannel Heat Sink.

MHE: Micro Heat Exchanger.

CFD: Computational Fluid Dynamics.

FVM: Finite Volume Method.

SIMPLE: Semi-Implicit Method for the Pressure-Linked Equation.

SIMPLEC: Semi-Implicit Method for Pressure Linked Equations-Consistent.

PISO: Pressure-Implicit with Splitting of Operators.

MWCNT: Multi-walled carbon nanotube.

SWCNT: Single-walled carbon nanotube.

CNT: Carbon nanotube.

DW: Distilled Water.

EG: Ethylene Glycol.

GNPs: Graphene nanoplatelets.

Ni: Nickle.

Al_2O_3: Alumina / Aluminium Oxide.

Fe: Iron.

Fe_2O_3: Iron Oxide.

Cu: Copper.

CuO: Copper Oxide.

TiO_2: Titania / Titanium Dioxide.

SiO_2: Silicon Dioxide.

ZnO: Zinc Oxide.

CeO_2: Cerium dioxide.

D: Tube diameter (m).

D_h: Hydrolic diameter (m).

k: Conductivity (W/m K).

T_w: Wall temperature (K).

T: Temperature (K).

q: heat flux (W/m^2).

A: Area (m^2)

L: length of the tube (m).

h: Heat transfer Coefficient (W/m^2 K).

h_{avg}: Average heat transfer coefficient (W/m^2 K).

Nu: Nusselt number.

Nu_{avg}: Average Nusselt number.

$\boldsymbol{V}$: Velocity vector.

u: The axial velocity of the fluid (m/s).

T_f : The bulk temperature of the fluid (K).

x: The distance from the tube inlet (m).

Kn: Knudsen number.

Po: Poiseuille number.

T_{h_out}: Temperature at the outlet of the heating tube (K).

T_{h_in}: Temperature at the inlet of the heating tube (K).

T_{c_out}: Temperature at the outlet of the cooling tube (K).

T_{c_in}: Temperature at the inlet of the cooling tube (K).

Num: Numerical.

Exp: Experimental.

l_p: The length of the CNT particle (μm).

d_p: The diameter of the particle (nm).

C_μ: Represents the eddy-viscosity.

K': Refers to the turbulent kinetic energy equation.

ε: Refers to the dissipation equation.

G_k: Represents the generation of turbulence kinetic energy due to the mean velocity gradients.

$C_{2\varepsilon}$ and $C_{1\varepsilon}$: Constants in the turbulent model equation.

σ_K and σ_ε : The turbulent Prandtl numbers for K' and ε, respectively.

S : The mean strain rate.

$\overline{\Omega_{ij}}$: The mean rate-of-rotation tensor.

$C_{2\varepsilon}$, A_0 and A_s: Turbulent model constants.

a: Thermal diffusivity (m^2/s).

a_{avg}: The average thermal diffusivity (m^2/s).

R: The thermodynamic constant (J/K mol).

K: The measure of the average viscosity of the fluid (The consistency index, $kg.s^{n-2}/m$).

K_{eq}: The equivalent of the measure of the average viscosity of the fluid (The consistency index, $kg.s^{n-2}/m$).

n: The measure of the deviation of the fluid from Newtonian (The power-law index).

n_{eq}**:** The equivalent of the measure of the deviation of the fluid from Newtonian (The power-law index).

H(T): The temperature dependence (Arrhenius law).

c_p: Specific heat (J/kg K).

$c_{p\text{-}eq}$: The equivalent specific heat (J/kg K).

T^*: The dimensionless temperature.

$T_W(x)$: The wall temperature at a specific axial location.

$T_f(x)$: The bulk fluid temperature at a specific axial location

$T(x,r)$: The fluid temperature at a specific point.

Pr: Prandtl number.

L_h: The hydraulic length.

L_{th}: The thermal length.

Δ : represents a non-Newtonian parameter.

Gr: Graetz number

Gr_L: Graetz number for x=L.

$\dot{V}$: The volume flow (m^3/s).

f : The fanning friction factor.

j: The Colburn j-factor (Dimensionless heat transfer coefficient)

St: Stanton number

JF: A dimensionless number evaluate the heat exchanger performance in comparison with a reference case.

f_R: The fanning friction factor of the reference case.

j_R: The Colburn j-factor of the reference case.

Nu_R: Nusselt number of the reference case.

R_{th}: The thermal resistance.

T_{max}: The maximum wall temperature (K).

Cf: Friction coefficient.

T_0: Shift temperature (K).

T_α: Reference temperature (K).

Pe: Peclet number.

R^2: Correlation factor (Fitness estimator).

NF_{group}: The nanofluid that represents the group.

NF_{eq}: The equivalent nanofluid.

Greek symbols:

ρ: Density (kg/m^3).

ρ_{eq}: The equivalent density(kg/m^3).

μ: Viscosity (mPa s).

μ_{cor}: Refers to the correlation viscosity results.

μ_{exp}: Refers to the experimental viscosity results.

τ : Wall shear stress (Pa).

φ: Particle volume fraction.

$\dot{\gamma}$: Shear rate (s^{-1}).

α: The ratio of the activation energy (J/mol) to the thermodynamic constant R (K).

α_{eq}: The equivalent of the ratio of the activation energy (J/mol) to the thermodynamic constant R (K).

δ: Boundary layer thickness.

η: The thermal performance factor.

Subscripts

out: Outlet of the tube.

in: Inlet of the tube.

w: Wall.

cor: Correlation.

Num: Numerical.

Exp: Experimental.

p: Particle.

f: fluid.

bf: Base fluid.

nf: Nanofluid.

eq: Equivalent.

max: Maximum.

th: Thermal.

h: Hydraulic.

R: Reference case.

L: Length of the tube.

avg: Average.

CHAPTER 1- INTRODUCTION

1.1 THESIS BACKGROUND AND MOTIVATION

Production and proper utilisation of energy are requisites to sustainable development. One of the most important fields of energy study is heat transfer, which has a wide range of applications in power generation, automotive, nuclear industries, aerospace application and research, marine and mining applications, chemical processing, petroleum, and several other areas. Industries have been experiencing continuous challenges to obtain higher efficiency levels and greater equipment reliability while reducing the overall size and cost of the design. Compact heat exchanger features a higher heat transfer performance, smaller geometric size and volume per heat load, lower fluid requirement and lower operational cost [1]. However, there are two problems still requiring further attention, namely the reduction in channel dimensions which is accompanied by higher pressure drop, and the amount of heat transfer which is limited by the used heat transfer fluid. Newton's law of cooling (Eq. 1-1) can describe the possibilities of achieving higher heat transfer flow (Q), through the increase of heat exchanger area (A), the temperature difference (ΔT), and convective heat transfer coefficient (h) [2].

$$\mathrm{Q} = \mathrm{h} \cdot \mathrm{A} \cdot \Delta\mathrm{T} \qquad \text{Eq. 1-1}$$

The most effective way to increase heat flow, where the minimization of the overall volume of the heat exchanger (CHEs) is required, can be by increasing the convective heat transfer coefficient. The latter can be achieved by enhancing the thermal conductivity (k) of the operated fluid (Eq. 1-2).

$$h = \frac{Nu \cdot k}{L} \qquad \text{Eq. 1-2}$$

Where (L) is a characteristic dimension of the system and (Nu) is Nusselt number. Another way is to increase heat transfer coefficient and Nusselt number by increasing the velocity of the fluid flow which requires higher pumping power.
However, the low performance of the employed conventional thermal fluids in micro heat exchanger applications such as water, ethylene glycol and oil have poor thermo-physical properties, led to a necessary need for new thermal fluid to intensify the heat transfer process through micro heat exchangers [3]. Thus, a new thermal fluid called nanofluid was firstly designed by Choi and Eastman [4] in 1995 by dispersing nanoparticles into a conventional fluid, presenting enhancements on the thermophysical properties. Later, several researchers have reported that a significant enhancement in thermal conductivity was occurred by suspending metallic and non-metallic nanoparticles in the base fluid [5]–[10]. Among the latter, Carbon Nanotubes (CNTs) have higher thermal conductivity than other particles [11], providing higher thermal conductivity to nanofluids. The superior thermophysical properties of CNTs nanofluids have attracted many researchers worldwide, recognising this fluid media as among the most interesting ones for heat exchanger applications [12]–[18]. Also, the enhanced thermo-physical and transport properties of these MWCNTs nanofluids (thermal conductivity and viscosity) with different nanoparticle geometries using mixtures of Distilled Water (DW) and Ethylene Glycol (EG) as base fluids at different nanoparticle concentration have been studied and modelled [19], [20] and [21]. Thus, this work intends to pursue those studies and provide further insight on fluid flow and heat transfer of those CNTs nanofluids when flowing though macro and microchannels.

The study of parameters such as fluid temperatures, Nusselt number, heat transfer coefficient, friction factor and pressure drop will enable to establish the importance of the nanofluids properties on the heat transfer phenomena and on the microchannels fluid flow dynamics. For this purpose, numerical simulations are considered a very useful approach to the interpretation of experimental data, where measurements of temperature fields and heat fluxes are obviously very difficult or impossible to obtain. It becomes an economic prediction technique by avoiding the need for numerous prototype tests. Thus, computational fluid

dynamics (CFD) has become a very significant research technique when tackling heat exchanger studies.

A validated numerical model of microscale heat transfer systems involving CNTs nanofluids is, therefore, a key element to justify and clarify their importance. Hence, this supports the current trend toward elements miniaturization and higher energy efficiency of all heat transfer applications in industry, achieving developed sustainability and enhanced energy usage with less environmental impact.

1.2 STATEMENT OF THE PROBLEM AND GENERAL OBJECTIVES

In the available literature, experimental and numerical investigations related to heat transfer of nanofluids flowing in a microchannel are not abundant. Moreover, most previous numerical investigations for predicting MCHE (Microchannel Heat Transfer) with nanofluids still present a certain degree of uncertainty mainly related to the nanofluid lack of knowledge and its poor definition, both in what concerns its thermo-physical as well as its transport properties.

A comprehensive experimental investigation has been carried out by Lamas et al. [22] and Abreu et al. [21] for assessing the thermal conductivity and defining the rheological behaviour of CNTs nanofluids, respectively, establishing the premises to understand this system's behaviour. The available experimental property data will, therefore, provide the means to accurately model the MWCNTs/DW+EG nanofluids behaviour under investigation and predict heat transfer phenomena and fluid flow.

Moreover, the experimental data on fluid flow and heat transfer which were measured in the team test rig will be used for validation purposes and establish appropriate and reliable numerical modelling of MWCNTs/DW+EG nanofluids behaviour on a macrochannel. A well-known fluid (water) will be modelled in a typical microchannel in order to fully exploit and address the uncertainties related to fluid flow and heat transfer through a microchannel. With the latter it is intended to establish a solid ground in what concerns numerical modelling of fluid flow and heat phenomena on Newtonian fluid flowing through

a microchannel, to better isolate and tackle the challenges on microchannel numerical modelling and hence establish the premises for further studies into the intended research on non-Newtonian fluid flow and heat transfer on microchannels. Such studies are considered of utmost importance to increase nanofluids industrialization level, since they will provide the required information for energy systems tailoring when considering equipment reliability, miniaturization, as well as higher energy efficiency.

1.3 LITERATURE REVIEW

In the following sections, it is presented a literature survey of the subjects related to heat transfer of nanofluids, particularly, CNTs nanofluids and their thermophysical properties, as well as the most important studies on fluid flow and heat transfer behaviour of nanofluids through microchannels.

1.3.1 Microchannel

Compact heat exchanger features a higher heat transfer performance, smaller geometric size and volume per heat load, lower fluid requirement and lower operational cost [1]. Therefore, microchannels for cooling devices were firstly introduced by Tuckerman and Pease [23], and they were indicated to achieve higher thermal performances in comparison with traditional heat exchangers, due to their larger surface area. The techniques of such microsystem and single phase microchannels have been enhanced [24], rendering them enormous potential for a vast number of practical applications.

Moreover, Morini et al. [25] have highlighted in detail the significant scaling effects such as viscous dissipation, independent-temperature thermophysical and entrance effects on the heat transfer and friction factor of fluid flow in microchannels.

Nevertheless, there is no obvious agreed definition in the literature for the dimensions of the microchannel. However, a literature review by Rosa et al.[26] considered the channels whose hydraulic diameter lies between 1 μm and 1 mm as a microchannel, following a study carried by Celata et al. [27].

1.3.2 Nanofluids and its applications

As mentioned before, the suspension of nanoparticles in conventional fluids produces the so-called nanofluids. These nanofluids achieved an advanced level in enhancing the effective heat transfer coefficient [4]–[10]. According to the literature, nanoparticles can be metallic or non-metallic such as Cu, Ni, Fe, Al_2O_3, Fe_2O_3, CuO, TiO2, SiO_2 and ZnO [28]. Nanostructured materials can be also carbon-based compounds such as graphene, graphene oxide, graphite or carbon nanotube [29].

1.3.2.1. Carbon nanotubes (CNTs) nanofluids (Structure)

So far, many researchers report a significant enhancement in thermal conductivity when metallic and non-metallic nanoparticles are suspended in the base fluid [5]–[10]. Among the latter, Carbon Nanotubes (CNTs) have higher thermal conductivity than other particles [11], which in turn have attracted several researchers worldwide to the superior thermophysical properties of CNTs nanofluids highlighting its potential to solve the reported limitations of conventional working fluids in heat transfer applications [12]–[18]. Researchers have, therefore, been paying considerable attention to the study of thermal conductivity of nanofluid, besides other properties namely colloidal stability, density and viscosity. All those fluid properties depend on several concepts involving preparation techniques, nanoparticle geometry, base fluid and volume fraction which explain the thermal performance of CNTs nanofluids in the literature.

Preparation methods:

The main used CNT particles in nanofluids are the single-walled carbon nanotube (SWCNT) and the multi-walled carbon nanotube (MWCNT), which are produced by several technique methods such as Arc discharge, laser ablation, chemical vapour deposition (CVD), in addition to diffusion and premixed flame methods [29]. Moreover, CNTs particles are exposed to chemical treatment (functionalization) or mechanical treatment in order to achieve the long-term stability of the nanofluid.

There are two techniques typically used to prepare the nanofluid: two-step method and single-step method. In the two-step method, nanoparticles are initially synthesized as dry powders via physical or chemical methods. Then, the synthesized dry powders are dispersed in a base fluid. Usually, ultrasonication is used as a physical mixing of the CNTs nanoparticles and the base fluid. While in the single-step method both of nanoparticles production and the preparation of nanofluid are carried out concurrently in a combined process [31] and [32]. However, a comparison study between the preparations methods of CNTs nanofluids in order to stabilize CNTs into several types of base fluids was carried out by Yazid et al. [30]. The authors have studied the chemical treatments (covalent and non-covalent functionalization) and physical treatment for several particle volume fractions and types of CNTs. They have reviewed the latest publications in the field of long-term stability and the preparation techniques of CNTs nanofluid. The study referred to the covalent functionalization and ultrasonication as an effective method in terms of obtaining long-term stability and homogenous CNTs nanofluids.

In addition, base fluid has an important effect on nanofluid performance. In this, it was found that carbon nanotubes generally display an excellent dispersion behaviour in most of the commonly used conventional heat transfer fluids such as Water, Ethylene Glycol, Decene, Kerosene, Silicon oil and Engine Oil [20], [32] and [33]. Lamas et al. [20] and Abreu et al. [21] selected the distilled water (DW) and ethylene glycol (EG) mixture at volume fractions of 30% and 60% as a base fluid due to their importance to numerous applications of heat transfer fluids and their properties such as density and viscosity, allowing to control the sedimentation performance toward a good level of stability and homogeneity.

Stability

Stability is one of the key features for any nanofluid in the heat transfer application. There is a strong propensity of nanoparticles to agglomerate in the fluid media which cause clogging the microchannels and break down the thermal properties of nanofluids. The stability of the nanofluid can be influenced by several factors such as surfactants, pH adjustment and preparation method [16] and [41].

Thermal Conductivity

The most significant thermo-physical property of nanofluids is the thermal conductivity which directly affects the heat transfer characteristics of the fluid flow. Thus, the thermal conductivity of CNTs nanofluids has been attracting many researchers which leads to suggest some physical models in order to predict the thermal conductivity of the CNTs nanofluids such as Patel et al.[35], Timofeeva et al.[36] and Nan et al.[37], considering the CNTs geometry, volume fraction and interfacial thermal resistance. Latterly, Lamas et al. [20] investigated the possibility of long-term MWCNTs nanofluids with stably high thermal conductivity. In their research, the functionalized MWCNTs particles with several geometries and concentrations were dispersed through a short period of sonication into a mixture of distilled water (DW) and ethylene glycol (EG). The results have shown that the nanoparticle geometry, concentration and base fluid are the most important parameters affecting the stability of MWCNTs nanofluids.

Viscosity

It must be noticed that adding nanoparticles to the base fluid not only increases the thermal conductivity but also increases the viscosity of the nanofluids and causes a change in the rheological behaviour of the resulted fluid. However, the increase in viscosity causes a higher pressure drop which requires greater pumping power. Furthermore, the change of the fluid viscosity affects Reynolds and Prandtl numbers which are related directly to the heat transfer coefficient. Therefore, Abreu et al. [21] have widely studied the viscosity and the control factors that have a respectable influence on the rheological behaviour of CNTs nanofluids. The latter enables to gather a strong database of the dynamic viscosity and rheological behaviour of CNTs nanofluids as a function of the base fluid, temperature, shear rate, and MWCNTs size and concentration.

1.3.2.2. Applications

One of the most promising applications of nanofluids is thermal systems. Some studies reported the ability to use nanofluids as a thermal energy storage media (phase change materials) or as absorption media for solar collectors [36]

and [37]. Whereas, heat transfer systems were considered as the most efficient usage for nanofluids, such as automotive, electronics, energy generation, and several other areas contain the heat transfer concept in the form of heat exchangers. Furthermore, important efforts were seen to use nanofluids as an advanced solution in compact heat exchangers applications where the high heat flux is located intensively such as computers, medical, transportation, energy, aerospace, and defence, Fig. 1-1 and [40].

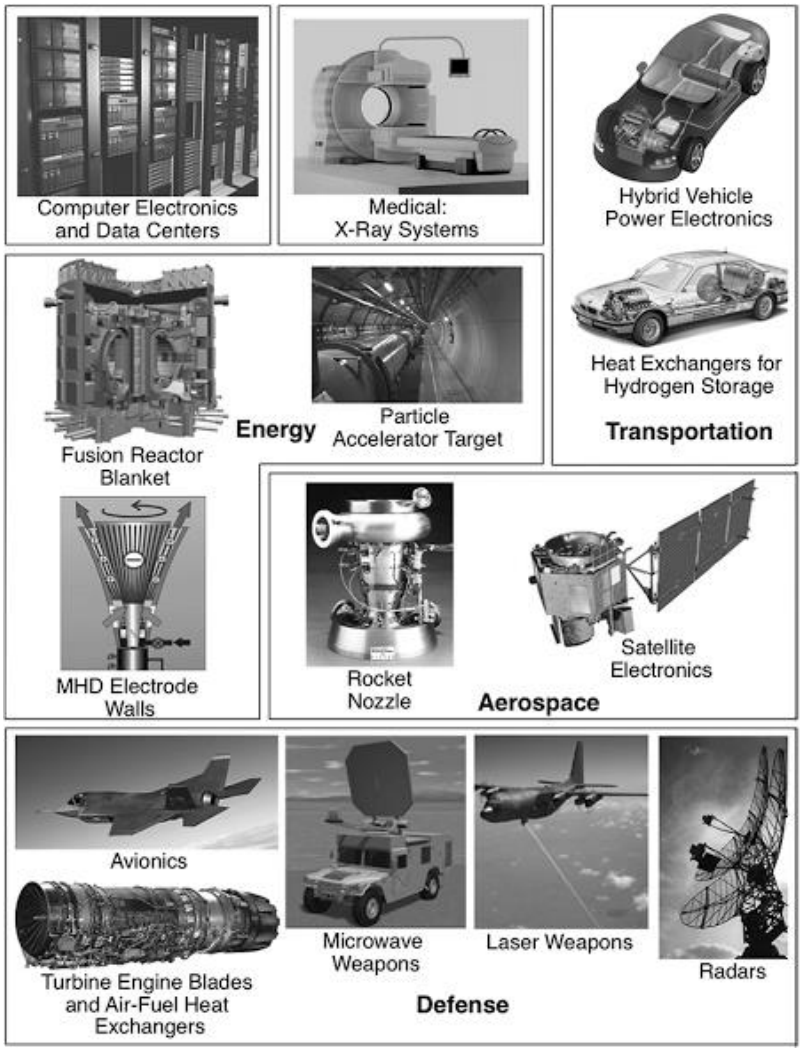

Fig. 1-1: Some applications of the micro heat exchangers [40].

1.3.2.3. Research trends

The research trends for nanofluids are growing yearly over the previous decade. This can be proved by the detailed increase of yearly publications on nanofluid presented in Fig. 1-2. Records retrieved from Scopus as of 25 October

2018 using ‘nanofluid’ or ‘nanofluid carbon nanotube’ as the keywords with or without an addition keyword ‘microchannel’. Based on the Scopus database, overall 13,042 publications on nanofluids and 386 publications on nanofluid Carbon Nanotubes (CNTs), appeared until 25/10/2018. Also, about 534 publications on nanofluid with microchannel [23–43]. The publications include all types of journals and conference articles, books, letters, and others.

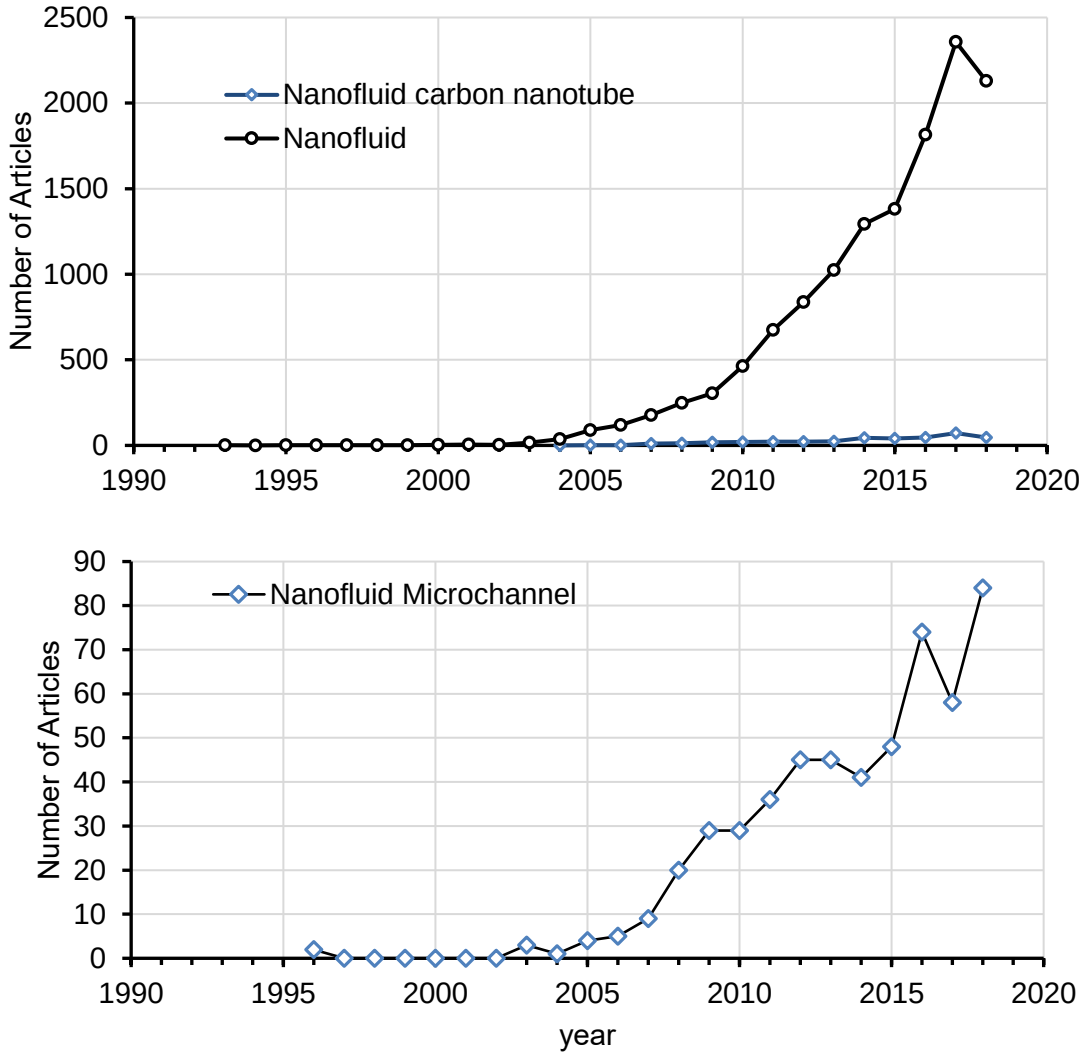

Fig. 1-2: The number of articles on nanofluid and CNTs nanofluid published from 1993 to 2018.

So far, a few articles have imperfectly reviewed the behaviour of CNTs nanofluids on heat and mass transfer [11], [31] and [60]. However, there isn’t any

review paper focused on the thermal performance of CNTs nanofluids in the microchannel.

Regarding the behaviour of this special type of nanofluid (CNTs nanofluid) in the microchannel, research and results from different publications are scattered with an absence of consistency. Hence, it is necessary and well-timed to provide useful and interesting information on the latest research results on the heat transfer behaviour of CNTs nanofluids in micro heat exchangers, hence contributing to the field of nanofluids and heat transfer which is developing rapidly.

1.3.3 Nanofluids in Microchannels

Several studies have been accomplished on the microchannel heat exchanger using nanofluids. A numerical study of Al_2O_3–water nanofluids flow through a microchannel heat sink (MCHS) was presented by Hung et al. [63]. The authors reported that the overall thermal resistance of the MCHS is reduced significantly by increasing the pumping power. Moreover, they have investigated the influence of the particle size and particle volume fraction on the thermal resistance of the device (MCHS).

An experimental investigation of TiO_2–water nanofluids in a microchannel has been realised by Manay et al. [64]. The results have shown an increase in heat transfer by increasing the particle volume fraction up to 1.5 vol%, accompanied by greater pressure drop and pumping power. Besides that, the heat transfer enhancement halts and a decrease start to occur, after reaching a specific high value of nanoparticles volume fraction (1.5 vol%), due to an increasing boundary layer thickness induced by high viscosity.

A numerical study of Alumina nanofluid flow through a circular microchannel was accomplished by Arjun et al. [65], where the heat transfer during both laminar and turbulent regimes has been solved using the viscous laminar and standard K-ε models. In their study, they found that the enhancement of heat transfer in laminar nanofluid flow was greater as compared to turbulent nanofluid flow with respect to its base fluid. The increase in Re number caused an increase in Nusselt numbers and pressure drop, whereas it caused a decrease in

the wall surface temperature, friction factor, thermal resistance and nanofluid temperatures. Moreover, the increase in particle volume fraction caused a rise in thermal conductivity, hence increasing the heat transfer coefficient and Nusselt number. Also, it was noticed a higher Nusselt number at the entrance regions of microchannels, where the higher variability on Nusselt numbers was achieved due to its hydrodynamically fully developed condition. Furthermore, it was noticed that the entrance length for fully developed flow is highly influenced by the nanofluid concentrations and Reynolds number.

A numerical study of three-dimensional incompressible steady fluid flow of a trapezoidal micro-channel heat sink (MCHS) using CuO/water nanofluid for laminar and turbulent flows were carried out by Yang et al. [66]. The study has shown that the pressure drop increases slightly for a nanofluid-cooled MCHS in the laminar flow case.

A numerical investigation study reported by Esmaeilnejad et al. [67] for incompressible, steady fluid flow through a rectangular microchannel using Al_2O_3 and CuO nanoparticles based nanofluid was analysed. From the results, it can be depicted a greater increment in the average heat transfer coefficient when compared with the base fluid. Moreover, it was observed that the thermal resistance of microchannel heat sink decreases with the increase of the nanoparticle volume fractions, while it decreases gradually with the increase of Peclet number.

A numerical investigation on a parallel square shaped microchannel heat exchanger (MCHE) to study the effects of using various types of nanofluids and Reynolds numbers on heat transfer and fluid flow characteristics was carried out by Mohammed et al. [68]. In this heat exchanger, there was a hot fluid (bottom channels) and 25 channels for the cold fluid (top channels). The bulk temperature, pumping power, effectiveness, performance index, pressure drop, wall shear stress and the heat transfer for the hot and cold water were reported to change in terms of nanoparticle volume fraction, Reynolds number and the type of nanoparticle. The results have shown an enhancement in the performance of the heat exchanger using nanofluids, accompanied by a slight increase in pressure drop. Also, it was shown that the increase of Reynolds number decreases the effectiveness of the micro heat exchanger.

A microchannel heat sink (MCHS) with several nanofluids were investigated numerically by Hung et al. [63]. The effects of the nanoparticles type, nanoparticle size and volume concentration, base fluid, and substrate material on the heat transfer performance of an MCHS were presented. The results have shown that the high thermal conductivity of the substrate material and less wall thickness cause more thermal enhancing. Also, base fluids having a lower dynamic viscosity provide better heat transfer performance. The overall thermal resistance of the MCHS was reduced significantly by increasing the pumping power. Moreover, the improvement in heat transfer obtained by decreasing the particle size was relatively limited compared to the improvement caused by varying the particle volume fraction.

Furthermore, the experimental and numerical investigations on single-phase flow of nanofluids in mini/microchannels were concisely reviewed by Hussien et al. [69]. The characteristics of heat transfer and fluid flow through mini/microchannels for nanofluids, in general, were discussed. The research analysed the scaling effects and the nanofluid thermophysical properties (thermal conductivity and viscosity), considering the volume fraction, size, material of the nanoparticles and pH value, the addition of dispersant and operation temperature of the medium. The review paper has shown that only a few investigations carried out in order to study the several scaling effects (design of mini/microchannel, entrance, roughness, conjugated heat transfer, viscous dissipation effect, gravity, temperature, electrical double layer (EDL), wall thickness and wall thermal conductivity effects). It has also been shown that the enhancement of convective heat transfer using nanofluid flow is particularly effective in the entrance region. This implies that short channels are more efficient for the enhancement of heat transfer coefficient in mini/microchannels. Most of these studies ignored the effect of gravity on heat transfer in microchannels on their numerical studies. They have also established a comparison between the two-phase and single-phase articles for different types of nanofluids. However, the authors have shown that there are limited studies on the enhancement of heat transfer coefficient on mini/microchannels using nanofluids, mainly in what concerns turbulent flow and circular channels emphasising the stability of nanofluids as the main challenge to overcome. Moreover, the same has been performed by the review carried out by

Mohammed et al. [1]. The latter also addressed issues concerning heat transfer and fluid flow characteristics in a microchannel heat exchanger using nanofluids including nanofluids properties and heat transfer characteristics, as well as their limitations in several applications.

Moreover, Wang et al. [70] studied water-based Al_2O_3 nanofluid as a coolant for various constraint conditions, such as the volume flow rate, pumping power, and pressure drop. The optimal geometric parameters were studied in terms of channels number, channel aspect ratio, and the ratio of channel width to the pitch. The results enabled to infer that the optimal geometric structure can be different under various boundary conditions, regarding the inlet volume flow rates, pumping powers, and pressure drops.

Also, Garg et al. [71] reported a high value of heat transfer coefficient achieved for a trapezoidal cross-section geometry at the beginning of the tube which then decreases considerably. Moreover, rectangular-trapezoidal geometries achieved the maximum value of the heat transfer coefficient along the tube once rectangular and rectangular-trapezoidal geometries were considered at the same aspect ratio. Moreover, for rectangular cross-section channels, the aspect ratio value of 4 was the optimum geometry in the Reynolds number ranging from 50 to 800, when the aspect ratio values of 2, 4 and 8 were used for the rectangular cross-section.

Another study by Kadja et al. [72] selected rectangular geometry as the best cross-section for enhancing heat transfer and reducing pumping power after examining nanofluid flow in the various microchannels geometries (elliptical, rectangular, and trapezoidal). They have also studied the sensitivity of the heat transfer to thermophysical properties dependence on temperature, realising that heat transfer increased by as much as 30 % when the latter was accounted for.

During the conducted survey, there were found several concepts presented to explain the heat transfer and fluid flow performance of nanofluids, as shown in Table 1-1.

Table 1-1: Most important effects behaviour parameters of nanofluids in microchannels – Literature highlights.

The concepts	Correlation	The influence	Ref.
The entrance length for fully developed region	$L_h = 0.05 \cdot Re \cdot D$ $L_{th} = L_h \cdot Pr$	It depends on nanofluid properties and Re number. There are higher Nusselt numbers in entrances region of microchannels	[65], [69]
Boundary layer thickness	$\delta = \frac{5 \cdot x}{\sqrt{Re}}$	The heat transfer performance decreases with the increase in the boundary-layer thickness.	[64], [26]
Knudsen number		It is the ratio of the mean free path to the characteristic length of the channel, used to provides a direct indication for the continuum regime.	[1], [73]
Poiseuille number	$Po = Re \cdot f$	Po decreases slightly with decreasing Re, for partially heated tubes. Po = 64, for fully heated tubes.	[74]
Microchannel section		Rectangle sections benefit heat performance, as well as high aspect ratio tubes.	[71]
Gravity		Often neglected, nevertheless its influence should be considered when studying vertical and oblique tubes.	
Wall thickness		Less wall thickness and substrate material with high thermal conductivity cause higher thermal performance.	[63]
Pumping power	$P_{pump} = \frac{\dot{V} \cdot \Delta p}{\eta_{pump}}$	Its increases cause an increase in pressure drop and a decrease in overall thermal resistance.	
Re number	$R_e = \frac{\rho \cdot u \cdot D}{\mu}$	The increase in Re number leads to an increase in velocity, pressure drop, HTC and Nu number.	[65]
Friction coefficient	$Cf = \frac{\tau}{\frac{1}{2} \cdot \rho \cdot u^2}$	It is higher for nanofluids in comparison with base fluid.	[64]
Peclet number	$P_e = Re \cdot Pr$	With increasing Peclet number, the heat transfer coefficient increases and thermal resistance decreases.	[1]
Prandtl number	$Pr = \frac{C_p \cdot \mu}{k}$	As Pr increases the difference between the wall and fluid temperature decreases, resulting in greater Nu number values.	[67]
Graetz number is	$Gz = Re \cdot Pr \cdot \frac{D_h}{L}$	For neglecting the entrance effect.	[69]

1.3.4 Heat transfer of CNTs nanofluid

Comparison against other nanofluids

Ebrahimnia et al. [75] studied numerically the performance of CNT/(water-EG) and other types of nanofluids flow through a straight circular pipe in a laminar flow regime. The results have shown that the heat transfer coefficient of CNTs nanofluid is much higher compared to Titanate nanotube and, the Al_2O_3 and CuO nanofluids. Also, a study by Kamali et al. [46] reported that by using MWCNT–water nanofluid instead of water in a typical heat sink, the mean reduction in thermal resistance for MWCNT–water and Al_2O_3–water, in comparison with using water are 18% and 1%, respectively. This shows the great advantages of using MWCNTs nanofluids in heat sinks in comparison with Al_2O_3 nanofluid. Moreover, some researchers [76], [77] and [59] have compared CNTs nanofluids with other types of nanofluids and they revealed a remarkable heat transfer coefficient for CNT nanofluids compared to other nanofluid types.

1.3.5 Characteristics of CNTs nanofluids in heat transfer studies

This section characterises the microstructure of the CNTs nanofluids that have been studied in the literature for the purpose of heat transfer. Over the years, nanofluids structures were under development in order to achieve high conductivity accompanied by high stability level and long shelf-life. Therefore, several types of nanoparticles have been designed which can be categorized regarding their dimensions (diameter and length), type (SWCNT or MWCNT) and treatment method (Covalent Functionalization). Also, it was used numerous types of the base-fluids (water, Ethanol, Oil ...) and various preparation methods for producing the CNTs nanofluids (one/two steps). The latter has an important impact on the structure and characteristics of the composed nanofluid, since these parameters influence several concepts such as Brownian motion, viscous resistance and particle-fluid interaction, hence affect the stability and other thermophysical properties of CNTs nanofluids such as conductivity and viscosity [21]and [22].

Therefore, a survey of some studies regarding the fluid flow and heat transfer of CNTs nanofluids is presented with a focus on the identification of the operated CNTs nanofluid, summarized in Table 1-2.

Experimental studies of CNTs nanofluid for fluid flow and heat transfer

The experimental investigations are of utmost importance to characterise and analyse the suitability of the new fluids under development. Moreover, the data acquired and stored will constitute knowledge to assist subsequent systems detail modelling and validation. Only a few experimental studies were carried out on CNTs nanofluid for heat transfer investigations due to the high cost of the devices and materials, as follows:

Paritosh et al. [78] have studied experimentally MWCNTs/water nanofluids in a tube with 914.4 mm length and 1.55 mm diameter under constant wall heat flux condition (q''=0.6 W/cm^2). Four samples of 1 wt% multi-walled carbon nanotube nanofluids were prepared. The samples have been studied considering the effect of dispersing energy (ultrasonication) on viscosity, thermal conductivity, and the laminar convective heat transfer. The results present a shear thinning behaviour of the MWCNTs nanofluids, followed the Power Law viscosity model. Also, the maximum enhancement in heat transfer coefficient was 32% at Reynolds number Re =600 and for ultrasonication of (40 min, e = 113 J/g). The enhancement in heat transfer coefficient was decreased for further ultrasonication time.

Amrollahi et al. [79] have studied experimentally the forced convective heat transfer coefficient of water/FMWCNTs nanofluids through a horizontal pipe of 1m length and 11.42 mm diameter for several particles volume fraction at laminar and turbulent flow regimes ($1592 \leq Re \leq 4778$). The results highlight that with the increase of nanoparticles volume fraction, Reynolds number and the temperature the heat transfer coefficient increases. The heat transfer enhancement was about 25% in comparison to the base fluid.

Akhavan-Behabadi et al. [80] measured the thermo-physical properties of MWCNTs–water nanofluids and investigated its overall performance inside a coil wire inserted into tubes under a constant heat flux. Also, Oliveira et al. [81] studied experimentally the thermal performance of MWCNTs/water–EG

nanofluids inside an automotive radiator. The results were analysed in terms of the heat transfer rate, Nusselt number and mass flow in comparison with distilled water.

Moreover, a research carried out by Hussein et al. [82] investigated MWCNTs/GNPs water-based hybrid nanofluid and a maximum enhancement on the heat transfer coefficient of 43.4% and a rise in pressure drop of 11% was achieved for the 0.25 MWCNTs + 0.035 GNPs hybrid nanofluid in comparison with distilled water at a Reynolds number of 200.

Kumaresan et al. [83] studied the heat transfer characteristics of MWCNTs/water–ethylene glycol mixture (70:30 by volume) in a tubular heat exchanger for nanofluids of 0.15, 0.3 and 0.45% particle volume fraction. The results indicated an increase in the Prandtl number by 115.8% at 0 °C and 180.2% at 40 °C for the nanofluids with 0.45 vol.% MWCNT in comparison to the base fluid. Also, the significant enhancement of the heat transfer coefficient was achieved in the entrance region.

Ding et al. [84] investigated the heat transfer behaviour of MWCNTs/water nanofluids for 0.1 and 0.5% particle volume fractions flowing through a straight copper tube with 970 mm length and 4.5 mm inner. The results indicated a significant enhancement of the convective heat transfer for nanofluids containing 0.5 wt.% CNTs at Re = 800.

Rashidi. et al. [85] studied the heat transfer behaviour of MWCNTs/water nanofluids for 0.5, 1 and 2% particle volume fraction flowing through a horizontal tube with a diameter of 6 mm for laminar flow under constant heat flux. The results show considerable enhancement in the convective heat transfer coefficient of nanofluids, rising with the increase of CNTs concentration and Reynolds number.

Chougule et al. [77] studied the convective heat transfer characteristics of CNT/water nanofluids through uniformly heated horizontal circular tube in the transition regime with helical twisted tape inserts for 0.15%, 0.45%, 0.60% and 1% particle volume fraction. The results observed that Nusselt number increases with a rise in Reynolds number and particle volume fraction. The maximum enhancement in heat transfer was obtained by using CNT/water nanofluid with

1% particle volume fraction. Moreover, the paper referred to the thinner thickness of the boundary layer at higher Reynolds number.

Thang et al. [86] used functionalized MWCNTs/distilled water nanofluid for cooling the computer processor experimentally. The MWCNTs particles have a diameter between 15 - 90nm and a length of 10 μm. As a result, the thermal resistance reduced with the increase of MWCNTs volume fraction due to the increase in thermal conductivity of the nanofluid, leading to reduce the saturated temperature of CPU by 7 °C compared to the base fluid, when the particle volume fraction was 1 gram/litter. Later, Thang et al. [87] studied the functionalized MWCNTs/(water-ethylene) nanofluid through the aluminium heat sink in order to cool the 450W LED floodlight. Their experimental results indicated a reduction in the saturated temperature of the device by 4.4 °C compared with the base fluid.

Furthermore, research to investigate the thermal performance of a copper-made heat sink with rectangular microchannels (w=0.25 mm, H=0.4 mm) using MWCNTs/water nanofluid carried out by Sarafraz et al. [15] for 0.05–0.1% particle volume fraction and laminar flow (Re<1400). The results referred to an enhancement in heat transfer coefficient by 29% in comparison to the base fluid and the maximum enhancement was observed at the entrance region of the microchannel.

Conversely, some researchers have concluded that nanofluids have a negative response, such as the study by Dietz et al. [88] that investigated the cooling of the electronics for laminar flow of CNTs nanofluids under forced convection conditions. The authors have noticed that CNTs nanofluids induced a higher pressure drop and a higher surface temperature, thus an increase in the thermal resistance.

Table 1-2: Experimental investigations on heat transfer performance of CNTs nanofluids

Reference	CNTs nanofluid components			Rheology	Stability	Device (D)	Fluid flow
	BF	Particle d_p and l_p	Volume fraction				
Kumarsan et al. [83]	Water+EG	MWCNTs 30-50 nm. 10-20 µm	0.15, 0.3 and 0.45%	-	-	Tubular heat exchanger D=12.7mm	Laminar
Ding et al. [84]	Water	CNTs - -	0.1 and 0.5%	Non-Newtonian	-	Tube D= 4.5 mm	Laminar
Rashidi. et al. [85]	Water + Gum Arabic	MWCNTs 5-50 nm. 10-20 µm	0.5, 1.0 and 2.0 %	-	-	Tube D=6mm	Laminar
Chougule et al. [77]	Water	MWCNTs 20-30 nm, 3-8 µm	0.15%	-	-	Helical screw D=10.5mm	Laminar
Akhavan-Behabadi et al. [80]	Water	MWCNTs 5–20 nm. -	0.05, 0.1 and 0.2 %	Newtonian	-	Coil wire inserted into tubes	Turbulent
Oliveira et al. [81]	Water+EG	MWCNTs - -	0.05-0.16 %	-	-	Radiator. D_h=7 mm	Laminar
Hussien et al. [82]	Water	MWCNTs+GNPs 15 nm. 1-5 µm	0.075, 0.125, and 0.25 %	-	-	Tube D= 1.1 mm	Laminar
Amrollahi et al. [79]	Water	FMWCNTs 150–200 nm. -	0.1, 0.12, 0.2 and 0.25 %	-	stable for months	Tube D=11.42 mm	Laminar and turbulent.
Paritosh et al. [78]	Water	MWCNTs 10–20 nm. 0.5–40 µm	1.0 %	Non-Newtonian Power Law viscosity	-	D=1.55mm	Laminar
Thang et al. [86]	water	FMWCNTs 10 µm. 15 - 90nm	0.2 and 1.2 gram/litre.	-	-	computer processor. heat sink -	Laminar
Microscale							
Sarafraz et al. [15]	water	MWCNTs 2µm 5-10 nm	0.05–0.1 Vol.%.	-	2-3 weeks.	MCHS w_c=0.25mm H_c=0.4mm	Laminar
Dietz et al. [88]	water	CNTs 10-80 µm 50 nm	-	-	-	MCHS w_c=4mm, H_c=0.15mm	Laminar

BF: Base Fluid. W_c: The channel width. H_c: The channel height.

1.3.6 Computational fluid dynamic (CFD)

The literature contains much detailed information about applying computational fluid dynamic (CFD) problems [89] and [90]. There are basically two ways of modelling a flow field; the fluid is either treated as a collection of molecules or a continuous and indefinitely divisible continuum modelling. In the

latter approach, velocity, temperature, pressure, etc. are all defined at every point in space and time, and the conservation of mass, momentum and energy lead to a set of nonlinear partial differential equations (Navier-Stokes) [91], see Fig. 1-3. The Navier–Stokes and energy equations are used to describe the flow and heat transfer in the channels. It was noticed a successful implementation of FVM in the fluid flow and heat transfer problems which can be explained by several reasons. For instance, the existence of several developed CFD codes (FLUENT, CFX and ..etc) which provide smooth and easy with numerical implementation [92]. Also, the lower required computational specifications, especially for the 2D approaches as well as the available conservation equations provide excellent control of the studied phenomena with the possibility of applying several choices such as the dependent-temperature thermophysical properties [93]. On the other hand, some assumptions are usually considered, for instance, the fluid is Newtonian and incompressible, single-phase, steady-state and constant thermophysical properties.

1.3.6.1. Numerical approach process

The numerical approach process of the CFD problem starts with the user inputs (geometry, boundary conditions and materials properties) which are determined based on the physical problem, Fig. 1-3. The proper mathematical model of the physical problem must be chosen based on some key physical principles and some suitable physical assumptions. Afterwards, the numerical solution can be implemented to the mathematical model and the selected variables (pressure, velocity, temperature, etc) may be obtained at the selected points on the mesh for detailed analysis [94]. Furthermore, for validation purposes, the results can be checked for consistency with the mathematical model (such as the behaviour at the boundaries) and if the numerical errors are acceptable.

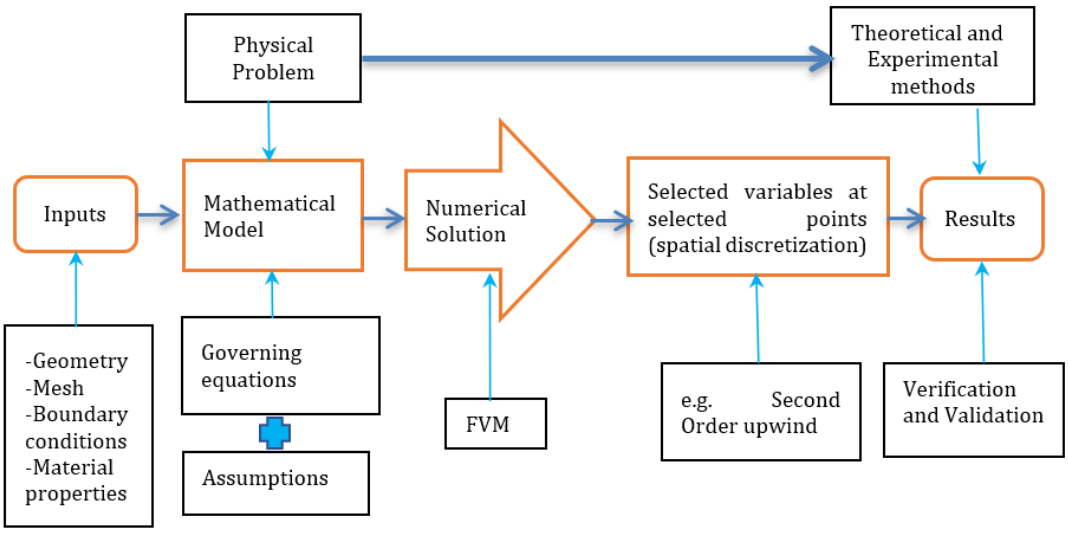

Fig. 1-3: A scheme of the numerical approach process of CFD [95].

Furthermore, the numerical results can be compared with available experimental data or by performing a theoretical analysis of the physical problem in order to validate the numerical model. This can lead to change some physical assumptions or the mesh structure, Fig. 1-3, [90].

However, the numerical study for a particular channel geometry is achieved by solving the main conservation laws for the fluid flow and the computational fluid dynamics (CFD) code, following three main steps when solving a problem [91], Fig. 1-4. These steps are as follows: a- Integrating the conservation equations, b- Converting the integral equations into algebraic equations by the discretization methods (FVM), c- Solve the obtained algebraic equations using the numerical iterative methods [94].

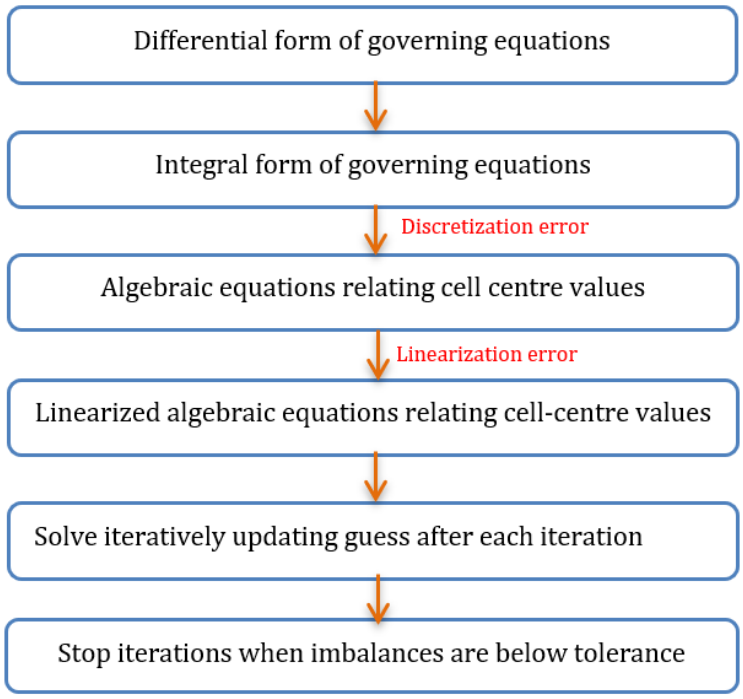

Fig. 1-4: A scheme of solving the governing equations by CFD tools [95].

The variables of the problem (pressure, velocity, etc are determined on the centre of each cell of the mesh in the domain by a process called discretization. The discretization has an error which can be reduced by using a higher number of cells in the mesh (mesh refinement) or by increasing the order of accuracy of the interpolation. Moreover, a linearization process may be used to decrease iterations solving, to account for imbalances of mass, momentum and energy to a certain selected tolerance [96].

Pressure-velocity coupling methods:

CFD tools such as ANSYS-Fluent provide several methods of pressure-velocity coupling: SIMPLE, SIMPLEC, PISO, and Coupled. Where the Semi-Implicit Method for the Pressure-Linked Equation (SIMPLE) coupling algorithm is a popular algorithm used for the single phase in order to couple pressure and velocity. The SIMPLE algorithm has been modified into a SIMPLER algorithm by an additional pressure equation [97]. It was presented that SIMPLER method requires less iterations than the SIMPLE method and it doesn't use guessed pressures, but extracts the pressure field from a given velocity field which should be a corrected one [94].

Discretization methods

In addition, ANSYS-FLUENT allows to choose the discretization methods for each governing equation: Second-Order Upwind discretization, First-Order Upwind discretization, Power law, QUICK and Third-Order Mascl. Second-order accuracy is automatically used for the viscous terms [94]. Single-phase problems are solved using second-order upwind discretization for the flow equations and all scalar equations except for those for turbulence quantities, which are solved using first-order upwind discretization. For triangular and tetrahedral meshes, since the flow is never aligned with the mesh, it will generally obtain more accurate results by using the second-order discretization. For quad/hex meshes, it will also obtain better results using the second-order discretization, especially for complex flows [97].

Solvers

There are two solver technologies available in ANSYS-FLUENT: 1- pressure-based and 2- density-based. The density-based solver was designed in order to approach the high-speed compressible flows. While, in the case of incompressible flows, the pressure-based solver is used [94].

1.3.6.2. Governing equations

The physical principles of the used governing equations, the contained assumptions and the boundary conditions are the most effective part of the numerical approach. The governing equations are based on the fundamental laws of fluid flow.

1.3.6.2.1. Laminar model

The dimensional governing equations for steady state and laminar flow condition using the single-phase model are as follows:

- Conservation of mass

$$\nabla \cdot (\rho \mathbf{V}) = 0 \qquad \text{Eq. 1-3}$$

- Conservation of momentum

$$\nabla \cdot (\rho \mathbf{V}\mathbf{V}) = -\nabla P + \nabla \cdot (\mu \nabla \mathbf{V}) \qquad \text{Eq. 1-4}$$

- Conservation of energy

$$\nabla \cdot \left(\rho C_p \mathbf{V} T \right) = \nabla \cdot (k \nabla T) + \Phi \qquad \text{Eq. 1-5}$$

where Φ is the dissipation function, representing the irreversible conversion of mechanical energy to internal energy as a result of the deformation of a fluid element [26].

$$\Phi = \frac{1}{2} \mu \cdot \nabla^2 \qquad \text{Eq. 1-6}$$

Moreover, the governing equation can be in a differential form or an integral form. In the differential form (Eq. 1-3, Eq. 1-4 and Eq. 1-5), the fundamental laws are applied to an infinitesimal fluid particle, while in the integral form the fundamental laws are applied to a finite volume in the flow domain [96] and [90].

1.3.6.2.2. Turbulent models

In addition to the governing equations of laminar flow, the turbulent model presents two further equations of conservation, particularly the turbulent kinetic energy equation (K') and the equation of dissipation (ε), Eq. 1-7 and Eq. 1-8. There are several types of turbulent models such as K'-ε models and K'-ω models. Also, there are three models of turbulent K'-ε (standard, RNG and Realizable K'-ε turbulence models).
Since the realizable model is a developed form of other K'-ε turbulence models, it satisfies certain mathematical constraints on the Reynolds stresses, consistent with the physics of turbulent flows [97].

Transport Equations for the Realizable K'-ε Model

The realizable-model was proposed by Shih et at. [98] in order to develop the traditional K'-ε model by considering a new eddy-viscosity formulation Eq. 1-11 (C_μ as a variable).

The turbulence kinetic energy (K') and its rate of dissipation (ε) are obtained from the following transport equations:

$$\nabla.(\rho \boldsymbol{V} K') = \nabla.\left[\left(\mu + \frac{\mu_t}{\sigma_K}\right)\nabla K'\right] + G_K - \rho\varepsilon \qquad \text{Eq. 1-7}$$

$$\nabla.(\rho \boldsymbol{V} \varepsilon) = \nabla.\left[\left(\mu + \frac{\mu_t}{\sigma_\varepsilon}\right)\nabla \varepsilon\right] + \rho C_{1\varepsilon} S\varepsilon - \rho C_{2\varepsilon}\frac{\varepsilon^2}{K' + \sqrt{\upsilon\varepsilon}} \qquad \text{Eq. 1-8}$$

Where

$$C_{1\varepsilon} = max\left[0.43, \frac{\eta}{\eta + 5}\right], \eta = S\frac{K'}{\varepsilon}, S = \sqrt{2S_{ij}S_{ij}} \qquad \text{Eq. 1-9}$$

In these equations, G_k represents the generation of turbulence kinetic energy due to the mean velocity gradients. $C_{2\varepsilon}$ and $C_{1\varepsilon}$ are constants. σ_K and σ_ε are the turbulent Prandtl numbers for K' and ε, respectively. S is the mean strain rate [97].

Turbulent Viscosity:

In contrast to other K'- ε models (standard and RSS), the eddy viscosity of realizable-model is not constant, and it is computed from Eq. 1-10:

$$\mu_t = \rho \cdot C_\mu \cdot \frac{K'^2}{\varepsilon} \qquad \text{Eq. 1-10}$$

Where;

$$C_\mu = \frac{1}{A_0 + A_s\frac{K'U^*}{\varepsilon}} \qquad \text{Eq. 1-11}$$

$$U^* = \sqrt{S_{ij}S_{ij} + \tilde{\Omega}_{ij}\tilde{\Omega}_{ij}} \qquad \text{Eq. 1-12}$$

$$\tilde{\Omega}_{ij} = \Omega_{ij} - 2\varepsilon_{ijK}w_K$$
$$\Omega_{ij} = \overline{\Omega_{ij}} - \varepsilon_{ijK}w_K \qquad \text{Eq. 1-13}$$

where $\overline{\Omega_{ij}}$ is the mean rate-of-rotation tensor viewed in a moving reference frame with the angular velocity w_k. The model constants ($C_{2\varepsilon}$, σ_K, σ_ε A_0 and A_s) have been established to ensure that the model performs well for certain canonical flows. The model constants are given by:
$C_{2\varepsilon} = 1.9,\ \sigma_K = 1.0,\ \sigma_\varepsilon = 1.2,\ A_0 = 4.04$ and $A_s = \sqrt{6}\cos\varphi$.

1.3.7 Numerical studies of CNTs nanofluid

Numerical simulations are considered a very helpful method to investigate several situations, where measurements of temperature and velocity fields are certainly very hard or impossible to obtain. Numerical methods may become an economic prediction technique by avoiding the need for various laboratory tests. The study of parameters such as fluid temperatures, Nusselt number, heat transfer coefficient, thermal resistance, friction factor and pressure drop will enable to establish the importance of the nanofluids modelled properties on the heat transfer phenomena and on the microchannel fluid flow dynamics. A survey of the numerical studies available in the literature for fluid flow and heat transfer of CNTs nanofluid, was conducted and both numerical methods and the way of computing the thermophysical properties of the nanofluid are summarized in Table 1-3.

Mini-scale

Rashmi et al. [99] have studied experimentally and numerical CNTs/water-Gum Arabic nanofluids through the concentric tube heat exchanger. The results indicated an enhancement of the heat transfer coefficient of 68.6% at 30 g/s flow rate in comparison with base fluid. The authors refer to a Newtonian behaviour of CNTs nanofluids at 0.01 Vol%. Numerical results exhibited good agreement with the experimental results when the model of 2D Fluent 6.3. was used under the

conditions of single-phase, steady state and incompressible flow to simulate the laminar flow of CNTs nanofluids.

Also, Kamali et al. [100] studied numerically aqueous 1.0 wt% MWCNTs nanofluids as single phase and Non-Newtonian fluid in a horizontal tube with a diameter of 1.55 mm under constant wall heat flux. The numerical results have shown an agreement with the experimental measurements of the local heat transfer coefficient. the latter renders the numerical approach of such MWCNTs nanofluids an important tool for analysing the fluid flow and heat transfer phenomena even with non-Newtonian behaviour. Also, the results indicated the significant effect of the near wall region on the heat transfer coefficient in the case of non-Newtonian behaviour of MWCNTs nanofluid.

Micro-scale

A few researchers have limitedly studied the behaviour of some CNTs nanofluids in microchannels. Arani et al. [60] investigated numerically the laminar flow and heat transfer behaviour of water/single-wall carbon nanotubes (SWCNTs) flowing through a double-layered microchannel heat sink (MCHS). The investigation carried out for particle volume fraction of 0.04 and 0.08, proposed Newtonian single-phase fluid with independent-temperature thermophysical properties. The test section consists of double silicon microchannels and the dimensions are 20mm length, 0.45mm height and 0.05mm width, for each channel. Significant enhancement in heat transfer coefficient was observed with the increase of Reynolds number and SWCNTs volume fractions, accompanied by an increase in pressure drop in comparison with distilled water. Moreover, the reduction in thermal resistance was observed with increase in particle volume fraction, allowing to reach the favoured dimensionless temperature in less distance of microchannel than distilled water.

Nikkhah et al.[52] numerically investigated water/ FMWCNT nanofluid in a 2D microchannel with slip boundary condition under a periodic heat flux. The study carried out for Reynolds number between 1 to 100 and particle volume fraction of 0.12% and 0.25%. The proposed fluid flow is Newtonian, single phase, laminar, steady and incompressible. Thermophysical properties of water and FMWCNT nanofluid were considered at a constant temperature of T = 306 K. The

results indicated an enhancement of Nusselt number when particle volume fraction, Reynolds number and slip velocity coefficient increase. Also, the Nusselt number has a maximum value at the inlet and decreases along the length of microchannel.

Arabpour et al. [61] numerically investigated the behaviour of temperature domain and hydrodynamic of laminar flow of kerosene/multi-walled carbon nanotubes in the microchannel heat sink for the two-dimensional double-layer microchannel. The study found that by increasing Reynolds number and volume fraction of nanoparticles, the maximum temperature factor reduces. The increase in dimensionless slip velocity coefficient causes the enhancement of heat transfer amount.

Nojoomizadeh et al. [58] investigated numerically the oil/(MWCNT) nanofluid in a two-dimensional microchannel under a fluctuating heat flux. The study highlights that the velocity of the nanofluid increases with the increase in Reynolds number, hence heat transfer needs less time which raises the local Nusselt number. The Nusselt number increased for high Reynolds numbers and low porosity.

A numerical study carried out by Ebrahimi et al. [101] to investigate the cooling performance of a microchannel heat sink with MWCNTs/water nanofluid. The results have shown that the use of MWCNTs/water in a microchannel heat sink causes lower thermal resistance in comparison with other nanofluids types.

A numerical study was conducted by Kamali et al. [46] for a laminar flow in a simplified microchannel. The results reported that the heat transfer performance of (MWCNT/water) achieved the lowest thermal resistance in comparison with (Al_2O_3/water) for 1.0% nanoparticle volume fraction when the same boundary conditions were applied. Moreover, the average heat transfer coefficient enhancement in the heat sink compared to the base fluid was by 36% for MWCNT/ water.

In another paper, Halelfadl et al. [47] have optimized the thermal resistance and the pumping power of MWCNTs/water nanofluid in a rectangular microchannel heat sink for laminar flow. The results have shown a significant enhancement in heat transfer behaviour compared with the base fluid at high temperatures.

Table 1-3: Heat transfer of CNTs Nanofluids– numerical modelling and fluid property definition

Research	Nanofluid	Thermal Conductivity	Viscosity /rheology	Device geometry	Numerical model	validation reference	assumptions
Rashmi et al.[99]	CNTs/ water-gum 0.01 vol.%	Exp. Constant-T	Exp. Constant-T Newtonian	Concentric tube heat exchanger D= 11.3 mm	Navier-Stokes, SIMPLE. Laminar	Exp. Water	2D, single-phase, no slip, incompressible
Kamali et al.[100]	CNTs/ Water 1 vol.%	Exp. Dependent -T	Exp. Constant-T Non-Newtonian	Tube D=1.55mm	Navier-Stokes, SIMPLE. Laminar	[78] Exp. CNTs nanofluid	2D, single-phase, no slip, incompressible
Arabpour et al.[102]	MWCNTs/ kerosene 4 and 8 vol.%	Exp. Constant-T	Exp, Constant-T -	MCHS H_c=50 µm	Navier-Stokes, SIMPLE. Laminar	[52] (numerical)	2D, single-phase, no slip, incompressible
Arani et al.[60]	SWCNTs/ water 0.04 and 0.08 vol.%	Exp. Constant-T	Exp, Constant-T -	MCHS W_c= 0.05mm H_c=0.45mm	Navier-Stokes, SIMPLE. Laminar	[103] Exp. Al_2O_3 and TiO_2 nanofluid	3D, single-phase, no slip, incompressible
Nikkhah et al. [52]	FMWCNTs / water 0.12 and 0.25 vol%	Exp. Constant-T	Exp, Constant-T -	Micro channel -	Navier-Stokes, SIMPLE. Laminar	[79], Exp. MWCNTs nanofluids, D=11.42mm and [104] (numerical)	0.001–0.1 for velocity slip, 2D, steady and incompressible - A periodic heat flux
Nojoomizadeh et al.[58]	- MWCNT/ Oil 0.1, 0.2 and 0.4 vol.%	Exp. Constant-T	Exp, Constant-T -	Micro channel -	Navier-Stokes, SIMPLE. Laminar	Teamah et al. 2011 (Numerical)	2D, single-phase, no slip, incompressible
Ebrahimi et al. [101]	MWCNTs/ water 1.0 vol.%.	Sabbaghzadeh model, 2007	Einstein model 1959 -	MCHS W_c/W=0.6 H/W_c=8.2	Navier-Stokes -	Jang et al. 2006 and Min et al. 2004 Exp. water	-
Kamali et al.[46]	MWCNT/ water 1.0 vol.%.	Exp, Constant-T	Exp. Constant-T -	MCHS W_c= 280 µm H_c= 430 µm	Navier-Stokes, SIMPLE. Laminar.	[105] (Numerical)	3D, single phase, -, incompressible

W_c: The channel width. H_c: The channel height. W: The MCHS width. H: The MCHS height.

It has appeared that the researchers have studied only some types of CNTs nanofluid in microchannels such as water/SWCNT, Kerosene/MWCNTs, and oil/MWCNT. None of the researchers seems to have studied the behaviour of (DW+EG)/MWCNTs nanofluids in the microchannel. Moreover, the CNTs nanoparticles were produced by different methods. Therefore, there are several characteristics of different CNTs nanofluids. Besides that, there is no serious investigation on the stability and the shelf life of the used CNTs nanofluid and the

thermophysical properties seem to have been modelled through mixture laws, with poor support from experimental data. However, an accurate thermophysical property database is very important when a numerical approach is applied to investigate the heat transfer phenomena and hydraulic behaviour of nanofluids. Furthermore, any generalization regarding nanofluids must be avoided, since misunderstanding may occur when expecting a specific behaviour for CNTs nanofluid.

1.3.8 Synthesis (State of the art identifying gaps in knowledge)

This section summarises the literature review with emphasis on recent studies regarding microchannel heat exchangers operated using nanofluids, particularly CNTs nanofluids. It has clearly appeared that there are emergency needs to increase the produced energy and rising the energy efficiency in most of the machines, industries and systems, required to enhance the heat transfer capacity by using nanofluids instead of conventional fluids. The most important ideas and concepts of the current literature review can be presented as follows:

- Most of the previous studies regarding CNTs nanofluids have reported significant enhancement in heat transfer coefficient and the results always challenge the restrictions of using conventional thermal fluids.

- The extension of this literature review for numerous nanofluids types highlights several options for simulating the CNTs nanofluids flow in microscale. The presented numerical studies have a good agreement with the correlated experimental data rendering the numerical approach method feasible and appropriate. In addition, a single channel seems to be more appropriate for studying nanofluid behaviour and its heat transfer phenomena. Thus, a numerical approach based on conventional CFD techniques can cover and measure all the important factors which are necessary for a complete understanding of the microfluidics phenomena.

- Most of the experimental and numerical investigations have reported Nusselt number, heat transfer coefficient, Reynolds number, Prandtl number, friction factor and pressure drop as the most important parameters addressed when studying heat transfer in a microchannel. Furthermore, the researchers

have used the temperature profile, thermal resistance, overall heat transfer coefficient, pumping power, overall performance index coefficient to evaluate the micro heat sink and MCHE performance.

- Nevertheless, experimental and numerical studies related to enhancing the heat transfer coefficient in a microchannel using nanofluids are limited. Also, there is still a lack in the investigation concerning CNTs nanofluids flowing through microchannels. Moreover, most numerical studies considered that the nanofluids properties are constant which causes inaccuracy when predicting MCHE, due to the large temperature differences in the MCHE and the strong temperature-dependent properties of nanofluids.

- Different characteristics of CNTs nanofluids have been presented in the studies of heat transfer and fluid flow. Parameters such as base fluid, particle size, particle volume fraction, and preparation method affecting the produced CNTs nanofluid have also been reported to have a direct influence on the CNTs thermophysical properties. Nevertheless, none of the reported studies has investigated the behaviour of (DW+EG)/MWCNTs nanofluid in a microchannel. It should, however, be mentioned, that most of the studies reviewed in this section, did not include a serious investigation on the thermophysical and transport properties of the used CNTs nanofluid.

-Most of the researchers have highlighted the necessity to further exploit the design of efficient compact heat exchangers for electronic cooling and other similar applications, since CNTs nanofluids are considered as promising coolants in microchannels

1.4 THESIS SPECIFIC OBJECTIVES AND RESEARCH QUESTIONS

This work comes in the continuation of the previous work developed by Lamas et al. [22] and Abreu et al. [21]. They have experimentally prepared the MWCNTs nanofluids in a wide range of volume fractions (φ=0.25, 0.5, 1.0 and 1.5%) and for different nanoparticle aspect ratios with two bases fluids (DW+60%EG and DW+30%EG).

The main objective of this work is to provide guidance for using CNTs nanofluid in micro heat exchanger applications. To accomplish the latter, the first objective of this work is to study MWCNTs nanofluid flow in a well-understood macroscale problem. This will enable to propose a tailored method for defining thermophysical properties of MWCNTs nanofluids, establishing new correlations of viscosity and conductivity to be used in a numerical approach for modelling heat transfer and fluid flow.

The second objective is to study the fundamental concepts of fluid flow through a microchannel for conventional fluids, in order to establish the fundamental basis for the study of MWCNTs nanofluid flow in a microchannel. This will test the level of accuracy and understanding of the problem, defining a proper methodology and acceptable assumptions for a numerical investigation on heat transfer and fluid flow in microchannels.

Based on the results of the previously established objectives, the third objective is to investigate numerically the fluid flow and heat transfer of MWCNTs nanofluids through a single microchannel. Here it is intended to analyse different samples of MWCNTs nanofluids (corresponding to different particles morphology and concentration, together with two ethylene glycol concentrations in the base fluid as single-phase fluid). The nanofluids thermophysical properties and rheological behaviour will be properly modelled so an extensive numerical investigation to evaluate the heat and momentum transport phenomena associated with the laminar flow of shear thinning fluids in microchannels will be carried out.

Moreover, based on the understanding of the heat transfer phenomena of MWCNTS nanofluids in microchannels, it will be also intended to evaluate the system overall performance taking into account the energy efficiency

enhancement, considering both the heat transfer gains and the pumping power increase due to the pressure drop.

The proposed research work contributes to the worldwide scientific knowledge answering to the following questions:

1- How do different MWCNTs nanofluids structures affect the heat transfer enhancement in microchannels for different flow conditions?
2- How will the performance of microchannel be when using MWCNTs nanofluids as a heat transfer fluid regarding Nusselt number and pressure drop?
3- How will the use of nanofluid in CHE contribute to enhancing the efficiency of the energy systems? What is the effect of that on the environmental and climatic change?

1.5 THESIS CONTRIBUTION

According to the previous literature review and the conclusions, it can be safely said that the amount of understanding and knowledge in this emerging field of CNTs nanofluid flow through microchannel is still at an early stage. Therefore, the strong database of carbon nanotubes nanofluids properties which were built by Lamas et al. [22] and Abreu et al. [21] can be used in further numerical investigations in order to have the necessary knowledge to fully establish the heat transfer concepts of CNTs nanofluid in a microchannel.

During the conducted survey, only a few studies explaining the heat transfer and fluid flow behaviour of CNTs nanofluids in microchannels were found. In addition to the work reported in the literature, the authors highlighted, dependent-temperature properties, rheology behaviour, viscous heating, entrance effects, inlet temperature and pressure drop as fundamental parameters to consider when modelling and designing systems involving CNTs nanofluids in microchannels. Table 1-4, summarizes the mechanism concepts that affect heat transfer and fluid flow of CNTs nanofluid in a microchannel.

Fig. 1-5 presents the methodology intended to be carried out to accomplish the highlighted contribution.

Table 1-4: Mechanism concepts that affect heat transfer and fluid flow of CNTs nanofluid.

Reference	**HTCE**	**BF**	**Φ%**	**T (K) Dependent-properties**	**Consider the rheology**	**viscous heating**	**Entrance effects**	**Pressure drop**
Arabpour et al.[102]	x		x					
Arani et al.[60]	x		x					x
Nikkhah et al.[52]	x		x					
Nojoomizadeh et al.[58]	X		X					
Ebrahimi et al.[101]	X		X					
Kamali et al.[46]	X							X
Halelfadl et al.[47]	X							
Rashmi et al.[99]	x							
Kamali et al.[100]	x			x	x			

HTCE = heat transfer coefficient enhancement. BF: Base Fluid. T: temperature.

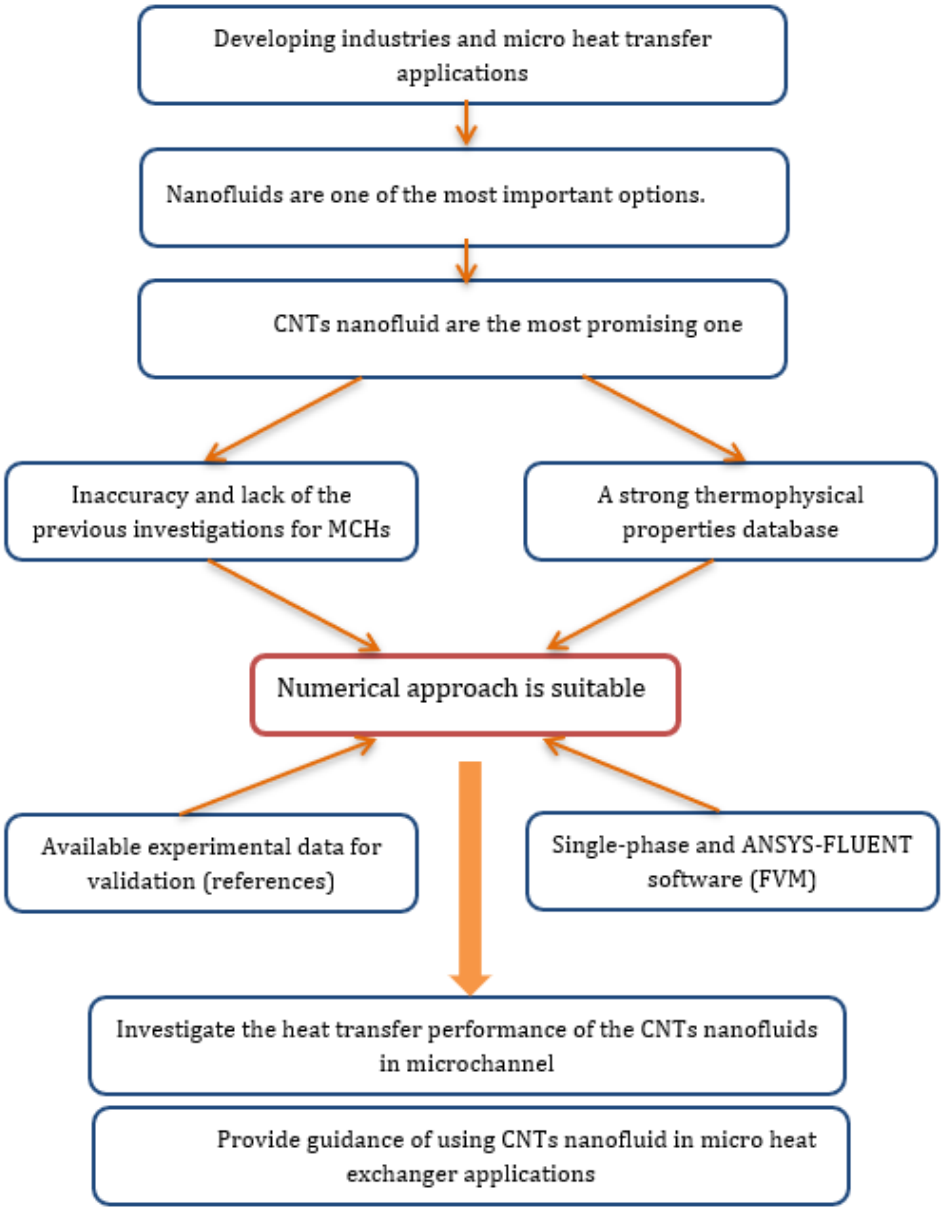

Fig. 1-5: A scheme clarifies the thesis contribution for the CNTs nanofluid in MCHE.

Therefore, this research aims to contribute to the required development in heat transfer applications by establishing guidance of using CNTs nanofluid in the micro heat exchanger. To this purpose, a validated numerical model can be a good tool for a wide range of investigations for many concepts and parameters that define the heat transfer performance of MWCNTs nanofluids in a microchannel. The acquired results are expected to contribute to present scientific knowledge as well as support for future work, both at the fundamental and engineering level.

1.6 THESIS ORGANIZATION

In Chapter-1 an overview of the relevant literature on heat transfer and fluid flow of nanofluids through the microchannel is presented, particularly for CNTs nanofluids and its thermophysical properties. The latter includes the experimental and numerical investigations, allowing to outline the gaps of knowledge besides the objectives and the challenges.

In Chapter-2 a numerical study, validated with experimental data, is carried out on convective heat transfer and laminar flow of MWCNTs nanofluids in a macrochannel, presenting new correlations for thermophysical properties of MWCNTs nanofluids to be used in a numerical approach (CFD) of heat transfer and fluid flow problems, particularly for the following intended step of micro heat exchangers.

Chapter-3 revises in detail some fundamental concepts of fluid flow through microchannel for conventional single-phase fluids (water). The latter intends to separate the fluid dynamics uncertainty rendered by the tube geometry (microscale) from the uncertainties introduced from a new fluid (nanofluid). In addition, a few case studies of fluid flow behaviour within a microchannel are selected to be reproduced by a developed numerical model in order to define and validate a proper methodology and the acceptable assumptions for the numerical investigation on the case.

Based on the results of the previous steps, Chapter-4 investigates the heat transfer and fluid flow of Non-Newtonian shear thinning fluids, particularly MWCNTs nanofluids, flowing in microchannels under a constant heat flux condition. The latter is carried out by using the presented correlations of the

thermophysical properties of MWCNTs nanofluid from Chapter-2, and the presented methodology of building a proper numerical approach for fluid flow and heat transfer in microchannel from Chapter-3. The nanofluids samples are analysed and modelled numerically depending on their thermophysical properties, mainly thermal conductivity and viscosity. Besides, this chapter assesses the overall energy efficiency enhancement for the studied non-Newtonian fluids (MWCNTs nanofluids). Finally, in Chapter-5 the major conclusions and future research objectives are given.

CHAPTER 2- Experimental and numerical study of convective heat transfer and laminar flow of MWCNTs nanofluid in a horizontal macroscale-tube

2.1 CHAPTER SYNTHESIS AND PURPOSE

During this chapter, it is carried out a numerical and experimental study in order to fully establish the efficiency of MWCNTs nanofluids in macroscale devices. The nanofluid behaviour and the capability of the numerical approach to compute the fluid thermophysical properties will be fully exploited. Moreover, the study of a well-understood macroscale problem, where an extensive fluid property database is available will be used to test the validity of the required thermophysical properties correlations to properly define the nanofluid behaviour in the numerical model, establishing the right premises for the intended following studies (i.e. MWCNTS nanofluid through microchannels).

The current chapter proposes a tailored method for defining thermophysical properties of MWCNTs nanofluids, mainly concerning the viscosity and the conductivity, establishing new correlations. The latter is used in a numerical approach for modelling heat transfer and fluid flow and the results are compared with experimentally obtained ones. Moreover, the method of using constant thermophysical properties of the nanofluid for the numerical approach is tested, besides the empirical method of using Shah equation.

This chapter also establishes a comparison between the theoretical, experimental and numerical results for heat transfer coefficient and Nu number as a function of Reynolds number for different MWCNTs nanofluids through a macroscale tube.

2.2 INTRODUCTION

Heat transfer is essential in a wide range of industries everywhere in the world, from power generation, automotive, chemical processing, oil extraction

and refining, renewable energy technologies to several other areas. Usually, these types of energy systems depend on thermal fluids to enhance heat transfer, such as water, ethylene glycol or oils. However, these conventional fluids have poor thermo-physical properties, limiting the effectiveness of such thermal systems when overall size and costs reduction are mandatory. As mentioned before, MWCNTs nanofluid is an important option to enhance heat transfer systems. Therefore, Lamas et al. [19] prepared Multi-Walled Carbon Nanotubes (MWCNTs) nanofluids and studied their thermo-rheological properties, experimentally. The colloidal stability, the thermal conductivity and viscosity for different MWCNTs volume fractions, for a wide range of temperatures, were investigated. Furthermore, to attain proper colloidal stability, the authors optimized the ultra-sonication mixing-time with a UV-vis spectrophotometer. The same research team reported that the colloidal stability benefits from a higher base fluid viscosity and reduced particle size, Lamas et al. [106]. Moreover, the authors also refer to the methods of producing high-quality nanofluids in terms of the balance between high conductivity and long shelf life [20]. The highest enhancement of thermal conductivity was reported to be about 17% for MWCNTs volume fraction of 1.5%. Besides that, the viscosity becomes larger with the increase of particle volume fraction, leading to an increased pressure drop, and pumping power. The obtained results suggest that MWCNTs with a smaller diameter enhance the quality and a good agreement between the experimental and numerical results was reported with a deviation of 3%. In addition, a numerical investigation on MWCNTs/water through a straight tube under laminar flow and constant heat flux conditions were carried out by Kamali et al. [100] using the finite volume method to numerically solve the Navier–Stokes equations coupled with the energy equation. The results confirmed that CNTs nanofluid has a better heat transfer performance than the respective base fluid and a good agreement of the computational results with the available experimental data for CNTs nanofluid regarding heat transfer coefficient, was found. It should be mentioned, however, that nanofluid tailoring prior to its extensive usage in any industrial application is fundamental since the knowledge of the dynamics of such promising systems is still embryonic. Despite that, among the literature, it is possible to encounter numerically studies for several types of nanoparticles beside the CNTs nanofluid [107]. For instance,

Ebrahimnia et al. [75] reported their evaluation of laminar convective heat transfer performance and pressure drop of different nanofluids flowing in a straight circular pipe. The authors found out that heat transfer coefficient and pressure drop of different types of nanofluids have similar behaviour with respect to changes in some parameters such as particle concentration and Reynolds number, while the heat transfer characteristics of nanofluids are highly affected by the type of base fluid and nanoparticle. Moreover, the study refers to the parameters which are important to choose a suitable nanofluid for each application such as the amount of heat transfer enhancement, pump power, stability and cost, whereas, some applications may need a low freezing temperature nanofluid.

It should, however, be referred that some researchers have concluded that CNTs nanofluids have a negative response, such as Dietz & Joshi [88]. These authors noticed that CNTs nanofluids caused a higher pressure drop and higher surface temperature leading to a thermal resistance rise. This numerical investigation of CNTs nanofluids used a single-phase approach, laminar and forced convection conditions through electronics cooling device. Furthermore, the CNTs nanofluids used in previous heat transfer studies [69], [108], [109] have different characteristics regarding many aspects namely: the preparation method, base fluid, nanoparticle geometry and operation conditions. In addition, it was noticed a lack regarding the ageing effect on the thermophysical properties, most of the times nothing is mentioned regarding the stability and shelf life investigations of the CNTs nanofluids that have been used in most of past studies.

Despite all the research effort put on nanofluids and regardless of their established potential, their application in industry is still not an accomplishment. The major drawback regarding poor industrialization lies essentially in model scattering within the research community, lack of agreement and robustness of assumptions, rendering heat transfer modelling integration very difficult or impossible. Validated numerical models of heat transfer systems involving nanofluids are, therefore, key elements to justify and clarify their importance and hence increase nanofluids industrialization level.

This chapter presents an experimental study complemented by a CFD simulation of a single-phase laminar flow of a well-characterized MWCNTs

nanofluid in a uniformly heated tube. The study operates on a new promising nanofluid which has been produced by dispersing 0.25% and 0.5% volume fraction of functionalized MWCNTs in a mixture of distilled water (DW) and 30% of ethylene glycol (EG) (30% EG +70% DW) as a base fluid. Furthermore, this chapter is carried out with the support of an experimental properties database that has been gathered for a few years for several types of MWCNTs for several particles geometry, different particle volume fractions, base fluid and a wide range of temperatures, nanofluid colloidal stability and thermophysical properties can be found in [19], [20], [22], [32], [106], [110], [21] and [111]. Moreover, the numerical approach has been validated against the measured data from the experimental work of Kim et al. [112]. The validation of the proposed numerical model with a new thermophysical properties correlations of MWCNTs nanofluids system is presented in this chapter where the numerical results are compared with experimental data that enabled to determine the impacts of stable MWCNTs nanofluid on the Nusselt number and heat transfer coefficient in a steady state system, and an acceptable agreement was observed.

2.3 EXPERIMENTAL SET-UP

In Fig. 2-1, it can be depicted a photograph of the experimental set-up developed by Abreu et al. [113] to evaluate the convective heat transfer phenomenon of nanofluids.

The experimental setup is composed of a reservoir (2), a peristaltic pump (3), a testing area (6) with a tubular heat exchanger, temperature probes to monitor the fluid inlet and outlet temperatures, a data acquisition system (5) and a shell and tube heat exchanger (4) for cooling the fluid.

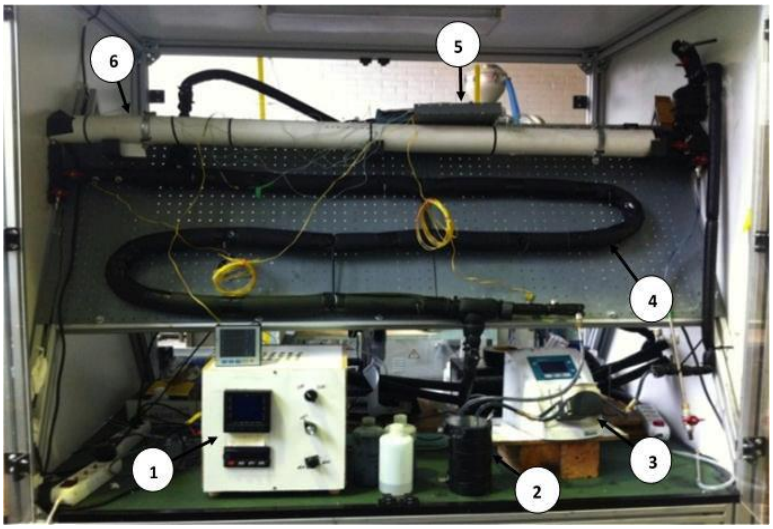

Fig. 2-1 Photography of the experimental device.

The operation of this looped system consists of a working fluid that is pumped out of the reservoir by means of a peristaltic pump and transported through silicone tubes to the testing section. Afterwards, the fluid enters a tubular heat exchanger where it is heated, and the temperature monitored. Next, the heated fluid enters the cooling shell and tube heat exchanger where the fluid is cooled by means of a thermal bath.

The test section consists of a 1420 mm long circular stainless steel (grade 316) tube, with internal and external diameters of 6 and 8 mm, respectively. These characteristics are disclosed in Table 2-1.

Table 2-1: The general characteristics of the experimental facility.

Equipment Features	
The overall length of the test section.	1420 mm
The internal diameter of the tube.	6 mm
The outside diameter of the pipe.	8 mm
The total number of thermocouples.	13
The number of surface thermocouples.	11
Distance between thermocouples.	127 mm
A minimum volume of fluid.	500 ml

The test section tube is heated using a rubber heating tape controlled by a potentiometer and a constant heat flux condition is applied. In order to minimize the heat losses, the heating tape is wrapped with aluminium tape and covered with glass wool. This straightforward setup allows for the determination of the temperature of the operating fluid at the tube inlet and outlet, as well as the outside tube surface temperature at intermediate positions. For this purpose, thirteen k-type thermocouples were used to evaluate the temperature at well-defined points.

2.3.1 Experimental methodology

To evaluate the heat transfer capability of different fluids, all the tests were performed according to the following methodology:

1) The thermocouples readings were verified by the dedicated software associated with the data acquisition system.
2) The fluid level in the reservoir (500ml) was checked.
3) Once the desired flow rate had been calibrated, the flow valves were placed in the required position to perform the test and then the thermal bath was switch on, enabling the control of the studied fluid inlet temperature. Any air bubbles that may exist in the system were eliminated during this step.
4) The heating tape was switch on, and constant power of 125W was imposed at the test-section walls.
5) This looped system was run until it stabilized, which was recognized when the desired flow and temperature were measured at the test section inlet. This was achieved by adjusting the flow rate and temperature of the thermal bath.

Finally, the temperatures recordings were saved by a data acquisition system at 2-second intervals. Each experimental test was conducted for at least 30 minutes.

2.3.2 Repeatability and uncertainty analysis

In order to ensure the reliability of the experimental apparatus, two calibration processes were conducted. Distilled water and a mixture of 30% of Ethylene Glycol and water were chosen as working fluids since their thermophysical properties are well known. During the tests, the tube wall and fluid temperatures were recorded at a time interval of 2 seconds. The tests were conducted at a constant heat flux of 125 W, at a Reynolds number of 1000 and an inlet temperature of 293.15 K for the deionized water. The calibration process with the mixture of 30%EG and water was performed at a heat flux of 125W, a Reynolds number of 1500 and an entry temperature of 313 K. The obtained results for both fluids presented a maximum experimental error of 5% for all the calibration tests. Furthermore, the uncertainty in the temperature and flow rate measurements was calculated for a confidence interval of 95%, and they were found to be less than 0.5% and 0.012%, respectively. Therefore, good repeatability and uncertainty were achieved.

2.3.3 The preparation of the nanofluid

The MWCNTs nanofluids used in this study were prepared in a similar fashion to Lamas et al. [19], [20], [22] and [111]. The selected base fluid is a mixture of distilled water (DW) and 30% of ethylene glycol (EG) (30%EG+70%DW). The chosen MWCNTs have a diameter of 20 to 40 nanometres and a length of 10 to 30 micrometres. This choice relies on the fact that nanofluids prepared with these nanoparticles present an expected lifetime between 10 to 20 years and a good thermal conductivity enhancement, as describe by Lamas et al. [20], [22] and [105]. The MWCNTs were produced by a catalysed chemical vapour deposition CCVD process by Cheaptubes Inc. These have a purity of (>95 wt%) and an ash content of (<1.5 wt%).

A medium at 413 K of nitric and sulfuric acid at 1:3 volume ratio was used to covalently functionalize the MWCNTs for thirty minutes, then proper washing with distilled water at 373 K was issued until the acidity fully disappeared, followed by drying for 72 hours. To account for good dispersion of the MWCNTs in the base fluid, ultrasounds combined with a magnetic stirrer were used for

optimized time periods. In order to analyse the nanofluids dispersion and assess their stability, the settling velocity of the MWCNTs-nanofluids was measured through a stability analyser LUMiSizer 6120. The latter allowed for the prediction of the required time to reach full settling of MWCNTs, defined as shelf life. For these nanofluids (i.e. MWCNTs with diameters of 5 to 30 nanometres and a length of 10 to 30 micrometres, volume fractions of 0.25% vol. and 0.5% vol) it was estimated a shelf life between 20 to 50 years. More detailed information can be found in [20].

2.3.4 The nanofluid properties

The thermo-physical properties of nanofluids play a significant role in heat transfer capability. The most important thermophysical properties are the density, the specific heat, the dynamic viscosity and thermal conductivity. In order to design a numerical approach to simulate the heat transfer of nanofluids, these properties must be properly characterized. In this study, the thermal conductivity of the considered nanofluids was experimentally assessed. It was used an ethylene glycol/distilled water mixture (30%EG+70%DW) as the base fluid, and different concentrations of MWCNTs with a diameter from 20 to 40 nanometres and lengths from 10 to 30 micrometres, were considered. The thermal conductivity was measured at different temperature levels by a KD2-pro thermal analyser, according to the procedure described by Lamas et al. [20] and [22]. The thermal conductivity measurements were performed by the coated-transient hot wire (THW) for temperature ranging from 283 K to 333 K at the MWCNTs volume fraction of 0.25% vol. and 0.5% vol. More than twenty readings for each temperature were done, remaining in each temperature for 5 hours, where the measurements are taken every 15 minutes.

The temperature of the samples was ensured by a circulating thermal bath in a double-jacketed bottle fitted in a block cavity of rigid polyurethane foam, to decrease the vibrations provided by the laboratory environment. Furthermore, the experimental apparatus was calibrated with the base fluid (DW+30%EG) and the maximum variation was 1.8% from the empirical values.

There is no standardized methodology to assess the viscosity of nanofluids. Despite that, the effective viscosity of the produced liquid samples was assessed by Abreu et al. [21] with the orientation of the International Organization for Standardization (ISO) and from the German Institute for Standardization (DIN), more particularly from ISO 3219, and the DIN 53019. These standards specify a methodology to determine the viscosity at a defined shear rate by means of rotational viscometers. Viscosity was assessed for a temperature ranging from 283 to 313 K and shear rates ranging from 50 to 400 s^{-1}, and more than ten repetitions were performed for each sample at each temperature, maintaining the sampler temperature constant during measurements. The results have shown that viscosity is influenced by several parameters namely, temperature, shear rate and particle volume concentration and its appropriate modelling requires further insight, more detailed information can be found in [21]. The density and specific heat of the nanofluids were calculated using the model proposed by Pak and Cho Eq. 2-1 [114] and the model of Xuan and Roetzel Eq. 2-2 [115], respectively,

$$\rho_{nf} = \varphi \cdot \rho_p + (1 - \varphi) \cdot \rho_{bf} \qquad \text{Eq. 2-1}$$

$$c_{p,nf} = \frac{\varphi \cdot (\rho \cdot c_p)_p + (1 - \varphi) \cdot (\rho \cdot c_p)_{bf}}{\rho_{nf}} \qquad \text{Eq. 2-2}$$

where the subscripts nf represent nanofluid, p the particle, and bf the base fluid. The thermophysical properties of nanofluids used for this numerical work at the tube inlet are summarized in Table 2-2.

Table 2-2: Thermophysical properties of the nanofluids at the tube inlet (293.15 K).

Fluid properties	**k (W/m. K)**	**ρ (kg/m³)**	**c_p (J/kg. K)**
BF+%0.25 CNT	0.463	1048	4480
BF+%0.5 CNT	0.465	1106	4384

Furthermore, this study suggests using variable-thermophysical properties of MWCNTs nanofluid for the numerical approach to achieve a high level of accuracy. Therefore, new conductivity correlations as a function of temperature were produced by performing a polynomial fitting curve on the conductivity experimental data of the MWCNTs nanofluids and base fluid (EG30%) [22], resulting well-fitted correlations of conductivity as function of the temperature, Table 2-3 (Eq. 2-3, Eq. 2-4 and Eq. 2-5), with a maximum deviation of 0.5%, as shown in Fig. 2-2.

Table 2-3 Thermal conductivity correlations.

Equation	$k = a\,T^3 + b\,T^2 + c\,T + d$				
Parameters	**a**	**b**	**c**	**d**	
0.25 vol%	4.444E-07	-4.026E−04	1.222E−01	-1.196E+01	Eq. 2-3
0.5 vol%	3.843E-07	-3.492E−04	1.065E−01	-1.042E+01	Eq. 2-4
EG30%	8.704E-07	-8.003E-04	2.458E-01	-2.476E+01	Eq. 2-5

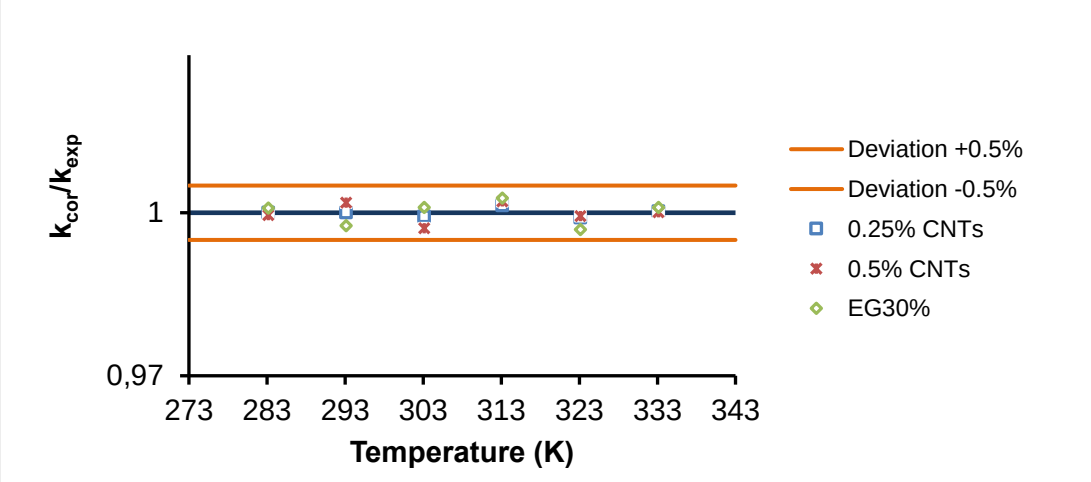

Fig. 2-2: Deviation of the proposed correlations of thermal conductivity in comparison with experimental data.

Furthermore, new viscosity correlations as a function of temperature and shear rate were produced by performing a Non-Newtonian power low viscosity fitting curve (Eq. 2-6, [97]) on the viscosity experimental data [21], considering

the observed non-Newtonian shear-thinning rheological behaviour of MWCNTs nanofluid.

$$\mu = K\,\dot{\gamma}^{n-1}\,H(T) \text{ where, } H(T) = exp\left[\alpha\left(\frac{1}{T-T_0}-\frac{1}{T_\alpha-T_0}\right)\right] \quad \text{Eq. 2-6}$$

Where, $H(T)$ is the temperature dependence (Arrhenius law). K, n, α, T_0 and T_α are input parameters. K is a measure of the average viscosity of the nanofluid (The consistency index), n is a measure of the deviation of the fluid from Newtonian (The power-law index, determined as n<1 for shear-thinning behaviour), α (K) is the ratio of the activation energy (J/K mol) to the thermodynamic constant R (J/mol). Also, T_α and T_0 are the reference temperature (T_α=293.15 K) and the temperature shift (T_0=273 K), respectively. $\dot{\gamma}$ is the shear rate (1/s).

The validation of the accomplished power-law correlations fitting curve of viscosity (Eq. 2-7 and Eq. 2-8) in comparison with experimental data is shown in Fig. 2-3. According to this figure, the MWCNTs nanofluids viscosity data fit well by the proposed correlations with a maximum deviation of 6%.

0.25 vol%: $$\mu = 2.589E-03\,\dot{\gamma}^{-0.01466}\,exp\left[2100\left(\frac{1}{T-T_0}-\frac{1}{293.15-T_0}\right)\right] \quad \text{Eq. 2-7}$$

0.5 vol%: $$\mu = 2.972-03\,\dot{\gamma}^{-0.02893}exp\left[2100\left(\frac{1}{T-T_0}-\frac{1}{293.15-T_0}\right)\right] \quad \text{Eq. 2-8}$$

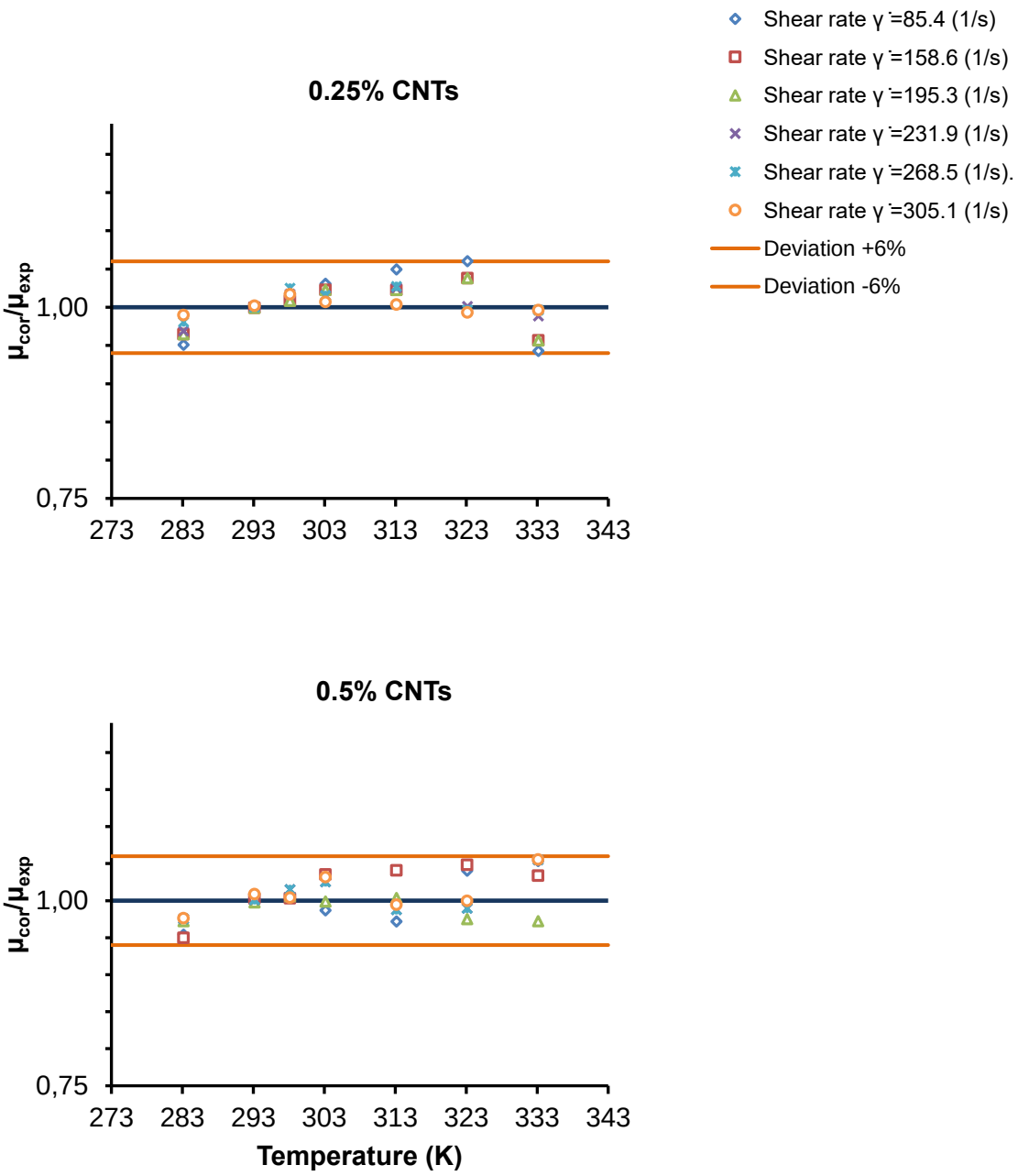

Fig. 2-3: The deviation of the proposed correlations of viscosity in comparison with experimental data for 0.25% and 0.5% MWCNTs nanofluids.

Also, the correlation of base fluid (EG30%) viscosity as a function of temperature (Eq. 2-9) was produced by performing a polynomial fitting curve on the experimental viscosity data of the base fluid (EG30%) [21]. The presented correlation achieved a maximum deviation of 1.5%.

EG30%: $\mu = -8.056E\text{-}09\ T^3 + 8.042E\text{-}06\ T^2 - 2.696E\text{-}0\ T + 3.046E\text{-}01$ Eq. 2-9

Consequently, dependent-temperature thermophysical properties correlations of the Non-Newtonian MWCNTs nanofluid were well-accomplished to be utilized in a numerical approach for fluid flow and heat transfer investigation.

2.4 MATHEMATICAL MODELLING

In the present study, the single-phase approach model is numerically implemented using the finite volume method (FVM) that transforms the governing equations to a form of algebraic equations that can be solved numerically. Moreover, a second order upwind method was used in order to include the convective and diffusive terms. Pressure and velocity were coupled using Semi-Implicit Method for Pressure-Linked Equations [SIMPLE] [90]. The simulations are carried out in the software code ANSYS-FLUENT version 18.2 environment [97].

2.4.1 Geometric configuration

According to the experiment setup, the numerical domain was established as a two-dimensional tube (2D) with 1.27 m length and 6 mm inner diameter as it can be depicted from Fig. 2-4. The imposed experimental boundary condition was a constant heat flux of 125 W at the tube's wall. For that purpose, the electrical heater was applied to the external wall of the test section and then covered by a layer of insulation material, see Fig. 2-1 for details. During the experiment, the current and voltage applied to the electrical heater were measured in order to check the respective power. The heat flux can be determined by dividing the electric resistance power by the test section surface area (0.0239 m^2). For that reason, the tube wall boundary condition was considered as a constant heat flux of 5224.3 W/m^2.

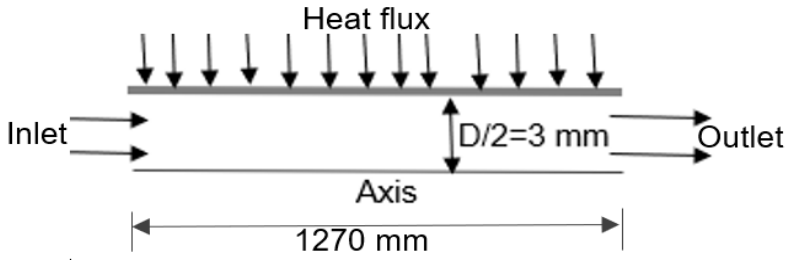

Fig. 2-4: Schematic diagram of the numerical region (test part).

2.4.2 Governing equations

The simulation has used the Navier-Stokes and energy equations to model the convective heat transfer and fluid flow since the Laminar model in the ANSYS-FLUENT software was applied. The dimensional governing equations for steady state and laminar flow condition using the single-phase model are presented in section 1.3.6.2.1, [116].

2.4.3 Boundary conditions

The process was accomplished assuming an incompressible fluid, a laminar flow and the heat losses to the surroundings by radiation or conduction were neglected, due to the appropriate thermal insulation. In addition, the thermophysical properties of the MWCNTs nanofluid and the base fluid at the inlet of the tube were obtained, Table 2-2, and were also used when modelling the constant-thermophysical properties numerical approach. Furthermore, when numerically modelling the Non-Newtonian MWCNTs nanofluid the temperature-dependent thermophysical properties correlations were used (Eq. 2-3, Eq. 2-4, Eq. 2-7 and Eq. 2-8). The inlet temperature (T_{in}) was considered at 293.15 K. Also, the uniform axial velocity profiles (u_{in}) at the tube inlet have been determined based on the experimental operation data and Reynold number as it is shown in Eq. 2-10 [2],

$$R_e = \frac{\rho \cdot u \cdot D}{\mu} \qquad \text{Eq. 2-10}$$

Where, (u) is the velocity of the fluid flow, (μ) is the viscosity and (ρ) is the density of the fluid. In addition, non-slip wall condition and a constant uniform heat flux were considered as the boundary conditions at the tube wall.

2.5 RESULTS AND DISCUSSION

2.5.1 Mesh optimisation and validation

In order to guarantee mesh-independent results, four different mesh distributions (47519, 139531, 104026 and 63021 nodes) were tested. The simulation has been done for the same test section and laminar flow of water was considered for three different Reynolds numbers, considering both cases of dependent-temperature and independent-temperature for the thermophysical properties of the fluid. In order to evaluate the mesh dependency of the numerical results, the simulations with increasing mesh resolution were carried out and the obtained Nu curves were compared, Fig. 2-5.

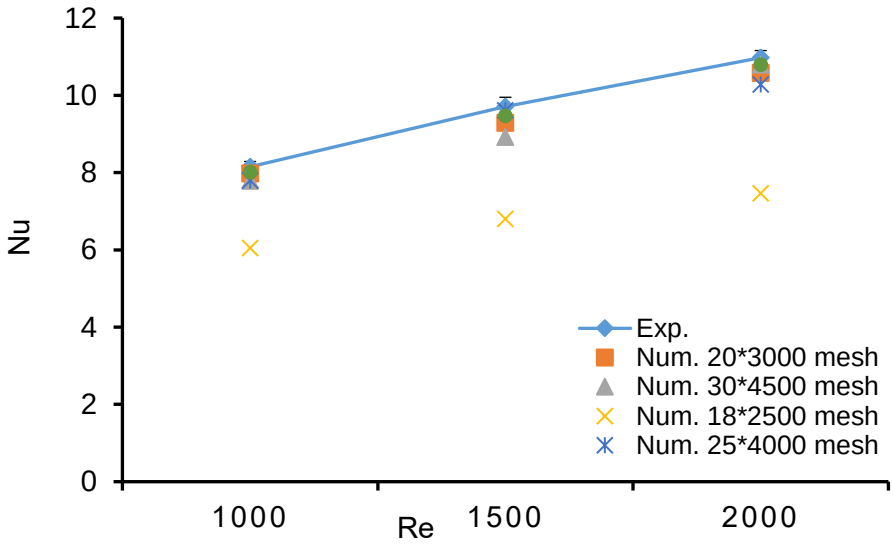

Fig. 2-5: Mesh independency for water flow according to Nusselt number as a function of Re number.

The results show that the mesh with 47519 does not agree with the experimental results, so the number of nodes was increased and it was noticed that for meshes with a numbers of nodes equal or higher than 63021 there is not

a significant change in the determined Nu, which was compared with the experimental results showing a deviation lower than 4% for both cases of using dependent and independent-temperature thermophysical properties conditions, leading to the conclusion that the 63021 nodes mesh is acceptable for simulation of this system, being a trade-off between accuracy and computational cost. Moreover, Nu number decreases with the Reynolds number in both experimental and numerical results until Nu= 8 at Re=1000 with a deviation between experimental and numerical values of 2%. These results lead to the conclusion that the mesh with 63021 nodes is adequate for the simulation of this system.

At the first stage, the CFD model was validated comparing CFD results with those determined by the correlation reported by Kim et al. [112] for water at the same boundary conditions. Then the results were evaluated along the tube in the axial direction and compared with experimental data at Re= 16520 and it was noticed a maximum deviation of 4%, likewise, the Nu number has shown a high value at the entrance region of the tube, decreasing along its axial direction, both for the numerical and experimental results, as it can be depicted from Fig. 2-6 .

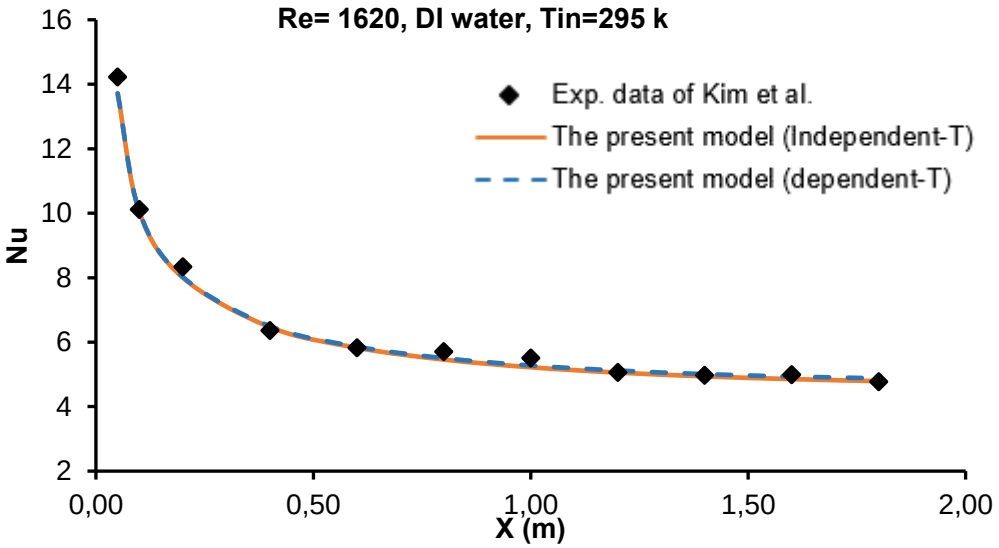

Fig. 2-6: Numerical and experimental Nusselt number as a function of axial position along the tube for distilled water, for Re=1620.

This procedure was repeated for the heat transfer coefficient for several Reynolds numbers and MWCNTs particle volume fractions, as presented in Fig.

2-10, Fig. 2-11 and Fig. 2-12, and a good representation of the experimental data was obtained.

2.5.2 Heat transfer

In general, adding nanoparticles to the base fluid results in an increase of thermal conductivity, which in turn enhances the heat transfer capability. As it can be depicted from Eq. 2-11, the heat transfer coefficient is assessed by Newton's law of cooling, where the temperature at the wall T_w, the bulk fluid temperature T_f, and the imposed heat flux must be evaluated. It can be noted that the decrease in the difference between the tube wall temperature and the bulk temperature of nanofluids is a sign and a measure of an enhanced heat transfer coefficient.

$$h = \frac{q}{T_w - T_f} \qquad \text{Eq. 2-11}$$

The bulk temperature of the fluid (T_f) can be numerically obtained by the Area-Weighted Average method at each location selected along the test section of the tube using ANSYS-FLUENT model, as well as for the temperature at the wall (T_w) which can be numerically determined at each wanted point on the test section model, Fig. 2-7. The temperature values are changing with the change of the fluid flow conditions.

Moreover, the bulk temperature of the fluid T_f can be calculated by Eq. 2-12,

$$T_f = T_{in} + \frac{q \cdot \pi \cdot D \cdot L}{\dot{m} \cdot c_p} \qquad \text{Eq. 2-12}$$

where (q) is the total heat flux, (T_{in}) is the inlet temperature measurement, and ($\dot{m}$) is the flow rate, (L) is the tube length and (D) is the tube diameter. Therefore, the required temperatures (T_f, T_w) of the tested fluid flows for the MWCNTs nanofluids (0.25% and 0.5%) and the base fluid (EG30%) were calculated and measured for several Reynolds number (Re=1000, 1500 and 2000). The numerical results of both cases (variable and constant-thermophysical

properties) were compared with the experimental data as it shown in Fig. 2-8 and Fig. 2-9.

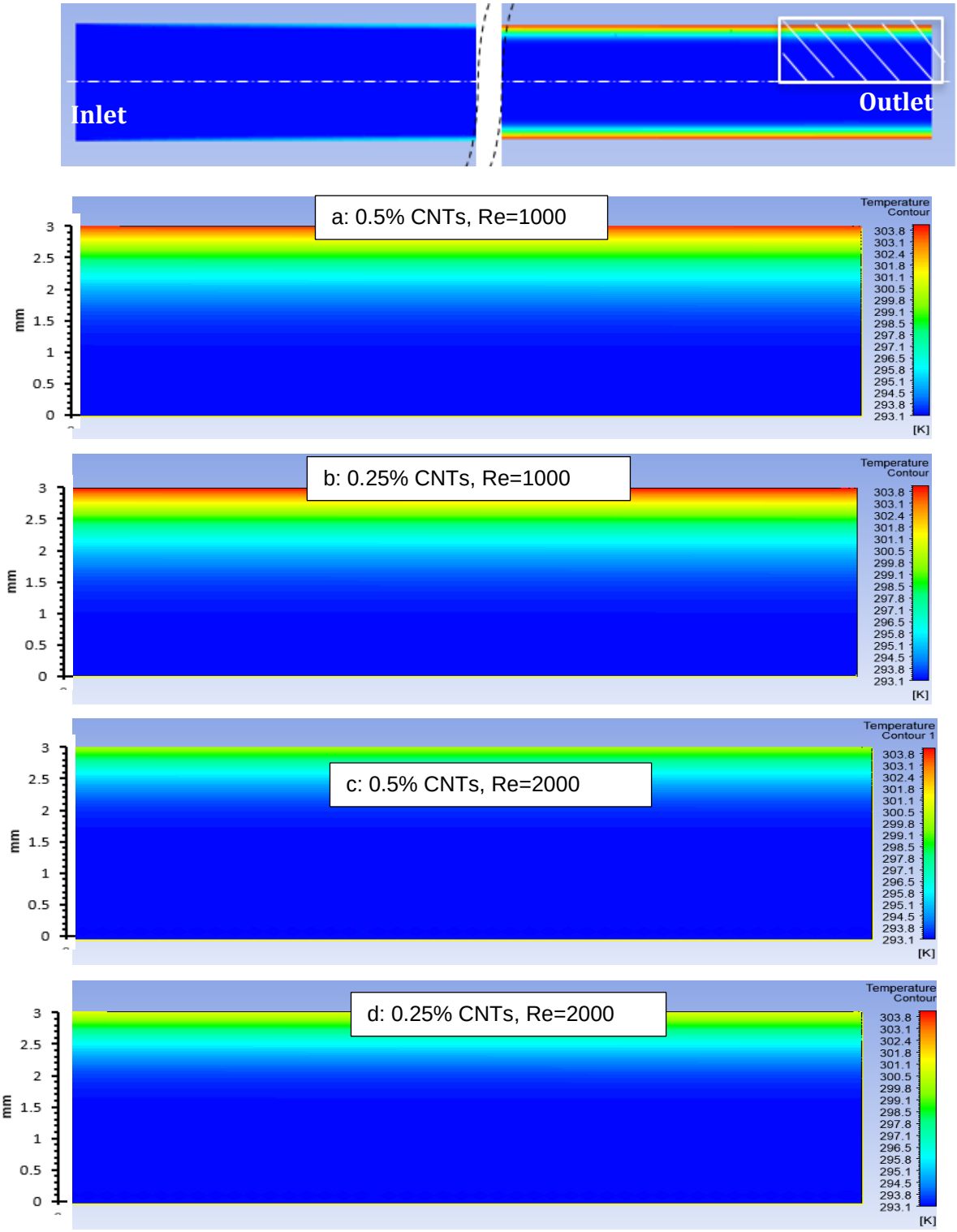

Fig. 2-7: The test section model showing the resulted temperature field at the outlet of the tube for deferent cases: (a: 0.5%CNTs-Re=1000, b: 0.25% CNTs, R e=1000, c: 0.5%CNTs-Re=2000 and d: 0.25%CNTs-Re=2000).

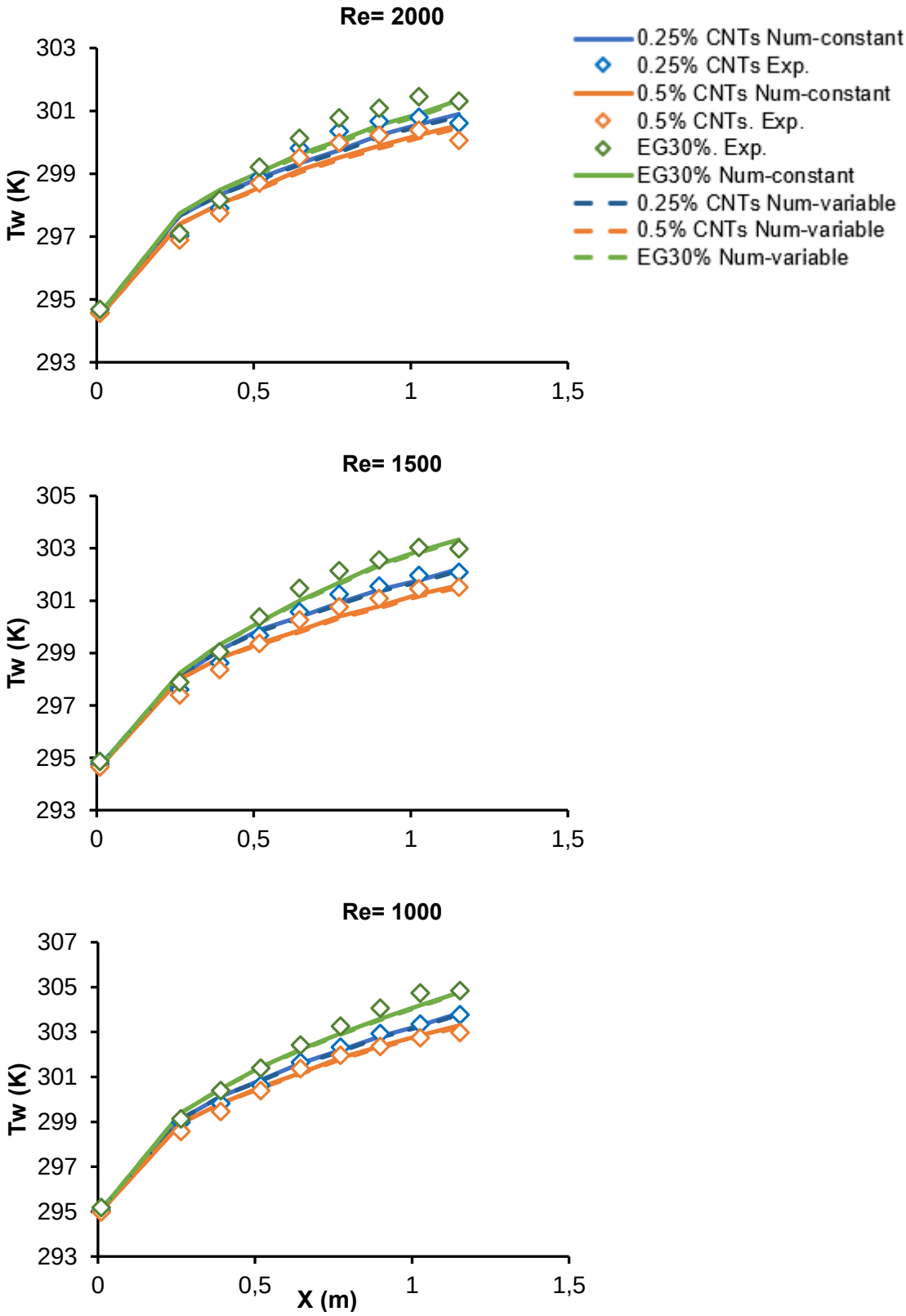

Fig. 2-8: Numerical and experimental wall temperature as a function of axial position along the tube for the base fluid and (0.25% and 0.5%) CNTs nanofluids for Reynolds numbers of (Re=2000,1500, and Re=1000).

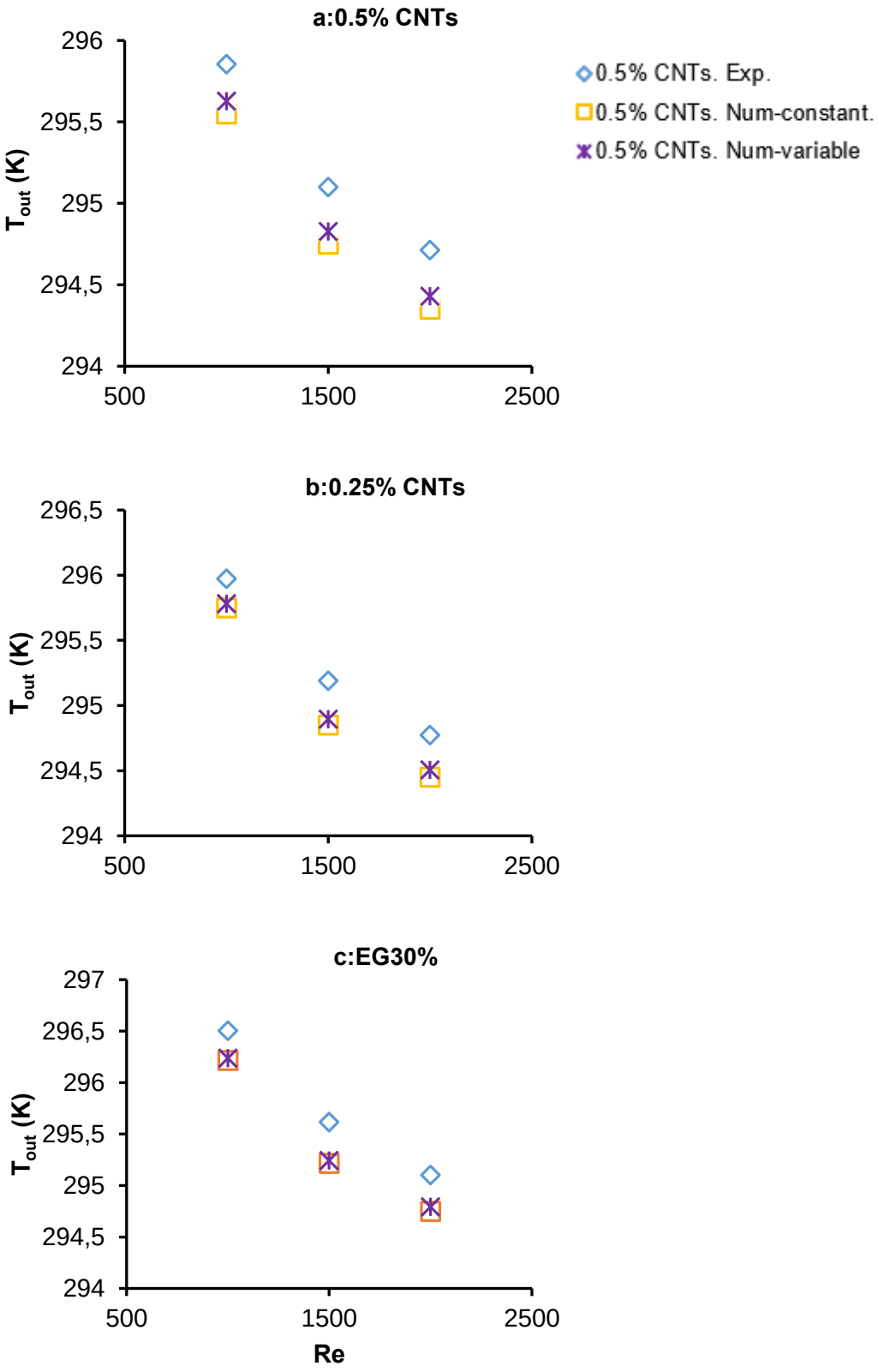

Fig. 2-9: Numerical and experimental fluid temperature at the outlet of the tube as a function of Reynolds number for (a:0.5%CNTs. b:0.25%CNTs. c: EG30%.).

It can be noticed a decrease in the wall temperature (T_w) with the increase of particle volume fraction and Reynolds number, which refers to the benefit of using MWCNTs nanofluids to reduce the surface temperature in cooling applications. Also, the wall temperature increases along the tube in the axial direction, rendering a good agreement between the numerical and experimental results for several fluid flow conditions, Fig. 2-8.

Moreover, with the increase of particle volume fraction and Reynolds number the outlet temperature ($T_{f,out}$) decreases, Fig. 2-9. The latter may be explained by Eq. 2-12, where it can be depicted that the temperature of the fluid decreases with the increase of fluid flow ($\dot{m}$) and the specific heat (c_p) of the operating fluid.

In addition, the average heat transfer coefficient h_{avg} *is* given by the Eq. 2-13:

$$h_{avg} = \frac{1}{L}\int_0^L h(x)\,dx \qquad \text{Eq. 2-13}$$

Furthermore, the convective heat transfer coefficient can be determined from Eq. 2-17 after calculating the Nusselt number using the following Shah Eq. 2-14 and Eq. 2-15 [117], for laminar flows under constant heat wall flux.

$$Nu = 1.953\left(Re \cdot Pr \cdot \frac{D}{x}\right)^{\frac{1}{3}} \qquad for \quad \left(Re \cdot Pr \cdot \frac{D}{x}\right) \geq 33.33 \qquad \text{Eq. 2-14}$$

$$Nu = 4.3640 + 0.0722 \cdot Re \cdot Pr \cdot \frac{D}{x} \qquad for \quad \left(Re \cdot Pr \cdot \frac{D}{x}\right) \leq 33.33 \qquad \text{Eq. 2-15}$$

where Pr is the Prandtl number, which is given by Eq. 2-16 [2], and k is the fluid thermal conductivity.

$$Pr = \frac{c_p \cdot \mu}{k} \qquad \text{Eq. 2-16}$$

$$h = \frac{Nu \cdot D}{k}$$ Eq. 2-17

The convective heat transfer coefficients, obtained numerically, were compared with those experimentally measured and those analytically calculated using Shah Eq. 2-14 and Eq. 2-15 for three Reynolds numbers (Re= 1000, 1500 and 2000), see Fig. 2-10, Fig. 2-11 and Fig. 2-12.

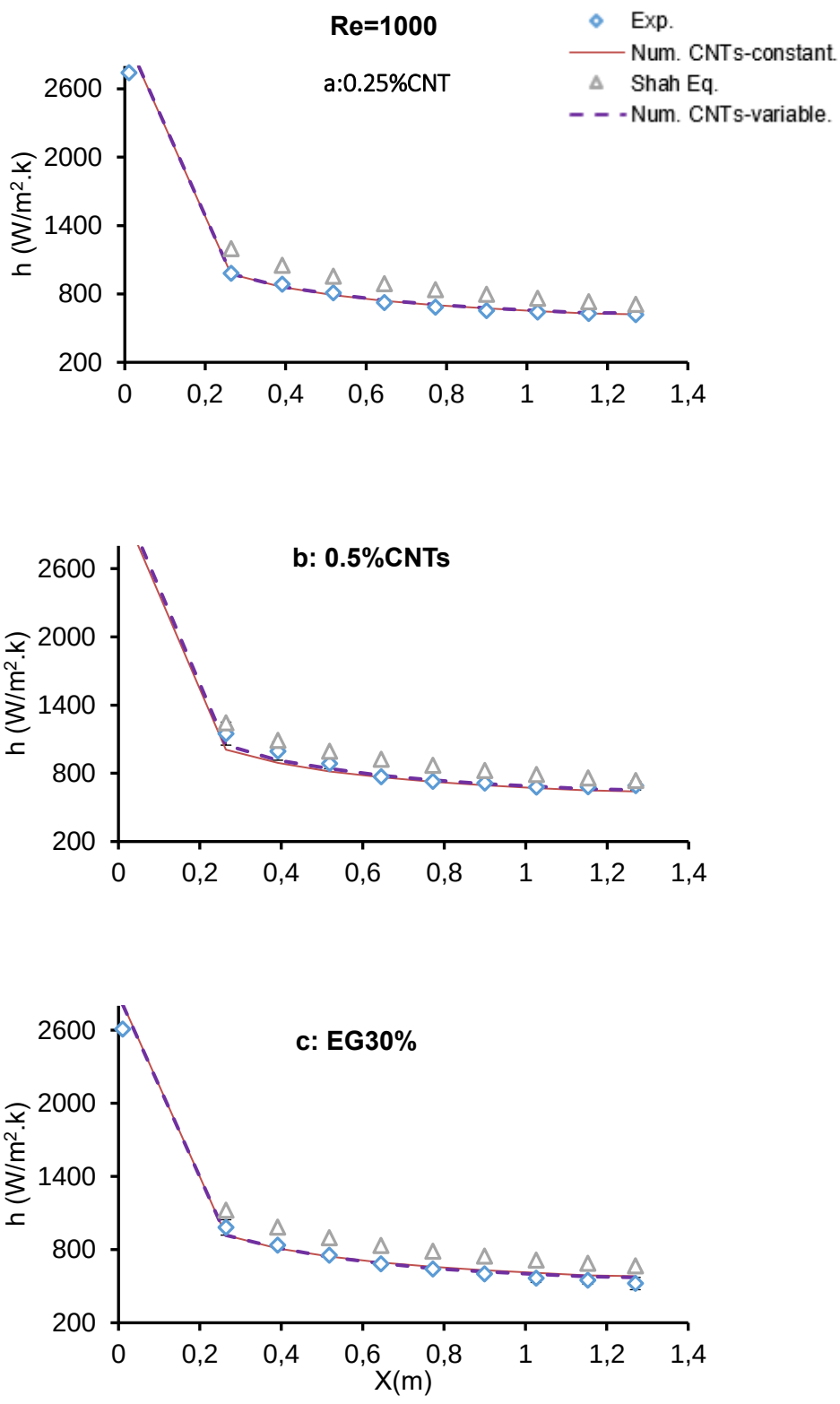

Fig. 2-10: Numerical and experimental convective heat transfer coefficient as a function of axial position along the tube for Re=1000 (a:0.25%CNTs, b:0.5%CNTs, c: EG30%).

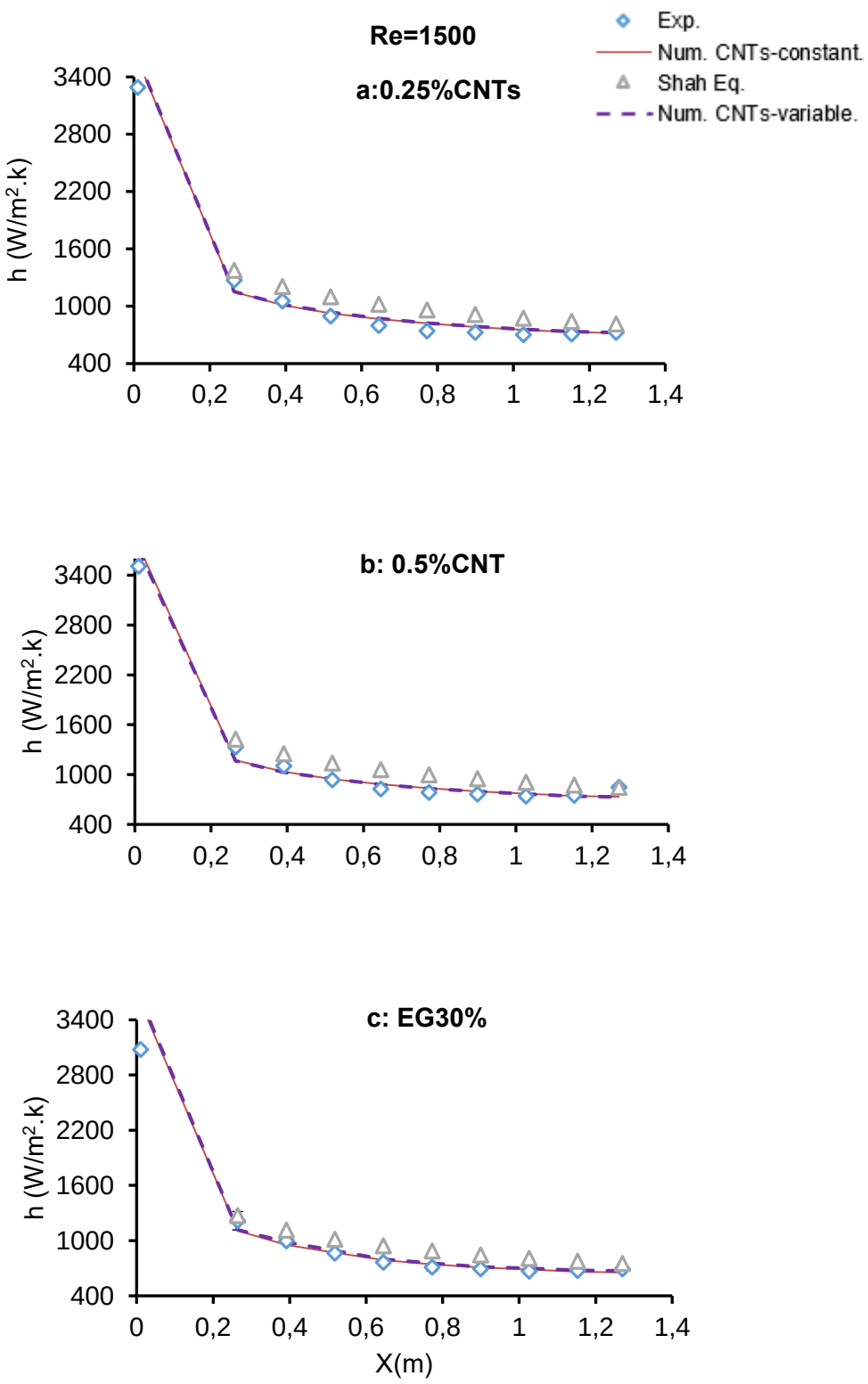

Fig. 2-11: Numerical and experimental convective heat transfer coefficient as a function of axial position along the tube for Re=1500 (a: 0.25%CNTs, b: 0.5%CNTs, c: EG30%).

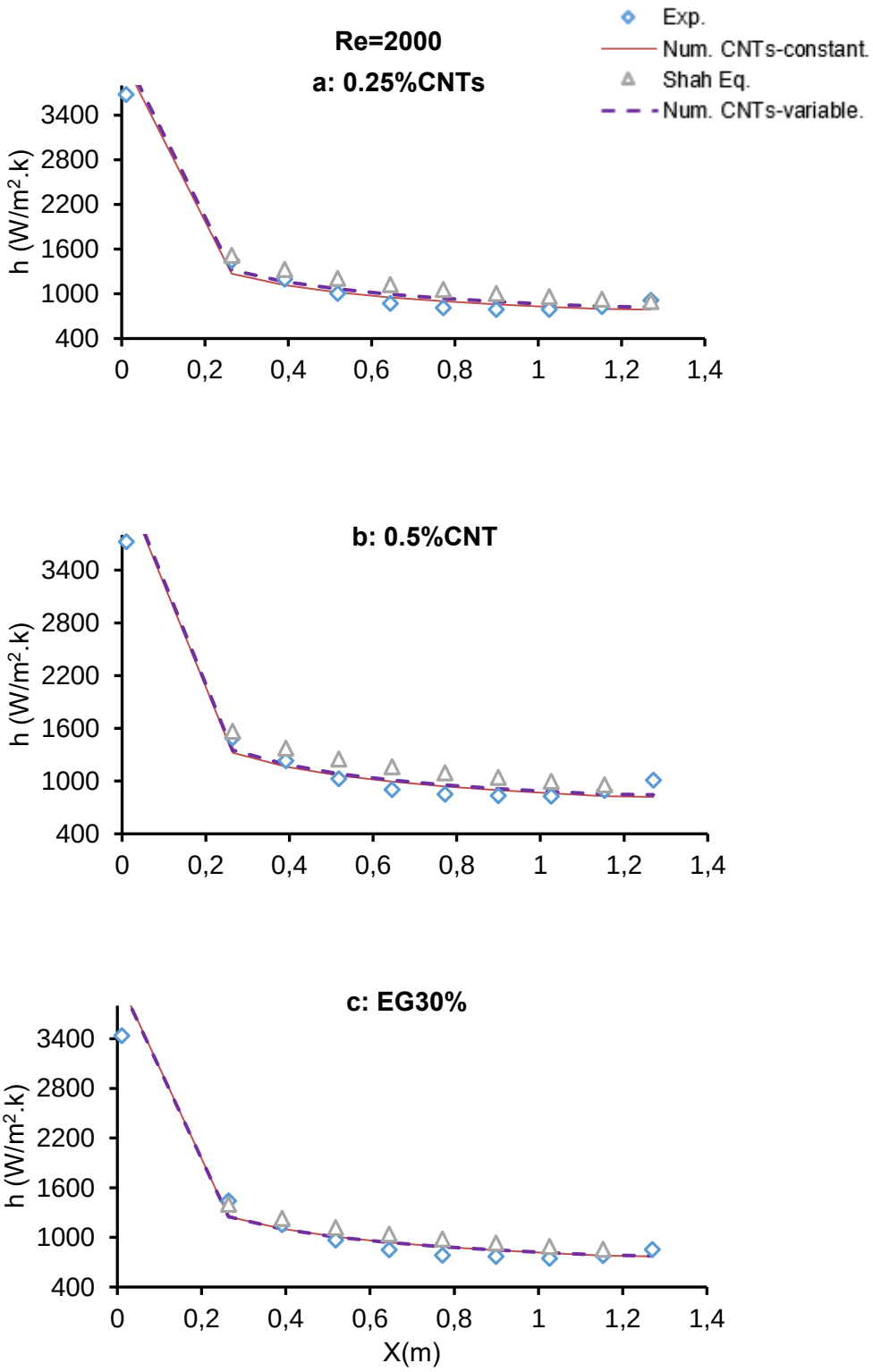

Fig. 2-12: Numerical and experimental convective heat transfer coefficient as a function of axial position along the tube for Re=2000 (a: 0.25%CNTs, b: 0.5%CNTs, c: EG30%).

From the obtained results, it can be clearly depicted that the numerical single-phase model provides a good approximation of the experimental data for all the cases studied (particle volume fractions and Reynolds numbers), achieving better results when variable-thermophysical properties are used. Moreover, the convective heat transfer coefficient of MWCNTs nanofluid enhances when the particle volume fraction increases. In addition, the numerical and experimental results denote a respectable enhancement in the heat transfer coefficient when the Reynolds number increases.

On the other hand, the predictions of the numerical model are in good agreement with the experimental results for the low particle volume fraction (0.25% and 0.5%) and laminar flows, particularly when variable thermophysical properties are used, Table 2-4. Moreover, the predictions of Shah's equation have shown a variation of 15 % with the experimental results, rendering to the numerical approach more capability for better predictions in comparison with the use of Shah's equation in laminar flow for MWCNTs nanofluid. It was also observed a high heat transfer coefficient at the entrance region of the tube for all the tests, which can be explained by a fully developed hydrodynamic boundary layer which affects the respective thermal layer. Almost constant heat transfer coefficients are achieved along the circular tube for all the tests, which refers to the benefit of short channels to achieve higher heat transfer coefficients.

The impact of nanoparticle volume fraction on the average heat transfer coefficient is shown in Fig. 2-13. The experimental and numerical data report an average enhancement in heat transfer coefficient by 10.3%, 9.6% and 9.2%, respectively for Re = 1000, Re = 1500 and Re=2000, because of adding 0.25% MWCNTs volume fraction to the base fluid. Whereas, for the nanofluid containing 0.5% MWCNTs volume fraction the average enhancements are about 12.85%, 14.30% and 14.63%, respectively for Re = 2000, Re = 1500 and Re=1000.

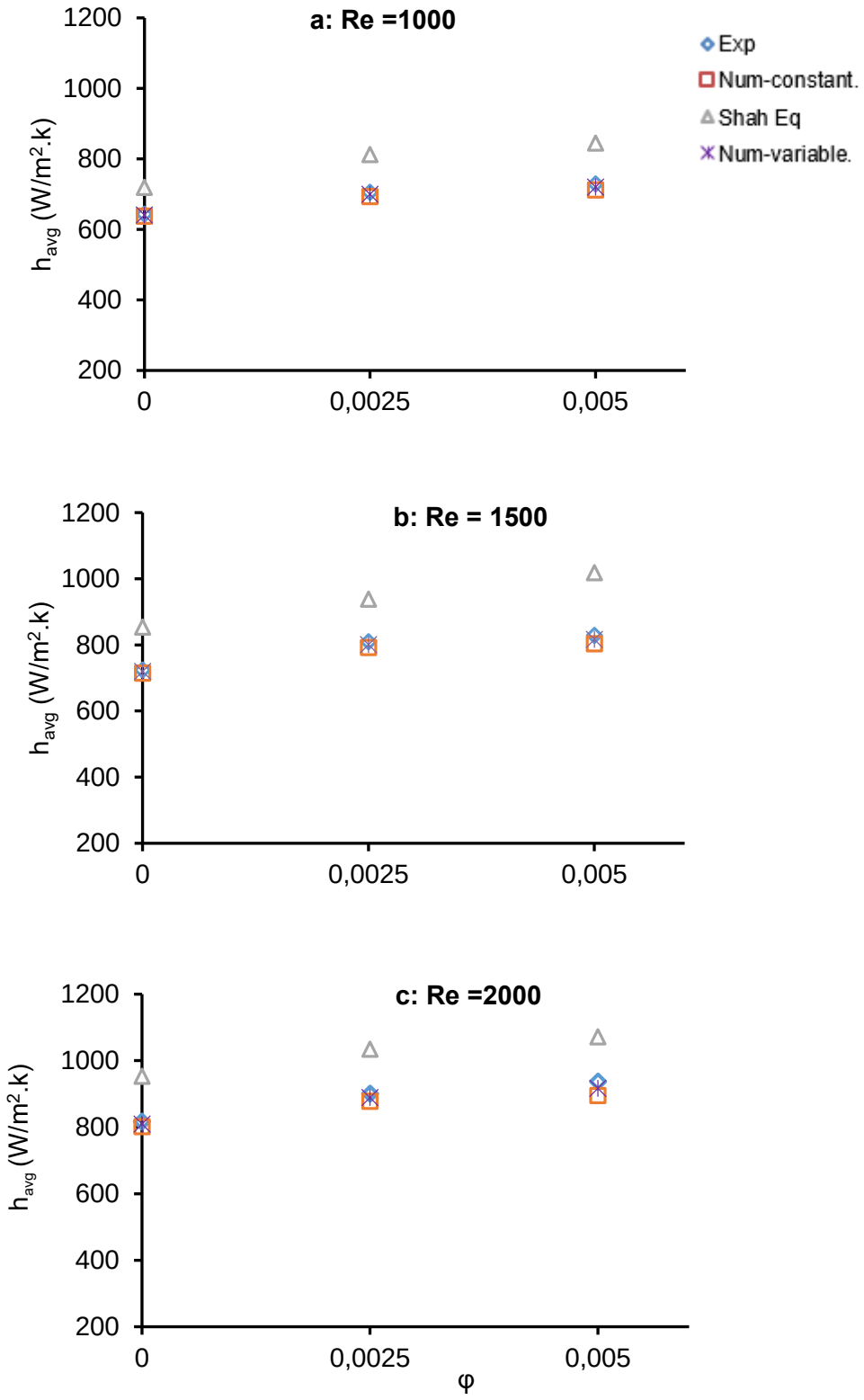

Fig. 2-13: Average convective heat transfer coefficient as a function of nanoparticle concentration. (a: Re =1000, b: Re = 1500, c; Re=2000).

Finally, the results determined with the numerical single-phase model, for both cases when using constant-properties and variable-properties, were compared with those obtained from the experimental data. The results show a maximum deviation of 5 % when the constant properties were used. While it shows a maximum deviation of 4 % when the correlations of the variable properties were used. Both numerical approaches, however, provide better-estimated results than those obtained by Shah equation. Moreover, with the increase of the Reynolds number, the deviation between the numerical results and experimental results increases as shown in Table 2-4.

Table 2-4: Average deviation between numerically predicted data and experimental results

Average Deviation			
0.25% MWCNTs nanofluid			
Re	**1000**	**1500**	**2000**
Shah Eq.	13.1%	13.9%	14.7%
Num. constant	1.0%	3.5%	4.5%
Num. variable	0.9%	2.7%	3.9%
0.5% MWCNTs nanofluid			
Shah Eq.	13.7%	14.2%	14.9%
Num. constant	2.7%	3.7%	4.8%
Num. variable	1.8%	2.9%	3.9%

2.5.3 Nusselt Number

As it would be expected per its definition the enhancement on the Nusselt number is consistent with the convective heat transfer coefficient enhancement noticed in figures Fig. 2-10, Fig. 2-11 and Fig. 2-12. From the latter, it can clearly be noticed that heat transfer coefficients rise as the particle volume fraction and the Re number increase. The same behaviour for Nusselt number was noticed in Fig. 2-14 where the variation of the computed Nusselt number for the nanofluids within evaluation is compared with the experimental data for the laminar flow regime. The average Nusselt number of the base fluid (30%EG+70%water) and the nanofluids increase is dependent on different parameters such as volume

concentration and Reynolds number. The results highlight that the average increase in Nusselt numbers for (0.25% MWCNTs) and (0.5% MWCNTs) nanofluids in comparison to that of the base fluid is linked with an increase in heat transfer coefficient. The obtained Nusselt numbers for nanofluids were enhanced with an increase in particle concentrations for equal Reynolds numbers.

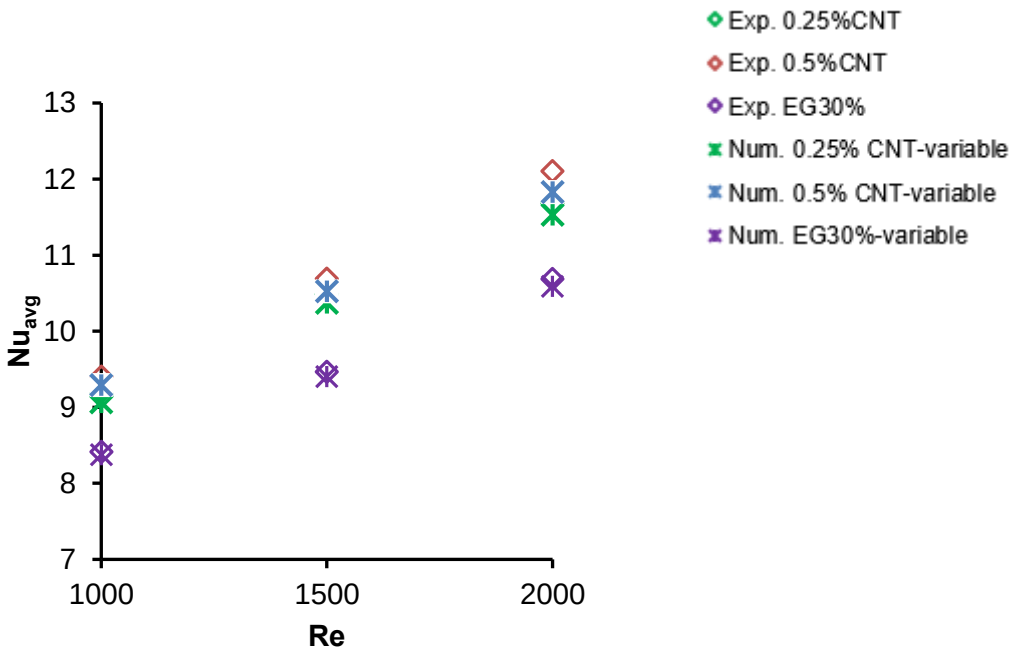

Fig. 2-14: Numerical and experimental Average Nusselt numbers as a function of Reynolds number.

In general, the addition of MWCNTs nanoparticles to a base fluid will increase the heat transfer rate, because of the high thermal conductivity of the mixture, which is due to the larger surface area of nanoparticles for molecular collisions [22], [32]. This is clearly shown in the last figures as an increase in nanoparticles volume fraction resulted in an enhanced heat transfer coefficient and Nusselt number.

2.5.4 Pressure Drop, Wall Shear Stress and Friction coefficient

The impact of heat flux and Reynolds number on the pressure drop and friction coefficient of the MWCNTs nanofluid flow along the circular tube is shown in Fig. 2-15 and Fig. 2-16. It can be noticed that the pressure drop is increasing while the friction coefficient decreases with Reynolds number rise. The friction coefficient is given by the following Eq. 2-18,

$$Cf = (2 \cdot \tau)/(\rho \cdot u^2) \qquad \text{Eq. 2-18}$$

where Cf is the friction coefficient of the MWCNTs nanofluid, τ is the wall shear stress of the MWCNTs nanofluid, ρ is the density of the nanofluid, and u is the axial velocity of the nanofluid.

By adding MWCNTs to the base fluid, not only the conductivity increases, but viscosity also increases which results in higher pressure drop due to the friction coefficient rise. As it would be expected, the highest-pressure drop was observed at a Re=2000 for 0.5%MWCNTs-basefluid (3185.1 Pa) followed by 0.25%MWCNTs-basefluid (2886.4 Pa) and base fluid (2679.3 Pa), respectively, when constant-thermophysical properties were considered, see Fig. 2-15. While slightly lower pressure drops were observed when variable-thermophysical properties are considered, in this case, the highest-pressure drop was (3089.8 Pa) at a Re=2000 for 0.5%MWCNTs-basefluid followed by 0.25%MWCNTs-basefluid (2860.5Pa) and base fluid (2664.249 Pa), respectively.

Moreover, the relative increase in pressure drop for MWCNTs nanofluids, when compared with the base fluid, in constant-properties case, was (16.2%) for 0.5%MWCNTs-basefluid and (9.8%) for 0.25%MWCNTs-basefluid. Whereas, in variable-properties case, it was (14.8%) for 0.5%MWCNTs-basefluid and (9.3%) for 0.25%MWCNTs-basefluid. The total pressure drop has been numerically calculated by the Area-Weighted Average method to determine the pressure difference between the inlet and the outlet of the test section model using ANSYS-FLUENT model [97].

The highest friction coefficient (0.0298) was found at Re = 1000 for the (0.5%MWCNTs-base fluid) and it decreases with the decreasing of particle volume

fraction for the same Reynolds number. From Fig. 2-16, it can be depicted that for the same particle volume fraction, the friction coefficient decreases with the increasing of Reynolds number, as it would be expected. Moreover, the variation between the numerical results of the friction factor in both cases (constant and variable-properties) is very low with a maximum deviation of 1.5%.

.

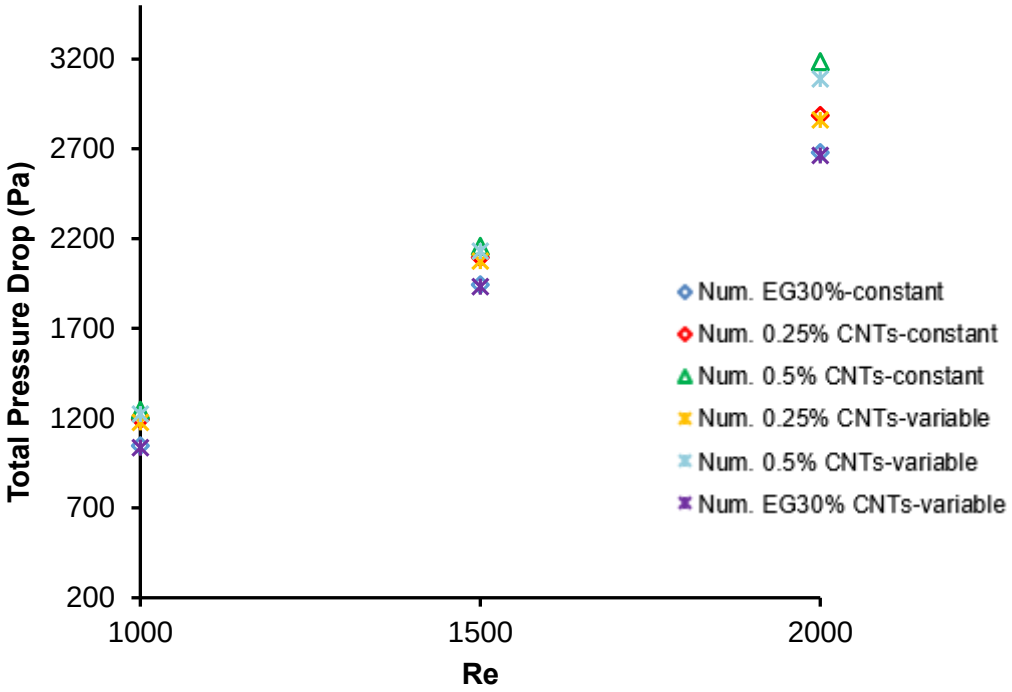

Fig. 2-15: Pressure drop for MWCNTs nanofluids and the base fluid as a function of Reynolds number.

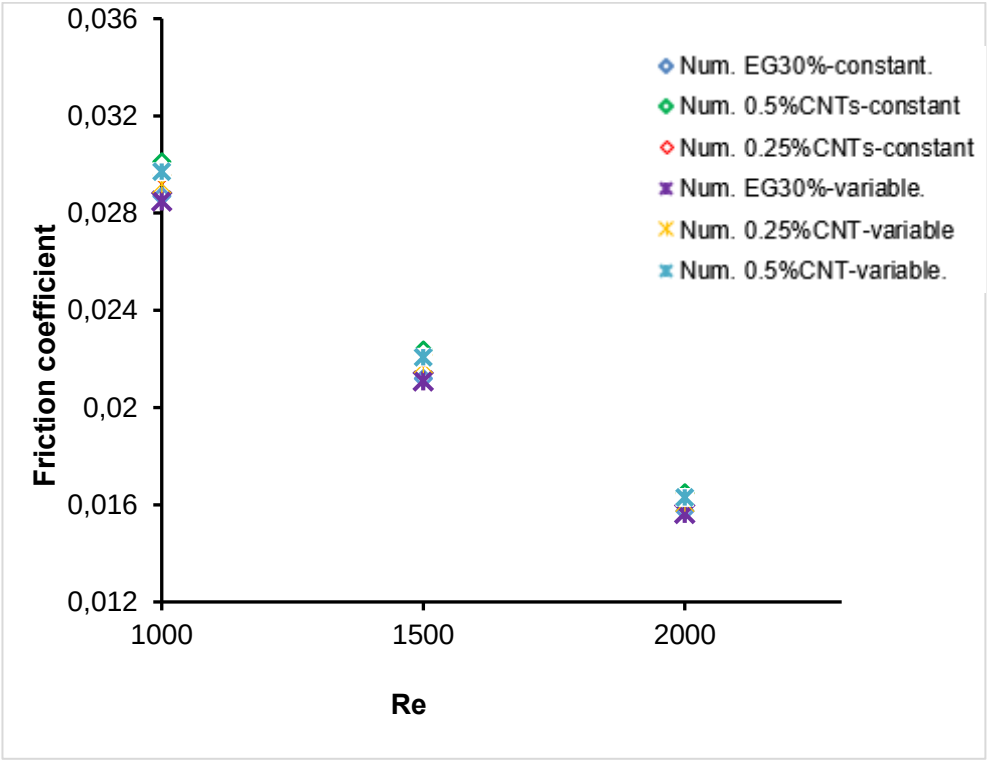

Fig. 2-16: Friction coefficient for MWCNTs nanofluids and the base fluid as a function of Reynolds number.

2.5.5 Wall Shear Stress

Wall shear stress is directly coupled to the pumping power as it is a function of pressure drop. Moreover, it is a combined function of viscosity, dimensions of the tube and the velocity, resulting in a nonlinear function. As the geometry is constant, the only variables left to influence the wall shear stresses are viscosity and velocity of the MWCNs nanofluids. Wall shear stress results for MWCNTs nanofluids are presented in Fig. 2-17. Since Wall Shear Stress can be obtained directly by the numerical model, it can be concluded that the wall shear stress for MWCNTs nanofluids increases when MWCNTs volume fraction is increased for equal Reynolds numbers conditions. In addition, as the MWCNTs particle volume fraction rises, the wall shear stress increases due to the enhancement of the nanofluid viscosity. The lower value was 2.01 Pa at Re=1000 for the base fluid, while the highest value observed was 5.61 Pa at Re= 2000 for 0.5%MWCNTs-base fluid nanofluid. It may be said, however, that wall shear stress consistently increased with Reynolds number, as it can clearly be seen in, Fig. 2-17. Moreover, it can be noticed from Fig. 2-15 and Fig. 2-17 that the variation between the achieved values for the different particle volume fractions at the same Reynolds number, rises as the Reynolds number increases, showing the effect of adding MWCNTs particles to the base fluid on the wall shear stress and pressure drop.

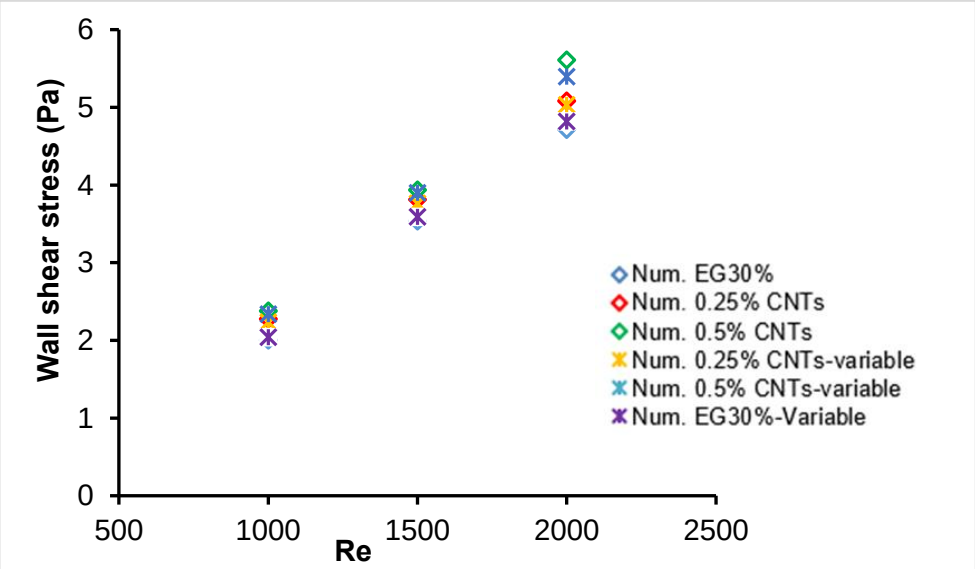

Fig. 2-17: Wall Shear Stress for MWCNTs nanofluids and base fluid as a function of Re number.

Furthermore, the deviation between the numerical results of wall shear stress in both cases (constant and variable-thermophysical properties) are shown in Fig. 2-18. A maximum deviation of 2.5% was observed at a Re=2000 for 0.5%MWCNTs-basefluid. The deviation rises with the increase of Reynolds number and particle volume fraction, and the highest deviation was noticed at the end of the tube. The latter can be explained by the effects of the conductivity and viscosity changes of MWCNTs nanofluid, according to the temperature and velocity gradients of the fluid flow.

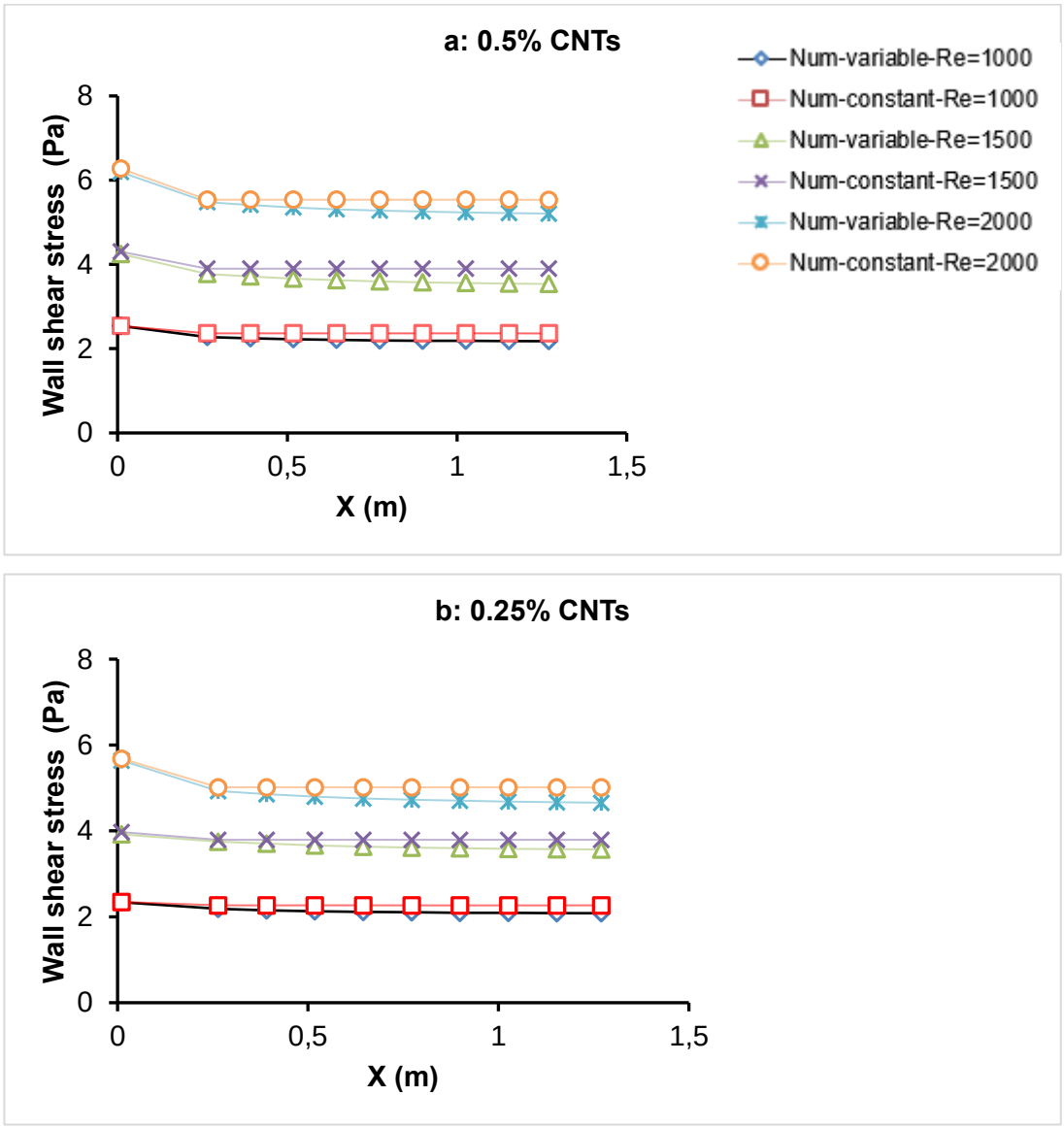

Fig. 2-18: Wall Shear Stress for MWCNTs nanofluids as a function of axial position along the tube for both cases: variable- thermophysical properties and constant-properties (a: 0.5%CNTs, b: 0.25%CNTs).

2.6 CHAPTER CONCLUSION

In this chapter, experimental work and numerical simulation on laminar flow and heat transfer performance in a circular tube were presented, in order to investigate the impacts of using a long-term MWCNTs/(DW+EG) nanofluid on the heat transfer. An experimental set-up was used to assess the heat transfer performance of MWCNTs/(DW+EG) nanofluids under steady-state laminar conditions. Moreover, CFD tools of ANSYS-FLUENT software were applied to develop a single-phase approach model. The comparisons between the numerical and the experimental results were carried out for the heat transfer coefficient and Nusselt number. The performance of MWCNTs/(DW+EG) nanofluids regarding heat transfer coefficient, pressure drop, friction coefficient and wall shear stress, were properly investigated. The main conclusions and results were drawn as follows:

1- The heat transfer coefficient and consequently, the Nusselt number, increased consistently with an increase of both Reynolds number and particle volume fraction. Almost a constant heat transfer coefficient was achieved along the circular tube due to its hydrodynamic fully developed nature, whereas the thermally developing conditions caused a higher heat transfer coefficient at the entrance region of the tube.

2- The average increase in the heat transfer coefficient for (0.25% MWCNTs) and (0.5% MWCNTs) nanofluids were about 10% and 14% in comparison to that of the base fluid, respectively.

3- The pressure drop and wall shear stress increase were consistent with an increase in both Reynolds number and particle volume fraction, whereas the friction coefficient decreased with the increase in Reynolds number. Moreover, the rise of pressure drop, in variable-properties case, was (14.8%) for 0.5%MWCNTs-basefluid and (9.3%) for 0.25%MWCNTs-basefluid, comparing with that of the base fluid. While, the rise of pressure drops, in constant- properties assumption case, was higher with a maximum deviation of (1.5%).

4- Also, this study presents the deviation of the numerical (variable and constant-properties cases) and empirical (Shah equation) results in

comparison with the experimental data. The highest deviation was observed for Shah equation results by (15%), followed by the numerical results of constant-properties assumption case (5%), and then by the numerical results of variable-properties consideration case (4%).

5- The numerical results present a good agreement with the experimental data for all tests, mainly when variable-thermophysical properties conditions of nanofluid were considered, which reports a good capability of the single-phase approach in investigating the MWCNTs nanofluid for other conditions and applications. Furthermore, the proposed correlations of viscosity and conductivity of MWCNTs nanofluid were validated and achieved good confidence for further numerical approaches of heat transfer studies about MWCNTs nanofluids, particularly for the following intended approach of fluid flow in microscale heat exchangers.

CHAPTER 3- FUNDAMENTALS OF FLUID FLOW AND HEAT TRANSFER IN MICROCHANNELS

3.1 CHAPTER SYNTHESIS

In this Chapter, the fundamental concepts of fluid flow through a microchannel for conventional fluids are presented, analysed and discussed, in order to establish the fundamental basis for the following intended approach: the study of MWCNTs nanofluid flow in a microchannel. The latter intends to separate the fluid dynamics uncertainty rendered by the tube geometry, particularly when CFD tools are concerned, from the uncertainties introduced from a new fluid, inferring to the overall problem further robustness.

To accomplish the above stated, in this chapter, the literature is reviewed on both available numerical and experimental models and methods to tackle fluid flow through a microchannel. Moreover, a few case studies are selected, and a numerical model developed to predict fluid flow behaviour within a microchannel, in order to test the level of accuracy and understanding of the problem. Furthermore, the obtained results when compared with experimental studies seem to indicate that a proper methodology is defined and those acceptable assumptions are established, when CFD tools are used to investigate heat transfer and fluid flow in microscale heat exchangers.

3.2 INTRODUCTION

There is a rapid development in microsystem technology involving microelectronic cooling systems, medicine engineering, power generation, automotive, nuclear industries, chemical processing, aerospace and other micro heat exchanger applications [40] and [118], which need a particular heat exchanger system for achieving the required temperature and increasing the device shelf life. The latter presents a continuing challenge to surpass the limitations of such thermal systems when overall size, saving energy and costs reduction is mandatory. Microchannels for heat transfer applications present high

thermal performance since they detain a wide respectable heat transfer surface area between the operating thermal fluid and the device, (see section 1.3.1, Chapter-1). On the other hand, the increase in pressure drop in a microchannel is believed to considerably lead to a considerable rise in pumping power. Moreover, proper consideration should be given to the so-called "scaling effects" since they may influence fluid flow and heat transfer characteristics through the microchannel, [119].

The literature highlights a few studies on convection heat transfer, concerning the performance of microchannels and their effectiveness regarding heat transfer enhancement [120], [121], [122], [123] and [124]. The studies have referred that, in contrast to conventional channels, in microchannels factors such as shape, viscous heating, dependent-temperature thermophysical properties and entrance region can't be neglected when studying heat transfer and fluid flow [26]. Moreover, as the hydraulic diameter of the channel decreases, the effects of thermophysical property variation and viscous dissipation increases and significantly affect the thermal and rheological behaviour of fluid flow through the microchannels, affecting heat transfer phenomena [125] and [126].

As previously stated, numerical methods do present themselves as advantageous solutions to exploit hydraulic and heat transfer phenomena, nevertheless it is mandatory to use accurate and validated numerical models to investigate microscale heat transfer systems. Gad-el-hak et al. [127] have studied the physics of fluid flow in microdevices, presenting several issues to be considered in terms of the validation of some assumptions such as continuum fluid, applying Navier-Stokes equations and boundary conditions. Furthermore, some researchers have studied fluid flow through microchannels experimentally, theoretically and numerically, as it will be reported further ahead.

3.3 NEWTONIAN FLUID FLOW IN MICROCHANNELS

The use of convective heat transfer of fluid flow in microchannels to cool microdevices has been recommended by several researchers which lead to the use of different approaches (both numerical and theoretical) besides the experimental

method for further investigations on the fluid flow and heat transfer phenomena through a microchannel.

3.3.1 Surface roughness effect and Transition Reynolds number.

The fluid flow conditions such as the smooth and rough surface of the microtubes or the transition Reynolds number from the laminar regime of the fluid flow into the turbulent regime were mentioned in the literature, as summarised in Table 3-1.

Li et al.[128] studied water flow in glass microtubes (79.9 < D < 166.3 μm), silicon microtubes (100.3 < D < 205.3 μm), and stainless steel microtubes (128.8 < D < 179.8 μm) with Reynolds number below 4000. The results have shown that in the case of using glass and silicon microtubes, friction factor (f) and transition Reynolds numbers were in good agreement with the classical theoretical predictions, (i.e. where $f = 64/Re$ for the friction factor and Re=2300 for the transition Reynolds number). For rough stainless-steel microtubes, the transition Reynolds number was Re= 1700-1900 and friction factors were 15–37% higher than the theoretical predictions ($64/Re$) in tubes with relatively smaller diameters, while a rough agreement was observed for larger tubes. The measured relative roughness was less than 0.1% for glass and silicon microtubes and 3.3–3.9% for stainless steel microtubes.

Moreover, Thompson et al. [129] measured the local velocities of the hydrodynamic developing flow in a circular microtube with an inner diameter of 180 μm. For this, micro-molecular tagging velocimetry (μMTV) was used for different Reynolds numbers of 60, 100, 140, 290, and 350. The results suggested the formation of a *vena contracta* for the locally turbulent flow and unsteady laminar flow, which is different from a macroscale experiment or numerical simulation, where the existence of a *vena contracta* in the laminar regime is typically not observed for Re <500. Along the microtube, the velocity profile developed to a parabolic distribution with a relatively constant fluid in the near wall region. Despite the existence of the *vena contracta*, the hydrodynamic development length in the microtube can be calculated approximately by ($x = 0.05 \cdot D \cdot Re$) which is like the macroscale.

Table 3-1: Transition Reynolds number in microchannels in some previous studies.

Researchers	Diameter (μm)	Length (mm)	Smooth/ rough	Fluid	Transition Re	Considered parameter
Wu et al.[130]	25.9 - 291	-	smooth	water	1500-2000	Nu number and Friction factor
Li et al.[128]	79-206	14-119	smooth rough	water	2000-2300 1700-1900	Friction factor
Yang et al.[131]	502-4010	200-1000	smooth	water	2200	Friction factor
Maynes et al. [132]	705	141.9	smooth	water	2200	Friction factor
Mala et al.[133]	50-254	55-88	smooth	water	1000-1500	Pressure gradient
Kandliker et al.[134]	620-1067	-	Rough	water	2000	Friction factor
Sharp et al.[135]	50-247	-	smooth	water	1800-2200	Friction factor

It can be depicted from the reviewed studies above, and summarised in Table 3-1, that the transition from laminar to turbulent flow in microchannels starts much earlier than it occurs in the conventional case (at macroscale case). The latter is believed to be related to the microtube diameter and its material since for smaller diameters and rough tubes, transition regime does seem to occur earlier. It may be worth noting, for future investigation purposes, that Reynolds numbers less than 1500 (see Table 3-1) establish the lower limit for the laminar regime on a microchannel.

3.3.2 Viscous dissipation effect

A few other studies have mentioned the viscous dissipation in their work concerning fluid flow in microchannels. Morini [25] highlighted the significant scaling effects particularly viscous dissipation on the heat transfer and friction factor of fluid flow in microchannels. The results referred to the role of viscous dissipation, conjugate heat transfer, and entrance effects (the effects of the thermal developing region) on the mean value of the Nusselt number. In addition, the impacts of scaling effects were changed when the working fluid or the microchannel geometry were modified.

Also, Koo et al. [136] studied numerically the fluid flow of water, methanol and isopropanol, in different conduit geometries. The results have shown that viscous dissipation was a strong function of the channel aspect ratio, Reynolds number, Eckert number, Prandtl number and conduit hydraulic diameter. Especially, for water flow in a tube with D_h < 50 μm, viscous dissipation became significant and should be considered.

However, CFD tools provide an option for considering the viscous dissipation factor in the energy equation, by an additional component. The latter has been described previously in section 1.3.6.2. Therefore, viscous dissipation is modelled and considered in numerical methodology here adopted and further discussed ahead.

3.3.3 Microchannels numerical modelling analysis

The comparison between the obtained numerical or theoretical results with experimental data is fundamental to validate a numerical model or to verify and understand the fluid flow behaviour. It should be mentioned, for example, the experimental investigation performed by Lelea et al. [74] on the fluid flow of distilled water in stainless steel microtubes with diameters of 100, 300 and 500 μm at Re = 50–800. The experimental heat transfer and fluid flow characteristics were compared with numerical and theoretical results in terms of Nusselt number and friction constant. Where Nu = 4.36 and Shah equation were used for the theoretical solution of Nusselt number, and the constant value of 64 for the friction factor multiplied by Re number ($f \cdot Re = 64$). The results refer that both conventional theories and numerical method are applicable for water flow through microchannel of the above sizes, presented a reasonable agreement with a deviation lower than the experimental uncertainty of the measurements (<8.9% for friction constant and <10% for heat balance).

Gao et al. [137] investigated the fluid flow of water through microchannels with diameters ranging between 200-2000 μm and Reynolds number ranging between 40 and 8000. The experimental results on Nusselt number were compared with the theoretical solution of Shah and London for laminar flow and have demonstrated a deviation of Nu_{avg}/Nu_{th}=0.88 (12%), where Nu_{th} is the

theoretical value calculated by Shah Equation. The deviation increased with the reduction of the channel size up to Nu_{avge}/Nu_{th}=0.4 (60%).

Also, Hetsroni et al. [138] have discussed several aspects of laminar flow in microchannels, such as pressure drop and transition from laminar to turbulent flow. The data from the literature have been collected and analysed for the circular, rectangle, triangular and trapezoidal microchannels with hydrodynamic diameters ranging from 15 μm to 4010 μm. The authors present a maximum deviation up to 12% when the theoretical results are compared with experimental results in terms of Poiseuille number (*Po*). The theoretical solution of Poiseuille number was applied by $Po = \lambda \cdot Re$, where λ is a constant defined by the microchannel shape. It should be mentioned that the uncertainty of the experimental results is not mentioned by Hetsroni et al. [138]. Moreover, the authors did not address the theoretical correlations for predicting the heat transfer parameters.

Harms et al. [139] conducted an experimental study for deionized water flow through rectangular microchannels with 1923 and 404 μm for Reynolds number ranging from 173 to 12900. They have tested a single channel system and a multiple one. The theoretical results were significantly lower than the experimental results in terms of Nusselt number in laminar flow, while closer results were obtained in terms of friction factor. However, the experimental uncertainties were 5.5% for Nusselt number and 8.5% for the friction factor. The significant deviations can clearly be noticed in their presented figures, despite not being quantified.

Bucci et al. [140], studied water flow through stainless steel microchannels with diameters of 172, 290 and 520 μm for Reynolds number ranging from 200 to 6000. The results were discussed in terms of friction factor and Nusselt number. At Reynolds number larger than 1000, laminar flow, the Nusselt number results of Hausen correlation have shown a deviation of 17% from the experimental data for the microchannel with the diameter of 520 μm, and deviation increased by up to 55% for a diameter of 172 μm. Furthermore, the experimental results of the friction factor agree with the results of Hagen-Poiseuille correlation, particularly for Reynolds number lower than 1000. The authors reported that the uncertainty

of the experiments for Nusselt number was equal to 22.25% and for friction factor was equal to 8.36%.

Most of the previously presented studies have reported a respectable deviation between the conventional theoretical results and the experimental data when the microchannels are used. This confirmed that microchannel fluid flows and heat transfer phenomena may not be explained by the conventional theories of the macro-scale channels, which are based on hypotheses such as**:** constant thermophysical properties of the fluid, negligible axial heat conduction and negligible viscous heating [2] and [90]. The latter leads to inconsistencies between the experimental and theoretical results of heat transfer and fluid flow through the microchannel, due to the dimensional and the near wall effects due to the large surface-to-volume ratio in these systems.

Moreover, several studies have focused on the validity of the numerical approach, for instance, an experimental study carried out by Wu et al. [130] for fluid flow of deionized water through smooth silicon microchannels with triangular and trapezoid cross-sections for the hydraulic diameter ranged from 25.9 to 291 μm. The experimental results were compared with the numerical results of Ma et al. [141] in terms of friction factor. The results confirmed that the Navier–Stokes equations are still valid for the laminar flow of deionized water in smooth microchannel having a hydraulic diameter as small as 25.9 μm, since the maximum relative deviation obtained was 10.9%, well within the experimental uncertainty, which was 11%. Moreover, for smooth channels with hydraulic diameters of 103.4–291 μm, transition from laminar to turbulent flow occurred at Re = 1500–2000.

Qu et al. [142] studied both experimentally and numerically heat transfer and fluid flow of water through a microchannel heat sink. The heat sink consisted of an array of rectangular micro-channels 231 μm wide and 713 μm deep. Each microchannel has a width of 57 μm and a depth of 180 μm, and are separated by a 43 μm wall. The Reynolds number ranged from 139 to 1672. A numerical code based on the finite difference method and the SIMPLE algorithm is developed to solve the governing equations. The numerical method includes Navier–Stokes and energy equations with some assumptions as follows: steady fluid flow and heat transfer, incompressible fluid, laminar flow, no-slip boundary condition, constant

fluid properties, negligible radiation heat transfer, negligible superimposed natural convective heat transfer. The numerical model was validated by comparing the numerical results with available experimental data in the literature and a good agreement was observed. Moreover, their experimental and numerical results achieved a satisfying agreement for most of the tests with a deviation within the experimental uncertainty of the study, outlined by error bars in the figures (they didn't report specific values). Although, one exception occurred for the inlet thermal resistance parameter at lower Reynolds numbers which was explained by the heat loss during the experiments which is more significant for small Reynolds numbers, because of the weak convective heat transfer of the fluid.

Tiselj et al. [143] evaluated experimentally and numerically heat transfer characteristics of water flowing through triangular silicon micro-channels with a hydraulic diameter of 160 μm in the range of Reynolds number 3.2 to 64. The results have shown an acceptable agreement between the experimental results and the numerical results in terms of fluid temperature. The study confirmed the validity of using Navier–Stokes and energy equations to describe the heat transfer of the fluid flow in microchannels as a common basis. It should be referred that the authors didn't present the values of the deviations and the experimental uncertainty.

A numerical investigation carried out by Lee et al. [144] on the laminar flow of water through rectangular microchannels with a hydraulic diameter between 318-903 μm for Reynolds number ranging between 300 and 3500. The authors found that numerical predictions based on a classical continuum approach are consistent with the experimental data with an average deviation of 5% which is less than the revealed experimental uncertainties ranging from 6% to 17%. The latter happened when the entrance and boundary conditions imposed in the experiment are accurately implemented in the simulation.

Table 3-2: Summary of some investigations studying the validity of using a numerical approach for microscale fluid flow.

Researchers	D_h (μm) Re	Fluid	Considered parameter	Deviation from experimental data
Qu et al. [142]	D_h=114.3 Re=140 - 1400	water	Nu number, Temperature, thermal resistance.	The deviation is within the experimental uncertainty.
Wu et al. [130]	D_h=103.4–291 Laminar	water	Nu number and Friction factor	A deviation of 10.9%, set within the experimental uncertainty <11%.
Lelea et al. [145]	D_h=100- 500 Re=50–800.	water	Nu number and Friction factor	A deviation was lower than the experimental uncertainty <10%.
Tiselj et al. [143]	D_h=160 Re =3.2–64.	water	Nu number and fluid temperature	-
Lee et al. [144]	D_h=318-903 Re=300-3500	water	Nu number	A deviation of 5% less than the experimental uncertainty <6%.

From the studies referred to above and briefly summarised in Table 3.2, one can conclude that the numerical approach based on the Navier–Stokes and energy equations with proper boundary conditions and acceptable assumptions is an appropriate option and it is valid for fluid flow and heat transfer investigations in a microchannel. Moreover, the presented comparative studies in the literature have investigated several fluid flow conditions (Re= 4-4000) in several microchannel geometries (D_i= 1-4010 μm) and materials (glass, nickel, copper and stainless steel) providing further insight and capabilities worth exploiting when imposing boundary conditions on the numerical approach. The authors confirmed in the presented studies above that the Navier–Stokes and energy equations can be applied for fluid flow through microchannels with a hydraulic diameter higher than 25.9 μm.

From sections 3.3.1 and 3.3.2, some conditions are clarified that must be considered when establishing a numerical approach for laminar flow in a microchannel, mainly the transition Reynolds number (Re< 1500) and the viscous dissipation (viscous heating). Also, an analysis has been carried out on the numerical models and assumptions used in the literature (section 3.3.3),

establishing good guidance for the implementation of a proper numerical methodology for the investigations into the subject, which are described in the following section.

3.4 Microchannel numerical model development and validation.

This section suggests a methodology to build a proper numerical approach for fluid flow through a microchannel, based on the previous investigations in the literature that have been discussed in section 3.3. Moreover, concerning the numerical model validation, therefore, some of the previous experimental studies (from literature) are reproduced numerically, following the suggested methodology and required assumptions.

3.4.1 Mathematical modelling

In order to reproduce numerically the experimental studies of fluid flow through microchannels, the numerical approach model is achieved using computational fluid dynamics (CFD) tools, mainly ANSYS-FLUENT version 18.2 environment [97]. The methodology for building the numerical approach is chosen according to the physics problem of the selected experimental study, following the steps and suggestions of the computational fluid dynamics (CFD) theory (See section 1.3.6, Chapter-1) and the available literature on the subject (Section 3.3.3, Chapter-3).

3.4.2 Assumptions and methodology

In order to build the numerical model, 2D Navier–Stokes and energy equations are used to describe the fluid flow and heat transfer, including the viscous dissipation effect in the simulations. Therefore, the finite volume method (FVM) is used to discretize the governing equations and the SIMPLE algorithm is chosen to couple pressure and velocity. Also, a second order upwind method is used in order to include the convective and diffusive terms. In addition, a pressure-based solver is implemented. The convergence criteria are set such that

the residual errors for continuity, momentum and energy are reduced to less than 10^{-6}.

Moreover, some assumptions were considered for the current simulations as following: (1) incompressible fluid; (2) continuum fluid flow and steady state; (2) laminar flow; (3) neglected radiation heat transfer; (4) neglected body force ; (5) neglected electrostatic force; (6) no-slip boundary condition at the wall; (7) fluid variable thermophysical properties (8) constant and uniform wall heat flux.

In this study, the numerical approaches take into consideration the variable thermophysical properties of the fluid. Therefore, third-order polynomial fitting curves of the experimental data [146] and [147] are used to obtain the correlations for the thermal conductivity (Eq. 3-1) and viscosity (Eq. 3-2) dependent-temperature of distilled water. Thus, the correlations of the conductivity and viscosity are as following:

$$k = -1.470E\text{-}07\ T^3 + 1.275E\text{-}04\ T^2 - 3.531E\text{-}02\ T + 3.701E+00 \qquad \text{Eq. 3-1}$$

$$\mu = -5.098E\text{-}09\ T^3 + 4.955E\text{-}06\ T^2 - 1.6156E\text{-}03\ T + 1.772E\text{-}01 \qquad \text{Eq. 3-2}$$

3.4.3 Mesh optimisation

The mesh optimisation and numerical results-independent process were carried out individually for each case of the reproduced studies. The number of nodes in axial and radial directions was changed according to the geometry of the tube in each case, and four different mesh distributions for each case were examined in comparison with the corresponding experimental data. The simulations have been done for the same test section and fluid flow conditions of the experimental setup. The mesh dependency of the numerical results is evaluated, and the simulations with increasing mesh resolution were carried out and the obtained numerical results were compared. The optimal mesh is chosen so that it achieves results-independency and good agreement with the experimental data, being a trade-off between accuracy and computational cost

(minimum number of nodes). Moreover, the nodes number are intensified near the microchannel wall where the velocity and temperature gradients are significant.

3.4.4 The validation of the numerical methodology

In this section, in order to validate the numerical model, the numerical results are compared with the experimental data of some literature studies. The chosen studies had investigated the fluid flow through a microchannel with different tube geometries and fluid flow conditions. The results are presented for each selected research as follows:

Comparison with the work of Zhuo et al. [148]:

The laminar flow and heat transfer characteristics of deionized water were investigated by Zhuo et al. [148] through smooth fused silica and rough stainless steel microtubes with the hydraulic diameters of 50–100 μm and 373–1570 μm, respectively. The Reynolds numbers ranged from 20 to 2400.

In this study, the numerical simulation is carried out for water flow through a stainless steel microtube with an inner diameter of 373μm, outlet diameter of 670 μm and length of 270mm at a Reynold number of 200, under wall heat flux condition of 36050 W/m^2. Also, the suitable mesh was selected as 756126. The numerical results of Nusselt number are compared with the experimental data along the tube and an acceptable agreement is observed with an average deviation of 5 %, considering dependent-temperature thermophysical properties (Num-variable), Fig. 3-1. It should be noted that a higher average deviation of 17% is observed when the simulation is repeated considering independent-temperature thermophysical properties (Num-constant, Fig. 3-1) for water, highlighting the significant impact of dependent-temperature properties on heat transfer and fluid flow through a microchannel, even at low Reynolds number (Re=200). The latter can be explained by the significant effect of the gradient viscosity and gradient conductivity on the fluid velocity and temperature profiles, particularly near the wall where the heat flux is applied. Thus, this factor is taken into account for the next simulations.

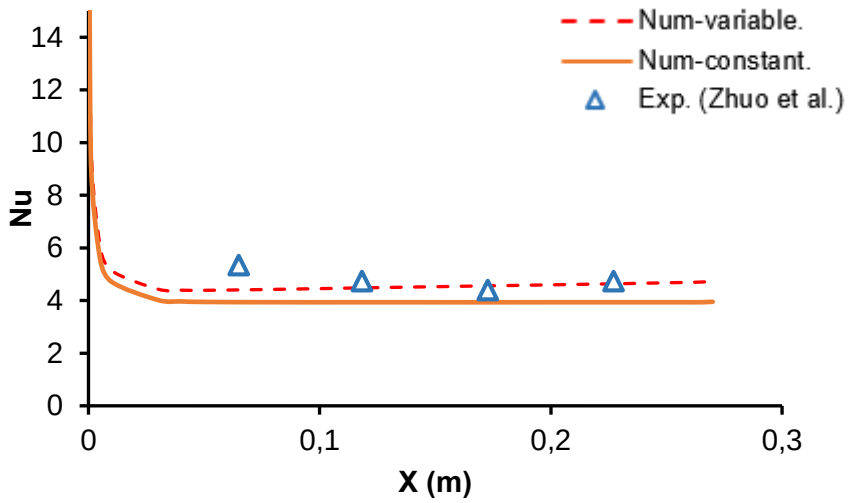

Fig. 3-1: Local distribution of Nu number of the tube (Di=373µm) at Re=200.

Comparison with the work of Mala et al. [133]:

Mala et al. [133] have investigated experimentally the water flow in microchannels with diameters ranging from 50 to 254 µm. The experimental results were compared with the results of the proposed conventional theory (Poiseuille equation for pressure drop), showing a good agreement for the large microtube diameters (100-254 µm). Also, the fluid flow behaviour was affected by the tube material. The fluid flow in the stainless Steel microtube caused less pressure drop gradient (ΔP/ΔL) values than Fused Silica due to the higher roughness of Fused Silica tube. The authors referred to the use of a numerical approach (Naiver-Stocks equations) for non-laminar flow and roughness tubes instead of conventional theory equations.

Therefore, in this study, a stainless-steel tube of 130 µm diameter and 0.01 length was chosen for Reynolds number ranging between 1000-1500 for the numerical simulations. The Mesh of 504126 nodes was chosen. The results are in accordance with those obtained experimentally and a maximum deviation of 7% is observed, Fig. 3-2. The deviation of the numerical results decreases with the reduction of the Reynolds number.

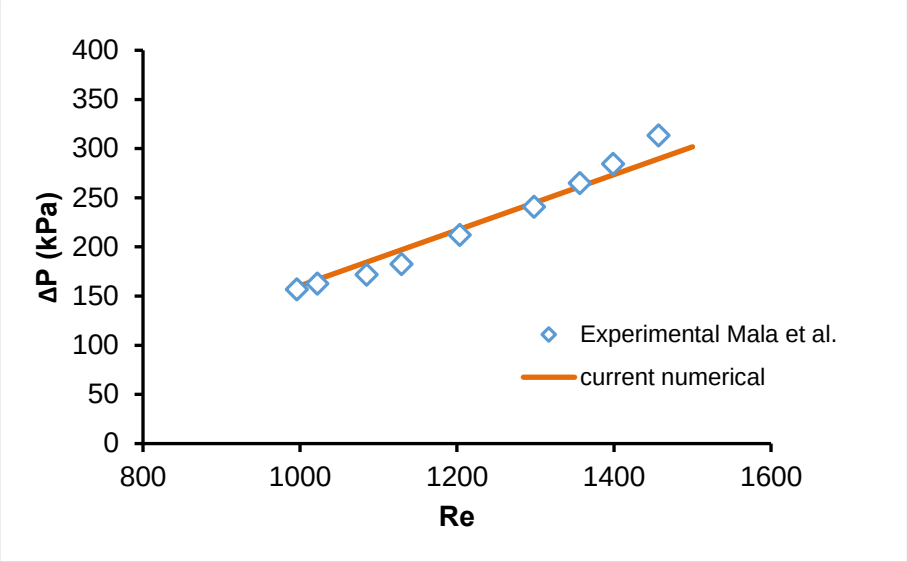

Fig. 3-2: Pressure drop (kPa) of water flow in microtube (D_i=130µm) as a function of Re number.

Comparison with the work of Sara et al. [149]:

Sara et al. [149] have investigated the fluid flow of distilled water in a microtube of 200 µm diameter and 0.0496 m length for Reynolds number ranging between 100-1100. The material of the tube was nickel.

In this study, the numerical model is built, and the suitable mesh is chosen as 567126. The results show a good agreement between the numerical results and the experimental data, with only one exception for Re=312, as presented in Fig. 3-3.

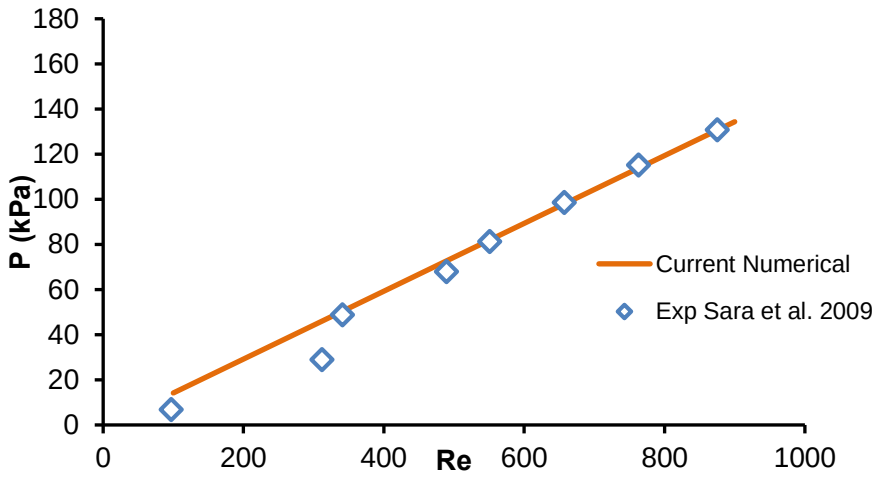

Fig. 3-3: Pressure drop (kPa) of water flow in microtube (D_i=200µm) as a function of Re number.

Comparison with the work of Lelea et al. [74]:

Lelea et al. [74] have carried out an experimental and numerical investigation on heat transfer and fluid flow in microchannels of 0.1, 0.3 and 0.5 mm diameters and for laminar flow with Re number range up to 800. The working fluid was distilled water and the tube material was stainless steel.

In this study, the numerical model is built for a tube diameter of 0.3 mm and the suitable mesh is chosen to be of 579726 nodes. The investigation carried out for the case of fluid flow without heat flux conditions (Q=0 W) and for the case of applying uniform heat flux of q=13409 W/m^2 (Q=2 W). The results are evaluated and compared with the experimentally obtained ones, for Nusselt number and friction constant ($f \cdot Re$). It is observed an acceptable agreement between the numerical results and the experimental data with an average deviation of 2% for friction constant, and with an average deviation of 5% for Nusselt number, as presented in Fig. 3-4 and Fig. 3-5.

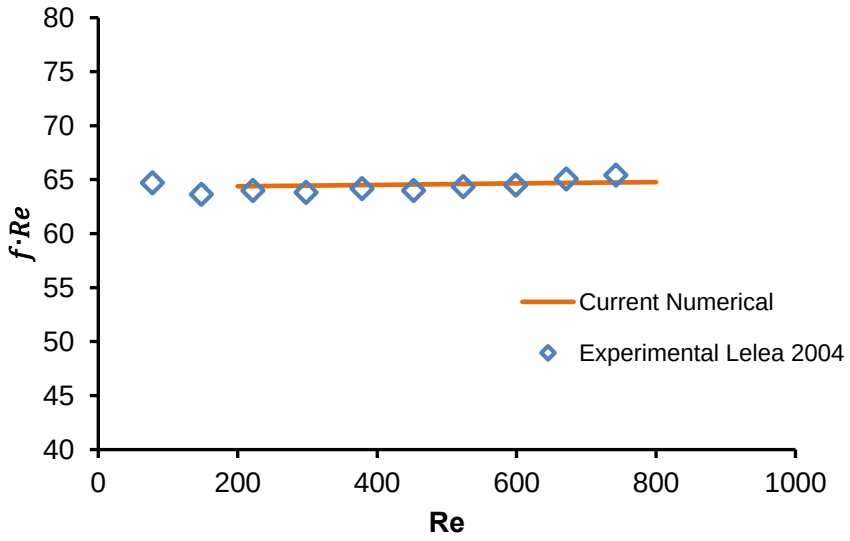

Fig. 3-4: Friction constant ($f \cdot Re$) of water flow in microtube as a function of Re number.

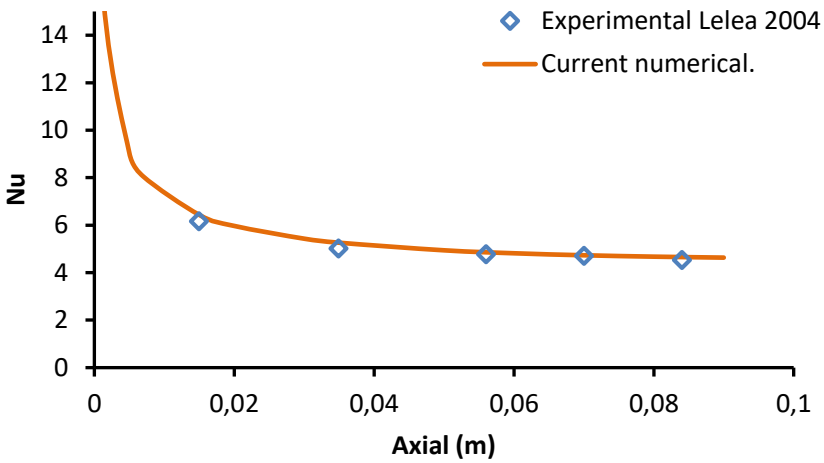

Fig. 3-5: Local Nusselt number of water flow in microtube as a function of the axial length of the tube for electrical power of Q=2 W and Re= 774.

The validated method and assumptions that have been used in the numerical approach referred to above are briefly summarized as follows:

- (2D) axisymmetric geometry (D_h>59 μm)
- The radial direction of the mesh has 80-150 nodes according to the diameter. While the axial direction various according to the tube length.
- Laminar-viscous Heating (Re<1500).
- Navier–Stokes and energy equations
- Single-phase, Incompressible and steady state conditions.
- Variable-thermophysical properties.
- Radiation heat transfer is neglected.
- The body force is neglected.
- The electrostatic force is neglected.
- Pressure-based solver.
- Second order upwind for the discretization.
- SIMPLE algorithm.
- The residual errors are less than 10^{-6}.

Moreover, the numerical results and the details of the reproduced studies referred to above are briefly summarised in Table 3-3. As a result, it is believed that the proposed numerical methodology in the sections 3.4.1, 3.4.2 and 3.4.3 for conventional fluids (water) in laminar flow through microchannels has been

conveniently validated, providing guidance for the next intended studies of nanofluids flow through a microchannel.

Table 3-3: Summary of the reproduced studies for heat transfer and pressure drop of single-phase Laminar fluid flow in microchannels.

Researcher	Fluid	Tube	Re	Q (W) T (K)	Considered parameters	Results
Zhuo et al.[148]	Water	D_i=373 µm L=270mm L/D=724 stainless steel	Re=200	Q=12W T_{in}=293K	Nu number.	5% deviation
Mala et al.[133]	Water	D_i= 130µm L=0.01m stainless steel	Re=1000-1500	Q=0 W T_{in}=293K	pressure drops.	7% deviation
Sara et al.[149]	water	Di=200µm L=0.0496 m nickel	Re=100-900	Q=0 W T_{in}=293K	pressure drops.	4% deviation
Lelea et al.[74]	water	D_i=300µm L=95mm stainless steel	1- Re=774 2-Re=200-800	1-Q=2W T_{in}=293K 2- Q=0W T_{in}=293K	Nu number and friction constant.	2% Deviation for friction coefficient, and 5% for Nu number.

Turbulent flow

In this section, the turbulent flow regime of water in the microchannel is numerically studied in order to determine the proper turbulent model for such numerical approach. In other words, a comparison between the provided turbulent models in ANSYS-Fluent (see section 1.3.6.2.2) against available experimental data in the literature is examined.

Comparison with the work of Adamas et al.[150]:

An experimental study of turbulent flows through microchannels was carried out by Adams et al. [150]. The operating fluid was distilled water flowing through copper microchannels with diameters between 0.102-1.09 mm. The research referred to higher experimental results than those obtained from the related conventional correlation (Gnielinski correlation) in terms of Nusselt

number. The deviation between the experimental and Gnielinski correlation results was higher for the smaller tube diameter.

In this section, a numerical approach is carried out using ANSYS-FLUENT version 18.2 environment [97] and the proposed methodology in section 3.4 to reproduce the experimental work of Adams et al. [150] numerically and compare the obtained results with the correlated experimental data. Thus, the simulations are carried out for an axisymmetric steady, forced turbulent convective flow of water through a horizontal circular tube having an inner diameter of 760 μm and a length of 50.8 mm, using the governing equations of single-phase turbulent flow (see section 1.3.6.2.2, Chapter-1) and the finite volume method. The SIMPLE algorithm procedure has been used for the velocity-pressure coupling. The second order upwind scheme has been applied to discretized momentum, turbulent kinetic energy and turbulence dissipation ratio equations. The mesh independency has been studied and the mesh of 513140 nodes has been adopted.

Moreover, to achieve the best results in turbulent flow, several turbulent models such as K'-ε models (Standard, realizable and RNG), K'-ω models (SST and Standard) and Reynolds Stress model, have been investigated and compared in terms of Nusselt number, Fig. 3-6. Among the latter, results show that standard and Realizable K'-ε model provides well agreement with the experimental data, particularly for low Reynolds number, with better results for Realizable K'-ε model. Furthermore, the comparison between the obtained results by several turbulent models against experimental data have shown a maximum deviation at the highest Reynolds number (14000) as follows: (33%) for K'-ε RNG results, (16.5%) for K'-ω Standard results, (15%) for K-ω sst results, (14%) for Reynolds Stress results, of (9.5 %) for K'-ε standard results and (7.5 %) for K'-ε Realizable results. Moreover, the computational time of the simulations in different models varied slightly. However, the most relevant result points out that K'-ε Realizable turbulent model correlates better with the experimental data. Thus, it is selected for further turbulent flow investigations into the subject of fluid flow and heat transfer in microchannels.

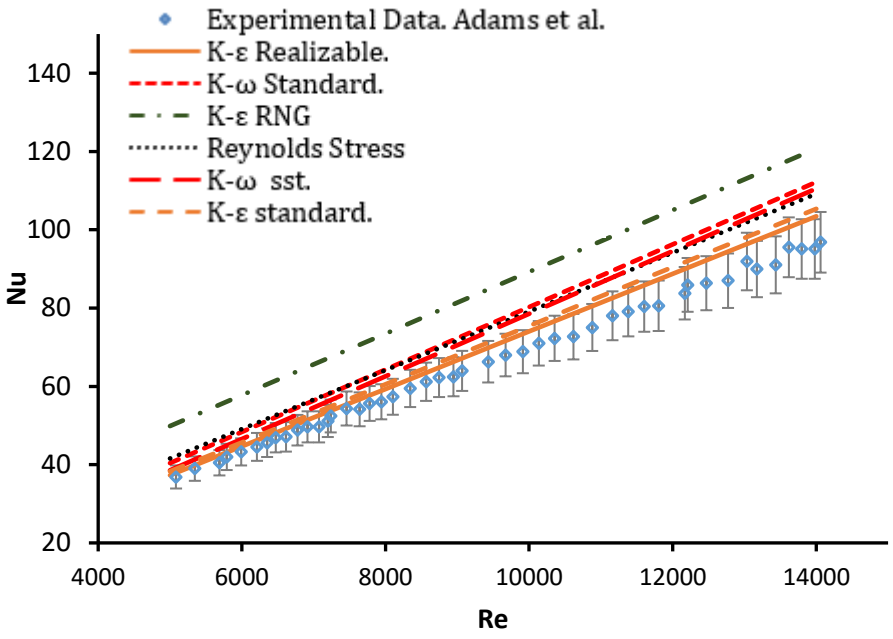

Fig. 3-6: The numerical results of several turbulence models in terms of Nusselt number as a function of Reynolds number.

3.5 CHAPTER CONCLUSION

In this chapter, several studies on conventional fluid flow and heat transfer through microchannels have been reviewed for a better understanding of the overall phenomena. The experimental, analytical and numerical methods in the field have been analysed by reviewing the literature. This allowed defining a proper methodology for a numerical investigation considering the microscale effects, mainly: dependent-temperature fluid properties, viscous heating and transition Reynolds number. The numerical methodology and acceptable assumptions have been established. The latter was then further used for reproducing numerically several experimental researches (different microchannel geometries and different operating conditions), providing confidence and establishing a proper validated methodology suitable to be used in future numerical investigations. Namely, the intended study of nanofluids flow through microchannels, presented in the following chapter.

CHAPTER 4- HEAT TRANSFER BEHAVIOUR OF MWCNTS NANOFLUIDS IN MICROCHANNELS

4.1 CHAPTER SYNTHESIS

In this chapter, a numerical approach to investigate heat transfer and fluid flow of MWCNTs nanofluids (0.25-1.5 vol%) as single-phase fluids under a constant heat flux boundary condition through microchannels is presented. Since the thermophysical properties (Thermal conductivity, viscosity, density and specific heat) characterize the single-phase fluids, the several MWCNTs nanofluids samples (In terms of the base fluid, particle concentration and particle geometry) are being modelled numerically depending on their thermophysical properties, mainly conductivity and viscosity. Then, these nanofluid samples are divided into four groups in terms of thermal diffusivity and viscosity. Each group is represented by one fluid, characterized by the average thermophysical properties.

The numerical code validation of a CFD approach based on the finite volume method using 2D Navier–Stokes and energy equations is conducted for CNTs nanofluids flow through microchannel by reproducing some available experimental researches. Then, the fully developed condition of the flow is studied and the geometric configuration of the test section is selected.

The MWCNTs nanofluids behaviour through the microchannel is evaluated by assessing the respective heat transfer coefficient, Nusselt number and pressure drop in comparison with that of the base fluid mixture. Moreover, the study includes the assessment of the above-referred parameters as a function of the Reynolds number and fluid velocity, establishing a detailed discussion regarding the mechanisms of heat transfer and flow characteristics of MWCNTs nanofluids in microchannels. From the obtained results, it will be possible to establish the relationship between the addition of nanoparticles to a base fluid and the associated heat transfer enhancement with extensive investigations on the case.

4.2 INTRODUCTION

As previously stated, the micro heat transfer systems depend significantly on the advantages of thermal fluids. It becomes an urgent need to use developed thermal fluids such as nanofluids instead of conventional fluids (water-ethylene glycol or oil) to intensify the heat transfer process via micro heat exchangers [3]. Recently, several investigations have been carried out on nanofluids for the potential application in micro heat transfer systems. Also, CFD tools have been considerably implemented for such problems.

Salman et al. [151] have numerically investigated the laminar flow of nanofluids for various nanoparticles (Al_2O_3, CuO, SiO_2 and ZnO) suspended into ethylene glycol as a base fluid through a microtube has a diameter of 50 μm under a constant heat flux. The use of different sizes of nanoparticles (diameters of 25, 45, 65 and 85 nm) with different particle volume fractions (1-4 Vol%) for Reynolds number ranging between 10-1500 was examined. The numerical approach based on solving 2D Navier–Stokes and energy equations are by finite volume method (FVM) with the SIMPLE algorithm choose to couple pressure and velocity. The numerical approach was validated by comparing the results with the work of Li et al. [148] for distilled water flow at Reynolds number of 80 under uniform heat flux of 9000 W/m^2 in terms of Nusselt number and a good agreement was observed. The results presented an enhancement of Nusselt number in comparison with the base fluid for all nanoparticles types and the highest Nusselt number was achieved for SiO_2–EG nanofluid. Also, it was noticed a decrease in Nusselt number and pressure drop with the increase in the size of the nanoparticles.

Lelea [152] has investigated numerically the laminar flow of Al_2O_3/water nanofluid through a microchannel heat sink has a hydraulic diameter of 50 μm under a constant heat flux of 35 W/m^2 for different particle volume fraction (1-9 Vol%) and several particle sizes (dp = 13, 28 and 47 nm). Finite volume method with Navier–Stokes and energy equations and SIMPLER algorithm method is used for the numerical model which was validated by comparing with the results with the experimental work of Lee et al. [153] for Al_2O_3/water nanofluid flow through micro heat sink has a hydraulic diameter 474 μm and a good agreement

was observed. The results showed an enhancement in heat transfer coefficient for nanofluid which increases with the increase of particle volume fraction and decreases with the increase of particle's diameter.

Sajadifar et al. [154] have studied numerically Laminar flow of non-Newtonian (pseudo-thinning plastic) nanofluid through a microtube has a diameter of 0.2 mm. The diameter of the (CMC)–Aluminium oxide nanoparticles is 25 nm. The validation of the numerical model was achieved by comparing the results with numerical work of Raisi et al [104] and with numerical work of Keshavarz et al.[155] and Akbari et al.[156] for nanofluids.

Jung et al [157] have studied experimentally Al_2O_3 nanofluids flow in rectangular microchannels have the dimensions of 50 * 50, 50 * 100 and 100 *100 μm^2 (Width*Hight) with 15 mm length. The nanoparticles have a diameter of 170 nm. The results showed that the convective heat transfer coefficient increased up to 32% in comparison with distilled water (base fluid) at a volume fraction of 1.8 Vol%. Also, heat transfer coefficients of all nanofluids are greater than those of their base fluids. In small the microchannel (50 * 50 μm^2), the heat transfer coefficient of fluid flow is higher than those obtained at large microchannels.

Haghighi et al. [158] have investigated experimentally the laminar flow of nanofluids with different nanoparticles types (Al_2O_3, TiO_2 and CeO_2) at 9 Vol.% concentration through a single microchannel tube has a diameter of 0.5 mm and length of 30 cm. The diameters of the suspended particles are 10 nm for Al_2O_3, 20-30 for TiO_2 and 50-100 nm for CeO_2.

Also, Kamali et al. [100] studied numerically the laminar flow of aqueous 1% MWCNTs nanofluids as single phase and Non-Newtonian fluid in a horizontal tube has a diameter of 1.55mm under constant wall heat flux at Reynolds numbers of 600, 900 and 1200. Moreover, the numerical results were compared with the experimental results of P. Garg et al. [78] and showed a good agreement in terms of local heat transfer coefficient, rendering the numerical approach of such MWCNTs nanofluids even with non-Newtonian behaviour an important tool for analysing the fluid flow and heat transfer phenomena of CNTs nanofluids in microchannels.

Table 4-1: Summary of some investigations on heat transfer performance of nanofluids with a reference to the hydrodynamic diameter of the microchannel (D_h) and the nanoparticle size (d_p).

Research	**nanofluids**	**d_p/D_h**	**Tube D_h**	**Tube length**
Salman et al. [151], Numerical	(Al_2O_3, CuO, SiO_2 and ZnO) /EG d_p=25–85nm	5E-04 –17.0E-04	50 μm	0.025 cm
Lelea [152], Numerical	Al_2O_3/water d_p=13–47nm	2.6E-4– 9.4E-04	50 μm	4.48 cm
Sajadifar et al. [154], Numerical	Al_2O_3/water d_p=25nm	1.2E-04	200 μm	0.5 cm
Mehrdad et al.[159] Experimental	TiO_2, Al_2O_3/water d_p=20nm	0.4E-04	502 μm	12 cm
Jung et al [157], Experimental	Al_2O_3/water dp=170nm	15E-04–30.0E-04	56.4 μm	1.5 cm
Kamali et al. [100] Numerical.	MWCNTs/water d_p=10–20nm, l_p=0.5–40 μm	0.4-5.10E-04	1.55mm	91.44 cm

However, to the best of authors' knowledge, the investigations of heat transfer and fluid flow of CNTs nanofluids through a microchannel in literature is quite limited (See section 1.3.5 and 1.3.7, Chapter-1). Besides, there aren't an overall investigation on the used CNTs nanofluids regarding the thermophysical properties, particularly stability and shelf life for several particles' geometries. Moreover, some important concepts such as dependent-temperature thermophysical properties of the nanofluid haven't been considered.

The present work uses a strong database of tested and developed MWCNTs nanofluids in a wide range of volume fractions (φ=0.25, 0.5, 0.75, 1.0 and 1.5). The preparation, stability, conductivity and viscosity of the nanofluids were investigated and achieved in previous work [20], [106] and [21]. To the authors´ knowledge, the literature does not contain other work with similar data and methodology coverage. Consequently, a numerical investigation on MWCNTs nanofluids through a circular microchannel is an appropriate set-up to study the different flow conditions and the heat transfer behaviour. The results of this study are analysed in terms of Heat Transfer Coefficient, Nusselt number, pressure drop and Reynolds number, allowing to a widely understand for the possible

applications of microthermal systems such as electronics and micro-electro-mechanical systems (MEMS).

4.3 NUMERICAL MODEL

As it was mentioned, the validity of using CFD tools for heat transfer and fluid flow of nanofluid through microchannels was examined by several researchers, Table 4-1, achieving a good agreement with the experimental data. In another hand, this section presents an investigation of using CFD for CNTs nanofluids through microchannel by reproducing some available experimental researches. Therefore, the assumptions and methodology that have been validated for conventional fluids in chapter-3 (Section 3.4) are considered here for the current numerical model using 2D Navier–Stokes and energy equations. Thus, the single-phase approach model is numerically achieved using the finite volume method (FVM) that transforms the governing equations to a form of algebraic equations that can be solved numerically. Moreover, a second order upwind method is used in order to involve the convective and diffusive terms. Pressure and velocity were coupled using Semi-Implicit Method for Pressure-Linked Equations [SIMPLE]. The simulations are carried out in the software code, ANSYS-FLUENT version 19.0 environment [97]. In additions, the boundary conditions regarding Non-Newtonian fluids are considered here, particularly the velocity at the tube inlet and the viscosity correlation as a function of shear rate.

4.3.1 Entrance velocity conditions

As it is known, the Reynolds number is important to determine the flow regime type. In addition, it will be used in the current study to calculate the fluid velocity at the inlet of the tube. The generalized Reynolds number for Newtonian fluid flow through a pipe is depicted by Eq. 4-1,

$$R_e = \frac{\rho \cdot u \cdot D}{\mu} \qquad \text{Eq. 4-1}$$

Where ρ is the density of the fluid, μ is the viscosity of the fluid, D is the tube diameter and u is the fluid velocity.

In the case of Non-Newtonian fluids, particularly the Power Law fluids (shear thinning fluids), Reynolds number was firstly introduced by Metzner and Reed [160]. The viscosity of Power Law fluid is given by:

$$\mu = \frac{\tau_w}{\dot{\gamma}} = \frac{K \cdot \dot{\gamma}^n}{\dot{\gamma}} = K \cdot \dot{\gamma}^{n-1} \quad \text{Eq. 4-2}$$

Where K is the consistency index and n is the shear thinning index of the power law Non-newtonian fluid. Also, the viscosity can be defined based on the flow characteristic in a pipe as:

$$\mu = \frac{\tau_w}{8 \cdot u/D} \quad \text{Eq. 4-3}$$

Where, τ_w is the shear stress at the wall.

Therefore, by comparing the equations Eq. 4-2 and Eq. 4-3, the viscosity can be defined as:

$$\mu = K \cdot (\frac{8 \cdot u}{d})^{n-1} = \frac{K \cdot u^{n-1} \cdot D^{n-1}}{8^{1-n}} \quad \text{Eq. 4-4}$$

Therefore, Reynolds number for Non-Newtonian fluid flow (Shear-thinning fluids) can be found by Eq. 4-4 and Eq. 4-1:

$$R_e = \frac{\rho \cdot u^{2-n} \cdot D^n}{K \cdot 8^{n-1}} \quad \text{Eq. 4-5}$$

The last equation Eq. 4-5 can be minimized to the final form of Re number equation Eq. 4-6 [154], [161] and [162], as:

$$R_e = \frac{\rho \cdot u^{2-n} \cdot D^n}{K} \quad \text{Eq. 4-6}$$

Therefore, all the MWCNTs nanofluids in the following investigations are subjected to determine the velocity (u) of the various nanofluids at the inlet of the tube in terms of the diameter of the tube D, Reynolds number, the density ρ, the consistency index K and the power-law index n, as it is shown in Eq. 4-6.

4.3.2 Numerical code validation (Comparative study):

In order to investigate the using of CFD tools for CNTs nanofluids flow through a microchannel, the numerical results are compared with correlated experimental data and presented for each selected research as follows:

Comparison with the work of P. Garg et al. [78]:

P. Garg et al. [78] have studied experimentally the laminar flow of 1 wt.% MWCNTs aqueous nanofluids through circular microchannel has an inner diameter of 1.55 mm under constant heat flux (0.6 W/cm^2) boundary conditions. Furthermore, the authors studied several dispersing energies (ultrasonication) based on processing time and four samples were investigated regarding the viscosity, thermal conductivity, and the laminar convective heat transfer. The suspended carbon nanotubes have an average outside diameter of 10–20 nm and length of 0.5–40 μm. Moreover, the thermophysical properties of the fluid were analysed and a shear-thinning behaviour was observed. Also, the four samples achieved good stability for over 1 month without sedimentation. The results indicated an enhancement in thermal conductivity and heat transfer coefficient of 20% and 32%, respectively in comparison with the base fluid.

Therefore, in this study, the numerical simulations are carried out for Sample A and Sample B, since they represent the limitations of the lowest and highest value in terms of thermal conductivity and viscosity. Also, the fluid flow conditions are determined for Reynolds numbers 600 and 1200, with the calculated velocity (Table 4-4) and a temperature of 288 k at the tube inlet. A suitable mesh was selected as 509691 nodes. Furthermore, the simulations carried out considering dependent-temperature of thermal conductivity and the Non-Newtonian nanofluid behaviour for the viscosity correlation, by fitting the

correlated experimental data [78]. The results of the obtained correlations are compared with experimental data in Fig. 4-1 and Fig. 4-2, achieving a good agreement with a maximum deviation of 6%. Thus, the correlations of the conductivity and viscosity are presented in Table 4-2 and Table 4-3. Furthermore, the velocity at the tube inlet for Sample A and Sample B at each Re number can be determined as shown in Table 4-4.

Table 4-2: The parameters of the viscosity correlations for Sample A and Sample B nanofluids.

MWCNTs					
Equation	$\mu = K\dot{\gamma}^{1-n} exp\left[\alpha\left(\frac{1}{T-T_0}-\frac{1}{T_\alpha-T_0}\right)\right]$				
Parameters	***K***	**n**	$\boldsymbol{T_\alpha}$	α	
Sample A	1.903E-03	0.924	288 K	2000	Eq. 4-7
Sample B	1.77E-03	0.963	288 K	1600	Eq. 4-8

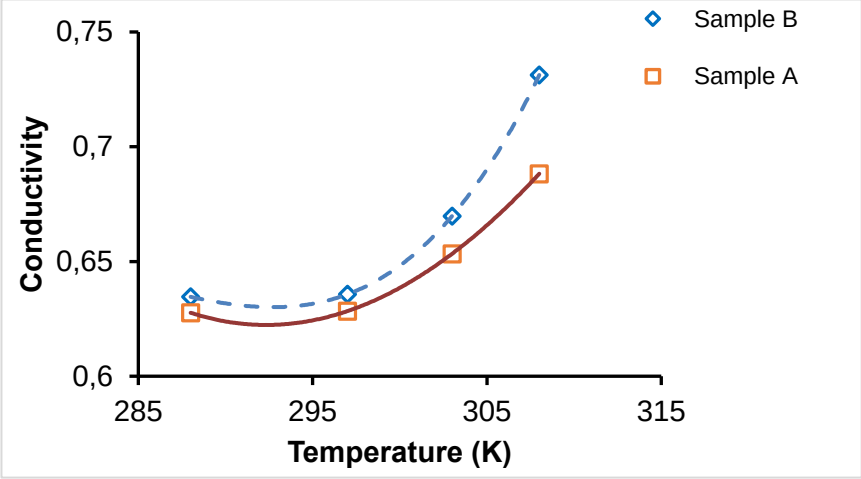

Fig. 4-1: The polynomial fitting curve of conductivity for the experimental data of Sample A and Sample B nanofluids.

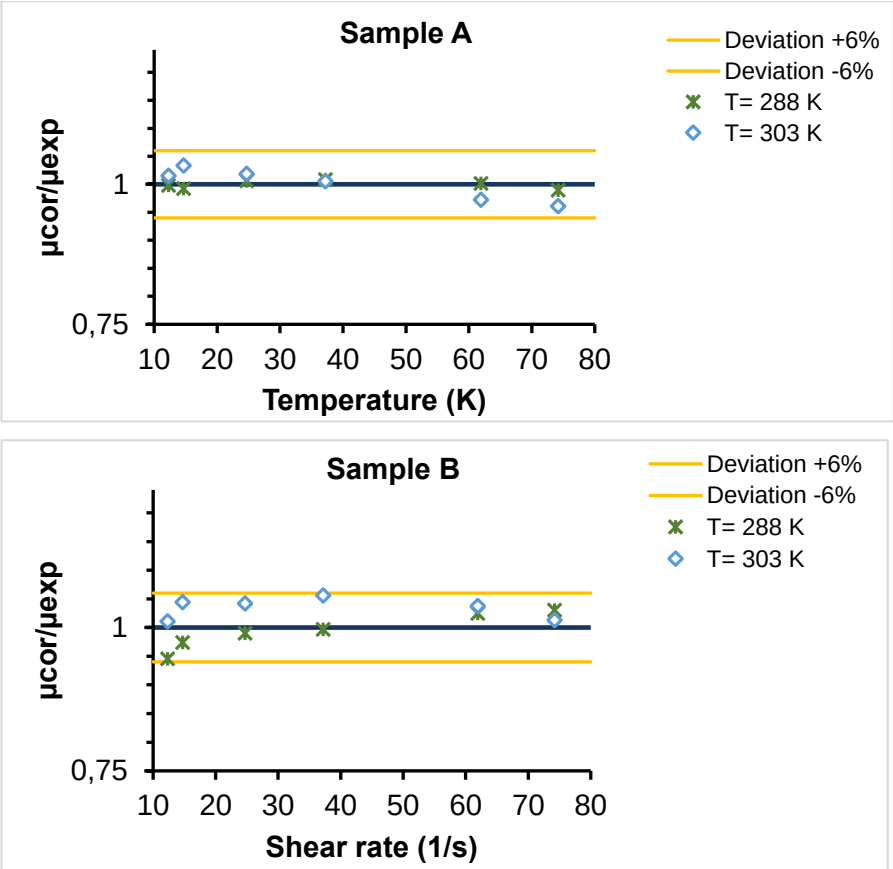

Fig. 4-2: The deviation of the proposed correlations of viscosity in comparison with experimental data of Sample B nanofluids.

Table 4-3: Thermal conductivity correlations.

	$k=aT^3+bT^2+cT+d$				
Parameters	**a**	**b**	**c**	**d**	
Sample A	-8.081E-07	9.896E-04	-3.714E-01	4.482E+01	Eq. 4-9
Sample B	1.152E-05	-9.864E-02	2.812E+00	-2.664E+02	Eq. 4-10

Table 4-4: The velocity of the nanofluids at the inlet of the tube.

u **m/s**		
Re	**1200**	**600**
Sample A	0.82	0.43
Sample B	0.97	0.50

The numerical results of heat transfer coefficient are compared with the experimental data along the tube, as shown in Fig. 4-3. A good agreement is observed with an average deviation of 6 %, and a maximum deviation of 14%, obtained for Sample-B at Re=1200. It should be mentioned that the uncertainty of their experimental results regarding the heat transfer coefficient is not presented by P. Garg et al. [78]. Therefore, if the uncertainty is higher or equal to 14%, the numerical results are quite accurate.

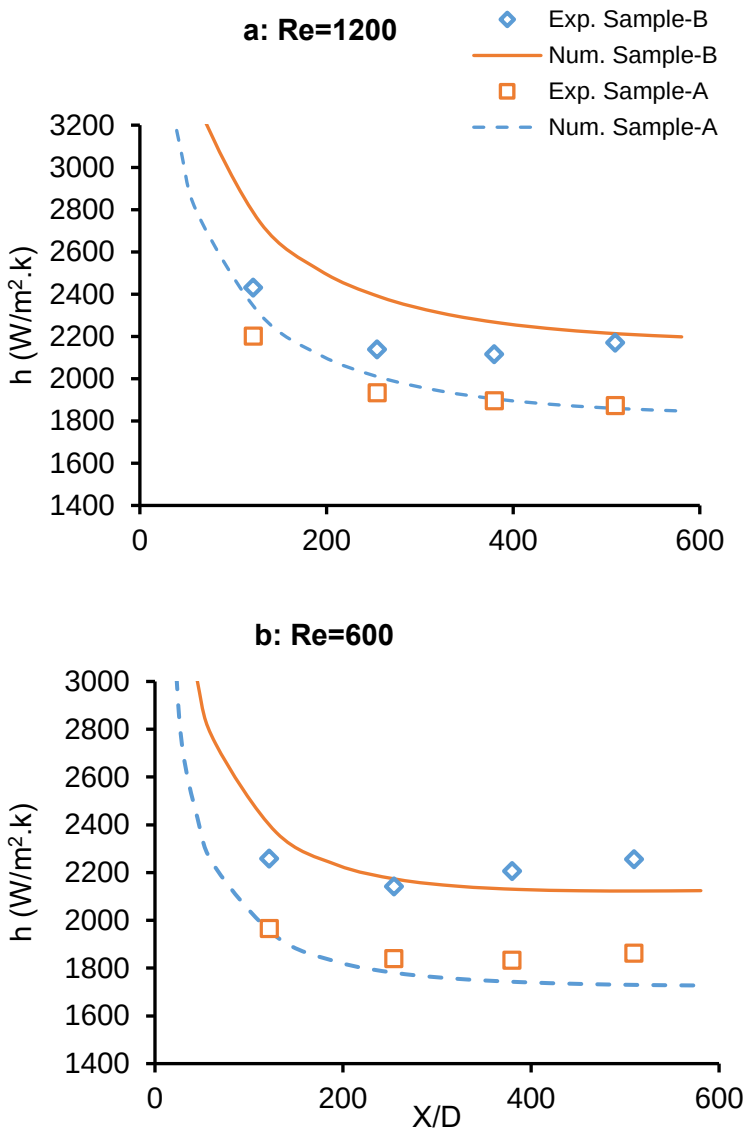

Fig. 4-3: Local heat transfer coefficient of Sample-A and Sample-B nanofluids flow in microtube (Di=1.55 mm) as a function of axial distance along the tube at a: Re=1200 and b: Re=1200.

Comparison with the experimental study of Hussien et al. [82]

Hussien et al. [82] have experimentally investigated the fluid flow of MWCNTs/ water nanofluid and MWCNTs/GNPs water-based hybrid nanofluids through a circular microtube (D_{in} = 1.1 mm) at Reynolds numbers ranging between 200-500 in terms of heat transfer coefficient, and pressure drop. The nanofluids were prepared for several particle weight concentrations of MWCNTs/water nanofluids (0.075, 0.125, and 0.25 wt.%) which mixed with (0.035 wt.%) GNPs for hybrid nanofluid. The used particles have an average diameter around 15 nm and an average length between 1-5 μm. The results indicated to a significant enhancement in heat transfer coefficient in comparison with the base fluid and maximum enhancement of 43.4% was obtained for 0.25 wt.%, accompanied with 11% increase in pressure drop.

Therefore, in this section, a numerical approach is carried out for the forced convective flow of MWCNTs/water nanofluid through a horizontal circular tube having an inner diameter of 1.1 mm and a length of 270 mm. The mesh independency has been studied and the mesh of 630000 elements has been selected.

Furthermore, the simulations carried out considering dependent-temperature of thermal conductivity and viscosity of nanofluid. It should be mentioned that the researchers didn't present data for viscosity as a function of shear rate. Thus, in order to consider the rheological behaviour of MWCNTs/water nanofluid, the correlated experimental data located in the literature [84] and [78] of viscosity as a function of shear rate are analysed. The data refer to the shear-thinning behaviour of MWCNTs/water nanofluid. Thus, the expected value of n (A measure of the deviation of the fluid from Newtonian) is taken from P. Garg et al. [78] (n=0.962) as an average value for several ultrasonication time at the temperature T=303 k. The latter is confirmed in our data base, where n value showed a range between 0.925 to 0.986 for the low MWCNTs concentration of nanofluids samples (see section 4.4.2 and Table C-1). And then K (A measure of the average viscosity) is determined for particle weight concentration of 0.125 wt.% and 0.25 wt.% so that achieving the presented viscosity value at a temperature of 310 K [82] 0.000735 and 0.000756 (Pa. s), respectively. This has been done after choosing the shear rate value as 200 1/s from the presented

viscosity data of MWCNTs nanofluid in [84], by comparing the viscosity values of Hussien et al. [82] and Ding et al. [84]. This leads to the expectation that Hussien et al. [82] has measured his viscosity data at a shear rate of 200 1/s. Therefore, the values of K for 0.125 wt.% and 0.25 wt.% are 0.000899 and 0.000924 kg.s^{n-2}/m.

As (n) and (K) are known now, it can find alpha (α) to compute the viscosity for temperatures range (300-330 K) by fitting the correlated experimental data of viscosity [82] using the Non-Newtonian power low viscosity fitting curve considering dependent-temperature and shear-thinning rheology behaviour. Furthermore, the final correlations of the viscosity (Eq. 4-11 and Eq. 4-12) have been validated in comparison with the experimental viscosity data of Hussien et al. [82], as shown in Fig. 4-4. Consequently, the velocity at the tube inlet can be determined as shown in Table 4-6.

Table 4-5: The viscosity correlations.

MWCNTs	$\mu = K\,\dot{\gamma}^{n-1}\,H(T)$ where, $H(T) = exp\left[\alpha\left(\frac{1}{T-T_0} - \frac{1}{T_\alpha - T_0}\right)\right]$				
Parameters	$\boldsymbol{K}$	**n**	$\boldsymbol{T_\alpha}$	α	
0.125wt%	0.899E-03	0.962	310 K	1800	Eq. 4-11
0.25wt%	0.924E-03	0.962	310 K	1800	Eq. 4-12

Table 4-6: The velocity of the nanofluids at the inlet of the tube.

$\boldsymbol{u}$ **m/s**		
Re	**200**	**470**
0.125 wt%	0.163	0.384
0.25 wt%	0.167	0.391

Furthermore, the thermal conductivity of nanofluid was determined by Hamilton and Crosser's model used by Hussien et al. [82] in his experimental research. Thus, the correlations of the conductivity (Eq. 4-13 and Eq. 4-14) are presented in Table 4-7.

Table 4-7: Thermal conductivity correlations.

	$k=aT^3+bT^2+cT+d$				
Parameters	**a**	**b**	**c**	**d**	
0.125wt%	-1.675E-08	5.528E-07	5.841E-03	- 7.327E-01	Eq. 4-13
0.25wt%	-1.679E-08	5.540E-07	5.855E-03	-7.344E-01	Eq. 4-14

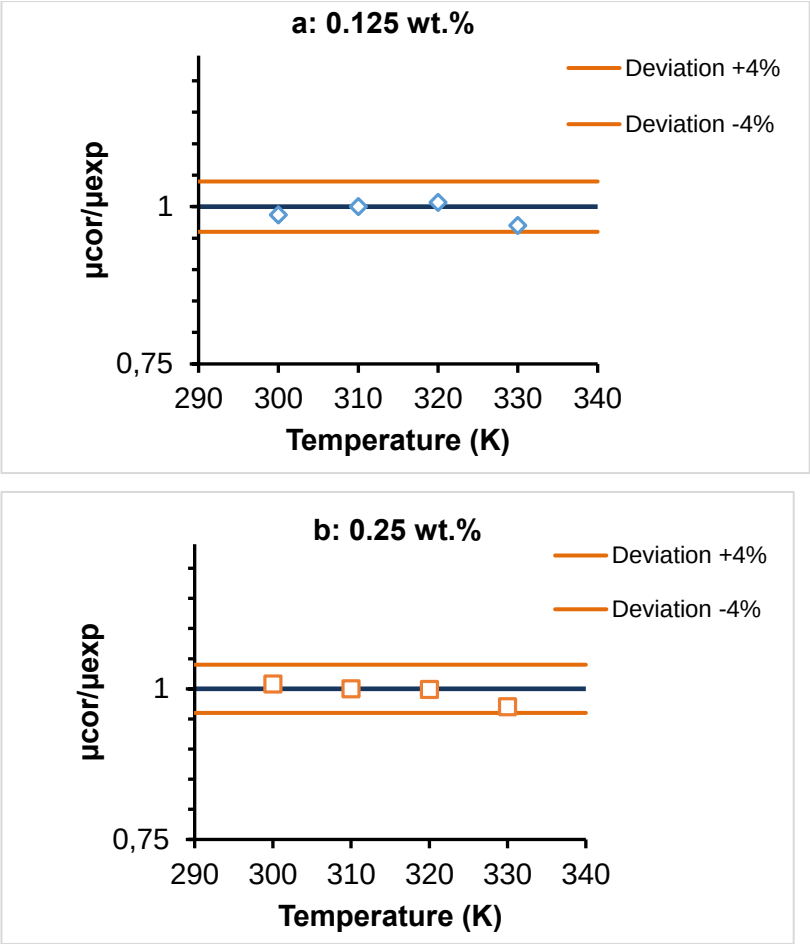

Fig. 4-4: The deviation of the proposed correlations of Non-Newtonian viscosity in comparison with experimental data for the concentrations of MWCNTs particles: a: 0.125 wt.% and b: 0.25 wt.%.

The numerical results are compared with the correlated experimental data for heat transfer coefficient (Fig. 4-5) and pressure drop (Fig. 4-6), presented a reasonable agreement, with an average deviation for heat transfer coefficient of 7% and a maximum deviation of 13% obtained for 0.25 wt.% nanofluid at Re=200. A lower deviation is obtained for pressure drop by 5%. It should be mentioned

that the researchers (Hussien et al. [82]) didn't report information about the uncertainty of their experimental results. In this, if the uncertainty of the experimental results regarding the heat transfer coefficient is higher or equal to 13%, the numerical results are quite accurate.

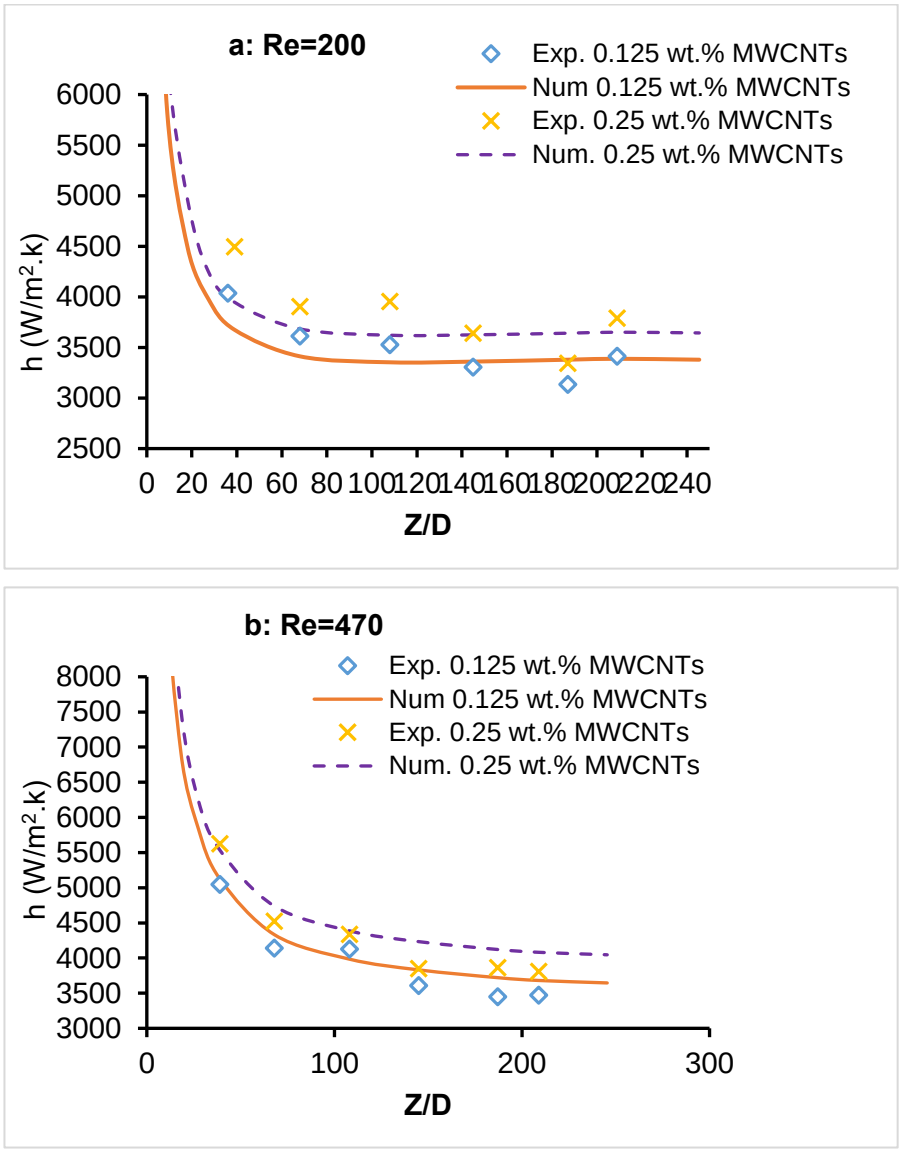

Fig. 4-5: Numerical and experimental convective heat transfer coefficient as a function of axial position along the tube for a: Re=200 and b: Re=470.

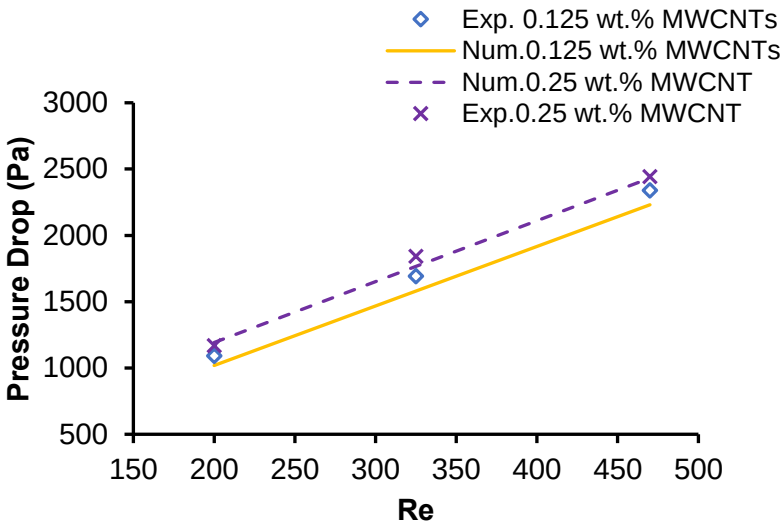

Fig. 4-6: Numerical results of pressure drop compared with the available experimental data of Hussien et al. [82].

4.4 NUMERICAL PARAMETERS AND PROCEDURE

It is presented in Chapter 3 a validated methodology for a proper numerical approach accompanied by the acceptable assumptions (Section 3.4) for conventional fluids (such as; water) flow through the microchannel. Which provides guidance for the numerical approach on the micro-scale fluid flow situation (Transition Reynolds number, Microchannel diameter, Viscous heating, Dependent-temperature thermophysical properties). In another hand, the latter was considered in the investigation of using CFD for CNTs nanofluids through a microchannel in section 4.3.2, showed a good validity of using the numerical model for such problem, since the numerical results agree with the correlated experimental data in terms of HTC and pressure drop. This leads to following the mentioned methodology for the next investigations in this Chapter too.

In the developed model, the Navier-Stokes and energy equations are applied to model the convective heat transfer and fluid flow using ANSYS- FLUENT software. Therefore, the governing equations for laminar flow for steady state and single-phase conditions are presented in section 1.3.6.2 of Chapter-1.

4.4.1 Geometric configuration

As mentioned earlier, CFD tools (ANSYS- FLUENT) with Navier-stocks and energy equations show an ability and validity for studying nanofluids flow through microtube. The numerical approach was validated for MWCNTs nanofluid flow through tubes have diameters of 1.55 mm and 1.1 mm. Moreover, the presented investigations on the fluid flow of nanofluids in microchannels (Table 4-1) refers to the acceptable ratio of nanoparticle diameter to the microchannel hydrodynamic diameter (d_p/D_h). Therefore, in this study, the numerical domain is established as a two-dimensional tube (2D) with 900 µm inner diameter achieving the highest value of ($d_{p\text{-}eq}/D_h$= 12.0E-04) for the largest MWCNT particle size. Where $d_{p\text{-}eq}$ is the equivalent diameter of the carbon nanotube particles, mentioned by Lamas et al.[22]. Furthermore, four Re numbers are chosen in the range 0< Re < 1500 to ensure the laminar flow (see the conclusion of Chapter-3), performed as Re=100, 600, 1000 and 1400. The geometric configuration is described in Fig. 4-7, where the length of the microchannel will be determined according to an investigation on the hydraulic and thermal development of the fluid flow in section 4.4.3.

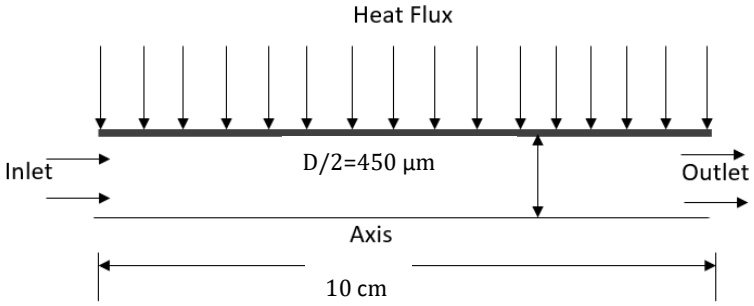

Fig. 4-7: Schematic diagram of the numerical region (test part).

4.4.2 Thermophysical properties of the Nanofluids Samples:

The preparation of MWCNTs nanofluids were carried out and explained by Lamas et al. [22] and Abreu et al. [21] for two aqueous fluids of ethylene glycol (EG) at volume fractions of 30% and 60% as base fluids and six aspect ratios of the geometry distribution of MWCNTs particles which suspended into each base fluid for different five concentrations, as shown in Table 4-8.

Table 4-8: The available samples of MWCNT nanofluids in the database.

Aspect ratio (l_p/d_p)	Volume fractions	Base fluids
333	0.25% Vol.	
667	0. 5% Vol.	
231	0.75% Vol.	DW+30%EG
125	1.0% Vol.	DW+60%EG
50	1.5% Vol.	
19		

As previously state, the thermophysical properties (Thermal conductivity, viscosity, density and specific heat) of the nanofluids are the key elements that influence the heat transfer behaviour through a microchannel. Therefore, the thermophysical properties of the available 60 nanofluid samples are presented in Table A-1 and Table A-2.

In this, the comparison study between the experimental and numerical results of fluid flow of MWCNTs nanofluids under heat flux conditions conducted in Chapter-2 enabled to develop validated thermophysical correlations of the thermal conductivity and the viscosity able to describe the behaviour of MWCNTs nanofluids when CFD tools are used. In this section, therefore, the correlations of computing conductivity and viscosity for several samples presented are produced via the same fashion that has been validated in Chapter-2. Thus, a curve fitting is performed on the conductivity data [163] as a function of temperature, and the resulted equations are summarized in Tables. Also, the viscosity correlations as a

function of temperature and shear rate are produced by performing a Non-Newtonian power low viscosity fitting curve [97] on the viscosity experimental data [21], considering the non-Newtonian shear-thinning rheological behaviour of MWCNTs nanofluid.

The density and the specific heat of the nanofluids are calculated using the model proposed by Pak and Cho [114] and the model of Xuan and Roetzel [115], respectively, presented in Chapter-2 (Eq. 2-1 and Eq. 2-2).

Moreover, thermal diffusivity (Eq. 4-15) for each sample is calculated and the nanofluid that achieves the highest value is determined as a reference nanofluid where it is expected to have a better heat transfer performance. As a result, Nanofluid-20 (NF20) is chosen from Table A-1 and Table A-2 as a reference fluid for studying the fully developed conditions (Thermal and hydraulic development of the fluid flow). It should be mentioned that Nanofluid-5 (NF5) is excluded since it is inconsistent with the whole results, Fig. 4-8.

$$a = \frac{k}{\rho \cdot c_p} \qquad \text{Eq. 4-15}$$

Where a is the thermal diffusivity of the fluid (m^2/s).

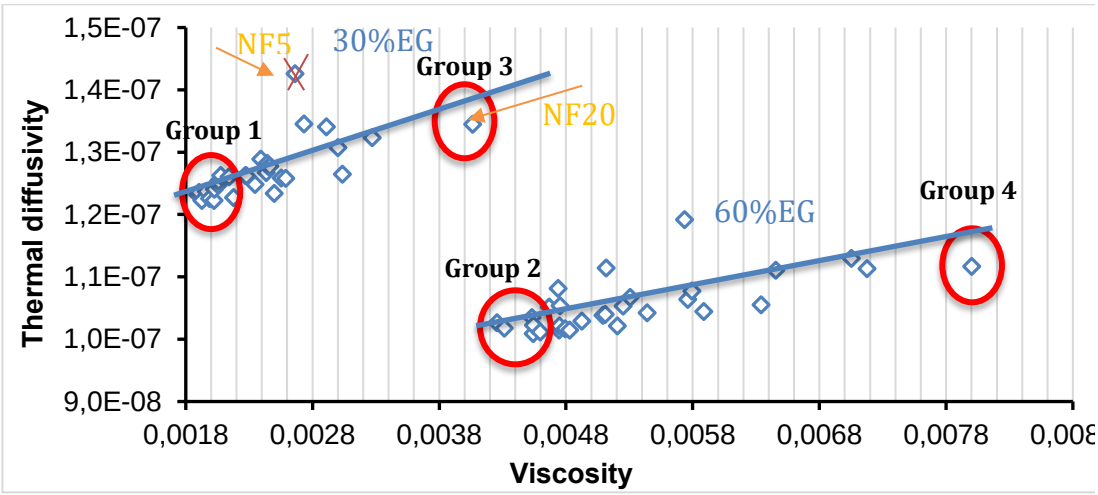

Fig. 4-8: The thermal diffusivity as a function of viscosity for the 60 nanofluid samples.

However, the high thermal diffusivity values may be accompanied by a high viscosity value which causes a higher pressure drop in the fluid flow. Therefore,

an analytical study is presented in Fig. 4-8 in order to choose several samples for further investigations. The reported data refers to Group-1, Group-2, Group-3 and Group-4 as the most interesting samples in terms of the high thermal diffusivity and the low viscosity. Where Group-1 and Group-3 achieve good levels of thermal diffusivity with good levels of viscosity. The nanofluid samples of these two groups (1 and 3) contain 30%EG as a base fluid, which provides a freezing point temperature of -16 °C and boiling temperature of 104 °C [164]. Furthermore, Group-2 and Group-4 contain 60%EG as a base fluid, which provides a freezing point temperature of -47 °C and boiling temperature of 110 °C [164].

For the heat transfer and fluid flow investigations, each group can be represented by one fluid, called the equivalent nanofluid (NF_{eq}). Therefore, the equivalent nanofluids for Group-1 and Group-2 can be obtained by calculating the average of the thermophysical properties of the nanofluids located in each group.

Moreover, from a rheological point of view, it is presented in Table C-1 the main parameters that describe the rheological behaviour of the nanofluid samples. Where K refers to the average viscosity of the nanofluid (The consistency index), n refers to the deviation of the fluid from Newtonian and α is the ratio of the activation energy to the thermodynamic constant.

Thus, the resulted thermophysical properties of the equivalent fluids are in Table 4-9, Table 4-10, Table B-1 and Fig. 4-9:

Table 4-9: The equivalent nanofluid in terms of rheological view for each group.

		n	K	α		n_{eq}	K_{eq}	α_{eq}
Group1	NF6	0.986	2.589-03	2100				
	NF21	0.985	2.520E-03	2300				
	NF16	0.925	3.590E-03	2150	Average	0.962	3.218E-03	2256
	NF17	0.912	4.050E-03	2300	Stdev	0.027	4.566E-04	127
	NF26	0.986	3.170E-03	2500	conf95%	0.021	3.817E-04	98
	NF11	0.967	3.076E-03	2300	upper limit	0.983	3.600E-03	2354
	NF7	0.971	2.97E-03	2100	lower limit	0.942	2.837E-03	2159
	NF1	0.967	3.150E-03	2300				
	NF22	0.977	2.970E-03	2300				
Group2	NF44	0.938	9.900E-03	2900				
	NF31	0.926	6.670E-03	3000	Average	0.957	7.548E-03	2950
	NF47	0.958	7.600E-03	3000	Stdev	0.021	1.203E-03	55
	NF36	0.98	6.748E-03	2900	conf95%	0.022	1.262E-03	57
	NF46	0.971	7.080E-03	2900	upper limit	0.979	8.810E-03	3007
	NF41	0.969	7.290E-03	3000	lower limit	0.935	6.286E-03	2893
Group3	NF20	0.911	9.460E-03	2200				
Group4	NF50	0.935	1.550E-02	2800				

Table 4-10: The equivalent nanofluid in terms of density and specific heat.

		ρ	c_p		ρ_{eq}	c_{p-eq}
Group 1	NF6	1048.4	3629.3			
	NF21	1048.4	3629.3			
	NF16	1048.4	3629.3	Average	**1049.1**	**3626**
	NF17	1051.2	3614.5	Stdev	1.290	7
	NF26	1048.4	3629.3	conf95%	1.078	6
	NF11	1048.4	3629.3	upper limit	1050.141	3631
	NF7	1048.4	3629.3	lower limit	1047.984	3620
	NF1	1051.2	3614.5			
	NF22	1048.4	3629.3			
Group 2	NF44	1097.8	3158.5			
	NF31	1089.8	3194.8	Average	**1091.6**	**3187**
	NF47	1092.5	3182.7	Stdev	3.25	15
	NF36	1089.8	3194.8	conf95%	3.41	15
	NF46	1089.8	3194.8	upper limit	1095	3202
	NF41	1089.8	3194.8	lower limit	1088	3171
Group 3	NF20	**1062.3**	**3555.9**			
Group 4	NF50	**1103.2**	**3134.8**			

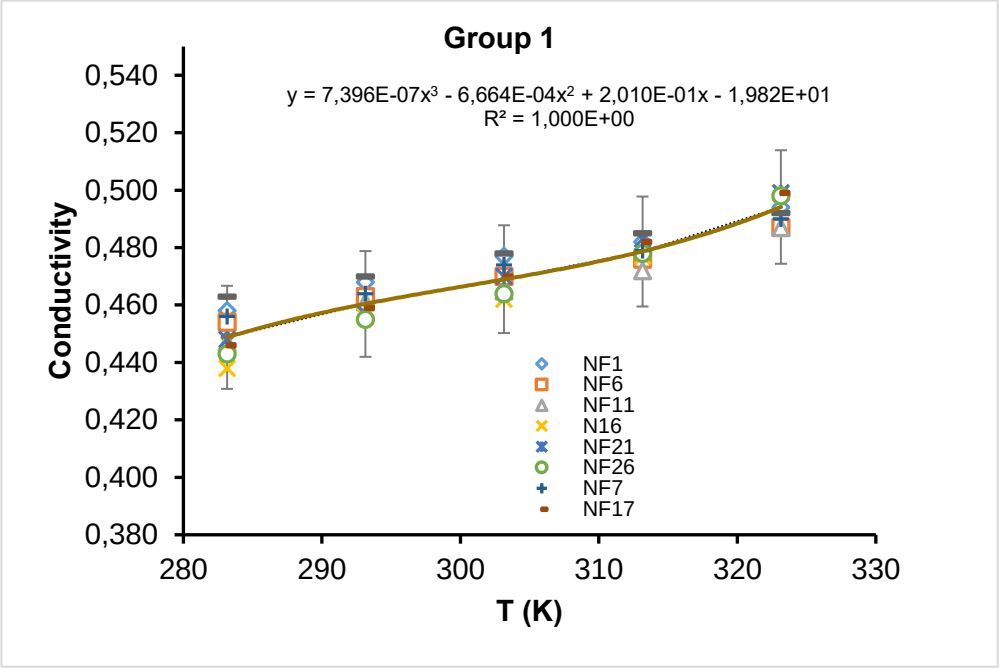

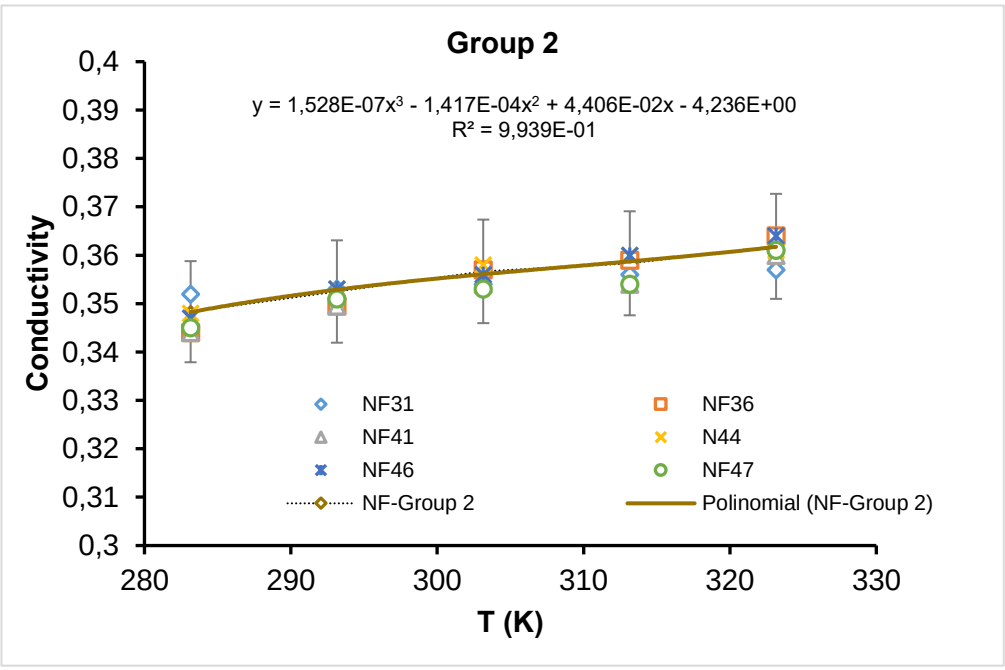

Fig. 4-9: The equivalent nanofluid in terms of thermal conductivity as a function of temperature.

4.4.3 Boundary Conditions

For this numerical study, the considered boundary conditions are the same referred at Chapter-3 (section 3.4.2), only the specific values of the tube geometry, inlet velocity and wall heat flux were adjusted as follow.

Tube geometry

The tube diameter selection was already explained at section 4.4.1. Here attention will be given to the tube length. As it is known, the entrance region gives a higher convective heat transfer coefficient and the value stabilizes after the entrance hydraulic development length. Therefore, a predictive analysis of the hydraulic development area is carried out in order to determine the suitable length of the tube for the current study. A numerical study conducted by Li et al. [165] for heat transfer in a micro-heat sink has defined the entrance length as the distance required for the centreline velocity to reach 99% of the fully developed value. Moreover, Li et al. [165], Sara et al. [149] and Lelea et al. [74] have estimated the microtube length of their studies achieving the hydraulic development of the fluid flow. For this, the widely used theoretical correlation is Eq. 4-16 [2]:

$$L_h = 0.05 \cdot Re \cdot D \qquad \text{Eq. 4-16}$$

Also, Garg et al. [78] have taken into account the achievement of thermal fully development of the flow by the correlation Eq. 4-17 [2]:

$$L_{th} = 0.05 \cdot Pr \cdot Re \cdot D \qquad \text{Eq. 4-17}$$

Taking into consideration the highest Re number in this study (Re=1400) and the selected reference nanofluid (Pr=30.7), the required length should be $L>L_h=0.063$m and $L>L_{th}=1.94$ m. Where Pr number for Non-Newtonian fluids, described by shear thinning behaviour can be found by Eq. 4-18 [154], [161] and [162] as follows:

$$Pr = \frac{c_p\ (u/D)^{n-1} \cdot\ K}{k_{nf}} \qquad \text{Eq. 4-18}$$

Where K is a measure of the average viscosity of the nanofluid (The consistency index), n is a measure of the deviation of the fluid from Newtonian (The power-law index). k_{nf} is the conductivity of the nanofluid. u is the mean velocity of the fluid flow. D is the diameter of the tube. c_p is the specific heat of the nanofluid.

To ensure the result, a numerical simulation is conducted for the flow of the reference nanofluid (Nanofluid-5) at the selected tube length (L=2.2 m > L_{th}). Moreover, an energy balance is performed (Eq. 4-19, [2]) in order to choose a heat flux value, avoiding the boiling of the fluid near to the wall. Where the variation between the outlet and inlet temperature of the fluid is determined as ($T_{out} - T_{in}$=19 °C), since the required heat flux value to obtain this temperature increase (19 °C) of the fluid, will cause a near wall temperature lower than the expected boiling point of the fluid (<104°C for the base fluid 30%EG [164]). As a result, a constant heat flux of 46000 W/m^2 is chosen.

$$q = \frac{c_p \cdot\ \dot{m}\ \cdot (T_{out} - T_{in})}{\pi \cdot\ D \cdot\ L} \qquad \text{Eq. 4-19}$$

Therefore, the numerical simulation is carried out for Nanofluid-20 (The highest thermal diffusivity) flow at Reynolds number of 1400 with a determined velocity (Table 4-11) and a temperature of 293.15 K at the tube inlet. Furthermore, the simulations carried out considering dependent-temperature of thermal conductivity and the Non-Newtonian nanofluid behaviour for the viscosity correlation, by fitting the correlated experimental data [78]. Thus, the correlations of the conductivity and viscosity (Eq. 4-20 and Eq. 4-21) are as following:

$$k = 3.333E\text{-}07\ T^3 - 2.817E\text{-}04\ T^2 + 7.987E\text{-}02\ T - 7.105{+}00 \qquad \text{Eq. 4-20}$$

$$\mu = 9.467E - 03\ \dot{\gamma}^{-0.0886}\ exp\left[2200\left(\frac{1}{T - T_0} - \frac{1}{293.15 - T_0}\right)\right] \qquad \text{Eq. 4-21}$$

Table 4-11: The velocity of the nanofluids at the inlet of the tube.

Non-Newtonian fluid			NF20	
CNTs	**K**	**n**	**Re number**	***u*** **m/s**
1.5 wt. %	9.46E-03	0.9114	1400	6.32

It can be noticed from Fig. 4-10 that the centreline velocity reaches the 99% of the fully developed value at the axial location is near to the predicted distance by Eq. 4-16 (X=0.063 m). Moreover, it is presented in Fig. 4-11 the results of the velocity of the cross section at several axial locations along the tube, showing a change in the parabolic velocity profile until the location X=0.063 m, then it keeps with almost a constant profile form.

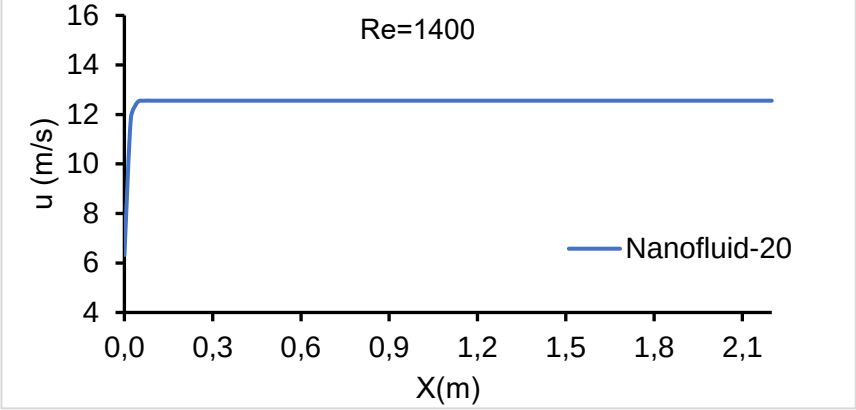

Fig. 4-10: The centreline velocity along the tube (L=2.2 m).

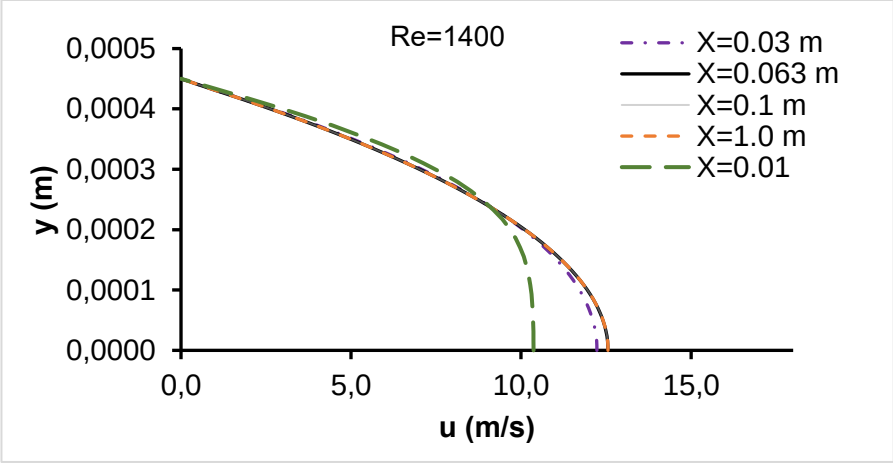

Fig. 4-11: The parabolic velocity profile at several axial locations along the tube.

Furthermore, the results of the thermal fully development are studied in terms of the dimensionless temperature profile, using the correlation Eq. 4-22 and presented in Fig. 4-12.

$$T^* = \frac{T_W(x) - T(x,r)}{T_W(x) - T_f(x)} \qquad \text{Eq. 4-22}$$

As it was expected, the parabolic dimensionless temperature profile is changing along the tube until it reaches an axial location near to X=1.94 m, then it keeps with almost a constant profile. This is agreed with the predicted results of the theoretical correlation Eq. 4-17.

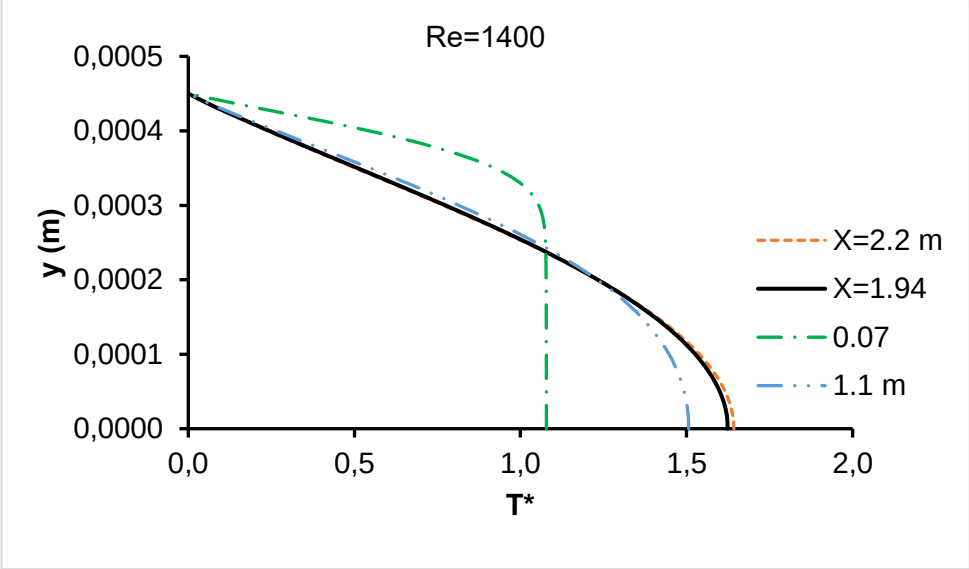

Fig. 4-12: The dimensionless temperature profile at several axial locations along the tube.

There is an agreement between the theoretical predictions and the obtained numerical results in terms of the velocity profile and dimensionless temperature profile for the fluid flow of Nanofluid-20 which has a Non-Newtonian (Shear-thinning) behaviour. This can be explained by the high rheology index value (n=0.9114) of the used fluid since the fully developed velocity and temperature profiles of the Non-Newtonian fluid become flattered and flatter as (n) decreases [166] as shown in Fig. 4-13.

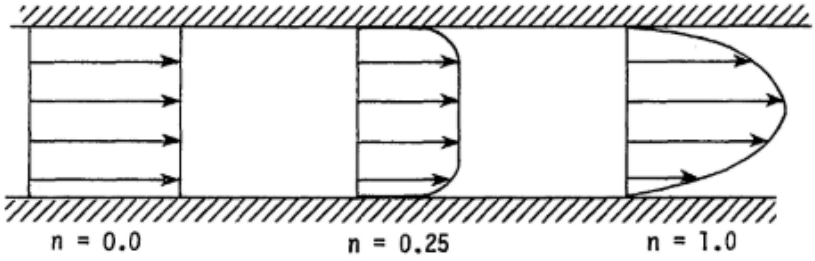

Fig. 4-13: The laminar velocity profiles for shear-thinning Non-Newtonian fluids (Pseudoplastic fluids) [166].

Moreover, the performance of the Nusselt number along the tube is presented in Fig. 4-14. The results refer to the high values of Nu number in the hydraulic development region (L<0.063 m). Then, it becomes much lower in the hydraulic fully developed region and slightly decreases under the influence of the thermal development region (L<1.94 m).

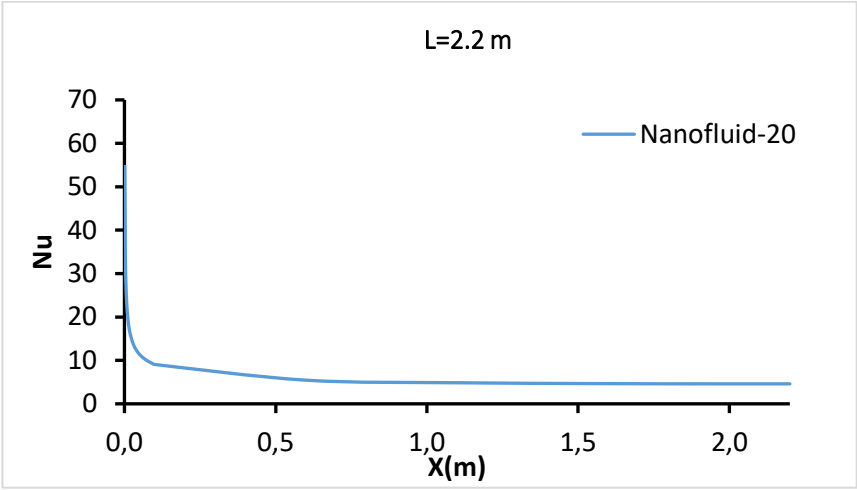

Fig. 4-14: The Nusselt number along the tube.

In this study, therefore, the tube length of 10 cm (L≈111×D) is chosen, achieving the requirements of the hydraulic development of the flow. Also, the expected applications are taken into consideration where the small sizes are required. For this, a summary of some researches carried out in the field is given in Table 4-12.

Table 4-12: Summary of some studies for heat transfer and Laminar fluid flow in microchannels with reference to the hydraulic developed conditions.

Researcher	fluid	Tube Diameter	Tube length	L/D	Re	L/DRe
Lelea [152],	Al_2O_3/water	50 μm	4.48 cm	89.6	107–1760	0.0509
Sajadifar et al. [154]	Al_2O_3/water	200 μm	0.5 cm	25	1, 10, 20	1.25
Mehrdad et al.[159]	TiO_2/water	502 μm	12 cm	24	200 - 2500	0.0096
Jung et al [157]	Al_2O_3/water	56.4 μm	1.5 cm	266	5 - 300	0.887
Mala et al.[133]	Water	130μm	1 cm	77	1000-1500	0.0513
Sara et al.[149]	water	200μm	4.96 cm	248	40-1400	0.177
Salman et al. [151]	ZnO /EG	50 μm	0.025 cm	5	80	0.0625

Inlet velocity

The velocity of the nanofluids at the tube inlet for each Reynolds number was calculated by Eq. 4-6, as shown in Table 4-13.

Table 4-13: The velocity of the nanofluids at the inlet of the tube for each Re number.

Non-Newtonian fluid							
				Re numbers			
NF	K	n		100	600	1000	1400
Group1	3.22E-03	0.962	u m/s	0.27	1.54	2.53	3.50
Group 2	7.55E-03	0.957	u m/s	0.58	3.24	5.29	7.30
Group 3	9.46E-03	0.9114	u m/s	0.56	2.9	4.64	6.32
Group 4	15.5 E-03	0.935	u m/s	0.96	5.33	8.60	11.80

Wall Heat flux

In order to choose a suitable heat flux value, the methodology of the energy balance was performed above (Eq. 4-19, [2]) is repeated here for the tube length of 10 cm at the lowest Reynolds number (Re=100). For this, the Nanofluid with the minimum thermal diffusivity (NF-group2) is used with the determined velocity in Table 4-13 and a temperature of 293.15 k at the tube inlet. As a result, a constant heat flux of 80 kW/m^2 is chosen. After defining the boundary conditions, the simulations are conducted using the parameters of the thermophysical properties, presented in Table 4-9, Table 4-10, Table B-1 and Fig. 4-9.

4.4.4 Mesh independence

The mesh-independent results are examined by four different mesh distributions (877500, 625000, 450000 and 210000). The mixture of distilled water (DW) and 30% of ethylene glycol (EG) (Base fluid) was simulated for the same test section and flow conditions presented in section 4.4.1 and section 4.4.3. The results, Fig. 4-15, show that for meshes with element numbers equal or higher than 625000 elements, the Nusselt number does not have a significant change, leading to the conclusion that the mesh that has 625000 elements is acceptable for simulation of this system, being as a trade-off between accuracy and computational time.

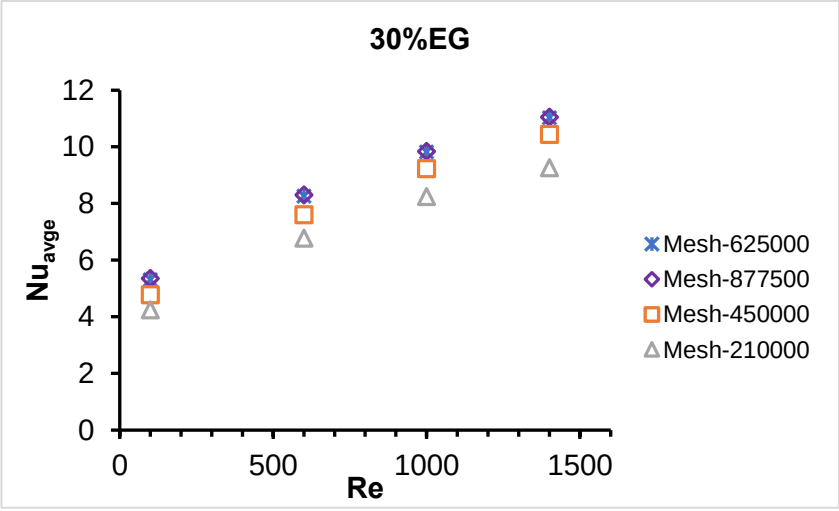

Fig. 4-15: Mesh independence for the base fluid (30% EG +70% DW) flow in the tube.

4.5 THE RESULTS

The main purpose of this chapter is to assess and study the factors affecting the heat transfer phenomena and fluid flow of MWCNTs based nanofluids in a microchannel. As mentioned earlier, an overall numerical investigation was carried out considering several operation conditions and characteristic parameters. The conducted literature review presented in Chapter-1 suggested that the heat transfer and fluid flow performance of nanofluids in microchannels can be explained by the same physical laws ruling used for common fluids flowing in macro channels, i.e., depending on wall and fluids temperatures, Nusselt number and friction coefficient. In order to assess the contribution of these parameters, its variation should be studied as a function of axial direction along with the tube, Reynolds number and particle volume fractions.

Moreover, the overall analysis of the previous investigations on heat transfer of nanofluids conducted in Chapter-1 identified that the thermophysical properties (Thermal conductivity, viscosity, density and specific heat) of the nanofluids are the key elements that influence the heat transfer and fluid flow behaviour through microchannels. These thermophysical properties, namely thermal conductivity and viscosity, depend on the particle concentration, particle geometry, and base fluid [22] and [21]. The increase of fluid conductivity leads to the increase of the Nusselt number resulting in an enhancement of the heat transfer rate by convection. The increase of fluid viscosity increases wall shear stress and friction factor resulting in a higher pressure drop, leading to higher pumping power. Also, it should be mentioned that the increase of the viscosity leads to an increase in the boundary-layer thickness which decreases the heat transfer performance.

However, it should be noted that the temperature and velocity gradients, the viscosity gradient, and the thickness of the boundary layer in a fluid flowing through a microchannel have a significant effect on the heat transfer phenomena, due to the micro scales involved. In addition, nanofluids may not show a Newtonian behaviour, therefore attention must be given to the fluid rheology modelling. Geometry scale effect on gradients and fluid rheology are the key aspects when modelling nanofluids flows in microchannels. The obtained results

are qualitatively coherent with the fluid properties and flow conditions, see Fig. 4-16, where the temperature distribution at the end of the tube for the highest and lowest Reynolds numbers when two different nanofluids are considered, are shown.

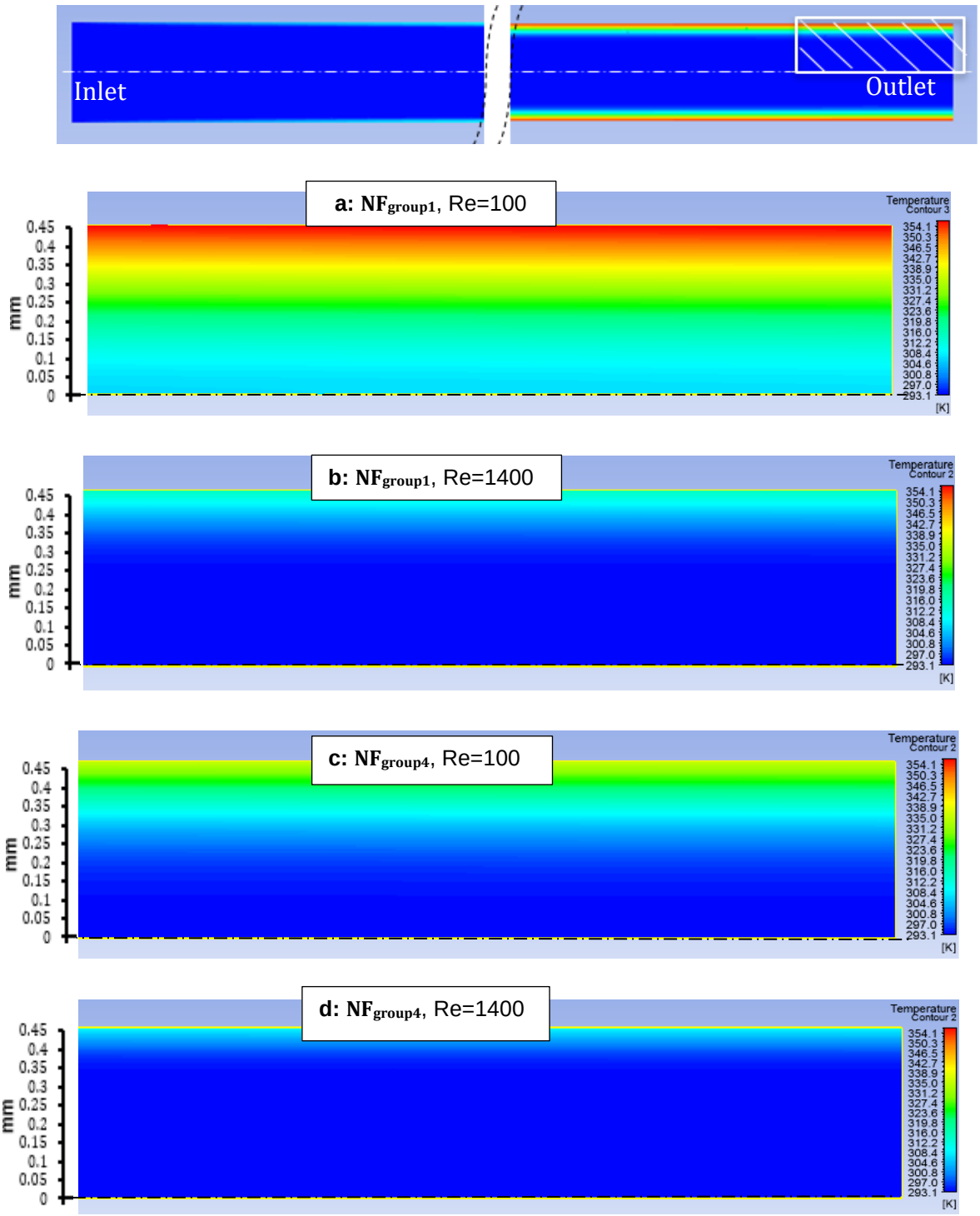

Fig. 4-16: The test section model showing the resulted temperature field at the outlet of the tube for deferent cases: (a: NF_{group1}-Re=100, b: NF_{group1}-Re=1400, c: NF_{group4}-Re=100 and d: NF_{group4}-Re=1400).

4.5.1 The heat transfer coefficient and pressure drop

The methodology of the heat transfer calculation presented for Chapter-2 (section 2.5.2) will be followed here. Consequently, the local heat transfer coefficient is calculated by Eq. 2-11, and the average heat transfer coefficient is found by Eq. 2-13. Then the local Nusselt number and average Nusselt number are calculated by Eq. 2-17. Also, pressure drop can be calculated theoretically using Eq. 4-23 [2].

$$\Delta p = \frac{64 \cdot L \cdot u^2 \cdot \rho}{2 \cdot Re \cdot D} \qquad \text{Eq. 4-23}$$

According to the nanofluids properties database, the increase of particle volume fraction enhances the thermal conductivity, increases the viscosity and degrades the specific heat of the nanofluid. This affects the heat transfer and fluid flow performance. Therefore, the heat transfer coefficient and pressure drop for the four representative nanofluids are compared at four Reynolds numbers (Re= 100, 600, 1000 and 1400).

From the obtained results, Fig. 4-17 and Fig. 4-18, it can be clearly depicted that the heat transfer coefficient enhances with increasing Reynolds number and thermal diffusivity, accompanied by an increase in pressure drop.

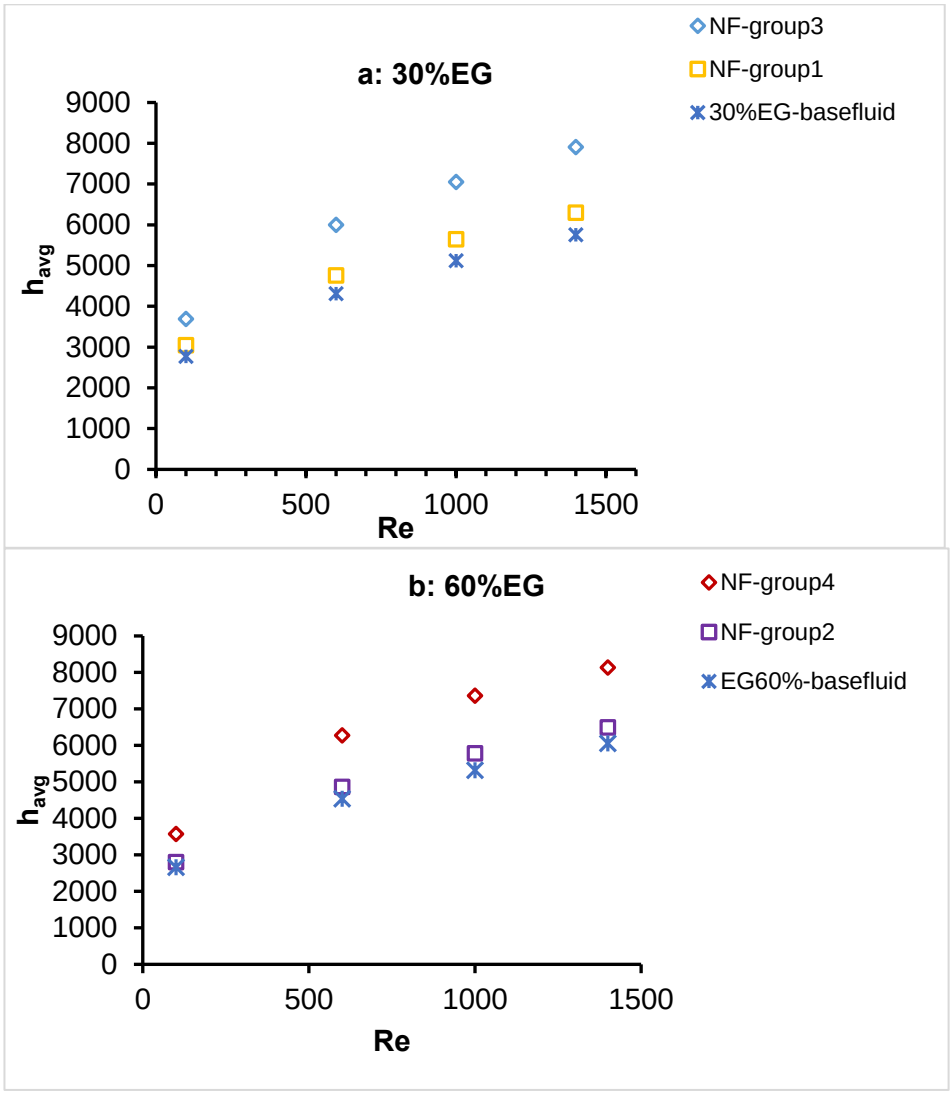

Fig. 4-17: Average heat transfer coefficient as a function of Reynolds number.

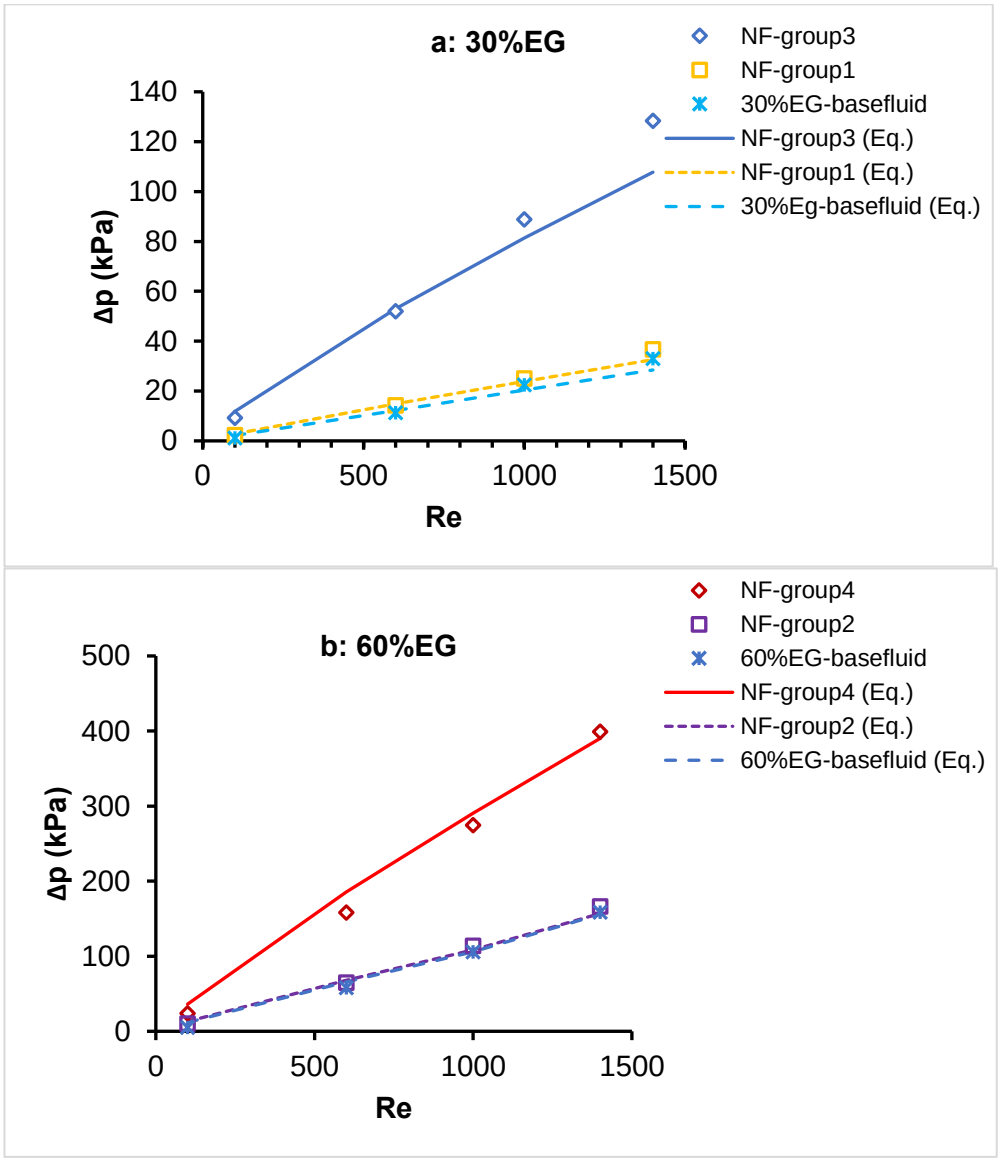

Fig. 4-18: Total pressure drop as a function of Reynolds number.

Moreover, the average enhancement of heat transfer coefficient and pressure drop for each nanofluid in comparison with the base fluid is presented in Table 4-14. The numerical results refer that the increase in pressure drop for NF_{group3} and NF_{group4} is much higher than the increase in heat transfer coefficient, because of their high viscosity. This leads to select NF_{group1} and NF_{group2} as the optimal nanofluids where the low-pressure drop is required at the same time with the heat transfer enhancement.

Table 4-14: Average increase of heat transfer coefficient and pressure drop.

	NF_{group1}	NF_{group2}	NF_{group3}	NF_{group4}
Average HTC	10.0%	7.1%	31.0%	28.2%
Pressure drop	16.2%	8.0%	315.3%	160.1%

Furthermore, the results in Table 4-15, report an enhancement in heat transfer coefficient with increasing Re numbers, such as for NF_{group1} it becomes by 10.3%, at Re=600, slightly decreases to 10.2% at Re=1000 and 9.5% at Re=1400. The further increase in Re number causes a larger decrease in heat transfer coefficient enhancement, accompanied by high-pressure drops by 25,041 kPa and 36,703 kPa for NF_{group1} at Re=1000 and 1400, respectively. This can be explained by the entrance length effect and the velocity of the fluid which increases with the increase of Re number. Thus, the effect of higher thermal diffusivity of the nanofluids on the heat transfer coefficient for high Re number becomes lower in comparison with the Re number effect.

Table 4-15: The enhancement of the heat transfer coefficient for several Reynolds numbers.

HTC	**100**	**600**	**1000**	**1400**
NF_{group1}	9.9%	10.3%	10.2%	9.5%
NF_{group2}	5.3%	8.0%	7.8%	7.2%
NF_{group3}	27.3%	33.2%	31.8%	31.5%
NF_{group4}	27.1%	29.9%	29.3%	26.3%

Also, the results show a decrease in heat transfer coefficient enhancement at the low Re number (Re=100), which can be explained by the higher boundary layer thickness (δ), as shown in Eq. 4-24 [2].

$$\delta = \frac{5 \cdot x}{\sqrt{Re}} \qquad \text{Eq. 4-24}$$

4.5.2 Performance evaluation

The evaluation of the heat transfer enhancement in a micro heat exchanger caused by using nanofluids must consider the energy losses related to the pressure drop increase, allowing to estimate the beneficial impact on saving energy. The extra energy costs of the pumping power are proportional with the pressure drop increase as shown in Eq. 4-25 [2].

$$P_{pump} = \dot{V} \cdot \Delta p \qquad \text{Eq. 4-25}$$

Where, $\dot{V}$ Is the volume flow rate (m^3/s).
Therefore, the ratio of the Colburn j-factor to the friction factor (*j/f*) in what is called ''Goodness factor'', proposed by Kays and London[167], was used to determine the overall thermo-hydraulic performance [168]. Where f is the Fanning friction factor, and Colburn j-factor is given by Eq. 4-26.

$$j = St \cdot Pr^{2/3} \qquad \text{Eq. 4-26}$$

where St is Stanton number, given by Eq. 4-27.

$$St = \frac{Nu}{Re \cdot Pr} \qquad \text{Eq. 4-27}$$

The latter has been adopted to evaluate the performance of ten radiator tubes by Olsson et al. [169], and a design for a parallel, finless heat exchanger by Li et al. [170]. Later, Zamzamian et al. [171] have used the Area goodness factor to assess the relative thermal–hydraulic performance enhancement of Plate-Fin Heat Exchangers with Cu-water nanofluids. Furthermore, a new dimensionless number JF (Eq. 4-28), based on the area goodness factor concept, was presented by Yun et al.[172] for evaluating the thermal-hydraulic performance of a heat exchanger in comparison with a reference case. This dimensionless number JF has been adopted by Erbay et al. [173] and Qi et al. [174] in their studies of heat exchangers evaluation.

$$JF = \frac{j/j_R}{(f/f_R)^{\frac{1}{3}}}$$ Eq. 4-28

where f_R and j_R are the f and j factors of the reference case.
A similar equation (Eq. 4-29) has been used by Wongcharee et al. [175] to define the thermal performance factor (η) of the heat exchanger with nanofluids.

$$\eta = \left(\frac{Nu}{Nu_R}\right)\left(\frac{f_R}{f}\right)^{\frac{1}{3}}$$ Eq. 4-29

where Nu_R is the Nusselt number of the reference case (Non-enhanced case).
Also, this equation (Eq. 4-29) has been adopted by Manay et al. [64] with a new form (Eq. 4-30), clearly described the evaluation of the micro heat sink performance in the case of using nanofluids (nf) in comparison with the base fluid case (bf).

$$\eta = \left(\frac{Nu_{nf}}{Nu_{bf}}\right)\left(\frac{f_{bf}}{f_{nf}}\right)^{\frac{1}{3}}$$ Eq. 4-30

In this study, the dimensionless number JF in Eq. 4-28 is used to evaluate the overall enhancement efficiency of the micro heat exchanger geometry, described in Fig. 4-7. For this, Fanning friction factor ƒ (Eq. 4-31, [2]) for the nanofluids and base fluids are calculated at each Re number. The results are presented in Fig. 4-19 and Fig. 4-20.

$$ƒ = \frac{2 \cdot \Delta P \cdot D}{\rho \cdot u^2 \cdot L}$$ Eq. 4-31

The nanofluids that achieve higher JF number values are preferred, since it provides better heat transfer with saving energy.

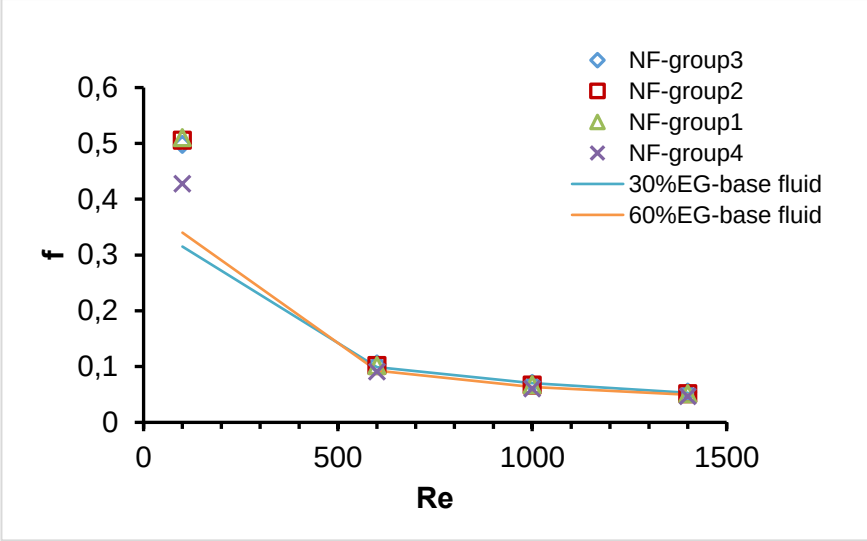

Fig. 4-19: Fanning Friction factor as a function of Re number.

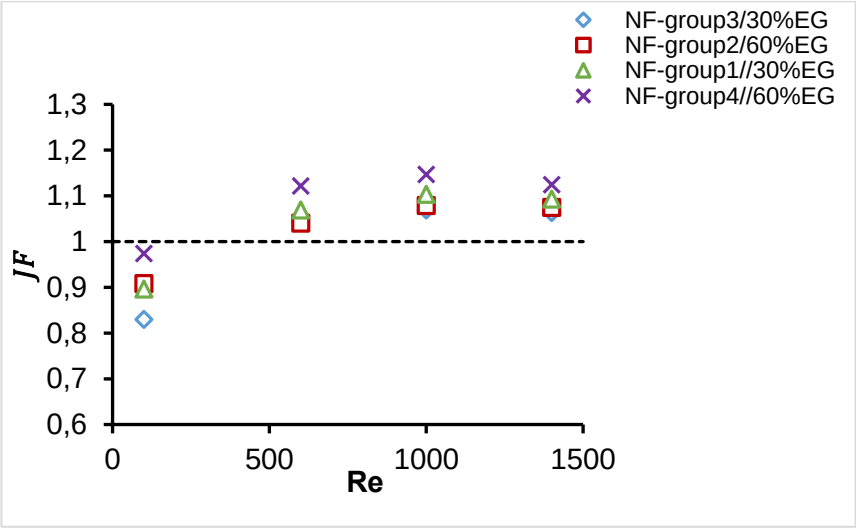

Fig. 4-20: *JF* number as a function of Re number.

The results show a decrease in JF number (<1) at the low Re number (Re=100), due to the high boundary layer thickness (δ), as shown in Eq. 4-24, which causes a higher pressure drop and lower heat transfer. This indicated to a useless of low Re numbers regarding saving energy. While it still can be beneficial according to the application's requirements in the field. Also, the nanofluids with higher thermal diffusivity shows higher JF number value, thus higher thermal performance. Whereas, the increase of Re number accompanied with an increase of JF number, but it goes down after a certain value (Re=1000). The latter agrees with the conclusion in the correlated literature [64] and [176].

On another hand, minimizing the thermal resistance of the micro heat exchangers was always an important objective in the literature [47], [177]–[179]. Therefore, it is presented in Fig. 4-21 the thermal resistance values for the four nanofluids and base fluids as a function of Re number, calculated by the given Eq. 4-32 [64].

$$R_{th} = \frac{T_{max} - T_{in}}{q \cdot A} \qquad \text{Eq. 4-32}$$

where R_{th} is the thermal resistance, T_{max} is the maximum wall temperature, T_{in} the inlet temperature, q is the heat flux and A the surface cylinder area of the microchannel.

The results indicate the highest values of thermal resistance are for the base fluids, becomes lower for NF_{group1} and $N_{Fgroup3}$, respectively for 30%EG-base fluid case (Fig. 4-21, a). In addition to a lower value for NF_{group2} and $N_{Fgroup4}$, respectively for 60%EG-base fluid case (Fig. 4-21, b).

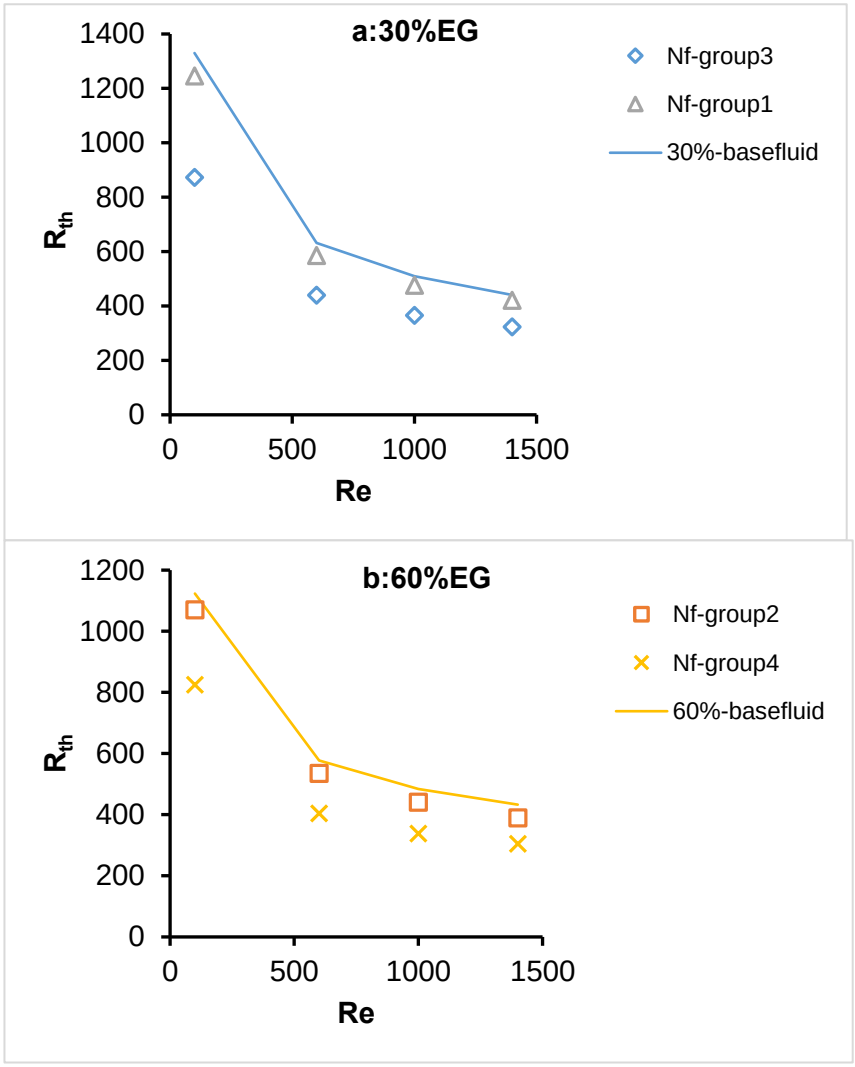

Fig. 4-21: Thermal resistance number as a function of Re number.

Nevertheless, the previous comparison of the four nanofluids was done at constant values of the Reynolds number. While in the case of considering a constant value of fluid flow the results will be deferent. For further investigation, a comparison study between NF_{group1} and NF_{group2} at the same volume fluid flow of $\dot{V}$=9.83E-07 m^3/s which meets the inlet velocity value of u=1.54 m/s (Re=600 for NF_{group1}) is conducted, since they represent nanofluids with different base fluids (30%EG and 60%EG) for the lowest viscosity (lowest particle concentration). The presented results in Fig. 4-22 refers to a better heat transfer performance for NF_{group1} with an average heat transfer coefficient of 4755 $W/m^2.K$, in comparison with NF_{group2} which achieves an average heat transfer coefficient of 3771 $W/m^2.K$.

Moreover, NF_{group1} achieves better results in terms of pressure drop (14.179 kPa) in comparison with NF_{group2} (28.916 kPa).

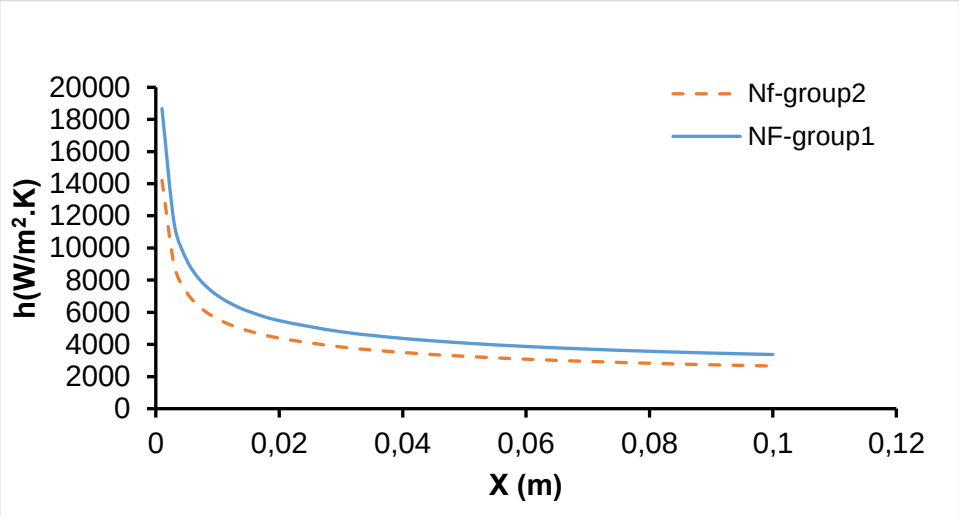

Fig. 4-22: Heat transfer coefficient as a function of axial distance along the tube for the same fluid flow value.

However, the applications of the nanofluids with 60%EG base fluid can be different from the applications of nanofluids with 30%EG base fluid. Because of the freezing points of 60%EG fluid and 30%EG fluid are (-47 °C) and (-16 °C), respectively, in addition to the boiling points which are (110 °C) and (104 °C) [164], respectively.

4.5.3 Nusselt number correlation

The wide range of heat transfer applications with several operating conditions, required to simplify the process of estimating the heat transfer performance. Therefore, a reliable analytical prediction of the average Nusselt Number commonly desirable as an engineering calculation. In the case of Newtonian fluids, some Nusselt number correlations have been produced for the heat transfer of laminar flow under a constant heat flux in a microchannel, such as Shah Eq., Leveque Eq. and McAdams Eq., as shown in Table 4-16.

Table 4-16: Some correlations of Nusselt number for Laminar flow.

Leveque Eq. Cited in [166]	$Nu = 1.75 \cdot (Gr)^{\frac{1}{3}}$
Shah Eq. [180]	$Nu = 1.953 \cdot \left(Re \cdot Pr \cdot \frac{D}{x}\right)^{\frac{1}{3}}$ for $\left(Re \cdot Pr \frac{\cdot D}{x}\right) \geq 33.33$
McAdams Eq. Cited in [180]	$Nu = 1.62 \cdot (Gr)^{\frac{1}{3}}$

Whereas, limited Nusselt number correlations are found in the literature for the case of Non-Newtonian fluids. A correlation for local Nusselt number (Eq. 4-33) found in [181] for laminar flow of Non-Newtonian fluids under a constant wall heat flux boundary condition for the thermally developing flow region in the dynamically fully developed flow.

$$Nu_x = 1.41 \cdot (\Delta \cdot Gr_x)^{\frac{1}{3}} \quad \text{Eq. 4-33}$$

In addition, another Non-Newtonian fluids correlation (Eq. 4-34) for the average Nu number was proposed by (Pigford, 1955) for macro-channels as cited by Joshi [166] and Pawar et al. [182], for laminar flows under constant heat wall flux at the entrance region.

$$Nu = 1.75 \cdot (\Delta \cdot Gr_L)^{\frac{1}{3}} \quad \text{Eq. 4-34}$$

where Gr is the Graetz number, which is given by Eq. 4-35. And, Δ represents a non-Newtonian parameter, Eq. 4-36.

$$Gr_L = Re \cdot Pr \cdot \frac{D}{L} \quad \text{Eq. 4-35}$$

$$\Delta = \frac{3n + 1}{4n} \quad \text{Eq. 4-36}$$

where Pr is the Prandtl number, which is given by Eq. 4-18.

In this study, therefore, the average Nu number for the Nanofluids (Non-Newtonian) and base fluids (Newtonian, Δ=1) is calculated by the correlation Eq. 4-34. The obtained results are compared with the correlated numerical results as shown in Fig. 4-23.

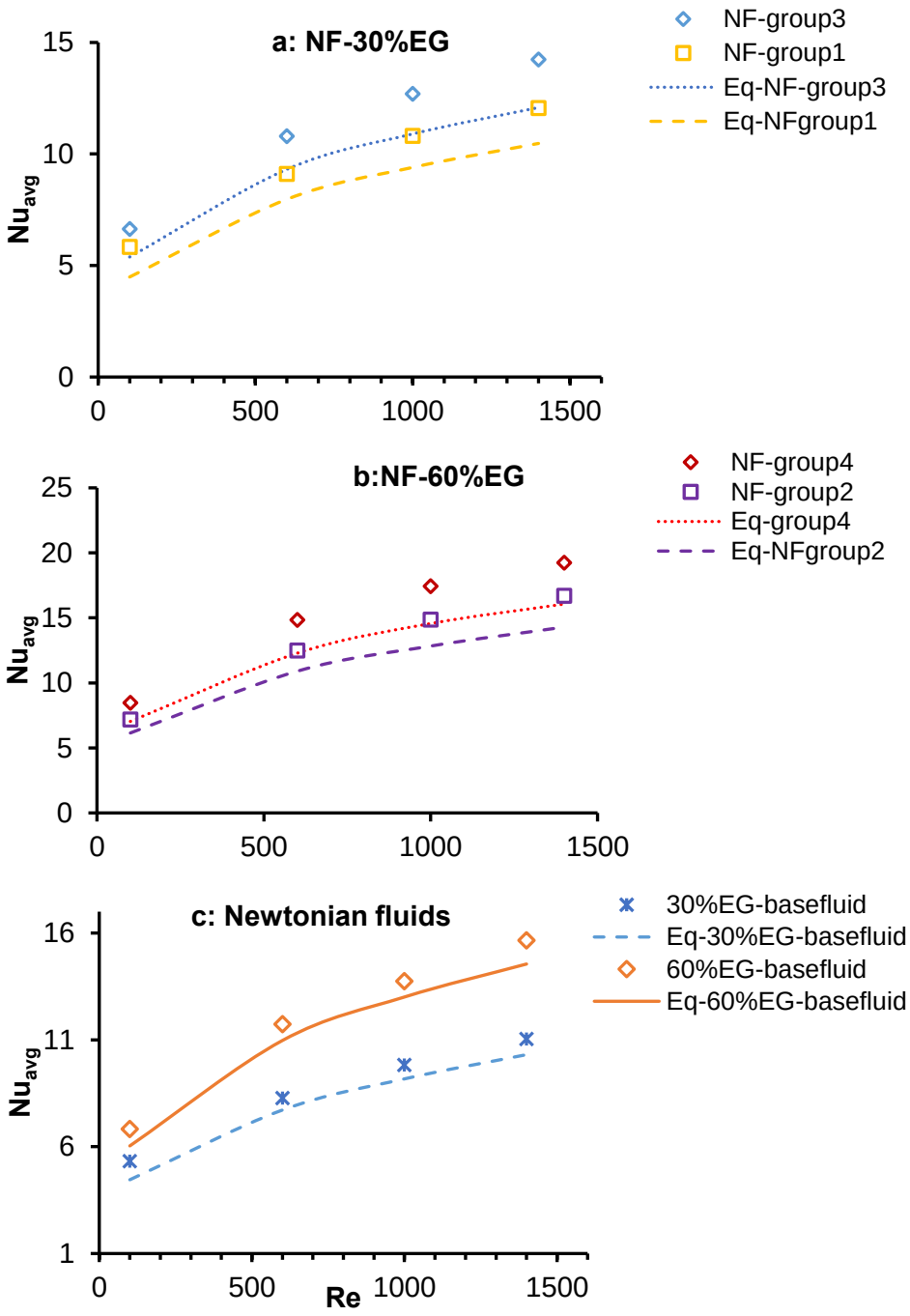

Fig. 4-23: The numerical results of Average Nu number in comparison with the results of the correlation for the Non-Newtonian fluids (**a** and **b**) and Newtonian fluids (**c**).

Moreover, the analytical results of the Eq. 4-34 show a deviation from the numerical results between 10% and 18% for the Non-Newtonian case. While a deviation between 7% and 12% for the Newtonian case.

The mentioned correlations for Non-Newtonian fluids (Eq. 4-34 and Eq. 4-33) and Newtonian fluids (Table 4-16) show that Nu number is governed by Graetz number (Gr) and Δ which reflexes the effect of Non-Newtonian behaviour of the fluid. As it is known, Graetz number determined by Eq. 4-35 based on Reynolds number (Re), Prandtl number (Pr) and the ratio (L/D). However, the current study intends to explore and develop the functional correlation between these parameters for the obtained numerical results. As previously state, the boundary conditions of the current study were for Reynolds number range between 100-1400, Prandtl number range between 18 < Pr < 81 and Non-Newtonian index between 0.911 < n < 0.975, under a constant heat flux. Also, the Graetz number for the whole tube length (Gr_L) has been calculated based on the data, giving values between 18< Gr_L <870.

In order to predict the average Nusselt number of non-Newtonian Nanofluids used in the present study, the numerical results of average Nusselt number are correlated as a function of Re number, Prandtl number and Δ (Nu=f (Re, Pr, Δ). It should be mention that this process is conducted for a fixed value of L/D=111. Therefore, the data are fitted via Multiple Variable Regression process to a correlation given by Eq. 4-37, enabling to find the intermediate values of the parameters a, a_1, a_2 and a_3.

$$Nu = a \cdot Re^{a_1} \cdot Pr^{a_2} \cdot \Delta^{a_3} \qquad \text{Eq. 4-37}$$

The resulting constant parameters are summarized in Table 4-17.

Table 4-17: The constants values of the correlation Eq. 4-37.

a	a_1	a_2	a_3	Deviation %Avg.	R^2
0.4709	0.3154	0.3361	-1.4254	2.63%	0.993

A good agreement is achieved when the predicted results of Eq. 4-37 are compared with the numerical results of average Nusselt number, presented an

average deviation of 2.71% and a correlation factor R^2=0.993. The positive values of the constants (a, a_1 and a_2) in the established Nusselt number equation are consistent with the fact that increasing Reynolds number and Prandtl number enhances the heat transfer [161].

Despite that, the physical analysis of the shear thinning behaviour of the fluids, described by the variable Δ, must refers to a positive effect on the heat transfer. This becomes stronger at low values of the Non-Newtonian index (n), [183] and [184]. In this, Azimian et al.[183] reported that the shear thinning fluid (n=0.7) has less pressure drop and less thermal resistance than a Newtonian (n=1) and shear thickening fluids (n=1.2) for Microchannel Heat Sinks. Also, Shojaeian et al.[184] have concluded that the increase in the power-law index (n) decreases Nusselt number value and the variation of thermophysical properties with the temperature of the fluid has an important effect on the heat transfer performance. This can be explained by the thinner boundary layers in shear thinning fluids[161] and the enhancement of the heat and mass transfer of the main flow and near-wall flow by the shear thinning viscosity [185].

Therefore, the Multiple Variable Regression fitting process of the data is repeated for a fixed value of a_3=1/3, chosen as the commonly used value in the found Nusselt number correlations (Eq. 4-34 and Eq. 4-33) for Non-Newtonian fluids. For this, the correlation form is given by Eq. 4-38 is used to find the intermediate values of the parameters a, a_1 and a_2.

$$Nu/\Delta^{1/3} = a \cdot Re^{a_1} \cdot Pr^{a_2} \qquad \text{Eq. 4-38}$$

The new resulting constant parameters are summarized in Table 4-18.

Table 4-18: The constants values of the correlation Eq. 4-38.

a	a_1	a_2	Deviation %Avg.	R^2
0.3972	0.3376	0.3374	2.33%	0.994

A good agreement is achieved when the predicted results of Eq. 4-38 are compared with the numerical results ($Nu/\Delta^{1/3}$), presented an average deviation of 2.33% and a correlation factor R^2=0.994. Moreover, the positive values of the parameters (a, a_1 and a_2) achieve the physical requirement. Furthermore, the

values of a_1 and a_2 are near to the standard value (1/3) in the common Nu number correlations of laminar flow under a uniform heat flux for Non-Newtonian fluids Eq. 4-34 and Newtonian fluids (Table 4-16).
The final form of the proposed equation can be written as follows (Eq. 4-39).

$$Nu = 0.3972 \cdot Re^{0.3376} \cdot Pr^{0.3374} \cdot \Delta^{0.3333} \qquad \text{Eq. 4-39}$$

The obtained results from the established correlation Eq. 4-39 for the four nanofluids samples (Non-Newtonian) were compared with the numerical results as shown in Fig. 4-24 (**a** and **b**). Also, the validity of using Eq. 4-39 correlation for Newtonian fluids was checked at Δ =1 (n=1) for the base fluids (30%EG and 60%EG) as shown in Fig. 4-24 (**c**), achieving an average deviation of 6.2% from the numerical results.

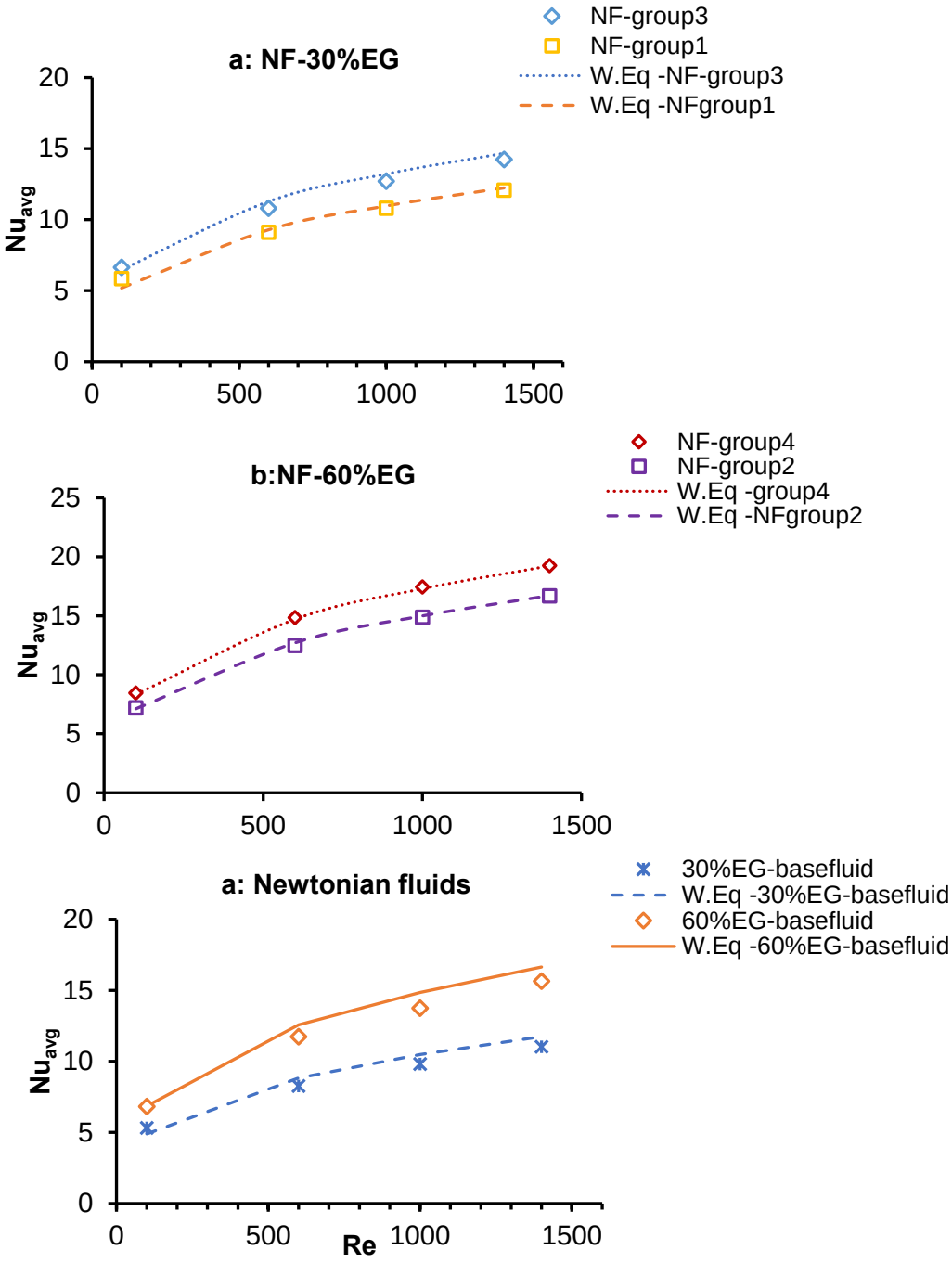

Fig. 4-24: The results of the new Average Nu number correlation in comparison with the numerical data as a function of Reynolds number.

4.6 CHAPTER CONCLUSION

This chapter clarifies and investigates the heat transfer characteristics of Non-Newtonian shear thinning fluids, particularly MWCNTs nanofluids, flowing in microchannels under a constant heat flux condition. The results show that MWCNT nanofluids enhance the thermal performance of microchannel heat exchangers with an increase in pressure drop. The Nu number achieves higher values for nanofluids with higher thermal diffusivity, increasing with the increase of Re number, but the extra pressure drop will somewhat decrease the beneficial effects. The most relevant conclusions of this study can be summarized as follows:

- A numerical code has been successfully validated with literature available containing experimental data for CNTs nanofluids flowing through microchannels.
- An investigation of the hydraulic and thermal fully development conditions has been conducted for Non-Newtonian nanofluids. A good agreement was found between the theoretical predictions and the obtained numerical results regarding velocity and dimensionless temperature profiles. It should be noted that for the considered fluids, the Non-Newtonian index, n, lies between 0.911 and 0.975 (n=1 corresponds to a Newtonian fluid).
- The laminar heat transfer coefficient and Nusselt number of all studied nanofluids were greater than those for the respective base fluid. On another hand, the obtained values regarding pressure drop suggested a more complex behaviour
- The increase in viscosity for NF_{group3} and NF_{group4} is much relevant than the increase in heat transfer coefficient, because of their higher particle concentration, resulting in a higher pressure drop. This leads to the selection of NF_{group1} and NF_{group2} as the best nanofluids among the studied ones, if a low-pressure drop is required.
- The maximum enhancement in heat transfer coefficient (33.2%) was obtained at Re= 600 for NF_{group3}. This effect slightly decreases by increasing the Re number.
- JF dimensionless number was used as a key performance indicator (KPI) of the studied fluids as it represents the overall energy efficiency

enhancement in heat transfer applications combining the thermal and hydraulic performances. A larger JF number corresponds to a higher performance heat transfer working fluid. The JF number was lower than the standard value (JF <1) at Re=100, due to the thick boundary layers. While it was higher than the standard value (JF >1) for all Nanofluids at Re higher than 600. This means that the use of MWCNTs nanofluids as heat transfer working fluid in micro heat exchangers is advantageous for Re>600 since the enhancement in heat transfer dominates over the losses due to pumping.

- The thermal resistance of the microchannel (R_{th}) decreases with the increase of Re number both for the base fluids and the nanofluids. However, the thermal resistance decreases when a nanofluid is used instead of the respective base fluid, irrespectively of its particle concentration. This is due to the decrease in the wall temperature obtained using Nanofluids.
- If priority must be given to heat transfer enhancement, without any concerns regarding pumping power, once EG concentration is adjusted to the freezing/boiling requirements, higher MWCNT particle loads should be selected.
- If priority must be given to energy efficiency (the combination of heat transfer enhancement and pressure drop limitation), once EG concentration is adjusted to the freezing/boiling requirements, nanofluids with lower MWCNT particle loads should be selected and operation should be tuned near Re=1000.
- A new Nu number correlation is proposed. The correlation was developed based on the CFD results for the following conditions: Reynolds number range of 100-1400, Prandtl number range of $18 < Pr < 81$ and Non-Newtonian index $0.911 < n < 0.975$, under a constant wall heat flux, and validated for a fixed microchannel geometry (L/D=111). This enables to see the influence of each parameter on enhancing heat transfer in the microchannel and provides an empirical method suitable for engineering applications in good agreement with an alternative more complex and time-consuming numerical approach.

CHAPTER 5- CONCLUSIONS

The general objective of this thesis was to investigate the transport phenomena associated with non-Newtonian nanofluids flowing in microchannels. The primary research programme application is the enhancement of heat transfer in micro heat exchangers, but there are many other applications such as microvalves development, biomechanics, microsensors and actuators, etc. In this context, the variation of nanofluid thermophysical properties has a significant effect on the heat transfer phenomena and fluid flow characteristics. Therefore, it was necessary to implement specific models describing the thermophysical properties of the nanofluids based on correlations considering the temperature and the fluid rheological behaviour.

The developed research programme comprised three different stages, with increasing complexity, towards the final research objective, namely:

1- the study/simulation of non-Newtonian fluid flow in macro channels

2- the study/simulation of Newtonian fluid flow in microchannels

3- the study/simulation of non-Newtonian fluid flow in microchannels

supported by previous and/or on-going experiential research work developed by the same research team or published results of other research groups.

As a result of the developed work plan, at a first stage, a numerical model for the fluid mechanics and heat transfer of non-Newtonian fluids flowing through macro-channels was proposed and validated. The considered non-Newtonian fluid was a nanofluid incorporating multiwalled carbon nanotubes (MWCNT)s in a water and ethylene glycol base fluid, showing a shear-thinning rheological behaviour. For validation purposes, experimental results of the convection heat transfer coefficient, measured in a team test rig and correlations for the thermophysical properties of the considered nanofluid (thermal conductivity and viscosity) for different temperatures and shear rates, measured by the same research team, were used. The computational results were compared with experimental data demonstrating good agreement.

At the second stage, a wide study was carried out for the fluid flow in microscale conditions for a well-known fluid (Water). Some concepts have been established for this case, which allowed to propose a suitable methodology and

acceptable assumptions to proceed to the third stage and build an accurate numerical approach for nanofluids in a microchannel, validated by reproducing available experimental results for CNTs nanofluids flowing through microchannels. After validation, sixty samples corresponding to different formulations of MWCNTs nanofluids (corresponding to different particles morphology and concentration, together with two ethylene glycol concentration in the base fluid) were analysed as single-phase fluid with appropriate thermophysical properties and rheological behaviour. These samples were represented by four reference fluids with representative thermophysical properties and used in an extensive numerical investigation to evaluate the heat and momentum transport phenomena associated with the laminar flow of shear thinning fluids in microchannels. The obtained results allowed to establish several relationships between different parameters affecting heat transfer in micro heat exchangers, including an overall performance evaluation considering the energy efficiency enhancement, considering both the heat transfer gains and the pumping power increase due to the pressure drop.

5.1 CONCLUSIONS

The first stage of this investigation started with a well-understood macroscale problem for heat transfer and fluid flow of MWCNTs nanofluids, known as shear thinning fluid. The study conducted in Chapter-2 established thermophysical properties correlations, namely for the viscosity and the thermal conductivity, to be used as input data of the numerical approach. A single-phase model using CFD tools (ANSYS-FLUENT) was built. The performance of MWCNTs/(DW+EG) nanofluids regarding heat transfer coefficient, pressure drop, friction coefficient and wall shear stress were investigated. A comparison between numerical, empirical and experimental data was made and investigated in detail. The highest deviation from experimental data was observed for Shah equation with a deviation of (15%), followed by the numerical results assuming constant-properties (5%). The smallest deviation was found for the numerical results considering variable properties (4%). Enhancement of heat transfer coefficient relative to the respective base fluid was observed showing an average

improvement of 10% and 14% for 0.25% MWCNTs and 0.5% MWCNTs nanofluids, respectively. A heat transfer coefficient enhancement relative to the respective base fluid was consistent with increases of Reynolds number and particle volume fraction. This effect was accompanied by a rise in pressure drop of 9.3% and 14.8%, respectively. The pressure drop and wall shear stress were found to rise with the increase of Reynolds number and particle volume fraction, while the friction coefficient registered a decrease with increasing Reynolds number. A good capability of the single-phase approach simulating shear thinning nanofluids was reported. Furthermore, the validity of the proposed correlations for viscosity and thermal conductivity of the considered nanofluids allowed to achieve good results, a promising output for further numerical studies involving MWCNTs nanofluids, namely in a microchannel.

To understand the effect of the micro-channel scale in the flow conditions, the fundamentals of fluid flow and heat transfer in microchannels for Newtonian fluids (water) were reviewed. The tiny dimensions of microchannels result in a large surface-to-volume ratio making near-wall effects particularly important. The temperature and velocity gradients near the wall and the boundary-layer thickness compared to microchannel dimensions have a significant effect on the heat and momentum transfer phenomena. Therefore, viscous heating, transition Re number and dependent-temperature thermophysical properties should be considered. The transition from laminar to turbulent flow starts much earlier in the microchannel fluid flow (e.g. Re=1500). At this stage, different experimental studies were numerically reproduced and a reasonable agreement was achieved between computational results and correlated experimental data. This result supports the conclusion that if a proper methodology and acceptable assumptions are followed it is possible to achieve accurate results for the simulated flow of conventional fluids in microchannels.

From the above stated, it may be said that the validated assumptions and methodology described in Chapter-3 may be considered suitable for further numerical investigations on heat transfer and fluid flow of shear thinning nanofluids flowing through microchannels. Moreover, the boundary conditions regarding Non-Newtonian fluids were considered and the related nondimensional numbers (Re and Pr) presented in chapter 4 were used.

The results have shown larger heat transfer coefficient and Nusselt number values for all nanofluids in comparison to the base fluid. The maximum enhancement in heat transfer coefficient (33.2%) has been obtained at Re =600 for NF_{group3}. The obtained results were used to propose a new correlation for the average Nusselt number ($Nu = 0.397 \cdot Re^{0.337} \cdot Pr^{0.337} \cdot \Delta^{0.333}$) describing the influence of Re number, Prandtl number and the Non-Newtonian index (n) on heat transfer performance. In addition, it provides a reliable analytical prediction to estimate the heat transfer performance under the current study conditions (L/D=111, 100 <Re<1400, 18 < Pr < 81 and 0.911 < n < 0.975, under a constant wall heat flux).

To assess the overall energy efficiency enhancement combining the thermal and hydraulic performances for the studied family of non-Newtonian fluids, the JF dimensionless number was used as a key performance indicator (KPI). The results indicated that the enhancement in heat transfer dominates the losses of the pumping energy caused by the increase in the pressure drop for Re number ranging from 600 to 1400. However, at low Reynolds number (Re=100), the results indicated a negative impact on energy efficiency due to the thick boundary layer that increases the pressure drops and reduces the heat transfer coefficient.

Despite the variation in the results between the four Nanofluids families studied, it is not easy to classify them as good or bad, since their applications can be different, as they have different thermophysical properties such as freezing and boiling temperatures.

In summary, the developed research programme succeeds in answering the questions raised in the objectives of the thesis, as follows:

1- *How do different MWCNTs nanofluids structures affect the heat transfer enhancement in microchannels for different flow conditions?*

   The heat transfer performance of four representative MWCNTs nanofluids was investigated. These nanofluids families differ regarding their thermophysical properties, namely thermal conductivity and viscosity. The obtained results reported that increasing the particle concentration enhances higher heat transfer

as well as pressure drop. In addition, for low particle concentrations, the comparison between two nanofluids with different base fluids points out to a better heat transfer performance for the one with lower viscosity and higher thermal conductivity (30%EG). However, it is not possible to do an absolute ranking since each nanofluid may have other specific properties such as boiling and freezing points, rendering it the better choice for a specific application. Nevertheless, if the JF non dimensional number is taken in account, it is possible to conclude that increasing the particle concentration can be useful for the higher percentage of EG in the base fluid (60%), while in the case of low percentage of EG in the base fluid (30%), reducing the particle concentration is preferred.

2- *How will the performance of microchannel be when using MWCNTs nanofluids as a heat transfer fluid regarding Nusselt number and pressure drop?*

It was verified a heat transfer performance enhancement for the four nanofluids if compared with the respective base fluid. Once EG concentration is adjusted to the freezing/boiling requirements, if priority must be given to heat transfer enhancement, without any concerns regarding pumping power, higher MWCNT particle loads should be selected. On the other hand, higher particle concentration leads to an increase of the viscosity resulting in a higher pressure drop. This leads to the selection of NF_{group3} and NF_{group4} as the best nanofluids among the studied ones if a high heat transfer performance is required, and to the selection of NF_{group1} and NF_{group2} if a low-pressure drop value is more important than a high heat transfer rate.

3- *How will the use of nanofluid in CHE contribute to enhancing the efficiency of the energy systems? What is the effect of that on the environmental and climatic change?*

The use of MWCNTs nanofluids enhances the overall energy efficiency of the heat exchanger system under specific fluid flow conditions (600<Re<1400). In these conditions, the enhancement in heat transfer given by MWCNTs nanofluids dominates the extra pumping energy required due to the increase in the viscosity. Therefore, if priority must be given to energy efficiency (the combination of heat transfer enhancement and pressure drop limitation), once EG concentration is adjusted to the freezing/boiling requirements, nanofluids with lower MWCNT particle loads should be selected and operation should be tuned near Re=1000. The increase in energy efficiency will reduce pollution emissions, providing a significant benefit to the environment and climatic change.

As a result of the developed research programme, it was possible to confirm, that the addition of MWCNTs to conventional thermal fluids enhances its heat transfer performance when used in microchannel heat exchangers.

5.2 FUTURE WORK

The conducted research programme answers successfully all the originally proposed research questions. Nonetheless, the developed work revealed additional questions and research ideas.

For future work, it is of the utmost importance to conduct experimental studies regarding heat transfer enhancement in a microchannel using nanofluids, particularly MWCNTs nanofluids. Also, it is needed to characterize the density and specific heat of MWCNTs nanofluids by a wide experimental study.

In addition, it is important to experimentally study nanofluids in turbulent flow conditions. Moreover, it will be a significant contribution to provide a validated viscosity model able to describe the rheological behaviour of Non-Newtonian fluids under turbulent flow conditions to be used in CFD tools for future numerical investigations.

Finally, further experimental investigations are required in this emerging field to fully explain heat transfer enhancement in microchannels employing nanofluids with stronger non-Newtonian behaviour.

REFERENCES

[1] H. A. Mohammed, G. Bhaskaran, N. H. Shuaib, and R. Saidur, "Heat transfer and fluid flow characteristics in microchannels heat exchanger using nanofluids: A review," *Renew. Sustain. Energy Rev.*, vol. 15, no. 3, pp. 1502–1512, 2011.

[2] F. P. INCROPERA, D. P. DEWITT, School, T. L. BERGMAN, and A. S. LAVINE, *Fundamentals of Heat and Mass Transfer*. John Wiley & Sons, Inc, 2007.

[3] D. Wen, G. Lin, S. Vafaei, and K. Zhang, "Review of nanofluids for heat transfer applications," *Particuology*, vol. 7, no. 2, pp. 141–150, 2009.

[4] S. U. S. Choi and J. A. Eastman, "Enhancing thermal conductivity of fluids with nanoparticles," *ASME Int. Mech. Eng. Congr. Expo.*, vol. 66, pp. 99–105, 1995.

[5] V. Trisaksri and S. Wongwises, "Critical review of heat transfer characteristics of nanofluids," *Renew. Sustain. Energy Rev.*, vol. 11, no. 3, pp. 512–523, 2007.

[6] S. U. S. Choi and J. A. Eastman, "Enhancing thermal conductivity of fluids with nanoparticles," *ASME Int. Mech. Eng. Congr. Expo.*, vol. 66, no. March, pp. 99–105, 1995.

[7] S. U. S. Choi, Z. G. Zhang, W. Yu, F. E. Lockwood, and E. A. Grulke, "Anomalous thermal conductivity enhancement in nanotube suspensions," *Appl. Phys. Lett.*, vol. 79, no. 14, pp. 2252–2254, 2001.

[8] J. A. Eastman, S. U. S. Choi, S. Li, W. Yu, and L. J. Thompson, "Anomalously increased effective thermal conductivities of ethylene glycol-based nanofluids containing copper nanoparticles," *Appl. Phys. Lett.*, vol. 78, no. 6, pp. 718–720, 2001.

[9] S. M. S. Murshed, K. C. Leong, and C. Yang, "Enhanced thermal conductivity of TiO2-Waterbased nanofluids," *Int. J. Therm. Sci.*, vol. 44, no. 4, pp. 367–373, 2005.

[10] M. Liu, M. Lin, and C. Wang, "Enhancements of thermal conductivities with Cu, CuO, and carbon nanotube nanofluids and application of MWNT/water nanofluid on a water chiller system," *Nanoscale Res. Lett.*, vol. 6, no. 1, p. 297, 2011.

[11] S. M. S. Murshed and C. A. Nieto De Castro, “Superior thermal features of carbon nanotubes-based nanofluids - A review,” *Renew. Sustain. Energy Rev.*, vol. 37, pp. 155–167, 2014.

[12] R. Sadri *et al.*, “A facile, bio-based, novel approach for synthesis of covalently functionalized graphene nanoplatelet nano-coolants toward improved thermo-physical and heat transfer properties,” *J. Colloid Interface Sci.*, vol. 509, pp. 140–152, 2017.

[13] G. Vakili-Nezhaad, M. Al-Wadhahi, A. M. Gujrathi, R. Al-Maamari, and M. Mohammadi, “Effect of temperature and diameter of narrow single-walled carbon nanotubes on the viscosity of nanofluid: A molecular dynamics study,” *Fluid Phase Equilib.*, vol. 434, pp. 193–199, 2017.

[14] M. Muruganandam and P. C. M. Kumar, “Experimental analysis of four-stroke diesel engine by using carbon nanotubes based nanofluids as a coolant,” *J. Appl. Fluid Mech.*, vol. 10, no. SpecialIssue, pp. 1–5, 2017.

[15] M. M. Sarafraz, V. Nikkhah, M. Nakhjavani, and A. Arya, “Fouling formation and thermal performance of aqueous carbon nanotube nanofluid in a heat sink with rectangular parallel microchannel,” *Appl. Therm. Eng.*, vol. 123, pp. 29–39, 2017.

[16] P. C. M. Kumar and M. Muruganandam, “Stability analysis of heat transfer MWCNT with different base fluids,” *J. Appl. Fluid Mech.*, vol. 10, no. SpecialIssue, pp. 51–59, 2017.

[17] N. S. Rajput, “Thermal Analysis of MWCNT/ Distilled Water Nanofluid on the Efficiency of Flat Plate Solar Collector,” vol. 8, no. 8, pp. 233–240, 2017.

[18] A. Hosseinian, A. H. Meghdadi Isfahani, and E. Shirani, “Experimental investigation of surface vibration effects on increasing the stability and heat transfer coefficient of MWCNTs-water nanofluid in a flexible double pipe heat exchanger,” *Exp. Therm. Fluid Sci.*, vol. 90, pp. 275–285, 2018.

[19] B. C. Lamas *et al.*, “EG/CNTs Nanofluids Engineering and Thermo-Rheological Characterization,” *J. Nano Res.*, vol. 13, pp. 69–74, 2011.

[20] B. Lamas, B. Abreu, A. Fonseca, N. Martins, and M. Oliveira, “Long-term MWCNTs nanofluids toward heat transfer capability improvement,” *J. Phys. Chem. C*, vol. 117, no. 24, pp. 12826–12834, 2013.

[21] B. Abreu, “Rheological Characterization and Modelling of CNT Nanofluids,”

2018.

[22] B. C. Lamas, “Nanofluids development and characterization for heat exchanging intensification,” 2013.

[23] D. B. Tuckerman and R. F. W. Pease, “High-performance heat sinking for VLSI,” *IEEE Electron Device Lett.*, vol. 2, no. 5, pp. 126–129, 1981.

[24] Z. Wu and B. Sundén, “On further enhancement of single-phase and flow boiling heat transfer in micro / minichannels,” *Renew. Sustain. Energy Rev.*, vol. 40, pp. 11–27, 2014.

[25] G. L. Morini, “Scaling effects for liquid flows in microchannels,” *Heat Transf. Eng.*, vol. 27, no. 4, pp. 64–73, 2006.

[26] P. Rosa, T. G. Karayiannis, and M. W. Collins, “Single-phase heat transfer in microchannels: The importance of scaling effects,” *Appl. Therm. Eng.*, vol. 29, no. 17–18, pp. 3447–3468, 2009.

[27] G. P. Celata, *Heat Transfer and Fluid Flow in Microchannels*. New York: Begell House Inc., 2004.

[28] M. Raja, R. Vijayan, P. Dineshkumar, and M. Venkatesan, “Review on nanofluids characterization, heat transfer characteristics and applications,” *Renew. Sustain. Energy Rev.*, vol. 64, pp. 163–173, 2016.

[29] N. M. Mubarak, E. C. Abdullah, N. S. Jayakumar, and J. N. Sahu, “An overview on methods for the production of carbon nanotubes,” *J. Ind. Eng. Chem.*, vol. 20, no. 4, pp. 1186–1197, 2014.

[30] M. N. A. W. M. Yazid, N. A. C. Sidik, R. Mamat, and G. Najafi, “A review of the impact of preparation on stability of carbon nanotube nanofluids,” *Int. Commun. Heat Mass Transf.*, vol. 78, pp. 253–263, 2016.

[31] H. Xie and L. Chen, “Review on the preparation and thermal performances of carbon nanotube contained nanofluids,” *J. Chem. Eng. Data*, vol. 56, no. 4, pp. 1030–1041, 2011.

[32] B. Lamas, B. Abreu, A. Fonseca, N. Martins, and M. Oliveira, “Critical analysis of the thermal conductivity models for CNT based nanofluids,” *Int. J. Therm. Sci.*, vol. 78, pp. 65–76, 2014.

[33] M. N. A. W. M. Yazid, N. A. C. Sidik, and W. J. Yahya, “Heat and mass transfer characteristics of carbon nanotube nanofluids: A review,” *Renew. Sustain. Energy Rev.*, vol. 80, no. June, pp. 914–941, 2017.

[34] A. Ijam, R. Saidur, P. Ganesana, and A. M. Golsheikh, “Stability, thermo-physical properties, and electrical conductivity of graphene oxide-deionized water/ethylene glycol based nanofluid,” *Int. J. Heat Mass Transf.*, 2015.

[35] H. E. Patel, K. B. Anoop, T. Sundararajan, and S. K. Das, “Model for thermal conductivity of CNT-nanofluids,” *Bull. Mater. Sci*, vol. 31, no. 3, pp. 387–390, 2008.

[36] E. V. Timofeeva, J. L. Routbort, and D. Singh, “Particle shape effects on thermophysical properties of alumina nanofluids,” *J. Appl. Phys.*, vol. 106, no. 1, 2009.

[37] C.-W. Nan, G. Liu, Y. Lin, and M. Li, “Interface effect on thermal conductivity of carbon nanotube composites,” *Appl. Phys. Lett.*, vol. 85, no. 16, pp. 3549–3551, 2004.

[38] T. B. Gorji and A. A. Ranjbar, “Geometry optimization of a nanofluid-based direct absorption solar collector using response surface methodology,” *Sol. Energy*, vol. 122, pp. 314–325, 2015.

[39] K. Y. Leong, H. C. Ong, N. H. Amer, M. J. Norazrina, M. S. Risby, and K. Z. Ku Ahmad, “An overview on current application of nanofluids in solar thermal collector and its challenges,” *Renew. Sustain. Energy Rev.*, vol. 53, pp. 1092–1105, 2016.

[40] I. Mudawar, “Recent Advances in High-Flux, Two-Phase Thermal Management,” *J. Therm. Sci. Eng. Appl.*, vol. 5, no. 2, 2013.

[41] A. Maqsood and M. Arshad, “Thermal transport properties of nanofluids containing carbon nanotubes,” in *Proceedings of the Sixth International ASME Conference on Nanochannels, Microchannels and Minichannels*, 2008, vol. 27, pp. 1830–1834.

[42] T.-H. Tsai and R. Chein, “Performance analysis of nanofluid-cooled microchannel heat sinks,” *Int. J. Heat Fluid Flow*, vol. 28, no. 5, pp. 1013–1026, 2007.

[43] H. Moon, S. Bindiganavale, Y. Nanayakkaras, and D. W. Armstrong, “Icnmm2009-82264 Digital Microfluidic Device Using Ionic Liquids,” in *Proceedings of the ASME 2009 7th International Conference on Nanochannels*, 2009, pp. 1–4.

[44] S. Ebrahimi, J. Sabbaghzadeh, M. Lajvard, and I. Hadi, “Heat sink with Nanofluids Containing CNTs,” in *Proceedings of the 2009 4th IEEE Internationa*, 2009, pp. 864–867.

[45] “2012 12th IEEE International Conference on Nanotechnology, NANO 2012,” in *Proceedings of the IEEE Conference on Nanotechnology*, 2012.

[46] R. Kamali, Y. Jalali, and A. R. Binesh, “Investigation of multiwall carbon nanotube-based nanofluid advantages in microchannel heat sinks,” *Micro Nano Lett.*, vol. 8, no. 6, pp. 319–323, 2013.

[47] S. Halelfadl, A. M. Adham, N. Mohd-Ghazali, T. Maré, P. Estellé, and R. Ahmad, “Optimization of thermal performances and pressure drop of rectangular microchannel heat sink using aqueous carbon nanotubes based nanofluid,” *Appl. Therm. Eng.*, vol. 62, no. 2, pp. 492–499, 2014.

[48] S. M. S. Murshed, D. Milanova, and R. Kumar, “Characteristics of Carbon Nanotubes-Nanofluids,” in *Proceedings of the ASME 2009 7th International Conference on Nanochannels, Microchannels and Minichannels*, 2014, pp. 2–7.

[49] L. F. Chen, H. Xie, Y. Li, and W. Yu, “ICNMM2009-82055,” in *Proceedings of the ASME 2009 7th International Conference on Nanochannels, Microchannels and Minichannels*, 2014, pp. 2–5.

[50] L. Chen, H. Xie, Y. Li, and W. Yu, “Preparation of Stable Silicone Oil Based Nanofluid Containing Multi-Walled Carbon Nanotube by Using Hexamethyldisiloxane as Dispersant,” in *Proceedings of ASME 2010 3rd Joint US-European Fluids Engineering Summer Meeting and 8th International Proceedings of the ASME 2010 3rd Joint US-European Fluids Engineering Summer Meeting and 8th International Conference on Nanochannels, Microchannels, an*, 2010.

[51] C.-Y. Chung, M. E. Warkiani, S. Mesgari, G. Rosengarten, and R. Taylor, “Thermoset polyester-based superhydrophobic microchannels for nanofluid heat transfer applications,” in *proceedings of spiedigital library*, 2015, vol. 9668, p. 96680D.

[52] Z. Nikkhah *et al.*, “Forced convective heat transfer of water/functionalized multi-walled carbon nanotube nanofluids in a microchannel with oscillating heat flux and slip boundary condition,” *Int. Commun. Heat Mass Transf.*, vol.

68, pp. 69–77, 2015.

[53] A. Karimipour, A. Taghipour, and A. Malvandi, “Developing the laminar MHD forced convection flow of water/FMWNT carbon nanotubes in a microchannel imposed the uniform heat flux,” *J. Magn. Magn. Mater.*, vol. 419, pp. 420–428, 2016.

[54] C. N. Nanofluid *et al.*, “Thermal and Hydrodynamic Performance of a Microchannel Heat Sink Cooled with Carbon Nanotubes Nanofluid,” *J. Teknol.*, vol. 790, pp. 69–77, 2016.

[55] S. Ahlatli, T. Mare, P. Estelle, and N. Doner, “Thermal performance of carbon nanotube nanofluids in solar microchannel collectors: An experimental study,” *Int. J. Technol.*, vol. 7, no. 2, 2016.

[56] J. Li and L. Fan, “An Experimental Study of Boiling Heat Transfer During Quenching,” in *Proceedings of the ASME 2016 Heat Transfer Summer Conference*, 2016, pp. 1–7.

[57] R. Nimmagadda and K. Venkatasubbaiah, “Multiphase Approach on Heat Transfer Performance of Micro-channel using Hybrid Carbon Nanofluid,” in *Proceedings of the ASME 2015 13th International Conference on Nanochannels, Microchannels, and Minichannels*, 2015, pp. 1–9.

[58] M. Nojoomizadeh and A. Karimipour, “The effects of porosity and permeability on fluid flow and heat transfer of multi-walled carbon nanotubes suspended in oil (MWCNT/Oil nanofluid) in a microchannel filled with a porous medium,” *Phys. E*, vol. 84, pp. 423–433, 2016.

[59] R. Nimmagadda and K. Venkatasubbaiah, “Two-Phase Analysis on the Conjugate Heat Transfer Performance of Microchannel With Cu, Al, SWCNT, and Hybrid Nanofluids,” *J. Therm. Sci. Eng. Appl.*, vol. 9, no. 4, p. 041011, 2017.

[60] A. A. A. Arani *et al.*, “Heat transfer improvement of water/single-wall carbon nanotubes (SWCNT) nanofluid in a novel design of a truncated double-layered microchannel heat sink,” *Int. J. Heat Mass Transf.*, vol. 113, pp. 780–795, 2017.

[61] A. Arabpour, A. Karimipour, and D. Toghraie, “The study of heat transfer and laminar flow of kerosene/multi-walled carbon nanotubes (MWCNTs) nanofluid in the microchannel heat sink with slip boundary condition,” *J.*

Therm. Anal. Calorim., no. m, 2017.

[62] M. N. A. W. M. Yazid, N. A. C. Sidik, and W. J. Yahya, "Heat and mass transfer characteristics of carbon nanotube nano fluids : A review," *Renew. Sustain. Energy Rev.*, vol. 80, no. May, pp. 914–941, 2017.

[63] T.-C. Hung, W.-M. Yan, X.-D. Wang, and C.-Y. Chang, "Heat transfer enhancement in microchannel heat sinks using nanofluids," *Int. J. Heat Mass Transf.*, vol. 55, no. 9–10, pp. 2559–2570, 2012.

[64] E. Manay and B. Sahin, "Heat Transfer and Pressure Drop of Nanofluids in a Microchannel Heat Sink," *Heat Transf. Eng.*, vol. 38, no. 5, pp. 510–522, 2017.

[65] K. S. Arjun and K. Rakesh, "Heat Transfer Enhancement Using Alumina Nanofluid in Circular Micro Channel.," *J. Eng. Sci. Technol.*, vol. 12, no. 1, pp. 265–279, 2017.

[66] Y.-T. Yang, K.-T. Tsai, Y.-H. Wang, and S.-H. Lin, "Numerical study of microchannel heat sink performance using nanofluids," *Int. Commun. Heat Mass Transf.*, vol. 57, pp. 27–35, 2014.

[67] A. Esmaeilnejad, H. Aminfar, and M. S. Neistanak, "Numerical investigation of forced convection heat transfer through microchannels with non-Newtonian nanofluids," *Int. J. Therm. Sci.*, vol. 75, pp. 76–86, 2014.

[68] H. A. Mohammed, G. Bhaskaran, N. H. Shuaib, and H. I. Abu-Mulaweh, "Influence of nanofluids on parallel flow square microchannel heat exchanger performance," *Int. Commun. Heat Mass Transf.*, vol. 38, no. 1, pp. 1–9, 2011.

[69] A. A. Hussien, M. Z. Abdullah, and M. A. Al-Nimr, "Single-phase heat transfer enhancement in micro/minichannels using nanofluids: Theory and applications," *Appl. Energy*, vol. 164, pp. 733–755, 2016.

[70] X. D. Wang, Bin An, and J. L. Xu, "Optimal geometric structure for nanofluid-cooled microchannel heat sink under various constraint conditions," *Energy Convers. Manag.*, vol. 65, pp. 528–538, 2013.

[71] H. Garg, V. S. Negi, N. Garg, and A. Lall, "Numerical and experimental analysis of microchannel heat transfer for nanoliquid coolant using different shapes and geometries," in *Proceedings of the Institution of Mechanical Engineers, Part C: Journal of Mechanical Engineering Science*, 2015, vol. 229, no. 11, pp. 2056–2065.

[72] M. Kadja and I. Rezaiguia, "Investigation of conjugate heat transfer in microchannels using variable thermophysical property nanofluids," *ASME International Mechanical Engineering Congress and Exposition, Proceedings (IMECE)*, vol. 15. 2013.

[73] M. A. Al-Nimr, M. Maqableh, A. F. Khadrawi, and S. A. Ammourah, "Fully developed thermal behaviors for parallel flow microchannel heat exchanger," *Int. Commun. Heat Mass Transf.*, vol. 36, no. 4, pp. 385–390, 2009.

[74] D. Lelea and S. Nishio, "The experimental research on microtube heat transfer and fluid flow of distilled water," *nternational J. Heat Mass Transf.*, pp. 2817–2830, 2004.

[75] E. Ebrahimnia-Bajestan, H. Niazmand, W. Duangthongsuk, and S. Wongwises, "Numerical investigation of effective parameters in convective heat transfer of nanofluids flowing under a laminar flow regime," *Int. J. Heat Mass Transf.*, vol. 54, no. 19–20, pp. 4376–4388, 2011.

[76] B. Sun, Z. Zhang, D. Yang, and H. Li, "Heat transfer and flow resistance characteristics with drag reducing nanofluids in circular tube," *Huagong Xuebao/CIESC J.*, vol. 66, no. 11, 2015.

[77] S. K. Sahu, "Comparative Study on Heat Transfer Enhancement of Low Volume Concentration of Al2O3–Water and Carbon Nanotube–Water Nanofluids in Laminar Regime Using Helical Screw Tape Inserts," *J. Nanotechnol. Eng. Med.*, 2014.

[78] P. Garg, J. L. Alvarado, C. Marsh, T. A. Carlson, D. A. Kessler, and K. Annamalai, "An experimental study on the effect of ultrasonication on viscosity and heat transfer performance of multi-wall carbon nanotube-based aqueous nanofluids," *Int. J. Heat Mass Transf.*, vol. 52, no. 21–22, pp. 5090–5101, 2009.

[79] A. Amrollahi, A. M. Rashidi, and M. E. Meibodi, "Convection heat transfer of functionalized MWNT in aqueous fluids in laminar and turbulent flow at the entrance region," *Int. Commun. Heat Mass Transf.*, vol. 37, pp. 717–723, 2010.

[80] M. A. Akhavan-Behabadi, M. Shahidi, M. R. Aligoodarz, and M. Ghazvini, "Experimental investigation on thermo-physical properties and overall

performance of MWCNT–water nanofluid flow inside horizontal coiled wire inserted tubes," *Heat Mass Transf.*, vol. 53, no. 1, pp. 291–304, 2017.

[81] G. A. Oliveira, E. Martin, C. Contreras, E. Pedone, and B. Filho, "Experimental study on the heat transfer of MWCNT / water nanofluid flowing in a car radiator," *Appl. Therm. Eng.*, vol. 111, pp. 1450–1456, 2017.

[82] A. A. Hussien, M. Z. Abdullah, N. M. Yusop, M. A. Al-Nimr, M. A. Atieh, and M. Mehrali, "Experiment on forced convective heat transfer enhancement using MWCNTs/GNPs hybrid nanofluid and mini-tube," *Int. J. Heat Mass Transf.*, vol. 115, pp. 1121–1131, 2017.

[83] V. Kumaresan, S. Mohaideen Abdul Khader, S. Karthikeyan, and R. Velraj, "Convective heat transfer characteristics of CNT nanofluids in a tubular heat exchanger of various lengths for energy efficient cooling/heating system," *Int. J. Heat Mass Transf.*, vol. 60, no. 1, pp. 413–421, 2013.

[84] Y. Ding, H. Alias, D. Wen, and R. A. Williams, "Heat transfer of aqueous suspensions of carbon nanotubes (CNT nanofluids)," *Int. J. Heat Mass Transf.*, vol. 49, no. 1–2, pp. 240–250, 2006.

[85] F. Rashidi and N. M. Nezamabad, "Experimental investigation of convective heat transfer coefficient of CNTs nanofluid under constant heat flux," in *Proceedings of the World Congress on Engineering 2011 Vol III*, 2011, vol. 3, pp. 6–11.

[86] B. H. Thang, P. Van Trinh, N. Van Chuc, P. H. Khoi, and P. N. Minh, "Heat Dissipation for Microprocessor Using Multiwalled Carbon Nanotubes Based Liquid," *Sci. World J.*, p. 6, 2013.

[87] B. H. Thang, L. Dinh Quang, N. Manh Hong, P. H. Khoi, and P. N. Minh, "Application of multiwalled carbon nanotube nanofluid for 450 W LED floodlight," *J. Nanomater.*, p. 6, 2014.

[88] C. R. Dietz and Y. K. Joshi, "Single-Phase Forced Convection in Microchannels with Carbon Nanotubes for Electronics Cooling Applications," *Nanoscale and Microscale Thermophysical Engineering*, vol. 12, no. 3, pp. 251–271, 2008.

[89] A. S. Mujumdar, "HANDBOOK OF NUMERICAL HEAT TRANSFER," *Dry. Technol.*, vol. 7, no. 4, pp. 843–845, Dec. 1989.

[90] S. Patankar, *Numerical heat transfer and fluid flow*. NewYork, 1980.

[91] A. N. Smith and P. M. Norris, *Microscale heat transfer*, no. May. 2003.

[92] H. K. Versteeg and W. Malalasekera, *An Introduction to Computational Fluid Dynamics*. 1995.

[93] S. Özerinç, A. G. Yazcoglu, and S. Kakaç, "Numerical analysis of laminar forced convection with temperature-dependent thermal conductivity of nanofluids and thermal dispersion," *Int. J. Therm. Sci.*, vol. 62, pp. 138–148, 2012.

[94] *ANSYS FLUENT 12.0 User's Guide*, vol. 123, no. 6. 2009.

[95] Corrnell University, "A Hands-on Introduction to Engineering Simulations: Computational Fluid Dynamics (CFD)." [Online]. Available: https://courses.edx.org/courses/course-v1:CornellX+ENGR2000X+1T2018/course/.

[96] J. Anderson, *Computational Fluid Dynamics: The Basics with Applications*. 1995.

[97] *ANSYS FLUENT 18.2 User's Guide*. 2017.

[98] T.-H. Shih, W. W. Liou, A. Shabbir, Z. Yang, and J. Zhu, "A New - Eddy-Viscosity Model for High Reynolds Number Turbulent Flows - Model Development and Validation," *Comput. Fluids*, vol. 24, no. 3, pp. 227–238, 1995.

[99] W. Rashmi, M. Khalid, A. F. Ismail, R. Saidur, and A. K. Rashid, "Experimental and numerical investigation of heat transfer in CNT nanofluids," *J. Exp. Nanosci.*, vol. 10, no. 7, pp. 545–563, 2013.

[100] R. Kamali and A. R. Binesh, "Numerical investigation of heat transfer enhancement using carbon nanotube-based non-Newtonian nanofluids," *Int. Commun. Heat Mass Transf.*, vol. 37, no. 8, pp. 1153–1157, 2010.

[101] S. Ebrahimi, J. Sabbaghzadeh, M. Lajvard, and I. Hadi, "Cooling performance of a microchannel heat sink with nanofluids containing cylindrical nanoparticles (carbon nanotubes)," *Heat Mass Transf.*, 2010.

[102] A. Arabpour, A. Karimipour, and D. Toghraie, "The study of heat transfer and laminar flow of kerosene / multi-walled carbon nanotubes (MWCNTs) nanofluid in the microchannel heat sink with slip boundary condition," *J. Therm. Anal. Calorim.*, vol. 131, no. 2, pp. 1553–1566, 2018.

[103] G. D. Xia, R. Liu, J. Wang, and M. Du, "The characteristics of convective heat

transfer in microchannel heat sinks using Al2O3 and TiO2 nano fluids," *Int. Commun. Heat Mass Transf.*, vol. 76, pp. 256–264, 2016.

[104] A. Raisi, B. Ghasemi, and S. M. Aminossadati, "A numerical study on the forced convection of laminar nanofluid in a microchannel with both slip and no-slip conditions," *Numer. Heat Transf. Part A Appl.*, vol. 59, no. 2, pp. 114–129, 2011.

[105] H. A. Mohammed, P. Gunnasegaran, and N. H. Shuaib, "Heat transfer in rectangular microchannels heat sink using nanofluids," *International Communications in Heat and Mass Transfer*, vol. 37, no. 10. pp. 1496–1503, 2010.

[106] B. Lamas, B. Abreu, A. Fonseca, N. Martins, and M. Oliveira, "Assessing colloidal stability of long term MWCNT based nanofluids," *J. Colloid Interface Sci.*, vol. 381, no. 1, pp. 17–23, 2012.

[107] S. M. Vanaki, P. Ganesan, and H. A. Mohammed, "Numerical study of convective heat transfer of nanofluids: A review," *Renew. Sustain. Energy Rev.*, vol. 54, pp. 1212–1239, 2016.

[108] N. Sher Akbar and Z. Hayat Khan, "Rheological Analysis of CNT Suspended Nanofluid with Variable Viscosity : Numerical Solution," *Commun. Theor. Phys.*, vol. 67, pp. 681–687, 2017.

[109] H. Taherian, J. L. Alvarado, and E. M. Languri, "Enhanced thermophysical properties of multiwalled carbon nanotubes based nanofluids. Part 1: Critical review," *Renew. Sustain. Energy Rev.*, vol. 82, pp. 4326–4336, 2017.

[110] B. Abreu, A. Valega, B. Lamas, A. Fonseca, N. Martins, and M. Oliveira, "On the Assessment of Viscosity Variability by Nanofluid Engineering: A Review," *J. Nanofluids*, vol. 5, pp. 23–36, 2016.

[111] B. Lamas, M. Oliveira, and N. Martins, *Long-term nanofluids for heat transfer intensification : Nanofluids development and characterization*. Scholars Press, 2014.

[112] D. Kim *et al.*, "Convective heat transfer characteristics of nanofluids under laminar and turbulent flow conditions," *Curr. Appl. Phys.*, vol. 9, no. 2, pp. e119–e123, 2009.

[113] B. Abreu and B. Lamas, "Experimental characterization of convective heat transfer with MWCNT based nanofluids under laminar flow conditions,"

Heat Mass Transf., vol. 50, no. 1, pp. 65–74, 2014.

[114] B. C. Pak and Y. I. Cho, "Hydrodynamic and heat transfer study of dispersed fluids with submicron metallic oxide particles," *Exp. Heat Transf.*, vol. 11, no. 2, pp. 151–170, 1998.

[115] Y. Xuan and W. Roetzel, "Conceptions for heat transfer correlation of nanofluids," *Int. J. Heat Mass Transf.*, vol. 43, no. 19, pp. 3701–3707, 2000.

[116] M. Izadi, A. Behzadmehr, and D. Jalali-Vahida, "Numerical study of developing laminar forced convection of a nanofluid in an annulus," *Int. J. Therm. Sci.*, vol. 48, no. 11, pp. 2119–2129, 2009.

[117] R. Lotfi, Y. Saboohi, and A. M. Rashidi, "Numerical study of forced convective heat transfer of Nanofluids: Comparison of different approaches," *Int. Commun. Heat Mass Transf.*, vol. 37, no. 1, pp. 74–78, 2010.

[118] M. M. Sarafraz, A. Arya, F. Hormozi, and V. Nikkhah, "On the convective thermal performance of a CPU cooler working with liquid gallium and CuO/water nanofluid: A comparative study," *Appl. Therm. Eng.*, vol. 112, pp. 1373–1381, 2017.

[119] H. Herwig and O. Hausner, "Critical view on ''new results in micro-fluid mechanics'': an example," *Int. J. Heat Mass Transf.*, vol. 46, pp. 935–937, 2003.

[120] W. Owhaib and B. Palm, "Experimental investigation of single-phase convective heat transfer in circular microchannels," *Exp. Therm. Fluid Sci.*, vol. 28, no. 2–3, pp. 105–110, 2004.

[121] H. Y. Wu and P. Cheng, "An experimental study of convective heat transfer in silicon microchannels with different surface conditions," *Int. J. Heat Mass Transf.*, vol. 46, no. 14, pp. 2547–2556, 2003.

[122] K. . Toh, X. . Chen, and J. . Chai, "Numerical computation of fluid flow and heat transfer in microchannels," *Int. J. Heat Mass Transf.*, vol. 45, no. 26, pp. 5133–5141, 2002.

[123] L. Jiang *et al.*, "Closed-loop electroosmotic microchannel cooling system for VLSI circuits," *IEEE Trans. Components Packag. Technol.*, vol. 25, no. 3, pp. 347–355, 2002.

[124] B. X. Wang and X. F. Peng, "Experimental investigation on liquid forced-convection heat transfer through microchannels," *Int. J. Heat Mass Transf.*,

vol. 37, no. 1, pp. 73–82, 1994.

[125] H. C. Chiu, J. H. Jang, H. W. Yeh, and M. S. Wu, "The heat transfer characteristics of liquid cooling heatsink containing microchannels," *Int. J. Heat Mass Transf.*, vol. 54, no. 1–3, pp. 34–42, 2011.

[126] K. Hooman and A. Ejlali, "Effects of viscous heating, fluid property variation, velocity slip, and temperature jump on convection through parallel plate and circular microchannels," *Int. Commun. Heat Mass Transf.*, vol. 37, no. 1, pp. 34–38, 2010.

[127] M. Gad-el-hak, "The Fluid Mechanics of Microdevices — The Freeman Scholar Lecture," *J. Fluids Eng.*, vol. 121, no. 1, pp. 5–33, 1999.

[128] Z. Li, D. Du, and Z. Guo, "Experimental Study on Flow Characteristics of Liquid in Circular Microtubes," *Microscale Thermophys. Eng.*, vol. 7, no. 3, pp. 253–265, 2003.

[129] B. R. Thompson, D. Maynes, and B. W. Webb, "Characterization of the Hydrodynamically Developing Flow in a Microtube Using MTV," *J. Fluids Eng.*, vol. 127, no. 5, pp. 1003–1012, 2005.

[130] H. Y. Wu and P. Cheng, "Friction factors in smooth trapezoidal silicon microchannels with different aspect ratios," *Int. J. Heat Mass Transf.*, vol. 46, pp. 2519–2525, 2003.

[131] C. Y. Yang, "Friction characteristics of water, r-134a, and air in small tubes," *Microscale Thermophys. Eng.*, vol. 7, no. 4, pp. 335–348, 2003.

[132] D. Maynes and A. R. Webb, "Velocity profile characterization in sub-millimeter diameter tubes using molecular tagging velocimetry," *Exp. Fluids*, vol. 32, no. 1, pp. 3–15, 2002.

[133] M. Mala and D. Li, "Flow characteristics of water in microtubes," *Int. J. Heat Fluid Flow*, vol. 20, no. November 1997, pp. 142–148, 1999.

[134] S. G. Kandlikar, S. Joshi, and S. Tian, "Effect of surface roughness on heat transfer and fluid flow characteristics at low Reynolds numbers in small diameter tubes," *Heat Transf. Eng.*, vol. 24, no. 3, pp. 4–16, 2003.

[135] K. V. Sharp and R. J. Adrian, "Transition from laminar to turbulent flow in liquid filled microtubes," *Exp. Fluids*, vol. 36, no. 5, pp. 741–747, 2004.

[136] J. Koo and C. Kleinstreuer, "Viscous dissipation effects in microtubes and microchannels," *Int. J. Heat Mass Transf.*, vol. 47, no. 14–16, pp. 3159–3169,

2004.

[137] P. Gao, S. Le, and M. Favre-marinet, “Scale effects on hydrodynamics and heat transfer in two-dimensional mini and microchannels,” *Int. J. ofThermal Sci.*, vol. 41, pp. 1017–1027, 2002.

[138] G. Hetsroni, A. Mosyak, E. Pogrebnyak, and L. P. Yarin, “Fluid flow in micro-channels,” *Int. J. Heat Mass Transf.*, vol. 48, no. 10, pp. 1982–1998, 2005.

[139] T. M. Harms, M. J. Kazmierczak, and F. M. Gerner, “Developing convective heat transfer in deep rectangular microchannels,” *Int. J. Heat Fluid Flow*, vol. 20, pp. 149–157, 1999.

[140] A. Bucci, G. P. Celata, M. Cumo, E. Serra, and G. Zummo, “Water Single-Phase Fluid Flow and Heat Transfer in Capillary Tubes,” *1st Int. Conf. Microchannels Minichannels*, no. June 2014, pp. 319–326, 2003.

[141] H. B. Ma, G. P. Peterson, H. B. Ma, and G. P. Peterson, “Laminar friction factor in micro- scale ducts of irregular cross section,” *Microscale Thermophys. Eng.*, pp. 253–265, 1997.

[142] W. Qu and I. Mudawar, “Analysis of three-dimensional heat transfer in micro-channel heat sinks,” *Int. J. Heat Mass Transf.*, vol. 45, no. 19, pp. 3973–3985, 2002.

[143] I. Tiselj, G. Hetsroni, and Z. Segal, “Effect of axial conduction on the heat transfer in micro-channels,” *Int. J. Heat Mass Transf.*, vol. 47, pp. 2551–2565, 2004.

[144] P. Lee, S. V Garimella, and D. Liu, “Investigation of heat transfer in rectangular microchannels,” *Int. J. Heat Mass Transf.*, vol. 48, pp. 1688–1704, 2005.

[145] D. Lelea and S. Nishio, “The experimental research on microtube heat transf and fluid flow of distilled water,” *Int. J. Heat Mass Transf.*, vol. 47, pp. 2817–2830, 2004.

[146] ASHRAE, *ASHRAE handbook: Fundamentals.* American Society of Heating, Refrigerating and Air-Conditioning Engineers, 2005.

[147] T. L. Bergman, A. S. Lavine, F. P. Incropera, and D. P. Dewitt, *Fundamentals of Heat and Mass Transfer*. John Wily & Sons Seventh, 2011.

[148] Z. Li, Y.-L. He, G.-H. Tang, and W.-Q. Tao, “Experimental and numerical studies of liquid flow and heat transfer in microtubes,” *Int. J. Heat Mass*

Transf., vol. 50, no. 17–18, pp. 3447–3460, 2007.

[149] O. N. Sara, Ö. Barlay Ergu, M. E. Arzutug, and S. Yapici, "Experimental study of laminar forced convective mass transfer and pressure drop in microtubes," *Int. J. Therm. Sci.*, vol. 48, no. 10, pp. 1894–1900, 2009.

[150] T. M. Adams, S. I. Abdel-Khalik, S. M. Jeter, and Z. H. Qureshi, "An experimental investigation of single-phase forced convection in microchannels," *Int. J. Heat Mass Transf.*, vol. 41, no. 6–7, pp. 851–857, 1998.

[151] B. H. Salman, H. A. Mohammed, and A. Sh. Kherbeet, "Numerical and experimental investigation of heat transfer enhancement in a microtube using nano fluids," in *International Conference on Heat Transfer, Fluid Mechanics and Thermodynamics*, 2014, vol. 59, no. 1069, pp. 88–100.

[152] D. Lelea, "The performance evaluation of Al2O3/water nanofluid flow and heat transfer in microchannel heat sink," *Int. J. Heat Mass Transf.*, vol. 54, no. 17–18, pp. 3891–3899, 2011.

[153] J. Lee and I. Mudawar, "Assessment of the effectiveness of nanofluids for single-phase and two-phase heat transfer in micro-channels," *Int. J. Heat Mass Transf.*, vol. 50, no. 3–4, pp. 452–463, 2007.

[154] S. A. Sajadifar, A. Karimipour, and D. Toghraie, "Fluid flow and heat transfer of non-Newtonian nanofluid in a microtube considering slip velocity and temperature jump boundary conditions," *Eur. J. Mech. B/Fluids*, vol. 61, pp. 25–32, 2017.

[155] M. K. Moraveji, S. Mohammad, H. Haddad, and M. Darabi, "Modeling of forced convective heat transfer of a non-Newtonian nano fluid in the horizontal tube under constant heat flux with computational fluid dynamics," *Int. Commun. Heat Mass Transf.*, vol. 39, no. 7, pp. 995–999, 2012.

[156] M. Akbari, A. Behzadmehr, and F. Shahraki, "Fully developed mixed convection in horizontal and inclined tubes with uniform heat flux using nanofluid," vol. 29, pp. 545–556, 2008.

[157] J. Y. Jung, H. S. Oh, and H. Y. Kwak, "Forced convective heat transfer of nanofluids in microchannels," *Int. J. Heat Mass Transf.*, vol. 52, no. 1–2, pp. 466–472, 2009.

[158] E. B. Haghighi *et al.*, "Cooling performance of nanofluids in a small diameter tube," *Exp. Therm. Fluid Sci.*, vol. 49, pp. 114–122, 2013.

[159] M. Karimzadehkhouei, S. E. Yalcin, K. Şendur, M. Pinar Mengüç, and A. Koşar, "Pressure drop and heat transfer characteristics of nanofluids in horizontal microtubes under thermally developing flow conditions," *Exp. Therm. Fluid Sci.*, vol. 67, pp. 37–47, 2015.

[160] A. B. Metzner and J. C. Reed, "Flow of non-newtonian fluids- correlation of the laminar, transition, and turbulent-flow regions," *AIChE J.*, vol. 4, no. 1, pp. 434–440, 1955.

[161] R. Shyam and R. P. Chhabra, "Effect of Prandtl number on heat transfer from tandem square cylinders immersed in power-law fluids in the low Reynolds number regime," *Int. J. Heat Mass Transf.*, vol. 57, no. 2, pp. 742–755, 2013.

[162] M. Shojaeian and A. Kos, "Convective heat transfer and entropy generation analysis on Newtonian and non-Newtonian fluid flows between parallel-plates under slip boundary conditions," vol. 70, pp. 664–673, 2014.

[163] S. J. Palm, G. Roy, and C. T. Nguyen, "Heat transfer enhancement with the use of nanofluids in radial flow cooling systems considering temperature-dependent properties," *Appl. Therm. Eng.*, vol. 26, no. 17–18, pp. 2209–2218, 2006.

[164] Ashrae, *ASHRAE Handbook: Fundamentals*. American Society of Heating, Refrigerating and Air-Conditioning Engineers, 2005.

[165] J. Li, G. P. Peterson, and P. Cheng, "Three-dimensional analysis of heat transfer in a micro-heat sink with single phase flow," *Int. J. Heat Mass Transf.*, vol. 47, no. 19–20, pp. 4215–4231, 2004.

[166] S. D. Joshi, "Heat transfer in in-tube flow of non-Newtonian fluids," 1978.

[167] W. M. Kays and A. L. London, *Compact Heat Exchangers*, Third edit. Melbourne, Australia: Krieger Publishing, 1984.

[168] Y. Sheikhnejad, R. Hosseini, and M. Saffar-avval, "Effect of different magnetic field distributions on laminar ferroconvection heat transfer in horizontal tube," *J. Magn. Magn. Mater.*, vol. 389, pp. 136–143, 2015.

[169] O. Olsson and B. Sundent, "Heat transfer and pressure drop characteristics of ten radiator tubes," vol. 39, no. 15, pp. 3211–3220, 1996.

[170] J. Li, C. Dang, and E. Hihara, "Heat transfer enhancement in a parallel , finless heat exchanger using a longitudinal vortex generator , Part A : Numerical investigation," *Int. J. Heat Mass Transf.*, vol. 128, pp. 87–97, 2019.

[171] A. Zamzamian and F. Hormozi, “Wavy Channel and Different Nanofluids Effects on Performance of Plate-Fin Heat Exchangers,” *J. Thermophys. Heat Transf.*, 2014.

[172] J. Yun and K. Lee, “Influence of design parameters on the heat transfer and flow friction characteristics of the heat exchanger with slit fins,” *Int. J. Heat Mass Transf.*, vol. 43, pp. 2529–2539, 2000.

[173] L. B. Erbay, B. Doğan, and M. M. Öztürk, *Comprehensive Study of Heat Exchangers with Louvered Fins*. 2017.

[174] Z. Qi, J. Chen, and Z. Chen, “Parametric study on the performance of a heat exchanger with corrugated louvered fins,” *Appl. Therm. Eng. 27*, vol. 27, pp. 539–544, 2007.

[175] K. Wongcharee and S. Eiamsa-ard, “Heat transfer enhancement by using CuO / water nanofluid in corrugated tube equipped with twisted tape,” *Int. Commun. Heat Mass Transf.*, vol. 39, no. 2, pp. 251–257, 2012.

[176] M. R. Sohel, S. S. Khaleduzzaman, R. Saidur, A. Hepbasli, M. F. M. Sabri, and I. M. Mahbubul, “An experimental investigation of heat transfer enhancement of a minichannel heat sink using Al2 O3 – H2O nanofluid,” *Int. J. Heat Mass Transf.*, vol. 74, pp. 164–172, 2014.

[177] S. P. Jang and S. U. S. Choi, “Cooling performance of a microchannel heat sink with nanofluids,” *Applied Thermal Engineering*, vol. 26, no. 17–18. pp. 2457–2463, 2006.

[178] A. Sarlak, A. Ahmadpour, and M. R. Hajmohammadi, “Thermal design improvement of a double-layered microchannel heat sink by using multi-walled carbon nanotube (MWCNT) nanofluids with non-Newtonian viscosity,” *Appl. Therm. Eng.*, vol. 147, no. September 2018, pp. 205–215, 2019.

[179] M. M. Sarafraz, V. Nikkhah, M. Nakhjavani, and A. Arya, “Thermal performance of a heat sink microchannel working with biologically produced silver-water nanofluid: Experimental assessment,” *Exp. Therm. Fluid Sci.*, vol. 91, no. November 2017, pp. 509–519, 2018.

[180] R. K. Shah and A. L. London, *LAMINAR FLOW FORCED CONVECTION IN DUCTS*. New York: Academic Press, 1978.

[181] F. T. Pinho and P. M. Coelho, *Non-Newtonian Heat Transfer in rheology*.

Oxford ,UK: Eolss Publishers, 2009.

[182] S. S. Pawar and V. K. Sunnapwar, “Experimental studies on heat transfer to Newtonian and non-Newtonian fluids in helical coils with laminar and turbulent flow,” *Exp. Therm. Fluid Sci.*, vol. 44, pp. 792–804, 2013.

[183] A. R. Azimian and M. Sefid, “Performance of Microchannel Heat Sinks with Newtonian and Non-Newtonian Fluids,” *Heat Transf. Eng.*, 2010.

[184] M. Shojaeian, M. Yildiz, and A. Koşar, “Convective heat transfer and second law analysis of non-Newtonian fluid flows with variable thermophysical properties in circular channels,” *Int. Commun. Heat Mass Transf.*, vol. 60, pp. 21–31, 2015.

[185] P. Li, Y. Xie, and D. Zhang, “Laminar flow and forced convective heat transfer of shear-thinning power-law fluids in dimpled and protruded microchannels,” *Int. J. Heat Mass Transf.*, vol. 99, pp. 372–382, 2016.

[186] World Commission on Environment and Development, “Our Common Future,” 1987.

[187] A. Maryam and B. Elham, “Deaths involving natural gas inhalation,” *Toxicol. Ind. Health*, vol. 26, no. 6, pp. 345–347, 2010.

APPENDIX

A. Thermophysical properties

Table A-1: Thermophysical properties of the nanofluid samples (30%EG base fluid).

lp/dp	%CNT	Nanofluid Number	Thermal diffusivity a_{avg} (m^2/s)	k_{avg} (W/m.k)	ρ (kg/m^3)	c_p (J/kg.K)	μ_{avg} Pa.s
231	0.25%	Nanofluid 1	1.24729E-07	0.4758	1043.135	3656.937	0.002056
	0.5%	Nanofluid 2	1.26747E-07	0.4828	1045.934	3641.89	0.002435
	0.75%	Nanofluid 3	1.28928E-07	0.4904	1048.733	3626.922	0.002392
	1.0%	Nanofluid 4	1.34538E-07	0.511	1051.533	3612.035	0.002732
	1.5%	Nanofluid 5	1.4264E-07	0.5402	1057.131	3582.496	0.002662
667	0.25%	Nanofluid 6	1.23208E-07	0.47	1043.135	3656.937	0.001893
	0.5%	Nanofluid 7	1.24069E-07	0.4726	1045.934	3641.89	0.002026
	0.75%	Nanofluid 8	1.24827E-07	0.4748	1048.733	3626.922	0.002346
	1.0%	Nanofluid 9	1.27746E-07	0.4852	1051.533	3612.035	0.002453
	1.5%	Nanofluid 10	1.32342E-07	0.5012	1057.131	3582.496	0.00327
50	0.25%	Nanofluid 11	1.22265E-07	0.4664	1043.135	3656.937	0.002023
	0.5%	Nanofluid 12	1.22756E-07	0.4676	1045.934	3641.89	0.002177
	0.75%	Nanofluid 13	1.23407E-07	0.4694	1048.733	3626.922	0.002499
	1.0%	Nanofluid 14	1.2585E-07	0.478	1051.533	3612.035	0.002588
		Nanofluid 15	1.26506E-07	0.4791	1057.131	3582.496	0.003037
125	0.25%	Nanofluid 16	1.22265E-07	0.4664	1043.135	3656.937	0.001927
	0.5%	Nanofluid 17	1.23701E-07	0.4712	1045.934	3641.89	0.001963
	0.75%	Nanofluid 18	1.26299E-07	0.4804	1048.733	3626.922	0.002076
	1.0%	Nanofluid 19	1.2822E-07	0.487	1051.533	3612.035	0.004361
	1.5%	Nanofluid 20	1.34507E-07	0.5094	1057.131	3582.496	0.004064
19	0.25%	Nanofluid 21	1.23575E-07	0.4714	1043.135	3656.937	0.001903
	0.5%	Nanofluid 22	1.25381E-07	0.4776	1045.934	3641.89	0.002057
	0.75%	Nanofluid 23	1.26246E-07	0.4802	1048.733	3626.922	0.002278
	1.0%	Nanofluid 24	1.25903E-07	0.4782	1051.533	3612.035	0.00255
	1.5%	Nanofluid 25	1.30757E-07	0.4952	1057.131	3582.496	0.003
333	0.25%	Nanofluid 26	1.22579E-07	0.4676	1043.135	3656.937	0.001987
	0.5%	Nanofluid 27	1.26064E-07	0.4802	1045.934	3641.89	0.002141
	0.75%	Nanofluid 28	1.26299E-07	0.4804	1048.733	3626.922	0.002271
	1.0%	Nanofluid 29	1.27798E-07	0.4854	1051.533	3612.035	0.002463
	1.5%	Nanofluid 30	1.34084E-07	0.5078	1057.131	3582.496	0.00291

Table A-2: Thermophysical properties of the nanofluid samples (60%EG base fluid).

lp/dp	%CNT	Nanofluid Number	Thermal diffusivity a_{avg}(m^2/s)	k_{avg} (W/m.k)	ρ (kg/m^3)	c_p (J/kg.K)	μ_{avg} Pa.s
231	0.25%	Nanofluid 31	1.02E-07	0.3544	1089.782	3194.825	0.004315
	0.5%	Nanofluid 32	1.05E-07	0.3658	1092.465	3182.74	0.004668
	0.75%	Nanofluid 33	1.08E-07	0.3756	1095.147	3170.655	0.004738
	1.0%	Nanofluid 34	1.11E-07	0.3864	1097.829	3158.569	0.005117
	1.5%	Nanofluid 35	1.19E-07	0.4122	1103.194	3134.84	0.005735
667	0.25%	Nanofluid 36	1.01E-07	0.3514	1089.782	3194.825	0.00454
	0.5%	Nanofluid 37	1.03E-07	0.3578	1092.465	3182.74	0.004926
	0.75%	Nanofluid 38	1.04E-07	0.362	1095.147	3170.655	0.005441
	1.0%	Nanofluid 39	1.08E-07	0.3736	1097.829	3158.569	0.005793
	1.5%	Nanofluid 40	1.11E-07	0.385	1103.194	3134.84	0.007177
50	0.25%	Nanofluid 41	1.01E-07	0.3523	1089.782	3194.825	0.004598
	0.5%	Nanofluid 42	1.01E-07	0.3528	1092.465	3182.74	0.004746
	0.75%	Nanofluid 43	1.02E-07	0.3548	1095.147	3170.655	0.005206
	1.0%	Nanofluid 44	1.03E-07	0.356	1097.829	3158.569	0.004256
		Nanofluid 45	1.04E-07	0.3596	1103.194	3134.84	0.00511
125	0.25%	Nanofluid 46	1.02E-07	0.356	1089.782	3194.825	0.004544
	0.5%	Nanofluid 47	1.03E-07	0.3598	1092.465	3182.74	0.004532
	0.75%	Nanofluid 48	1.05E-07	0.366	1095.147	3170.655	0.004753
	1.0%	Nanofluid 49	1.07E-07	0.37	1097.829	3158.569	0.005306
	1.5%	Nanofluid 50	1.12E-07	0.3864	1103.194	3134.84	0.0080
19	0.25%	Nanofluid 51	1.02E-07	0.354	1089.782	3194.825	0.004795
	0.5%	Nanofluid 52	1.01E-07	0.3528	1092.465	3182.74	0.004829
	0.75%	Nanofluid 53	1.05E-07	0.3658	1095.147	3170.655	0.005251
	1.0%	Nanofluid 54	1.06E-07	0.369	1097.829	3158.569	0.005761
	1.5%	Nanofluid 55	1.13E-07	0.3908	1103.194	3134.84	0.007051
333	0.25%	Nanofluid 56	1.02E-07	0.3556	1089.782	3194.825	0.004749
	0.5%	Nanofluid 57	1.04E-07	0.361	1092.465	3182.74	0.005091
	0.75%	Nanofluid 58	1.04E-07	0.3628	1095.147	3170.655	0.005886
	1.0%	Nanofluid 59	1.06E-07	0.366	1097.829	3158.569	0.00634
	1.5%	Nanofluid 60	1.11E-07	0.3842	1103.194	3134.84	0.006457

B. Conductivity

Table B-1: Thermal conductivity correlations of the four nanofluids and base fluids.

	$k = a\,T^3 + b\,T^2 + c\,T + d$				
Parameters	**a**	**b**	**c**	**d**	
NF-Group1	7.396E-07	- 6.664E-04	2.010E-01	- 1.982E+01	Eq. B-1
NF-Group2	1.528E-07	- 1.417E-04	4.406E-02	- 4.236E+00	Eq. B-2
NF-Group3	3.333E-07	- 2.817E-04	7.987E-02	7.105+00	Eq. B-3
NF-Group4	1.667E-07	- 1.544E-04	4.797E-02	- 4.605E+00	Eq. B-4
30%BF	8.704E-07	-8.003E-04	2.458E-01	-2.476E+01	Eq. B-5
60%BF	1.610E-07	- 1.517E-04	4.806E-02	4.762E+00	Eq. B-6

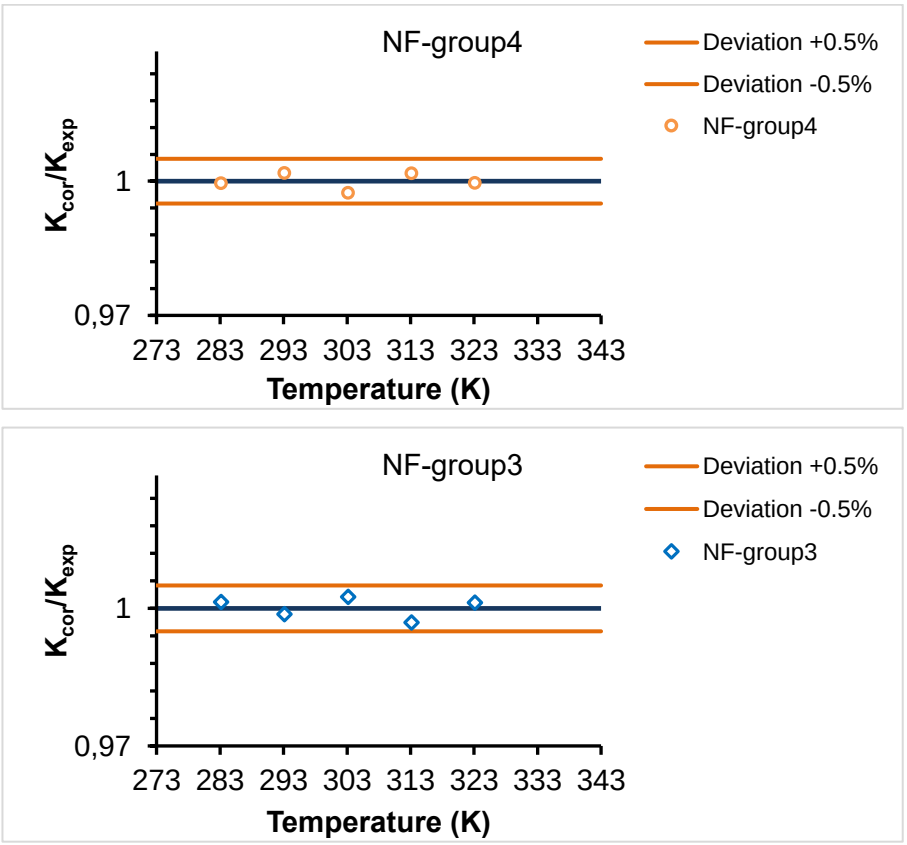

Fig. B-1: The deviation of the proposed correlations of thermal conductivity in comparison with experimental data (NF-group3 and NF-group4).

C. Viscosity

The viscosity parameters of the accomplished power-law correlations (for 60 nanofluid samples) produced by the fitting curve are presented in Table C-1. The obtained results from these correlations are compared with experimental data as shown in Fig. C-2, Fig. C-3, Fig. C-4, Fig. C-5, Fig. C-6, Fig. C-7 and Fig. C-8. According to these figures, the MWCNTs nanofluids viscosity are fitted well by the proposed correlations with a maximum deviation of 10%.

Also, the viscosity correlations of EG60% and EG30% base fluids as a function of temperature (Eq. C-2 and Eq. C-2) was produced by performing a polynomial fitting curve on the experimental viscosity data of the base fluid (EG60%) [21]. The presented correlation achieved a maximum deviation of 1.5% as presented in Fig. C-1.

EG30%: $\mu = -8.056E\text{-}09\ T^3 + 8.042E\text{-}06\ T^2 - 2.696E\text{-}0\ T + 3.046E\text{-}01$ Eq. C-1

EG60%: $\mu = -3.830E\text{-}08\ T^3 + 3.778E\text{-}05T^2 - 1.247E\text{-}02\ T + 1.380E+00$ Eq. C-2

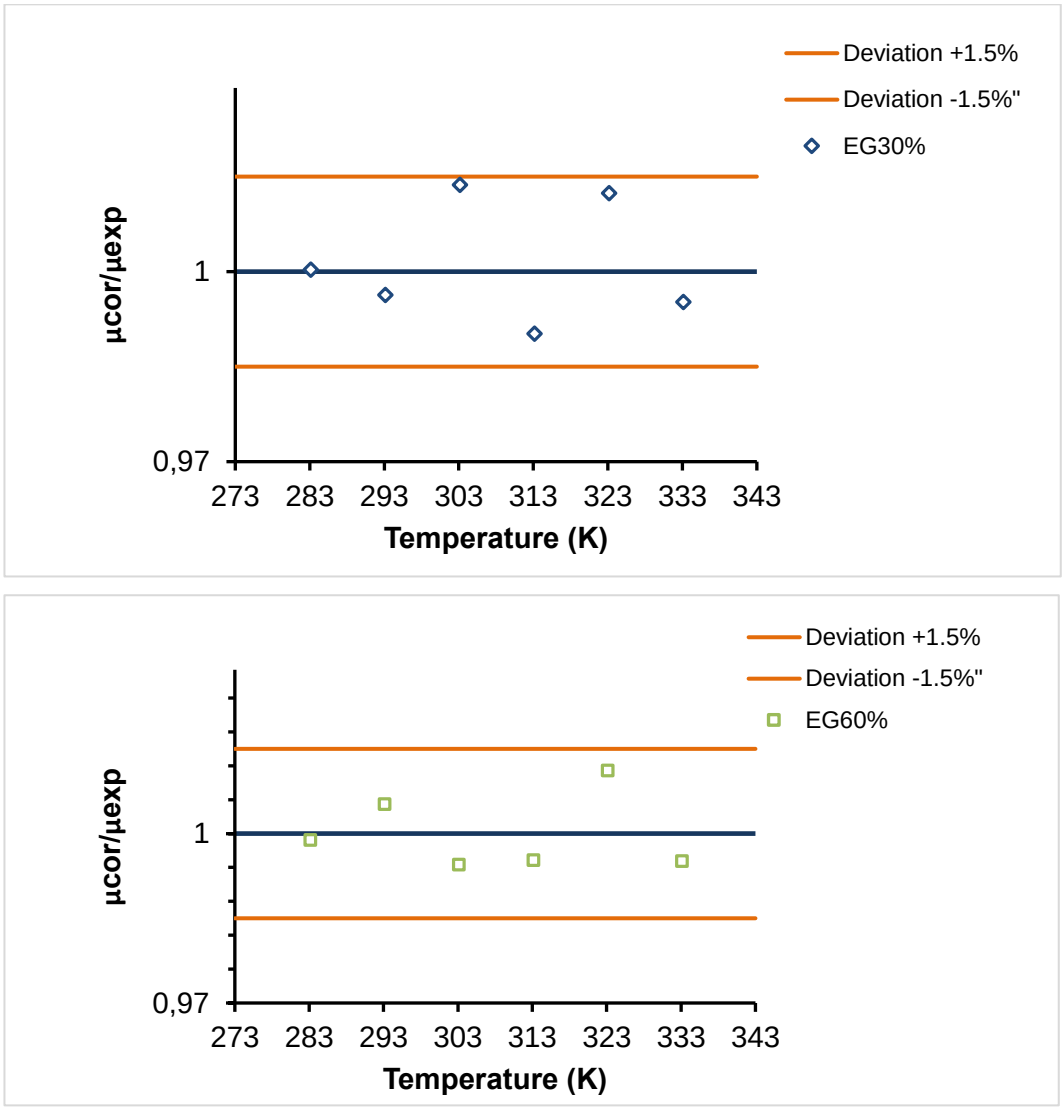

Fig. C-1: The deviation of the proposed correlations of viscosity in comparison with experimental data for EG60% and EG30% base fluids.

Table C-1: Rheological parameters of the nanofluid samples.

lp/dp	%CNT	NF number	n	K	α	NF number	n	K	α
231	0.25%	NF 1	0.967	3.150E-03	2300	NF 31	0.926	6.670E-03	3000
	0.5%	NF 2	0.973	3.60E-03	2300	NF 32	0.966	7.510E-03	3000
	0.75%	NF 3	0.958	3.780E-03	2250	NF 33	0.949	8.300E-03	2950
	1.0%	NF 4	0.926	4.900E-03	2500	NF 34	0.939	9.4700E-03	3000
	1.5%	NF 5	0.926	4.937E-03	2300	NF 35	0.919	1.1700E-02	2900
667	0.25%	NF 6	0.986	2.589-03	2100	NF 36	0.98	6.748E-03	2900
	0.5%	NF 7	0.971	2.97E-03	2100	NF 37	0.926	9.710E-03	3000
	0.75%	NF 8	0.927	4.35E-03	2300	NF 38	0.949	9.560E-03	3000
	1.0%	NF 9	0.914	4.89E-03	2400	NF 39	0.937	1.0800E-02	2950
	1.5%	NF 10	0.942	5.63E-03	2300	NF 40	0.973	1.1200E-02	3100
50	0.25%	NF 11	0.967	3.076E-03	2300	NF 41	0.969	7.290E-03	3000
	0.5%	NF 12	0.926	4.05E-03	2300	NF 42	0.985	6.900E-03	3000
	0.75%	NF 13	0.984	3.470E-03	2500	NF 43	0.95	9.100E-03	3000
	1.0%	NF 14	0.942	4.4920E-03	2400	NF 44	0.938	9.9000E-03	2900
		NF 15	0.95	4.9990E-03	2350	NF 45	0.932	1.2700E-02	2950
125	0.25%	NF 16	0.925	3.590E-03	2150	NF 46	0.971	7.080E-03	2900
	0.5%	NF 17	0.912	4.050E-03	2300	NF 47	0.958	7.600E-03	3000
	0.75%	NF 18	0.931	3.770E-03	2150	NF 48	0.949	8.300E-03	2900
	1.0%	NF 19	0.914	4.830E-03	2125	NF 49	0.946	9.4700E-03	3000
	1.5%	NF 20	0.911	9.460E-03	2200	NF 50	0.935	1.5500E-02	3500
19	0.25%	NF 21	0.985	2.520E-03	2300	NF 51	0.974	7.400E-03	3000
	0.5%	NF 22	0.977	2.970E-03	2300	NF 52	0.964	7.850E-03	3000
	0.75%	NF 23	0.972	3.414E-03	2350	NF 53	0.959	8.760E-03	3000
	1.0%	NF 24	0.953	4.298E-03	2350	NF 54	0.928	1.1200E-02	2900
	1.5%	NF 25	0.959	4.830E-03	2350	NF 55	0.916	1.4700E-02	3000
333	0.25%	NF 26	0.986	3.170E-03	2500	NF 56	0.969	7.500E-03	2950
	0.5%	NF 27	0.92	4.116E-03	2300	NF 57	0.967	8.100E-03	3250
	0.75%	NF 28	0.898	4.838E-03	2250	NF 58	0.953	1.010E-02	2950
	1.0%	NF 29	0.9219	4.6400E-03	2125	NF 59	0.89	2.0500E-03	3150
	1.5%	NF 30	0.8876	6.5100E-03	2150	NF 60	0.906	1.4000E-02	2800

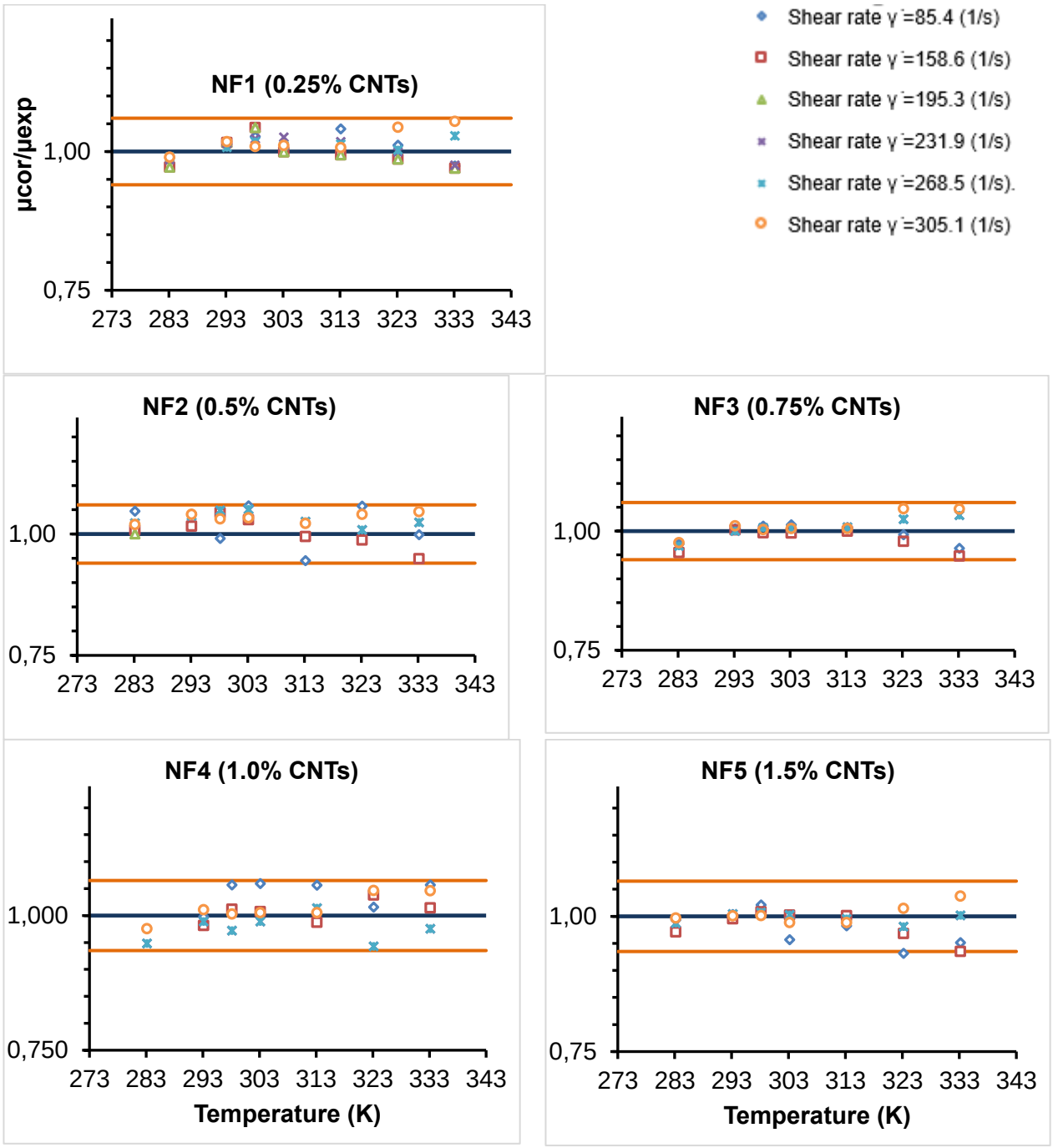

Fig. C-2: Deviation of the proposed correlations of viscosity in comparison with experimental data for 0.25%, 0. 5%, 0.75%, 1.0% and 1.5% MWCNTs nanofluids (NF1-5) for the particle dimensions of l_p/d_p=231 (d_p=50-80 nm and l_p= 10-20 μm) and 30%EG+DW as a base fluid.

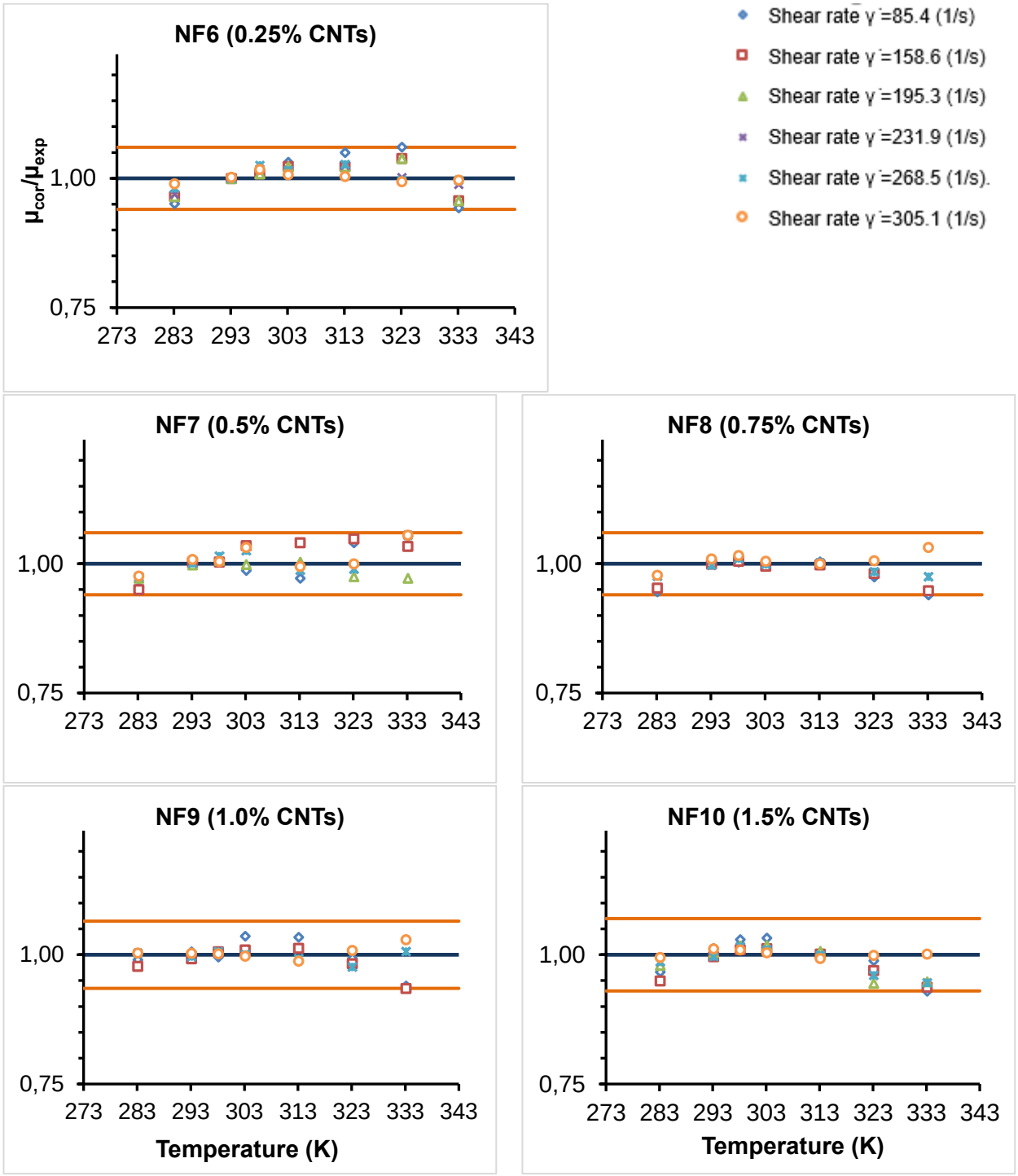

Fig. C-3: Deviation of the proposed correlations of viscosity in comparison with experimental data for 0.25%, 0. 5%, 0.75%, 1.0% and 1.5% MWCNTs nanofluids (NF6-10) for the particle dimensions of l_p/d_p=667 (d_p=20-40 nm and l_p= 10-30 μm) and 30%EG+DW as a base fluid.

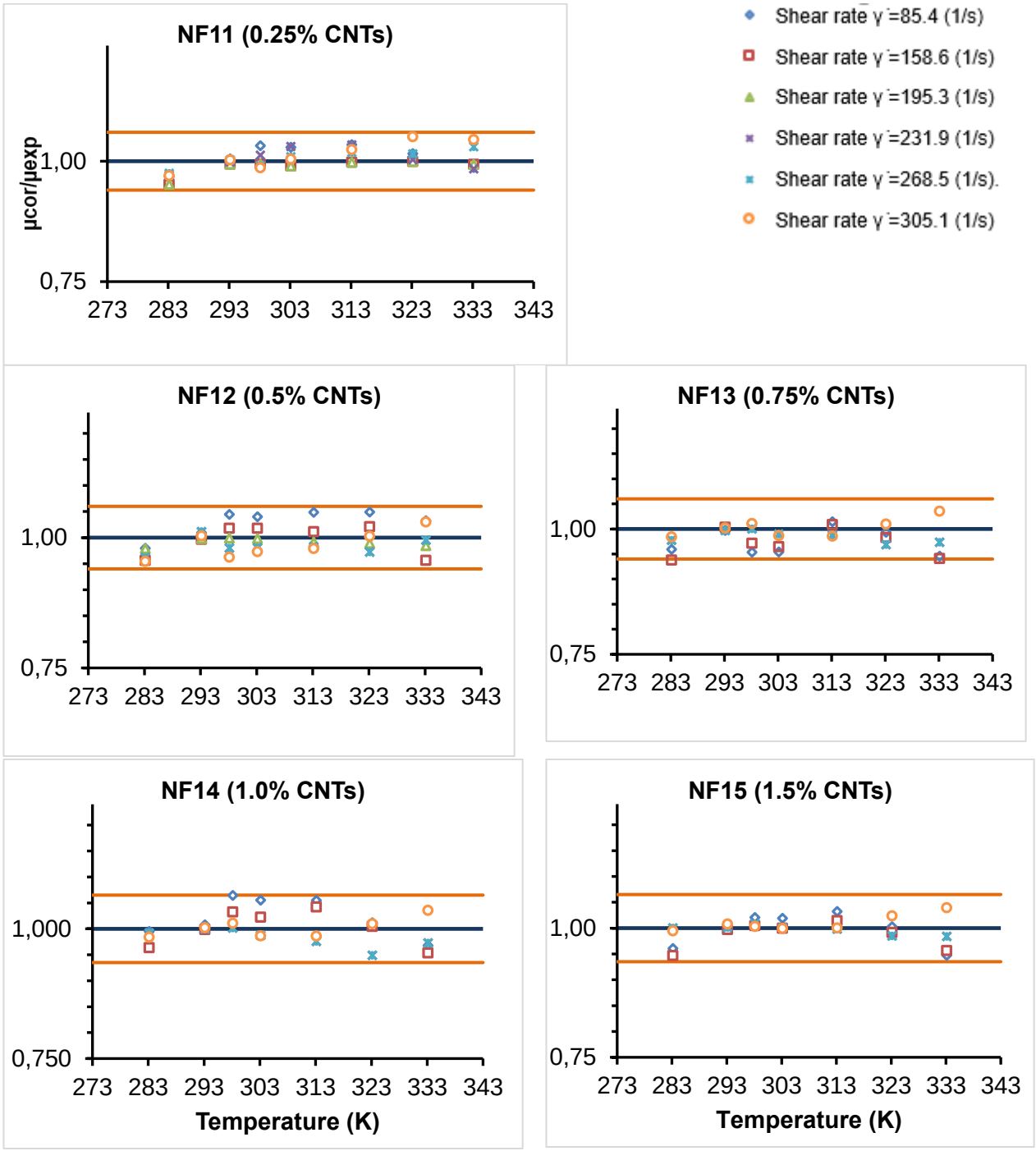

Fig. C-4: Deviation of the proposed correlations of viscosity in comparison with experimental data for 0.25%, 0. 5%, 0.75%, 1.0% and 1.5% MWCNTs nanofluids (NF11-15) for the particle dimensions of l_p/d_p=50 (d_p=20-40 nm and l_p= 1-2 μm) and 30%EG+DW as a base fluid.

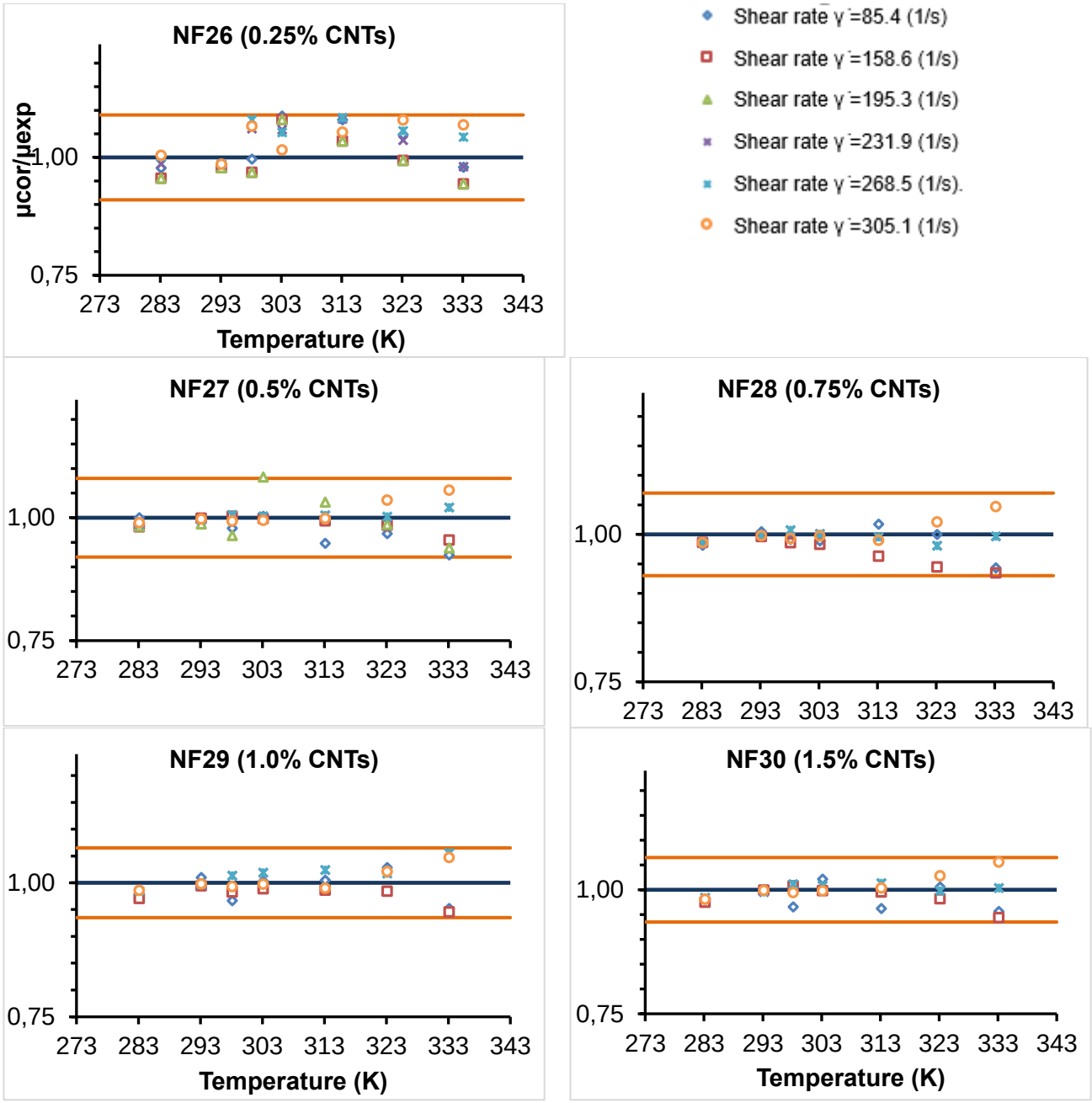

Fig. C-5: Deviation of the proposed correlations of viscosity in comparison with experimental data for 0.25%, 0. 5%, 0.75%, 1.0% and 1.5% MWCNTs nanofluids (NF26-30) for the particle dimensions of l_p/d_p=333 (d_p=20-40 nm and l_p= 5-15 μm) and 30%EG+DW as a base fluid.

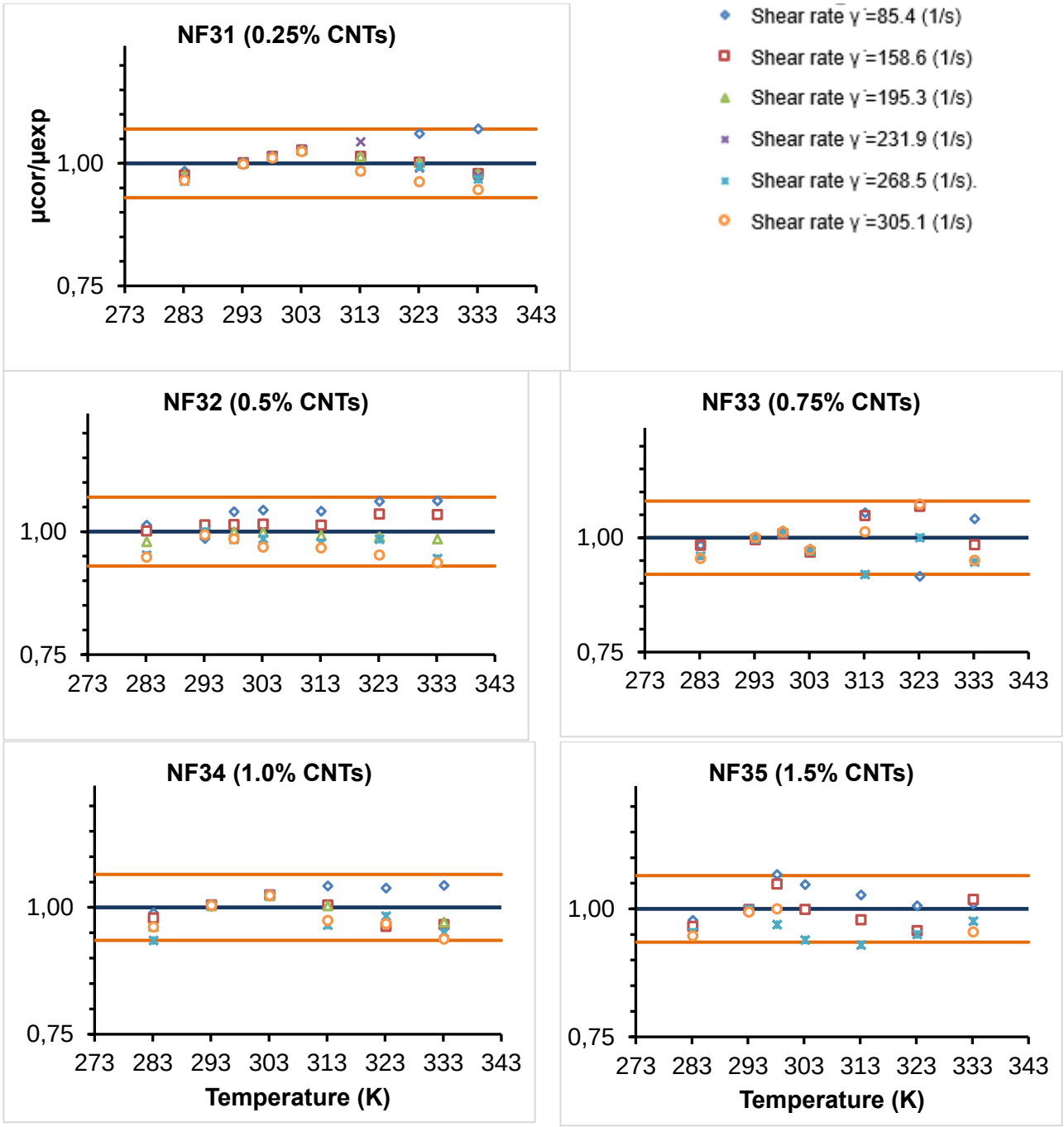

Fig. C-6: Deviation of the proposed correlations of viscosity in comparison with experimental data for 0.25%, 0. 5%, 0.75%, 1.0% and 1.5% MWCNTs nanofluids (NF31-35) for the particle dimensions of lp/dp=231 (d_p=50-80 nm and l_p= 10-20 μm) and 60%EG+DW as a base fluid.

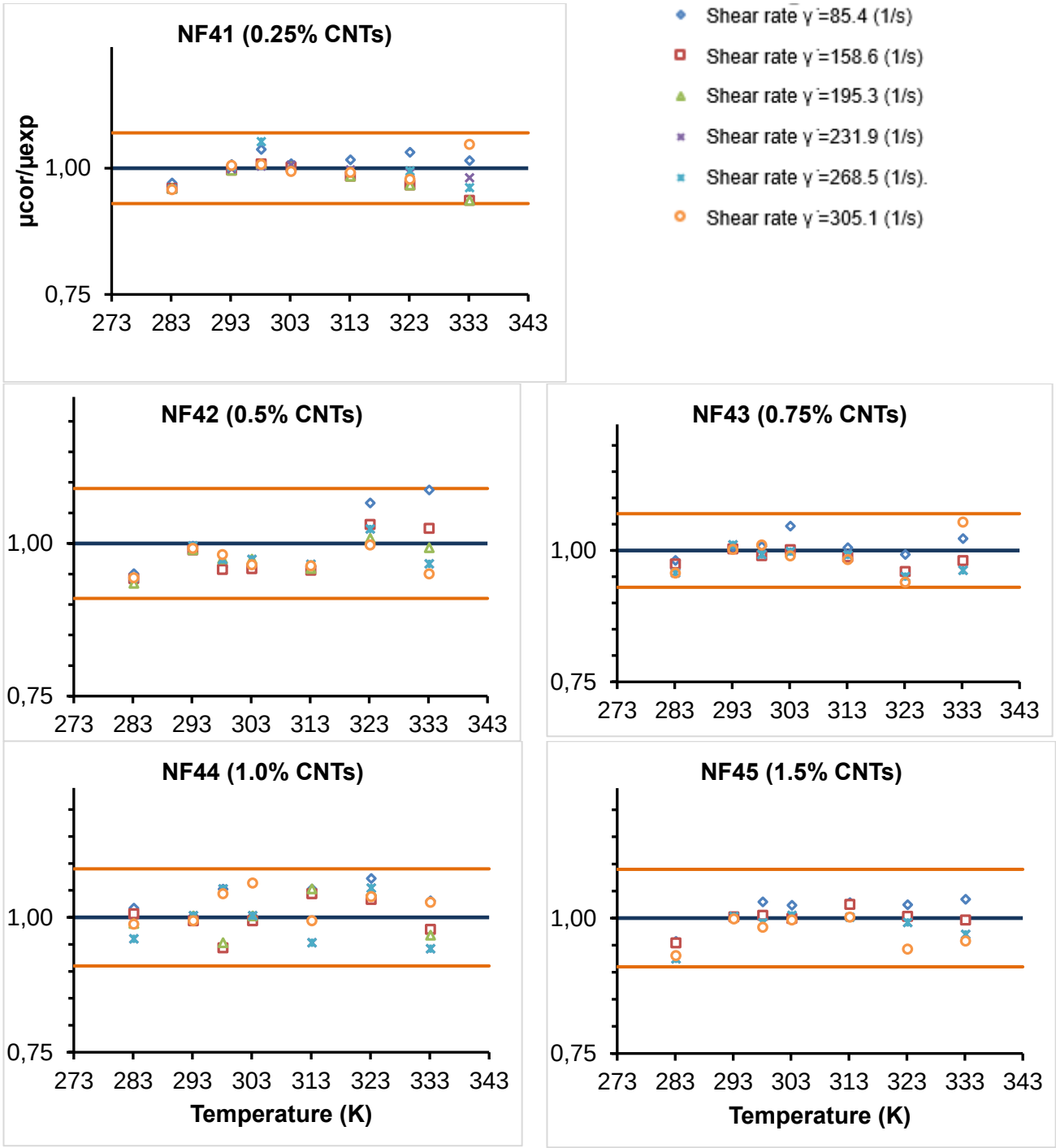

Fig. C-7: Deviation of the proposed correlations of viscosity in comparison with experimental data for 0.25%, 0. 5%, 0.75%, 1.0% and 1.5% MWCNTs nanofluids (NF41-45) for the particle dimensions of l_p/d_p=50 (d_p=10-20 nm and l_p= 1-2 μm) and 60%EG+DW as a base fluid.

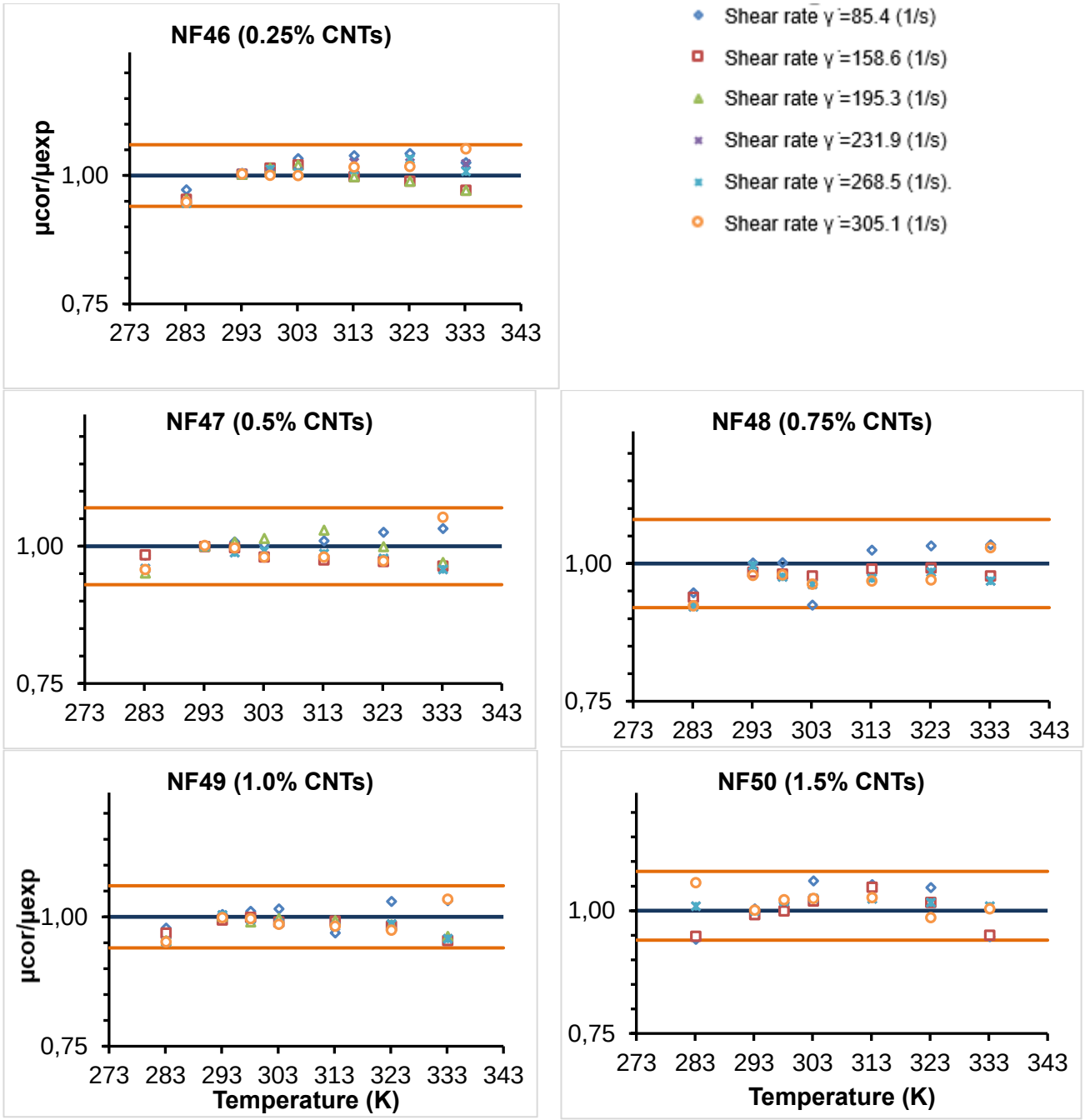

Fig. C-8: Deviation of the proposed correlations of viscosity in comparison with experimental data for 0.25%, 0. 5%, 0.75%, 1.0% and 1.5% MWCNTs nanofluids (NF46-50) for the particle dimensions of l_p/d_p=125 (d_p=60-100 nm and l_p= 5-15 μm) and 60%EG+DW as a base fluid.